Evaluation and Design of the DopTrackBox Concept

Development of a Satellite Doppler Tracking Network Using Commercial Off-the-Shelf Components

Master's Thesis

Dylano van Oijen

Delft University of Technology

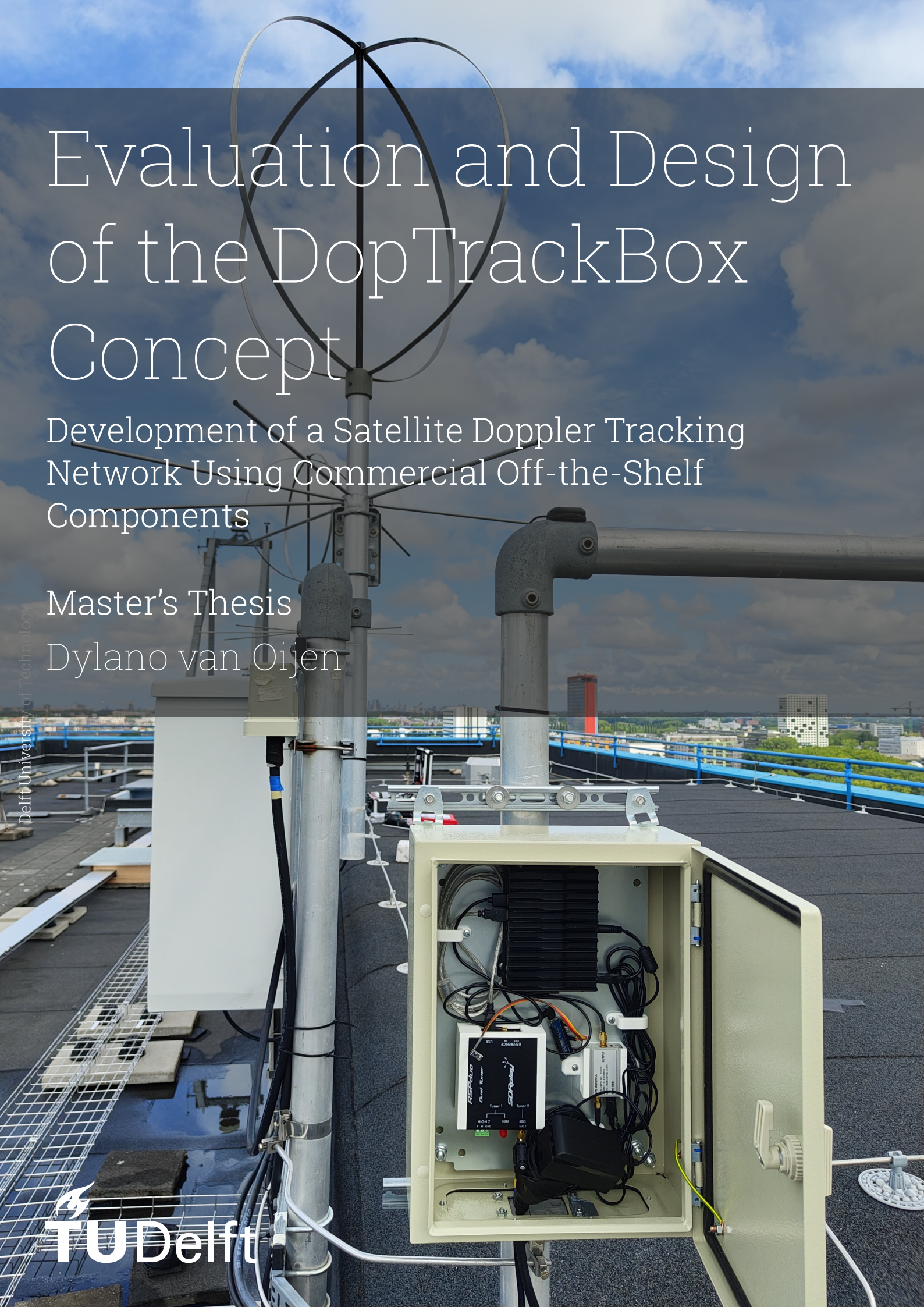

TU Delft

Evaluation and Design of the DopTrackBox Concept

Development of a Satellite Doppler Tracking Network Using Commercial Off-the-Shelf Components

by

Dylano van Oijen

to obtain the degree of Master of Science

at the Delft University of Technology,

to be defended publicly on Monday November 17, 2025 at 12:30.

Student number:	5414253	
Project duration:	Febrary 4, 2025 – November 2, 2025	
Thesis committee:	Dr. ir. B. C. Root,	TU Delft, Responsible Supervisor
	M. H. A. Søndergaard,	TU Delft, Additional Supervisor
	Dr. S. Gehly,	TU Delft, Independent Examiner
	Dr. ir. J. G. De Teixeira da Encarnacao,	TU Delft, Chair

An electronic version of this thesis is available at http://repository.tudelft.nl/.

TU Delft

Preface

What do you choose as a thesis topic when you have a background in physics, some limited background in electrical engineering, but are pursuing a master's degree in aerospace engineering? And you like working with computers but are also interested in learning about hardware? Apparently, you end up at the DopTrack project!

When I first learned about DopTrack at TU Delft, it seemed like a very interesting project, as it spans everything from hardware to simulations and signal processing. So, when I first stepped into Bart Root's office to discuss potential thesis topics, one sentence particularly stuck with me, someone who is generally more of a theorist than an experimentalist: "Your thesis is likely the last chance to really step outside your comfort zone in a safe way and do something that you wouldn't otherwise do." As a result, instead of pursuing a project that could be accomplished by mere computer simulation or analysis work, I chose to work on something practical in the form of continuing the development of DopTrackBox. The result is the thesis in front of you.

First of all, I want to thank Bart Root for providing me with the opportunity to conduct this thesis under his supervision. Although doing a topic that you like is important, having a supervisor that you like, makes time for your questions, is willing to think along, and is properly excited about your work is in my opinion at least equally important. All I can say is that Bart Root is excellent at that!

I would also like to thank Martin Søndergaard for joining the weekly discussions with Bart Root to provide valuable feedback on the progress of the project. In addition, I want to thank him for taking the time to provide me with access to the roof whenever something was not working, required inspection, or needed to be changed once again for additional tests.

Finally, I want to thank my family, in particular my caring and loving parents, for always supporting me during these years of studying. Having the privilege to study at all, let alone complete two master's degrees, is not something everyone has. I am therefore forever grateful to them for helping me achieve this in whatever way they could.

With the completion of this thesis, my time as a student will come to an end. Even though this time has not always been easy, wherever life may take me next, I will always cherish my time as a student at both UvA and TU Delft. Yet, I am also incredibly excited and look forward to what lies ahead of me.

Ad astra per aspera!

Dylano van Oijen
Delft, November 2025

Abstract

Doppler tracking is a widely adopted method of tracking spacecraft for high-profile missions, using networks of vast and expensive dedicated tracking equipment. Though, amateur astronomers are sometimes also capable of tracking these missions using comparatively simple and cheap radio hardware, typically when a spacecraft uses VHF, UHF, LoRa or S-band to communicate with groundstations.

A similar effort is made using the DopTrack project of the Delft University of Technology, with the goal of being able to estimate and predict satellite orbits to similar accuracy as NORAD's TLEs. To this end, a concept was developed to use standardized commercial off-the-shelf components that could be turned into a cheap and reliable tracking network. Preliminary studies showed that this concept is a viable solution, but questions remained regarding the frequency stability of the hardware and the influence of an observation time bias on the estimated orbits. In addition, no design had been made yet that accounted for environmental constraints on the components and the protection thereof.

The aim of this study was to first investigate the frequency stability of the GPS clock and software defined radio that were intended for the concept, in order verify that the desired estimation accuracy could be met. Then, this study investigated what the impact of a time bias in the observations is on the orbit estimation capabilities of the system. Subsequently, a prototype was developed and installed to record satellite passes in a realistic environment. This data was used to provide an estimation of the time bias in the real system, as well as compare its performance with the current DopTrack system.

It was found that the hardware recommended by the preliminary study satisfies the stability requirements of the project. Although it was also found that the system exhibits an observation time bias on the order of one second, the effects of this bias could be mitigated by estimating this bias during the orbit estimation.

The data gathered by operating the prototype revealed two issues with the design. First, even in the Dutch weather, the components occasionally overheated, leading to reduction of the operational period of the system. Further investigation is needed to determine if different hardware components should be used, or if it can be mitigated by redesigning the box with cooling options.

Secondly, the signal-to-noise ratio of the recorded satellites does not meet the expectations set by earlier work, nor does it satisfy the established requirements. Investigations presented in this work show that the likely cause of this is an excess amount of noise picked up by the software defined radio when operated on the roof. Further investigation is needed to find if this can be mitigated by shielding of the equipment, or placing it at locations with less noise.

Contents

1

Introduction

1.1. Context and Motivation

Over the years, more and more time and resources in the field of space engineering have been dedicated to making satellites more capable, but also smaller and cheaper. This has led to a space industry that is more accessible than ever, with small businesses, universities and small nations being able to build and operate their own satellites. To support the operations of such satellites, it is often required to communicate with the satellites and track their orbital state. The TU Delft is involved in the research and development of a Doppler tracking groundstation, called DopTrack. The operation principle of DopTrack is to extract the satellites range-rate from the observed Doppler shift in VHF or UHF radio beacon of the satellite.

The goal of the DopTrack project is to provide students with hands-on experience with orbit determination, as well as providing an alternative orbital state estimate to the North American Aerospace Defense Command's (NORAD) two-line element sets (TLEs) (Søndergaard, 2018; González Martínez, 2017). To this end, DopTrack should be a cheap and simple setup from using commercial of the shelf (COTS) components, such that other universities and interested parties can participate and form a network. Compared to a single station, a network should increase the performance significantly. One concept in that direction is DopTrackBox: a simpler version of DopTrack using smaller and cheaper COTS components. A preliminary study by Sprenkels (2023) has investigated the feasibility of potential DopTrackBox hardware and software configurations, but several aspects of the design require further investigation. Therefore, the goal of this project is to refine the design of DopTrackBox and assess its performance, such that the concept is ready to be cloned and used in a network capable of competing with NORAD.

1.2. Satellite Tracking Networks

In modern times, a wide range of solutions exists for the orbit determination of satellites, but all of them have in common that the orbit is estimated based on a set of position and/or velocity measurements of the spacecraft with respect to some reference frame. Performing these measurements can be done from the ground, on-board, or a combination of both, depending on the chosen navigation solution.

Historically, the tracking of satellites started using the same methods as how the movements of celestial bodies were studied: observing the reflected visible light of the body over time allows for a determination of its celestial coordinates. This method is referred to as optical tracking, and is still in use today using (networks of) automated telescope and camera systems. Another form of optical tracking is satellite laser ranging. This method uses pulses of laser light emitted from a ground station and bounced off a satellite to compute the range from a measurement of the round-trip time.

As an alternative to visible light, radio waves can be used to track satellites as well. RADAR tracking systems rely on the same method as described above, but using radio waves. In addition, radio waves emitted by the satellite itself can be used to acquire range and range-rate measurements of the satellite. Variations of these methods also include direction measurements in addition to the range and range-rate. Additionally, two-way variants of these methods also exist, requiring active dedicated on-board hardware on the satellites. Another on-board method is to use a GNSS receiver on the satellite. (Wertz and Larson, 2008).

Currently, NORAD is the only provider of publicly available orbital state elements for a wide range of satellites. Supposedly, their orbit determination is performed using a combination of range and range-rate measurements, provided by radar and optical groundstations from the US Space Surveillance Network (SSN). A common rule of thumb for NORAD's TLEs is that their position error at epoch is on the order of 1 kilometer for LEO satellites, but the real error depends on multiple factors, including the shape and orientation of the orbit (pericynthion, 2014; Flohrer, Krag, and Klinkrad, 2008).

Two open-source satellite network projects are TinyGS (*TinyGS* 2025; Galile0, 2025), and SatNOGS (*SatNOGS* 2025), which both operate in same VHF and UHF bands as the DopTrack project. However, these networks seem to be focused on the decoding of telemetry signals instead of orbit determination and should therefor not be regarded as tracking networks. Based on publicly available SatNOGS blog posts, members have made multiple attempts at extracting Doppler curves from the data of the SatNOGS network in order to perform orbit determination, but the exact status of these attempts is not publicly known (*Orbit Determination from SatNOGS data - SatNOGS* 2024; Janes, 2019; *SOCIS 2019* 2019).

1.3. The DopTrack Project

At the time of writing, the DopTrack project consists of a single groundstation located at the satellite and orbital mechanics laboratory of the Delft University of Technology. The station is equipped with two eggbeater antenna's that are placed at the roof of the Aerospace Engineering faculty building. One of them is optimized to receive VHF frequencies, while the other is optimized to receive UHF frequencies. Both are connected to a low-noise amplifier to boost the signal. The roof also hosts a GPS antenna to receive GPS signals. The antenna cables then go into the lab, where the VHF and UHF antenna outputs feed into into an antenna selector, of which the output goes into an Aor AOR5001DX radio. The radio tunes to the correct frequency and sends the still analog signals to a Ettus Research USRP N210 Software Defined Radio (SDR), which then samples the signal at the desired sampling rate and then digitizes the signal samples before sending them to the host computer. The antenna cable of the GPS antenna feeds into a spectracom Epsilon EC20S GPS clock. This GPS clock is used to provide both a stable reference frequency to the radio and SDR, as well as a 1 pulse-per-second (1PPS) signal to synchronize the SDR and computer in time. Figure 1.1 shows a schematic drawing of this hardware setup.

Works by González Martínez (2017) and Søndergaard (2018) investigated the performance of the setup described above. The former focused on the orbit estimation capabilities and limitations of the system, when comparing DopTrack data with TLE. It found that perturbations on the initial guess bigger than 1 km and 0.5 m/s tend to lead to poor convergence of the estimation, and provided suggestions for the a priori orbital state and measurement error uncertainties. The latter focused on analyzing the range-rate performance of the system and the different error contributions to the residuals when comparing the observations to expectations based on TLE.

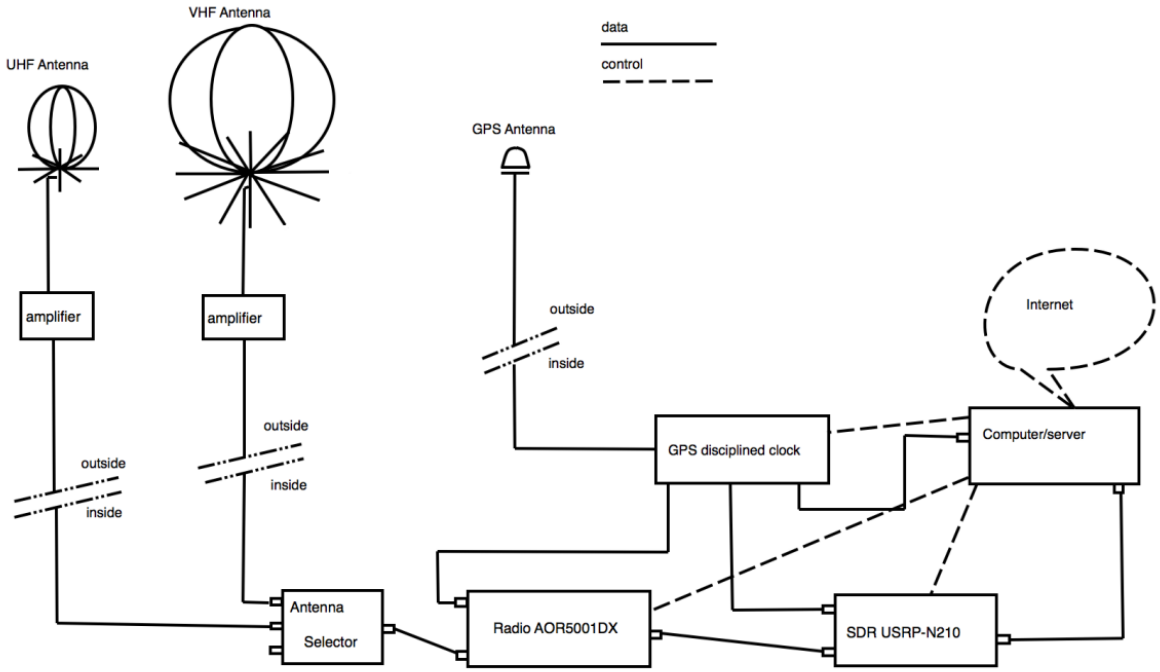

Figure 1.1: A schematic drawing of the DopTrack hardware setup (Root et al., n.d.).

1.4. The DopTrackBox Concept

As the goal of the DopTrackBox concept is to be a more cost effective solution than the Delft DopTrack station, there are a few possibilities of how the DopTrackBox concept could differ from the Delft DopTrack station. One is to not have a separate radio between the antenna and the SDR, but instead let the tuning be done by the SDR as well. Another option is to have an SDR that might be stable enough eliminate the need of an external reference clock if an alternative way to synchronize the sample time exists. The last option is to use cheaper components that still provide enough performance to meet the requirements. In the work of Sprenkels (2023), an alternative and cheaper SDR and GPS radio have been investigated. These are respectively the SDRPlay RSPduo and Leo Bodnar mini-GPS clock. It was found that although these components should together be capable enough to satisfy the requirements, in practice this expected performance was not achieved.

In the DopTrackBox concept investigated by Sprenkels (2023), the host computer was first represented by a Raspberry Pi3B computer, but it was found that it did not have sufficient data processing capacity to successfully record satellite passes consistently. Therefore, for this thesis, the Raspberry Pi3B has

been replaced by a Compulab Fitlet3 Atom x6425E computer as default for operating the DopTrackBox and taking measurements with its components.

With respect to the work of Sprenkels (2023), the scope and goals of DopTrackBox have been slightly altered. Primarily, the focus on the portability aspect has been removed. The consequences of this are that for the purposes of this thesis it is assumed that power and Ethernet will be available. In addition, the directional Yagi antenna is switched for a mostly omnidirectional eggbeater antenna. This removes the need for a person to manually point the antenna or an antenna rotator.

1.5. Research Questions

In order to achieve the goal of the DopTrackBox project, there are several open questions that this thesis aims to answer. These questions have been split into researchable questions covering topics from hard-ware selection and physical design to real-world performance.

1.5.1. Hardware selection

In order to obtain accurate orbit estimates, the Doppler range-rate measurements need to be as low-noise as possible. Therefore, the first question is:

1. "Is the current Leo Bodnar mini-GPS and SDRplay RSPduo combination capable enough to compete with NORAD?"

Because earlier work did not find that the Leo Bodnar mini-GPS clock led to less noisy range-rate measurements, even though theoretically it should have, more investigation is needed to address if these sufficient to reach the desired performance requirements. Therefore, the two subquestions to be answered are:

1A. "Is the Leo Bodnar mini-GPS clock output sufficiently stable for the desired range-range accuracy?"

1B. "Is the frequency stability of the SDRplay RSPduo sufficient for the desired range-rate accuracy when using the Leo Bodnar mini-GPS clock as an external reference clock?"

Earlier work used an interface circuit between this clock and the SDR to remove the DC offset of the Leo Bodnar mini-GPS clock and make the signal more stable. According to the SDR manufacturer this is not strictly needed for this model (*External Reference Clocks* 2020), thus the next subquestion is:

1C. "How does the use of an interface circuit after the output of the Leo Bodnar mini-GPS clock influence its output frequency stability?"

To achieve an orbit solution that is as accurate as possible, not only low-noise range-rate measurements are needed, but also the time of recording of these measurements needs to be known with as high precision as possible. Expensive SDRs such as the Ettus Research USRP products used in DopTrack have software support to time synchronization of samples using GNSS time and an accompanying 1 Pulse Per Second (1PPS) signal (*USRP Hardware Driver and USRP Manual: Device Synchronization* 2025), but cheaper SDRs such as the SDRplay RSPduo do not have these capabilities. Preliminary tests showed that there can be more than a second between a commanded start of recording and the samples being taken with the RSPduo. To find out if the RSPduo is capable of achieving the desired orbit estimation accuracy, the following research question will be investigated:

1D. "What sample timing accuracy is required to achieve the desired orbit estimation accuracy?"

Although the RSPduo is currently the primary option to use as SDR, the results from question 1B and 1D could show that it is not capable enough to satisfy the requirements. Work by Csete and Christiansen (2020) showed that the RSPduo should be the best low-price SDR usage as a satellite ground station, so in that case the second option is to use a much more expensive Ettus Research USRP N210, which is currently in use in the DopTrack station. To characterize the performance of that potential alternative design, the following research question will be investigated:

1E. "What is the frequency stability of the Ettus Research USRP N210 when using the Leo Bodnar mini-GPS as an external reference clock?"

1.5.2. Physical design

The current design specifies potential components of the setup, but does not provide a design for the physical layout and form factor of the setup. Therefore, a design should be made that ideally provides the station with a compact placement of components, while also being compliant with requirements regarding factors such as temperature stability, weatherproofing, and electromagnetic coupling between the components. This question is encompassed by the second research question:

2. "What is the best physical design for DopTrackBox that satisfies the environmental and performance constraints?"

To answer this question, it must first be investigated what environments DopTrackBox will encounter and what the resulting constraints are. Therefore, the first subquestion is:

2A. "What are the environmental constraints the DopTrackBox must be capable of enduring for continuous operations?"

Various people have reported that fluctuating temperatures influence the stability of the Leo Bodnar GPS clock oscillator significantly (*Question about the Bodnar mini GPSDO unit* 2025; *Another question about the Bodnar Mini GPS Unit* 2025). As the Fitlet3 computer can generate significant heat, it is important to investigate how much the temperature fluctuates and how that influences the stability of the GPS clock. Therefore, the following subquestion will be investigated:

2B. "Is passive temperature control of the box sufficient to satisfy the frequency stability requirements?"

As DopTrackBox should be capable of operating in the outside environment for extended periods of time, a box will be acquired or designed to make the setup resilient against different weather conditions. Therefore, the following research question will be investigated:

2C. "What box design makes DopTrackBox compliant with weather requirements?"

1.5.3. Improved Design Performance

After answering the research questions discussed before, a new refined DopTrackBox design should emerge that satisfies the requirements and is ready to be copied. To verify compliance with the requirements and find the performance limits of the setup, the refined DopTrackBox setup will be put under test to evaluate the research question:

3. "What is the performance of the refined DopTrackBox setup?"

To concretize this research question, it is split into two subquestions related to the two performance requirements that have a direct impact on the signal extraction and orbit determination capabilities of

the network: the signal-to-noise ratio and the range-rate error. The subquestions that characterize the DopTrackBox performance are therefore:

3A. "What is the minimum signal-to-noise ratio measured by the refined DopTrackBox setup for elevations above 20 degrees during a satellite pass?"

3B. "What is the time bias of the DopTrackBox system?"

1.6. Structure of the Report

After defining the context of the research and presenting the questions aimed to be answered in this thesis in Chapter 1, Chapter 2 will provide more background information for the project by discussing the key physical principles, used in the thesis, a more in depth explanation of the hardware used to track satellites in this thesis, and an oversight of the expected operational environments and measures to shield DopTrackBox against it.
Then, in Chapter 3, to account for changes in project scope, the project requirements established by earlier work are evaluated and updated to provide a new baseline for the capabilities and constraints that DopTrackBox should satisfy. This is followed by Chapter 4, in which the methods are discussed that have been used to verify DopTrackBox's satisfaction of these requirements.
Chapter 5 presents the results of these experiments, followed by Chapter 6 which provides an interpretation of these results and discusses the limitations of the analyzes presented in this thesis.
Lastly, Chapter 7 provides the conclusions of this project by tying back to the research questions and project requirements, and gives recommendations for future investigations and an improved DopTrackBox design.

2

Theoretical Background

This chapter presents the theoretical foundation on which the analysis of this thesis is based. It starts by presenting the main physical principles used for the Doppler tracking of satellite orbits in Section 2.1. This is followed by Section 2.2 in which a more in-depth exposition of the satellite tracking hardware is presented. Lastly, Section 2.3 studies the expected environments in which the system should be operable and the possible ways in which this could be achieved.

2.1. Physical Principles

This Section presents an introduction into radio waves in Subsection 2.1.1, followed by its application to Doppler tracking in Subsection 2.1.2. The section concludes with Subsection 2.1.3 about satellite orbits and state representations of these orbits.

2.1.1. Radio waves

Radio waves are electromagnetic waves with a frequency between 10kHz and 100GHz (ITU, 2024). Because electromagnetic waves travel at the speed of light, c, these characteristic frequencies can be expressed as a wavelength using the relation $c = f \cdot \lambda$, where f is the frequency of waves and λ the wavelength. As a result, the characteristic wavelengths of radio waves range from about 100km to about 0.1mm. This range is divided into 12 bands that each span one order of magnitude and in frequency and wavelength, and contain various civil, scientific, and military applications. This thesis focuses on the VHF and UHF bands, which both contain sub-bands reserved for amateur radio applications, including amateur radio satellites. These typically operate at the 145 MHz (VHF) and 435 MHz (UHF) bands, which are often also referred to as the 2 meter and 70 centimeter amateur bands respectively.

Although the speed of light in a vacuum is constant, in a medium the propagation speed depends on the refractive index of the medium, which is influenced by factors such as molecular composition, pressure and temperature of the medium (ITU-R, 2016). As a result, radio waves are refracted when traveling through the atmosphere, leading to a curved path between the a transmitter and an observer that is always longer than the direct line-of-sight path between them. Because of this and the fact that the

speed of light is slower in a medium, radio waves that travel through a medium arrive at an observer with a delay compared to when the wave would travel in a vacuum.

2.1.2. Doppler tracking

The physical principle that Doppler tracking utilizes is the Doppler effect: an effect that alters the observed frequency and wavelength of a wave when there is a non-zero relative velocity in the line-of-sight direction between the transmitter and the observer. In daily life, this effect is most commonly known as the effect that causes an ambulance to have a higher pitch when approaching you, shifting to a lower pitch when moving away from you.

As the velocity of satellites is small with respect to the speed of light, for all intents and purposes of this thesis the Lorentz gamma factor can be assumed to be equal to 1, meaning that any relativistic Doppler effects can be neglected. In that case, the ratio of the observed frequency f_r and transmitted frequency f_t is simply given by the equation

$$\frac{f_r}{f_t} = 1 - \frac{\Delta v}{c}, \tag{2.1}$$

where Δv is the relative velocity between the transmitter and the observer along their line of sight direction, and c is the speed of light (González Martínez, 2017). In Doppler tracking, this relative velocity along the line of sight direction is often called the range-rate, $\dot{\rho}$.

When a low Earth orbit satellite passes over an observing groundstation, the observed frequency will exhibit a distinct S-shape curve as a function of time. An example of this S-curve shape is shown in Figure 2.1. The mid-point of this S-curve is the point at which the satellite moves exactly parallel to the observer, which means that the satellite is at its closest to the observer and the observed frequency is equal to the transmitted frequency. So by measuring the observed frequency as a function of time during a satellite pass, the transmitted frequency can be deduced. Together with the observed frequencies themselves the range-rate can then be computed as a function of time using equation 2.1.

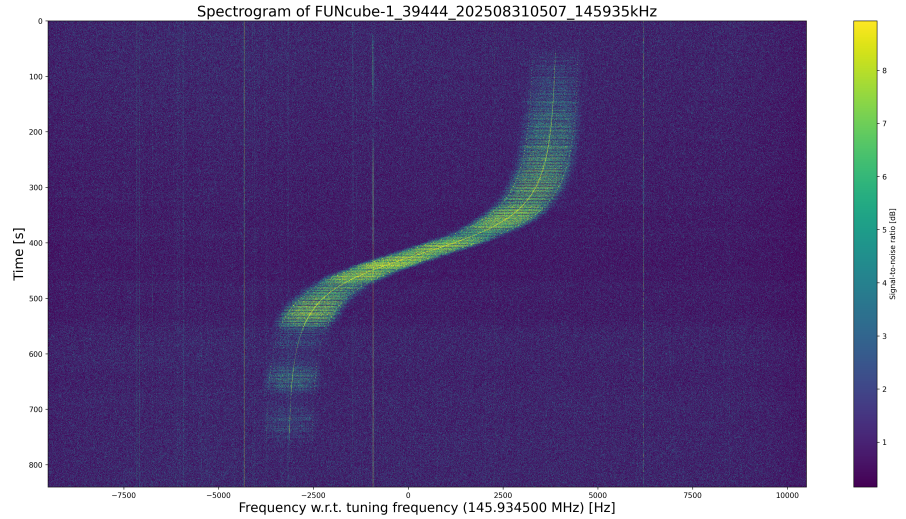

Figure 2.1: A spectrogram of a satellite pass recorded by DopTrack, showing the distinct S-shape in the frequency due to the Doppler effect.

2.1.3. Orbital Mechanics & States

When approximating the Earth as having a spherical mass distribution and assuming no forces other than gravity are acting on a satellite, its orbit around the Earth will follow a perfectly elliptical path with the Earth in one of the focal points. A common way to describe the shape and orientation of this ellipse around the Earth and the satellite's location along the ellipse is using Kepler elements. Figures 2.2 and 2.3 show the physical representation of five of the six Kepler elements, with the eccentricity missing, but defined as $e = \sqrt{1 - \frac{a^2}{b^2}}$, where a and b are the semi-major and semi-minor axes respectively.

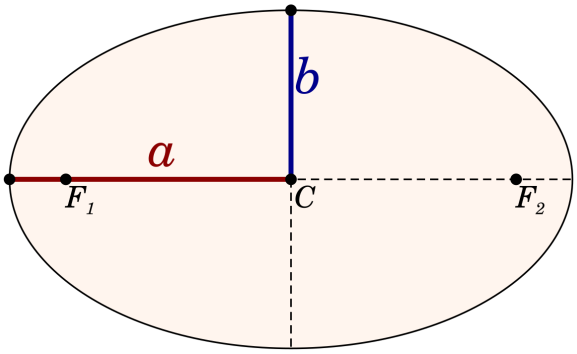

Figure 2.2: An ellipse with with focal points F_1 and F_2, semi-major axis a, semi-minor axis b (*Semi-major and semi-minor axes* 2025).

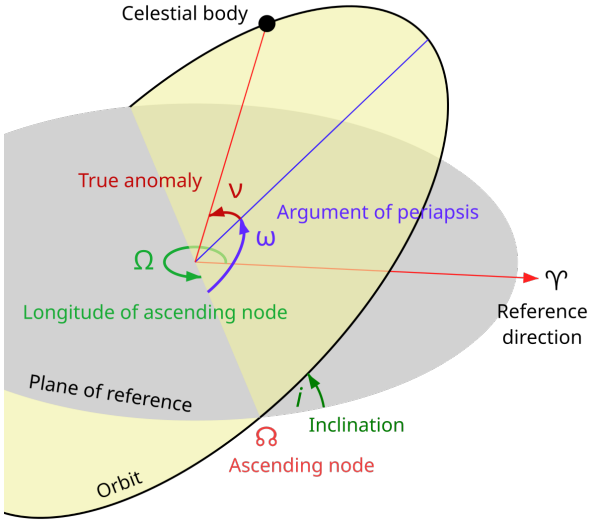

Figure 2.3: A depiction of the classical Kepler Elements describing the orientation of the orbital plane (*Orbital elements* 2025).

The benefit of using Kepler elements over Cartesian states is that if the assumptions above hold, the true anomaly would be the only element that changes over time which allows for a simpler propagation of the state, and a more intuitive understanding of the orbit. But when computing the estimation error of an orbital state it can still be useful to look at the Cartesian elements instead of Kepler elements.

In reality, the Earth does not have a perfectly spherical mass distribution and real satellites also experience forces from atmospheric drag, solar radiation pressure and gravitational third bodies. As a result, the orbits of satellites are not perfect Kepler orbits, but the Kepler elements can still be used to

describe the orbit at a certain epoch. The perturbations will be visible as oscillations and drifts of the Kepler elements. As some of these oscillations average out over a single or multiple orbits, NORAD TLEs contain mean orbital elements, whose exact definition is not in the public domain and should only be propagated using the corresponding SGP4 models (Harding, 2019).

SGP4 is often used as a general collective term for five different models, which SGP4 is only one from. Three of the five models are simplified general perturbation (SGP) models that contain, as the name suggests, predictive models of the the perturbing effects of the Earth's shape, atmospheric drag, solar radiation pressure, and gravitational perturbations causes by third bodies. The other two models are simplified deep space perturbation (SDP) models, used for satellites with orbits with period longer than 225 minutes.

2.2. Tracking Hardware

After being familiar with the physical principles used in the Doppler tracking of satellites, this section delves into the hardware used to perform this Doppler tracking in this thesis. Section 2.2.1 first covers the workings of the SDRs examined in this thesis, followed by an exposition on oscillators, clocks and their stability in Section 2.2.2. Section 2.2.3 then covers the theory used to express the stability of the aforementioned components.

2.2.1. Software Defined Radio

A Software Defined Radio (SDR) is a radio in which some components that historically used to be analog have been replaced by software, by first sampling the analog signal into a digital signal. As a result, SDRs are much more flexible and versatile than conventional radios and can handle various communication protocols with the same device (Akeela and Dezfouli, 2018). The drawbacks of SDRs is that they typically have a poorer dynamic range and higher power consumption then conventional radios that would be designed for the same specific task (Chadwick, n.d.).

Figure 2.4 shows the typical components of an SDR. From the antenna, analog signals first go to an amplifier to increase the signal strength, as a significant part of the noise in the final digital signal will originate from the SDR components themselves. Amplifying the signal beforehand will thus boost the signal-to-noise ratio of the output. The analog signal then goes to a tuner, which selects the frequency around which the signals are to be measured and typically shifts the signal to an intermediate frequency (IF). The Analog-to-Digital Converter (ADC) then samples the resulting analog IF signal into a digital signal. The digital output then feeds into a mixer, which mixes the now digital signal with a reference frequency provided by a local oscillator to shift the signals to a lower frequency range centered around zero. After this, the signal is filtered further using a low-pass filter, before it is ready to be processed.

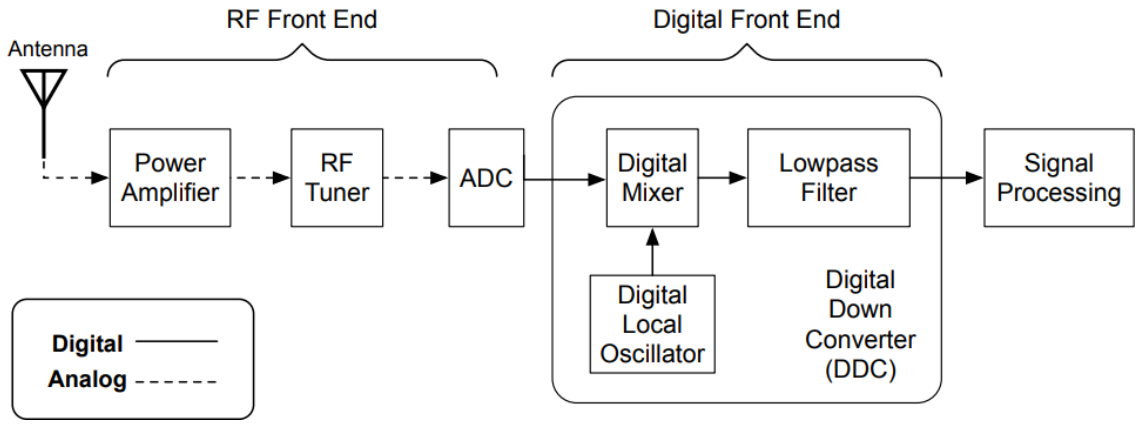

Figure 2.4: A schematic of a typical SDR (Akeela and Dezfouli, 2018).

Figure 2.5 shows a simplified diagram of the SDRPlay RSPduo. Instead of having a single tuner, it has two antenna inputs and tuners, enabling the device to tune to two completely different frequencies simultaneously, for example, one at VHF and one at UHF. This can only be done if the tuners are operated in a ”low-IF” mode with a maximum bandwidth of 2 MHz, instead of a maximum bandwidth of 10 MHz in ”zero-IF” mode (*Introduction to the RSPduo* n.d.). However, this limited bandwidth would be sufficient to capture the satellite signals of interest. In that case, the analog signals from each tuner are converted to digital by their own ADC in the MSI2500 block.

As a local oscillator is used during the selection and shifting of the measured signals, the frequency stability of this local oscillator has a direct impact on the frequency stability of the measured signals. To provide an option to improve this stability for applications that demand it, the RSPduo features a connection for an external oscillator. In a similar way, the Ettus Research USRP features a similar option to connect an external oscillator.

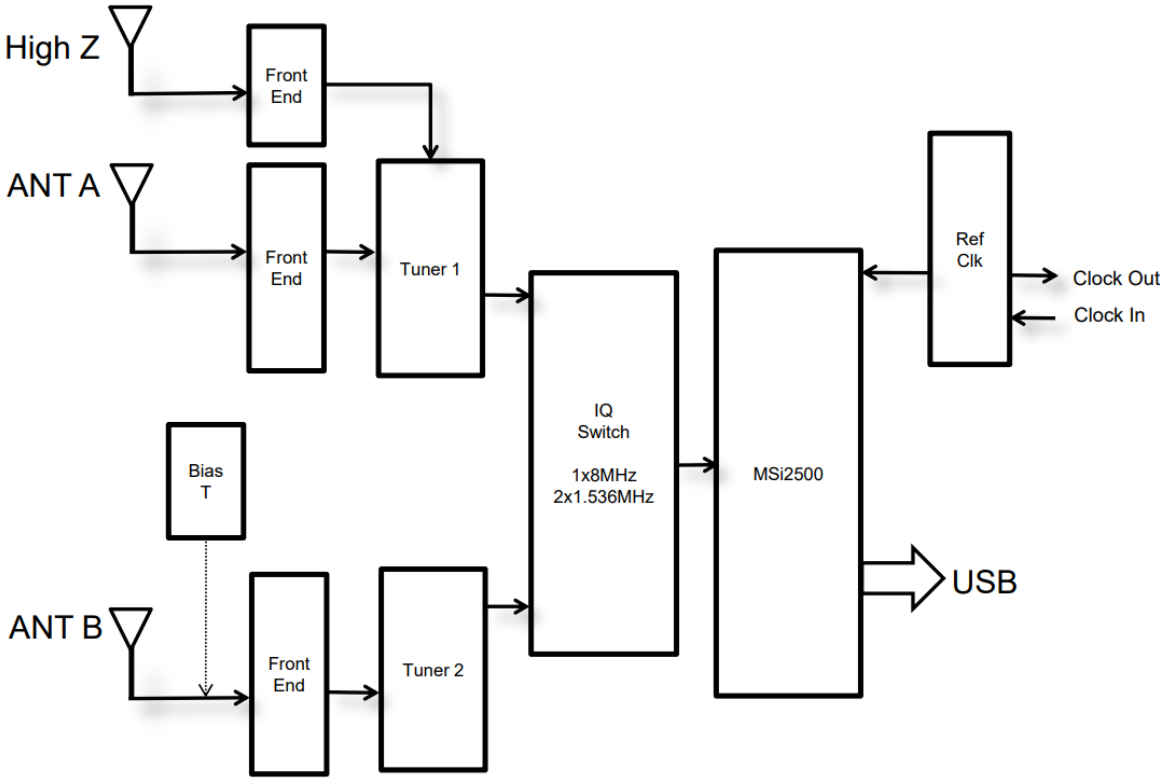

Figure 2.5: Schematic drawing of the SDRPlay RSPduo (*Introduction to the RSPduo* n.d.)

2.2.2. Oscillators, Clocks and Stability

Modern digital electronics are built on the foundation of gate combinations that are synchronized on a clock cycle. To generate such a clock cycle, one needs a signal that oscillates at a regular interval. To achieve this, electronic oscillators are used. At the same time, oscillators are also used to provide stable reference frequencies for electronic equipment such as radios, as described in section 2.2.1. Although the term ”oscillator” or ”reference signal” and ”clock” are often used interchangeably, some literature explicitly refers to clocks as being able to generate multiple different output frequencies, while an oscillator only produces one. In the same way, oscillators typically output a sine wave, while clocks often output a square wave, sawtooth or triangular wave, but this definition is not always enforced.

Electronic oscillators can be divided into roughly two categories based on the principle used to achieve oscillation: harmonic oscillators and relaxation oscillators. The former can be further divided into tuned oscillator circuits, RC oscillators, crystal oscillators and negative resistance oscillators (Garg, Dixit, and Yadav, 2008). The tuned oscillator circuits, RC oscillators and crystal oscillators have in common that the oscillation is induced by a feedback loop in the circuit. While tuned oscillator circuits are typically used for older analog tuners, modern reference frequencies and clocks are typically generated using crystal oscillator circuits.

The crystal oscillator uses the mechanical resonance of a vibrating crystal to generate a stable frequency: When an electric field is applied to a certain crystals, the (inverse-)piezoelectric effect deforms it. When this electric field is no longer present, the crystal relaxes to its original shape while generating its own electric field. If it is placed in a feedback loop with an amplifier this could result in a resonance,

leading to an output signal that oscillates at a theoretically constant frequency (Vig, 1997).

However, the resonance frequency of a crystal changes with temperature. As a result, the frequency will drift when the crystal heats up or cools down. To mitigate this effect, more advanced crystal oscillator circuits have been invented.

The first example of this is a Temperature Compensated Crystal Oscillator (TCXO). It utilizes a temperature sensor to measure the change in temperature and apply a correction voltage using a compensation network to pull the crystal to its nominal frequency. The second is an Oven-Controlled Crystal Oscillator (OCXO). This type has the crystal kept inside an oven to regulate the temperature of the crystal, preventing changes in temperature instead of correcting for it. These OCXOs typically have a more stable frequency than TCXOs (Vig, 1997). The SDRPlay RSPduo and Ettus Research USRP N210, investigated in this thesis, both utilize a TCXO as an internal local oscillator by default.

In addition to temperature fluctuations, there are several other factors that lead to noise and instability of the signal's frequency. The most important long-term effect is the "aging" of the crystal: Over time, the crystal moves and deforms slightly, which causes the resonance frequency of the crystal to change, leading to a frequency drift. In the short term, random vibrations of the crystal and thermal noise in both the crystal and oscillation circuit are dominant contributions.

For applications that need even higher stability, especially over long periods of time, atomic clocks are used. These utilize the fixed energy transition frequency of Rubidium or Cesium atoms in a feedback loop to discipline a quartz crystal oscillator, leading to a much more stable output frequency.

In order to synchronize such oscillators to an absolute time, oscillators are sometimes combined with GNSS receivers. The time information provided by the GNSS receiver can also discipline the local oscillator, leading to a long-term stability that approaches that of the atomic clocks on board of the GNSS satellites. Such devices are called a GPS clock or a GPS disciplined oscillator (GPSDO).

The stability of an oscillator signal is typically expressed as a dimensionless fraction of the original frequency, using the equation

$$y = \frac{\delta f}{f_0}, \tag{2.2}$$

where y is the dimensionless stability, δf the size of the fluctuations, and f_0 the nominal oscillator frequency. Alternatively, some literature express the stability in Parts Per Million (PPM) or Parts Per Billion (PPB), by multiplying the dimensionless stability with 10^6 or 10^9 respectively. Table 2.1 shows the typical stability of the oscillators discussed in this section, according to Vig (1997).

Oscillator Type	**Stability [-]**
TCXO	1×10^{-9}
OCXO	1×10^{-12}
Rubdium	3×10^{-12}
Cesium	5×10^{-11}

Table 2.1: Typical oscillator stability for an averaging time of one second, assuming constant environmental conditions. Values obtained from Vig (1997).

But as different noise sources are dominant at different timescales, it is often not sufficient to express the frequency stability as single constant, but needs to be expressed as a function of the averaging

time over which it is measured, called τ.

2.2.3. Allan Deviation

To quantify the frequency stability over different averaging periods, different mathematical quantities have been invented, each with their own characteristics. The first such quantity that was widely adopted is the Allan deviation, named after the inventor of its concept, David W. Allan (Allan, 1966). The value of the Allan deviation corresponding to a certain averaging time τ can be interpreted as the expected standard deviation of the difference in frequency between two measurements taken a time τ apart from each other. In order to compute the Allan deviation, one needs to measure the phase difference, x, or fractional frequency error, y, of a signal with respect to a reference signal that is known to have a higher stability. From a set of N measured phases at a measurement interval τ_0, the Allan variance of the fractional frequency error, $\sigma_y^2(\tau)$, can then be computed as

$$\sigma_y^2(\tau) = \frac{1}{2(N-2)\tau^2} \sum_{i=1}^{N-2} [x_{i+2} - 2x_{i+1} + x_i]^2, \tag{2.3}$$

where x_i is the ith phase measurement (Riley and Riley, 2008). From this, the Allan Deviation can be computed as

$$\sigma_y(\tau) = \sqrt{\sigma_y^2(\tau)}, \tag{2.4}$$

and is a measure of the expected dimensionless frequency stability y from equation 2.2 for a specific averaging period τ.

To improve the uncertainty on the Allan Deviation for the same dataset, the overlapping Allan deviation was invented. Instead of using only consecutive intervals of samples τ apart, the overlapping Allan Deviation uses all possible intervals with samples that are spaced τ apart to increase the number of samples used in the computation Riley and Riley, 2008. As a result, the measurement intervals will overlap, hence the name of the overlapping Allan deviation. Similar to the Allan deviation itself, the overlapping Allan deviation needs to be computed from its variance counterpart, which is defined as:

$$\sigma_y^2(\tau) = \frac{1}{2(N-2m)\tau^2} \sum_{i=1}^{N-2m} [x_{i+2m} - 2x_{i+m} + x_i]^2, \tag{2.5}$$

where m is called the averaging factor, which defines the number of samples that an interval spans and is defined as $\frac{\tau}{\tau_0}$. The overlapping Allan deviation can then be computed from the overlapping Allan variance using equation 2.4.

Examples of other quantities that are used as a measure of stability and improve in various aspects with respect to the Allan Deviation are the Modified Allan Deviation, time variance, Hadamard Deviation and Total Deviation, but the goal of these methods is to better distinguish different noise types and reduce the sensitivity to certain effects, neither of which are relevant for the purpose of the stability measurement in this thesis.

2.3. Environment & Physical Design

When operating in an outside environment, the system will encounter different environmental effects, depending on its location. This section investigates the expected environmental effects and potential ways to mitigate these effects.

2.3.1. Expected Environments

Before a design for the system could be made, the expected environmental factors at potential DopTrackBox locations needed to be investigated. The current DopTrack setup is located in Delft, The Netherlands, so to test and compare the system with DopTrack, the prototype was operated here as well. A first remote test location considered for this project is Zambujeira, Portugal. Additional DopTrackBox locations are taken from the work of González Martínez (2017) and represent locations that host a Technical University and are separated around the world with minimal overlap. The typical minimum and maximum temperatures during the coldest and hottest months of the year, together with the absolute minimum and maximum are shown for each of these locations in Table 2.2.

Location	Closest data city	Absolute minimum [°C]	Typical minimum [°C]	Typical maximum [°C]	Absolute maximum [°C]
Delft, The Netherlands	The Hague	-17.5	-5.5	30.0	35.5
Zambujeira, Portugal	Faro	1.0	3.5	36.0	44.4
Las Palmas de Gran Canaria, Spain	Gran Canaria	9.4	12.0	33.0	39.0
Astana, Kazakhstan	Astana	-42.0	-31.5	35.0	40.1
Khartoum, Sudan	Khartoum	-	11.0	45.5	-
Johannesburg, South Africa	Johannesburg	-	-2.5	30.5	-
Mumbai, India	Mumbai	8.5	12.5	39.0	42.0
Kuala Lumpur, Malaysia	Kuala Lumpur	-	22.0	36.0	-
Shanghai, China	Shanghai	-8.0	-3.0	38.0	42.0
Sydney, Australia	Sydney	3.0	5.0	38.0	46.0
Paramaribo, Suriname	Cayenne, French Guiana	18.6	21.0	34.0	35.2
Lima, Peru	Lima	11.5	14.0	30.0	33.0
São Paolo, Brazil	São Paolo	-	8.0	33.5	-
Punta Arenas, Chile	Punta Arenas	-14.2	-7.5	21.5	28.0
Reykjavik, Iceland	Reykjavik	-15.0	-10.0	19.5	25.7
Princeton, USA	Philadelphia	-20.6	-12.5	36.5	40.6
Burnaby, Canada	Vancouver	-15.2	-6.5	28.0	34.4
Mexico-city, Mexico	Mexico-city	-2.0	1.5	30.0	33.0
Honolulu, USA	Honolulu	11.7	15.5	33.0	35.0

Table 2.2: Typical and absolute minimum and maximum temperatures at a variety of potential DopTrackBox locations. Data extracted from the closest city to the potential location using (*Climates to Travel - world climate guide* 2025).

Although the occurrences and intensity of precipitation and lightning differ from one location to another, all locations on Earth experience these weather phenomena. Therefore, the box should be protected against these phenomena as well.

2.3.2. Weatherproofing

The most important task of an enclosure for the electronics is to protect the contents from the outside environment. One of the biggest factors is protection against rain and dust. Nowadays, standards exists to express the protection against these factors.

Liquids and Solids Ingression

The International Electrotechnical Commission (IEC) has developed a standardized rating system to classify enclosures based on their protection against ingression of foreign objects (IEC, 2013). The system is often referred to as the IP-rating of an enclosure and consists of two numbers. The first number indicates the protection against solid particulate intrusion, and the second against liquid ingression. On rare occasions, the rating also contains a supplementary letter, but its meaning is not relevant for this thesis. The IEC definition of the protection levels for solid particulate and liquid are shown in Tables 2.3 and 2.4 respectively.

First characteristic numeral	Brief Description	Definition
0	Not-protected	-
1	Protected against solid foreign objects of 50 mm Ø and greater	The object probe, sphere of 50 mm Ø, shall not fully penetrate
2	Protected against solid foreign objects of 2,5 mm Ø and greater	The object probe, sphere of 12,5 mm Ø, shall not fully penetrate
3	Protected against solid foreign objects of 1 mm Ø and greater	The object probe, sphere of 2,5 mm Ø, shall not penetrate at all
4	Protected against solid foreign objects of 1 mm Ø and greater	The object probe of 1,0 mm Ø, shall not penetrate at all
5	Dust-protected	Ingress of dust is not totally prevented, but dust shall not penetrate in a quantity to interfere with satisfactory operation of the apparatus or to impair safety
6	Dust-tight	No ingress of dust

Table 2.3: Solid particle intrusion protection definitions (IEC, 2013)

Second characteristic numeral	Brief Description	Definition
0	Non-protected	–
1	Protected against vertically falling water drops	Vertically falling drops shall have no harmful effects
2	Protected against vertically falling water drops when enclosure tilted up to 15°	Vertically falling drops shall have no harmful effects when the enclosure is tilted at any angle up to 15° on either side of the vertical
3	Protected against spraying water	Water sprayed at an angle up to 60° on either side of the vertical shall have no harmful effects
4	Protected against splashing water	Water splashed against the enclosure from any direction shall have no harmful effects
5	Protected against water jets	Water projected in jets against the enclosure from any direction shall have no harmful effects
6	Protected against powerful water jets	Water projected in powerful jets against the enclosure from any direction shall have no harmful effects
7	Protected against the effects of temporary immersion in water	Ingress of water in quantities causing harmful effects shall not be possible when the enclosure is temporarily immersed in water under standardized conditions of pressure and time
8	Protected against the effects of continuous immersion in water	Ingress of water in quantities causing harmful effects shall not be possible when the enclosure is continuously immersed in water under conditions which shall be agreed between manufacturer and user but which are more severe than for numeral 7

Table 2.4: Liquid intrusion protection definitions (IEC, 2013)

For an outdoor enclosure that contains electronics, an IP rating of IP65 is generally considered to provide sufficient protection, but when very heavy rain or flooding is expected, an IP rating of IP67 is recommended (Ames, 2025; Cao, 2025). COTS boxes for outdoor electronics can be roughly divided into the following categories:

- **Junction boxes**: Used to host small electronics or electronic cable connections in an outside environment. They are typically made from plastic, and their prices range from €20 to €150, depending on factors such as build quality, dimensions, and other features such as the presence of pre-made cable glands. The internal mounting of components often either needs to be designed by the customer, or the box comes with with a perforated grid plate to secure the components. The external mounting of these boxes is typically made for wall-mounting.
- **Outdoor cabinets without ventilation**: Typically used for larger electronics that do not generate much heat or are very temperature resilient. They are often made from metal and rely on convection, conduction and radiation of the closed system to lose heat. The prices of these boxes range from about €30 to €200, again depending on build quality, size and the presence of other features.

(a) Junction Box **(b)** Wihout Ventilation **(c)** With Ventilation

Figure 2.6: Visual examples of typical boxes in the ”junction box”, ”outdoor cabinet without ventilation” and ”outdoor cabinet with ventilation” categories.

The internal mounting is typically a mounting plate from sheet metal. The external mounting is typically designed for wall-mounting, and in rare cases also pole mounting.

- **Outdoor cabinets with ventilation**: These are typically used to house larger electronics in a serverrack-like mounting (either horizontally or vertically). As this type of electronics generally produces a lot of heat and can be sensitive to high temperatures, these cabinets have air ventilation sluices on one or more sides. Some rely on natural convection and wind to refresh the air inside the box to reduce the temperature, while others contain fans to aid in cooling. Prices for these boxes typically range from about €300 to €700, depending on the presence of fans and the size of the box. As these boxes tend to be significantly heavier, they are often designed to be placed on a pedestal or wall-mounted, but some of the smaller models also have options to be mounted to a pole.

A visual example of a box in each category is shown in Figure 2.6.

Temperature Control

Although fans can aid in cooling the equipment by enhancing the air convection in the box, this cannot cool the equipment to lower temperatures than the temperature of the air used to cool the equipment. As such, when the air temperature is higher than the maximum tolerable temperatures by the equipment, different methods of cooling need to be used. The options fall in two categories:

- **Thermo-mechanical Heat Pump**: This is the operating principle of many common devices such as refrigerators, but also air-conditioners and ground source heat pumps used to cool and heat buildings. Electrical energy is used to drive a mechanical system that ’pumps’ thermal energy from one location to another, utilizing a refrigeration cycle.
- **Thermo-electric Heat Pump / Peltier Element**: These devices use the Seebeck and Peltier effects to heat or cool two sides of a material when a current is supplied to it. These are less commonly used than thermo-mechanical heat pumps due to their low efficiency and thus higher power consumption to achieve significant cooling. The benefit of these kind of devices is that they contain no moving parts.

Table 2.5 shows the temperature limits of the electronic components considered for DopTrackBox, for as far as they can be retrieved. It must be noted that the Fitlet3 is also available in an ”Extended Temperature” variant and ”Industrial Temperature” variant. These have operational ranges between -20°C and 70°C, and -40°C and 85°C.

Component	**Minimum [°C]**	**Maximum [°C]**
Fitlet3	0	45
Fitlet3 power supply	-	40
RSPduo	-10	60
N210	0	55
LB mini-GPS	0	-
LB LBE-142	0	-
Interface circuit	-	-

Table 2.5: Temperature limits of the hardware components under consideration for DopTrackBox

Lightning Protection

To protect electronics against lightning strikes, a surge protector can be placed between the antenna and the rest of the electronics. However these typically only protect against surges caused by indirect hits. For the work of this thesis the risk was accepted to potentially lose the equipment due to a lightning strike, by not having a surge protector in the setup.

3

Requirements Analysis

In the work of Sprenkels (2023), a set of requirements had been established for the DopTrackBox concept, but with the change in scope that was described in Section 1.4, these requirements need to be revisited. This chapter will therefore first evaluate the established requirements in Section 3.1. Then, in Section 3.2, changes to these requirements and several new requirements are proposed. Lastly, Section 3.3 provides a summary of the dated requirements.

3.1. Current Requirements

The requirements have been split into operational requirements and technical requirements. According to Sprenkels (2023), the operational requirements were derived from the intended goals and functionalities of the system, which were then translated into technical requirements that the hardware and software must achieve. The established operational requirements (DTB-OPS) are given in Table 3.1, and the technical requirements (DTB-TECH) in Table 3.2.

Identifier	Requirement
DTB-OPS-1.01	DTB shall be no larger than 0.45 × 0.30 × 0.10 m
DTB-OPS-1.02	DTB shall include a computer
DTB-OPS-1.03	DTB shall include an SDR
DTB-OPS-1.04	DTB shall include a GPS clock
DTB-OPS-1.05	DTB shall include an antenna
DTB-OPS-1.06	DTB shall include an external data storage medium
DTB-OPS-1.07.1	DTB shall include a system to receive electrical power
DTB-OPS-2.01	DTB shall be able to record automatically scheduled satellite passes
DTB-OPS-2.03	DTB shall be able to operate without active internet connection during satellite passes
DTB-OPS-2.04	DTB shall be able to record satellite passes without crashing
DTB-OPS-2.06.1	DTB shall be able to operate on battery power for at least 60 minutes
DTB-OPS-2.07	DTB shall be able to store satellite data of at least 150 passes
DTB-OPS-2.08	DTB shall be able to record satellite data with a mean SNR of 3.0 dB or higher
DTB-OPS-2.09	DTB shall be able to record satellite data with a RMS range rate difference of 100 m/s or lower
DTB-OPS-2.10	The SNR difference between DTB and DT shall be no smaller than -3 dB
DTB-OPS-2.11	The RMS range rate difference between DTB and DT shall be no larger than 50 m/s

Table 3.1: Initial DopTrackBox operational requirements (Sprenkels, 2023)

Identifier	Requirement
DTB-TECH-1.01.1	The computer shall have at least 1 USB type A port
DTB-TECH-1.02	The computer shall have the capability of connecting to the internet
DTB-TECH-1.04	The computer shall have the means to connect to a Human Interface Device for interaction with the system
DTB-TECH-1.05	The computer shall have a minimum internal storage capacity of 32 GB
DTB-TECH-1.06	The computer shall be able to run Python 3.9 or newer
DTB-TECH-1.07	The computer shall be able to process a data stream of 2 MB/s
DTB-TECH-2.01	The SDR shall have a connection for the antenna
DTB-TECH-2.02	The SDR shall be connected to the computer via a USB type A connection
DTB-TECH-2.03	The SDR shall be capable of receiving VHF signals from 30 to 300 MHz
DTB-TECH-2.05	The SDR shall be capable of sampling at a sample rate of 250 kHz
DTB-TECH-3.01	The GPS clock shall be physically compatible with the rest of the DTB system
DTB-TECH-4.01	The antenna shall be capable of receiving VHF signals from 30 to 300 MHz
DTB-TECH-4.03	The antenna shall be physically compatible with the SDR
DTB-TECH-5.01	The external storage shall not have any moving parts
DTB-TECH-5.02	The external storage shall be connected to the computer via a USB type A connection
DTB-TECH-5.03	The external storage shall have a minimum capacity of 256 GB
DTB-TECH-6.01	The Operating System shall be based on Linux
DTB-TECH-6.02	The recorder software shall be compatible with the SDR
DTB-TECH-7.01	The VM shall be capable of USB passthrough
DTB-TECH-7.02	The VM shall be capable of running a Linux based Operating System
DTB-TECH-7.03	The VM shall have a minimum allocated storage capacity of 32 GB
DTB-TECH-7.04	The VM shall have a minimum allocated RAM capacity of 3 GB

Table 3.2: Initial DopTrackBox technical requirements (Sprenkels, 2023)

3.2. Proposed Modifications

In Section 1.4 it was already established that for this thesis, power and Ethernet will be assumed to be present. As such, requirements *DTB-OPS-2.06.1: "DTB shall be able to operate on battery power for at least 60 minutes"* and *DTB-OPS-2.03: "DTB shall be able to operate without active internet connection during satellite passes"* become meaningless. In the future, these requirements might become relevant again, so they will be kept, but no particular efforts will be made to comply with them during this project. As the portability aspect is no longer a focus of the design, requirement *DTB-OPS-1.01: "DTB shall be no larger than 0.45 × 0.30 × 0.10 m"* should be abolished. This does not mean that a compact form factor might be considered a criterion for a good box, but that the design and choice of components is not restricted by a requirement on the physical dimensions of the system.

Since requirement *DTB-OPS-1.02: "DTB shall include a computer"* exists, in addition to corresponding technical requirements for the computer to make it capable of operating the entire system, there should be no need to run a Virtual Machine anymore. As such, the requirements on the Virtual Machine, DTB-TECH-7.01 till DTB-TECH-7.04 can be removed. In addition, as the exact computer model to use is not specified in the requirements, the usage of an external storage device is not strictly necessary, as an internal storage device might provide sufficient storage. Therefore, it is proposed to remove

requirements *DTB-OPS-1.06: "DTB shall include an external data storage medium"* and *DTB-TECH-5.02: "The external storage shall be connected to the computer via a USB type A connection".* For the same reason, it is proposed to change requirement *DTB-TECH-5.01: "The external storage shall not have any moving parts"* to *"Any data storage medium shall not have any moving parts".*

The size of the needed storage is established in requirement *DTB-TECH-5.03: "The external storage shall have a minimum capacity of 256 GB"*. This number is based on an expected data rate of 1.44 GB per average pass of 12 minutes, and the requirement *DTB-OPS-2.07: "DTB shall be able to store satellite data of at least 150 passes"*. It is not clear what the rationale for 150 passes is, but it is suspected to be based on the ability to record three satellites with five passes per day each, for ten consecutive days in case no internet is available. After ten days, the accuracy of TLEs is too low to make accurate predictions of the passing times, and when no internet is available to retrieve new TLE's that would be a suitable point in time to stop recording passes until internet connection has been restored. To future-proof the concept, in this project it will be assumed that many more satellites will be tracked, with the consequence that the station could be recording almost continuously.

In that case, the data rate would be $24 \cdot \frac{60}{12} \cdot 1.44 \approx 172$ GB per day. One of the variables that dictates this data rate is the sampling rate of the recording. To fully capture the Doppler-shifted signals, a sample rate of about 30 kHz should be sufficient. Yet, DopTrack records at 250 kHz, because the hardware does not support recording at a much lower sampling rate. The RSPduo, the primary candidate SDR intended to be used in DopTrackBox, does support lower sampling rates, with a minimum of 62.5 kHz. Changing the sampling rate to 62.5 kHz would reduce the data rate by a factor of 4 to only 43 GB per day, while maintaining sufficient bandwidth to fully capture the signal even when its frequency drifts over time, as long as the recording frequency is updated regularly. Maintaining the same 10 days limit of continuous recording, the 43 GB per day translates to 432 GB per 10 days. The nearest common storage size that satisfies this minimum is 512 GB, so it is proposed to change requirement *DTB-TECH-5.03* to *"The data storage medium shall have a minimum capacity of 512 GB"*.

Currently there are two requirements related to DopTrackBox's performance with respect to DopTrack. These are requirements *DTB-OPS-2.10: "The SNR difference between DTB and DT shall be no smaller than -3 dB"* and *DTB-OPS-2.11: "The RMS range-rate difference between DTB and DT shall be no larger than 50 m/s"*. These requirements should not be interpreted as a design requirement, but as a guideline to monitor if the stations perform as expected when operated under the same circumstances. However, as the hardware is not identical, in particular the noise level could be significantly different between DopTrack and DopTrackBox, leading to a different signal-to-noise ratio.

As the range-rate difference can only be computed when operating the DopTrack and DopTrackBox stations side by side, it can only be used to monitor the station in the limited case that the DopTrackBox station is next to DopTrack for testing. To make the requirement more suitable to monitor stations over a longer period (even when placed in remote locations), it is proposed to change requirement *DTB-OPS-2.11* to *"The RMS of the range-rate difference over a single pass between DTB and the predicted orbit shall be no larger than 50 m/s."*

In addition to these requirements, there are requirements based on the desired orbit estimation performance of DopTrackBox. One of these is requirement *DTB-OPS-2.08: "DTB shall be able to record satellite data with a mean SNR of 3.0 dB or higher"*. In contrast to the SNR requirement with respect to DopTrack, this requirement actually is a design requirement as it is related to the current approximate

limit for which the processing script can still extract the signal from the sample recordings. However, as the received signal power depends on multiple factors, including the transmitted power of the satellite and its elevation above the horizon during the pass, the current requirement is not specific enough to evaluate. Therefore, it is proposed to change this requirement to *"DTB shall be able to record FUNcube-1 passes with a mean SNR of 3.0 dB or higher when its elevation is above* 20°*."*

Another orbit estimation performance requirement is *DTB-OPS-2.09: "DTB shall be able to record satellite data with a RMS range-rate difference of 100 m/s or lower"* exists, but this project proposes a change for this requirement from 100 m/s RMS error to 5 m/s RMS error in the range-rate based on the following grounds: a rule of thumb about NORAD's TLEs is that their position error at epoch is on the order of 1 kilometer for LEO satellites, but the real error depends on multiple factors, including the shape and orientation of the orbit (pericynthion, 2014; Flohrer, Krag, and Klinkrad, 2008). To compete with this, DopTrackBox should aim for about an order of magnitude lower, which is about 100 meters. As a rule of thumb, the Doppler range-rate error in meters per second should be a factor 20 lower than the position error in meters, which converts to about 5 m/s. Therefore, it is proposed to change *DTB-OPS-2.09* to *"DTB shall be able to record satellite range-rates with a RMS error less than 5 m/s"*. From this requirement, a technical requirement on the performance of the SDR and possible GPS reference clock can be derived: as the range-rate is computed from the change in frequency using the Doppler equation, the required frequency stability can be computed using the same equation when the required range-rate RMS error is known. From Equation 2.1, the RMS range-rate error as a consequence of a frequency stability δf, with respect to the transmitted frequency f_t can be written as:

$$\frac{\delta f}{f_t} = \frac{\delta v}{c}, \tag{3.1}$$

by defining the RMS error as δv and $\delta f = f_c - f_t$ (Reeve, 2020).

As the frequency stability of a signal measured by the SDR is directly related to the frequency of the local oscillator, using this equation, a requirement on the stability of the local oscillator as fraction of the carrier frequency can be found. Using a 5 m/s RMS range-rate requirement, a fractional stability requirement of 1.68×10^{-8} can be found. To keep some margin and stay conservative, the following technical requirement is proposed: *The SDR shall have a fractional frequency stability better than* 10^{-8}*"*. Typically, SDRs have a relatively low stability oscillator, with the option to connect an external reference clock to increase the stability, which is for the proposed DopTrackBox setup the GPS clock. Therefore, the following additional requirement could be added: *"The GPS clock shall provide an output with a fractional frequency stability better than* 10^{-8}*"*. Although requirement *DTB-OPS-1.04: "DTB shall include a GPS clock"* seems to be not strictly necessary, because it seems reasonable that an alternative SDR exists which has an oscillator that is stable enough to not need an external clock to meet the requirement, in practice this is unlikely as GPS disciplining is needed to maintain long-term stability. For sake of clarity, it is proposed to change requirement *DTB-TECH-3.01: "The GPS clock shall be physically compatible with the rest of the DTB system"* to several separate requirements that describe the physical compatibility. These will be: *"The GPS clock shall be capable of producing the reference frequency required by the SDR"*, *"The GPS clock shall be capable of producing the reference signal at the shape, voltage and current required by the SDR"* and *"The GPS clock output shall be capable of being connected physically to the SDR"*.

There are currently a few requirements on the DopTrackBox computer. One of these is *DTB-TECH-1.01.1: "The computer shall have at least 1 USB type A port"*. As the currently proposed GPS clock

needs a USB connection to the computer in order to be configured, as well as the SDR for transfer of data, it is proposed to change this requirement to *"The computer shall have at least 2 USB type A ports"*. In addition, to allow for fully remote operations, the following technical requirement is proposed: *"The computer shall be capable of access via SSH"*. Linked to this, the following operational requirement is proposed: "DTB shall be able to be operated fully remotely after initial setup".

Currently, there are no requirements regarding the Box part of DopTrackBox, apart from the requirement on the dimensions that was proposed to be removed. However, although the portability aspect of DopTrackBox is removed, it is still in scope to place the setup in an outside environment. Therefore, the following operational requirements are proposed: *"DTB shall be operable in an outside environment"* and. To facilitate this, the following technical requirements are proposed: *"DTB shall be dust and waterproof up to at least IP65*, and *"DTB shall be protected against lightning surges"* and *"DTB shall be operational in temperatures between TBD and TBD degrees Celcius"*. Although the dust and waterproofing shall be taken into account during the design in this thesis, the lightning protection shall not be taken into account. Although the temperature behavior of the system will be investigated and temperature control methods are discussed in this thesis, a tradeoff between designing the system to work in any temperature environment versus less environments but with a simpler system without cooling is beyond the scope of this thesis. Therefore, no numerical value on the environmental temperature limit have been set in the updated version of the requirements.

3.3. Updated Requirements

After updating Tables 3.1 abd 3.2 with the proposed modifications, the full set of operational and technical requirements are shown in Tables 3.3 and 3.4 respectively. Compliance of the design developed in this thesis with the requirements will be verified again in Section 7.1.

Identifier	Requirement
DTB-OPS-1.02	DTB shall include a computer
DTB-OPS-1.03	DTB shall include an SDR
DTB-OPS-1.04	DTB shall include a GPS clock
DTB-OPS-1.05	DTB shall include an antenna
DTB-OPS-1.07.1	DTB shall include a system to receive electrical power
DTB-OPS-2.01	DTB shall be able to record automatically scheduled satellite passes
DTB-OPS-2.03	DTB shall be able to operate without active internet connection during satellite passes
DTB-OPS-2.04	DTB shall be able to record satellite passes without crashing
DTB-OPS-2.06.1	DTB shall be able to operate on battery power for at least 60 minutes
DTB-OPS-2.07	DTB shall be able to store satellite data of at least 150 passes
DTB-OPS-2.08.1	DTB shall be able to record FUNcube-1 passes with a mean SNR of 3.0 dB or higher when its elevation is above 20°
DTB-OPS-2.09.1	DTB shall be able to record satellite range-rates with a RMS error less than 5 m/s
DTB-OPS-2.10	The SNR difference between DTB and DT shall be no smaller than -3 dB
DTB-OPS-2.11	The RMS of the range-rate difference over a single pass between DTB and the predicted orbit shall be no larger than 50 m/s
DTB-OPS-2.12	DTB shall be able to be operated fully remotely after initial setup
DTB-OPS-2.13	DTB shall be operable in an outside environment

Table 3.3: Proposed DopTrackBox operational requirements.

Identifier	Requirement
DTB-TECH-1.01.2	The computer shall have at least 2 USB type A ports
DTB-TECH-1.02	The computer shall have the capability of connecting to the internet
DTB-TECH-1.04	The computer shall have the means to connect to a Human Interface Device for interaction with the system
DTB-TECH-1.05	The computer shall have a minimum internal storage capacity of 32 GB
DTB-TECH-1.06	The computer shall be able to run Python 3.9 or newer
DTB-TECH-1.07	The computer shall be able to process a data stream of 2 MB/s
DTB-TECH-1.08	The computer shall be capable of access via SSH
DTB-TECH-2.01	The SDR shall have a connection for the antenna
DTB-TECH-2.02	The SDR shall be connected to the computer via a USB type A connection
DTB-TECH-2.03	The SDR shall be capable of receiving VHF signals from 30 to 300 MHz
DTB-TECH-2.05	The SDR shall be capable of sampling at a sample rate of 250 kHz
DTB-TECH-2.06	The SDR shall be capable of recording with a fractional frequency stability better than 10^{-8}
DTB-TECH-3.02	The GPS clock shall provide an output with a fractional frequency stability better than 10^{-8}
DTB-TECH-3.03	The GPS clock shall be capable of producing the reference frequency required by the SDR
DTB-TECH-3.04	The GPS clock shall be capable of producing the reference signal at the shape, voltage and current required by the SDR
DTB-TECH-3.05	The GPS clock output shall be capable of being connected physically to the SDR
DTB-TECH-4.01	The antenna shall be capable of receiving VHF signals from 30 to 300 MHz
DTB-TECH-4.03	The antenna shall be physically compatible with the SDR
DTB-TECH-5.01.1	Any data storage medium shall not have any moving parts
DTB-TECH-5.03.1	The data storage medium shall have a minimum capacity of 512 GB
DTB-TECH-6.01	The Operating System shall be based on Linux
DTB-TECH-6.02	The recorder software shall be compatible with the SDR
DTB-TECH-7.01	DTB shall be dust and waterproof up to at least IP65
DTB-TECH-7.02	DTB shall be protected against lightning surges
DTB-TECH-7.03	DTB shall be operational in temperatures between TBD and TBD degrees Celcius

Table 3.4: Proposed DopTrackBox technical requirements.

4

Methods

Having established the updated requirements that DopTrackBox should satisfy, this chapter presents the methods used to analyze in what potential hardware configurations DopTrackBox this could be achieved. To this end, Section 4.1 first describes the methods used to analyze the frequency stability of the SDRs and GPS clock. Then, Section 4.2 describes the simulations conducted to study the impact of a time bias in the satellite observations on the accuracy of the orbit estimation. This is followed by Section 4.4, in which the setup is described that was used to study the signal-to-noise ratio and time bias performance of the prototype DopTrackBox system developed during this thesis project. As the results of this analysis depend on the proper functioning of all components of the prototype, Section 5.6 provides a description of the methods used to systematically verify if all system components were working as expected.

4.1. Frequency Stability

Section 3.2 established the range-rate accuracy needed to reach the desired orbit estimation accuracy, and the subsequent requirement on the frequency stability of the SDR and GPS clock. Although Section 2.2.3 already described how the Allan deviation can be used to assess the stability of such devices, as both the GPS clock and the SDR produce an output that is not a phase or frequency error directly, separate methods and techniques are needed to evaluate their stability.

4.1.1. GPS Clock

The Leo Bodnar GPS clocks output a 3.3 V peak-to-peak square wave at a selected frequency f_0. To obtain the phase or frequency error of the output, needed to compute the Allan deviation, the GPS clock was connected to a TinyPFA. This device is a modified Vector Network Analyzer (VNA) that can operate as a phase/frequency analyzer (PFA). This means that it is capable of comparing the outputs of two frequency sources and determining the phase and frequency difference between them. If one of the sources is more stable than the other, the measured phase and frequency difference can be assumed to come from the less stable device. In this experiment, the output of the Leo Bodnar GPS clock was compared against the output of the Spectracom EC20S GPS clock used in the DopTrack

station.

The stability of the EC20S should be better than 3×10^{-11} for averaging periods longer than 1 second, and 3×10^{-12} for averaging periods longer than 100 seconds, while the Leo Bodnars are expected to achieve a similar stability between 5×10^{-11} and 3×10^{-12} (Spectracom, 2018; *Mini Precision GPS Reference Clock : Leo Bodnar Electronics* 2025). Although these values are close to each other, the values for the EC20S are minimum performance values while the values for the Leo Bodnar are actually measured performances by the manufacturer.

When the output of the Leo Bodnar is used as external reference to the RSPduo, the output should be 24 MHz, in this experiment the output frequency is set to 10 MHz. This is needed as the TinyPFA requires the compared frequencies to be as close as possible, and the EC20S is only capable of generating a 10 MHz sine-wave output.

Furthermore, the TinyPFA requires the connected sources to have a power between -20 and 0 dBm, and preferably between -10 and -5 dBm to achieve the best performance (*tinydevices.org | TinyPFA / First Use* 2025). To achieve this, the ECS20 was connected to a 20 dB attenuator, bringing its power level to -4 dBm. Similarly, for the measurements where the Leo Bodnar mini-GPS clock was the device under test, it was connected using a 15 dB attenuator to bring its power to -7 dBm while operating at a configured drive strength of 8 mA. When the Leo Bodnar LBE-1421 was the device under test, a 15 dB attenuator was used to bring the power to -3dBm. For this experiment, the LBE-1421 was configured in ”Phase Locked Loop” (PLL) rather than ”Frequency Locked Loop” (FLL) mode, because as the name suggests, this mode should have a stable phase in addition to a stable frequency.

After connecting the GPS clocks to the TinyPFA, the TinyPFA was configured for taking measurements by ’nulling’ the EC20S frequency, setting the configured output to ”unwrapped phase”, a minimum tau of 0.1 seconds and a decimation of 10. After this, the USB output was enabled and the TinyPFA connected to a Windows laptop running the Timelab software. A schematic overview of the measurement setup is shown in Figure 4.1.

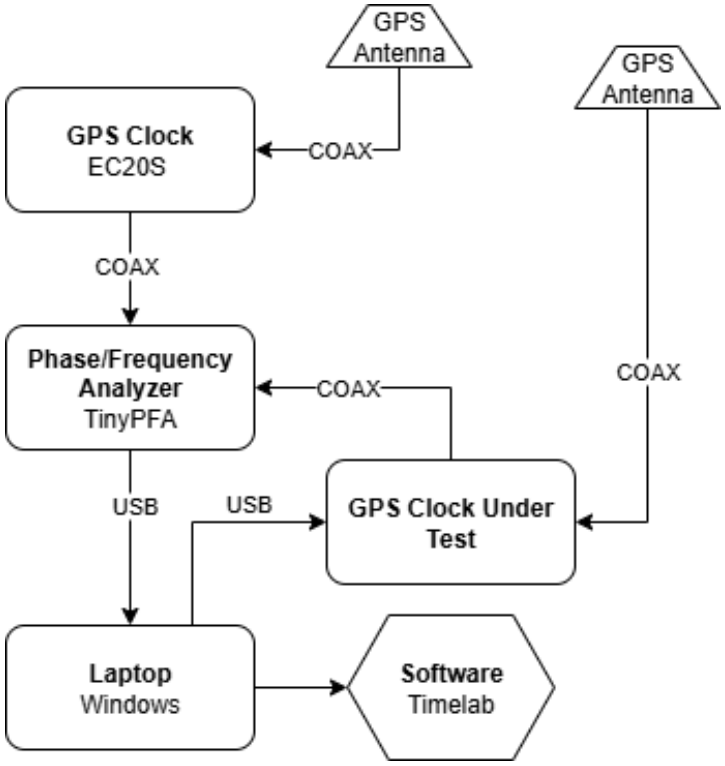

Figure 4.1: Measurement setup to perform Allan Deviation measurements of the Leo Bodnar GPS clocks.

Three phase measurement runs of 1 hour each were taken with each of the two Leo Bodnar GPS clock models in an air-conditioned laboratory environment. Between each of the measurements, a 15 minute break was held to allow the equipment to cool down. For the mini-GPS clock, the second and third runs were performed while the GPS clock was enclosed in a cardboard box in an attempt to limit temperature fluctuations due to duty cycling of the air-conditioning and opening and closing of a door to an unconditioned hallway. For the third run, an experimental 'correct pulling' setting was turned on in the TinyPFA, which attempts to correct for a frequency pulling effect between the inputs that could occur if the frequencies of the connected sources are relatively far apart (*tinydevices.org | TinyPFA / Menu Tree* 2025; Erik Kaashoek, 2023).

The measured phase was then exported in the form of an unwrapped phase, which means that the phase difference is continuous instead of wrapped between 0 and 2π when the difference between the signals is greater than the period of the signal. Using this data, the overlapping Allan deviation was then computed with Equation 2.5 by the Allantools python package. The results of this analysis are presented in Section 5.1.

The range of interest for the stability is constrained by a shorted and longest averaging time of interest. The shortest averaging time of interest is the length of a single Fourier bin in the spectral analysis of satellite data. This is typically 0.5 or 1 second. The longest time is the time of a full satellite pass. A typical pass recording has a maximum duration of 15 minutes, or equivalently approximately 10^3 when rounded to a logarithmic number.

4.1.2. Software Defined Radio

When recording samples using an SDR, the output is often a stream of IQ samples. IQ samples are typically represented by a complex number of which the components are an in-phase (I) and quadrature (Q) component of the received signal. Together, they provide information about both the amplitude and phase of a signal. This means that by providing the antenna input of the SDR with a strong signal with known frequency, the phase difference of the measured signal can be computed with respect to the expected phase, which should be a measure of the stability of the SDR under the assumption that the stability of the input signal is higher than the stability of the SDR. This phase difference can then be converted into an unwrapped phase similar to the previous section needed to compute the overlapping Allan deviation.

The 10 MHz output of the EC20S GPS clock was used as a stable frequency source to measure. As the waveform of this output signal is a sinusoid, the phase of this signal is well defined for all points in time. To not cross the maximum safe continuous power input of the RPSduo (0 dBm) and Basic RX daughterboard of the N210 (+10 dBm), the output of the EC20S was again connected to a 20 dB attenuator to bring its power to -4 dBm.

When the RSPduo was used as device under test, measurements were taken in three configurations: no external reference clock, using the Leo Bodnar mini-GPS as an external reference clock directly, and using the mini-GPS as external reference clock, but through an interface circuit. In each of these configurations, three consecutive measurements of 4000 seconds each have been performed in the air-conditioned lab. Between each of the measurements, a 10 minute break was held to allow for cooling down of the equipment and re-configuration of the electronics. This whole series of measurements has been repeated using a new cable between the Leo Bodnar mini-GPS and SDR, as the original one might have been defective. All measurements with the RSPduo were performed using the Fitlet3 as a host computer, using *rx tools* to record the samples.

In the measurements where the N210 was the device under test, both the Leo Bodnar mini-GPS as well as the LBE-1421 have been used as external reference clock. In addition, the LBE-1421 has been operated in both the FLL mode and PLL mode described in the previous section. In each of these configurations, two measurements have been performed in the air-conditioned lab. The measurements using the LBE-1421 are 4000 seconds each, but due to time constraints the measurements using the mini-GPS are only 3600 seconds each. Between each of the measurements, 10 minutes of break have been kept to allow for cooling down of the equipment and re-configuration of the electronics. Unlike with the RSPduo, the measurements with the N210 could not be performed using the Fitlet3 as measurement device. Attempts at configuring the N210 and recording with it failed numerous times with the Fitlet3, so a Windows laptop was used instead. More details on the error and the troubleshooting steps taken are discussed in Section C.4.4.

A schematic overview of the measurement setup is shown in Figure 4.2.

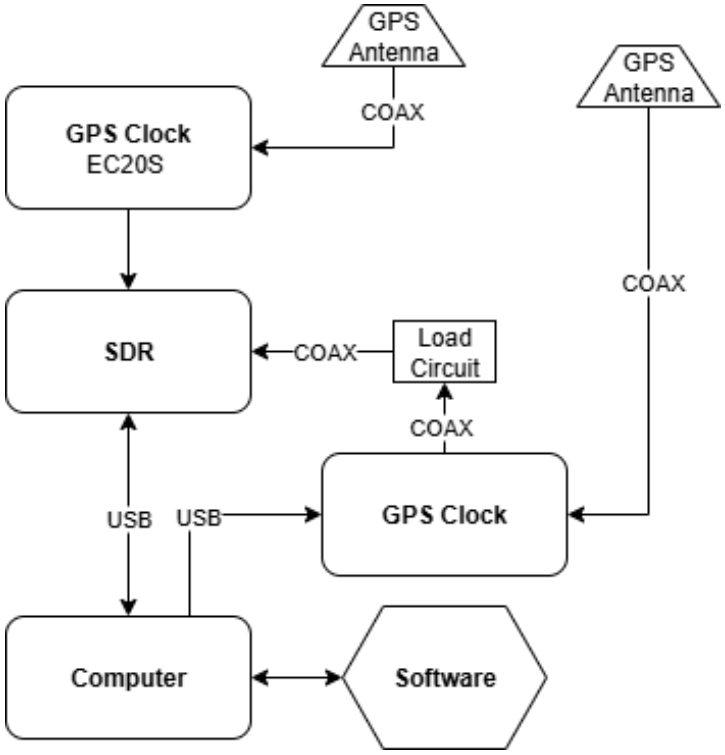

Figure 4.2: Measurement setup to perform Allan Deviation measurements of the SDRs.

To avoid measuring a potential DC-spike instead of the supplied signal, the measurements were performed at an offset-tuning of -5 kHz. The sampling rate was set to $f_s = 62.5$ kHz in the case of the RSPduo, while it was $f_s = 250$ kHz for the N210. After collecting the IQ samples, the measurements were processed by first shifting the IQ samples by -5 kHz to the zero-frequency, because the EC20S signal should be present at +5 kHz with respect to the tuning frequency due to the offset-tuning. This frequency shift was achieved using the equation

$$s' = s \cdot e^{2i\pi f_{\text{shift}}/f_s}, \tag{4.1}$$

where s' is now the shifted IQ signal, and f_{shift} is the size of the frequency shift. The phase of the measured signal with respect to the SDR's oscillator was then computed by converting the complex phase into a phase angle. After this, the phase angle was unwrapped to obtain the continuous phase difference between the SDR and the EC20S. At this stage, the unit of the phase difference is expressed in radians, so to convert it into seconds, the phase was divided by 2π and multiplied by the reciprocal of the 10MHz signal frequency.

After this, the Allantools package was again used to compute the Allan deviation of this unwrapped phase difference. In addition, for each set of two consecutive phase points, the instantaneous frequency was determined by numerically differentiating the phase. The results of this are shown in Section 5.2.

4.2. Observation Time-Bias

To find the impact of a potential time bias in the observed range-rates on the orbit estimation capabilities, simulations have been performed on a hypothetical case-study satellite in a similar orbit to Delfi-C3 in 2020. The orbit is a Low Earth Sun Synchronous orbit of which the orbital parameters are expressed in Kepler elements in Table 4.1.

Parameter	Value
Semi-major Axis [km]	6927.395
Eccentricity [-]	0.00123
Inclination [deg]	97.498
Argument of Perigee [deg]	173.369
Longitude of the Ascending Node [deg]	136.635
True Anomaly [deg]	18.702

Table 4.1: Initial orbit parameters of the simulated satellite at epoch. The angle parameters and semi-major axis have been rounded to thee decimals, and the eccentricity to five.

4.2.1. Observation Simulations

The satellite orbit was propagated for a 6-day period using the TU Delft Astronomy Toolkit (TUDAT) python package. The numerical integrator used to propagate the Cartesian state of satellite is a fixed-step 4th order Runge-Kutta integrator, with a stepsize of 4 seconds. In Appendix A it is shown that this integration scheme should lead to sufficient numerical precision for the purposes of this thesis.

The dynamical model used in the simulations contains a spherical harmonic Earth gravity field with degree and order 2, atmospheric drag, solar radiation pressure, and point mass gravity of the Sun, Moon, Venus, Mars and Jupiter. The satellite properties that influence the resulting forces on the satellite are shown in Table 4.2 and should be representative for a 3U cubesat similar to Delfi-C3.

Parameter	Value
Mass [kg]	2.2
Aerodynamic Drag Area [m^2]	0.035
Drag Coefficient [-]	1.2
Solar Radiation pressure Coefficient [-]	1.2

Table 4.2: Physical parameters of the simulated satellite.

Using the simulated orbit, the observed range-rate at three hypothetical Earth ground station locations were computed using TUDAT: Delft (The Netherlands), Sydney (Australia) and near Sao Paulo (Brazil). The Delft location is chosen as it is home to the current DopTrack setup, and the other locations are chosen as two hypothetical locations from Section 2.3.1, that are far from Delft, and each other. The coordinates of the station locations are shown in Table 4.3.

Location	Latitude [deg]	Longitude [deg]
Delft (The Netherlands)	52.0116	4.3571
Sydney (Australia)	-33.9300	151.2200
Sao Paulo (Brazil)	-23.2000	-45.8500

Table 4.3: Simulated groundstation locations

As the real-world range-rate noise of the DopTrackBox setup is not yet known, a gaussian noise has been applied to the range-rate observations with varying values of $\sigma_n = 0, 0.1, 1$ and 10 m/s. The real

range-rate performance will likely fall within this range, assuming that the requirement of 5 m/s on the range-rate noise will be achieved.

The simulated range-rate observations were then shifted in time on a pass-by-pass basis to simulate a time bias due to inaccurate timestamping of a satellite recording. As the time bias of a real system might not be a constant factor, but have some variability, for each satellite pass, the applied time bias t_b is obtained from a Gaussian distribution with mean μ_b and standard deviation σ_b. A pseudo-observation set has been generated for each combination of values for $\mu \in [0, 0.1, 0.5, 1, 5, 10]$ seconds, and $\sigma \in [0, 0.05, 0.1, 0.5, 1, 5, 10]$ seconds, with the exception of the cases where $\sigma > \mu$. Before applying the randomly drawn time bias, it is clipped at 0, to prevent a time bias that is unphysical.

4.2.2. Orbit & Parameter Estimation

The TUDAT package was then used to perform the estimation using a batch least-squares algorithm. For the estimation, the same dynamical model and integrator were used as for the simulation, except that the fixed timestep was 8 seconds to make the estimation less computationally expensive, while keeping the same dynamical model

Theoretically, all pseudo-observations together could be used to estimate a single orbital state. Generally, the more observations are used, the better the estimated state should become. However, in practice, achieving a converging estimation becomes more difficult the more the observations are spread out in time. As such, the observations were split into separate tracking arcs of different lengths, for which one cartesian state was estimated per arc: one arc per satellite pass, one arc per day, and one arc per three days.

In all estimations, the observation weight was set to $w = \frac{1}{\sigma_n^2}$, except for the case in which $\sigma_n = 0$. In that case, the weight was left at the default value of 1.

To investigate if the effect of a time bias on the observations could be reduced by estimating a per-pass time bias, estimations were performed in such a configuration as well. As the effects of a time bias might be absorbed by estimating the atmospheric drag coefficient (per arc) or a bias on the observed range-rate (per pass), estimations using these parameters were performed as well, including combinations with each other, and an observation time bias simultaneously.

The least squares estimation was terminated when a maximum of 25 iterations had been reached, or more than three iterations occurred in which the residuals changed by less than 0.1 mm/s. It has been empirically observed that the latter led to iterations with typically less than 100 meters of change in the position estimates, while the former ensured that the estimation did not become too computationally expensive for too slowly converging cases.

As an initial guess for the Cartesian states, estimations have been performed where the initial guess was perfect, as well as where a perturbation of 500 m on the position components, and 0.1 m/s on the velocity components had been applied. The initial guess of the range-rate and drag parameters was set to the true values, and for the observation time bias estimations have been performed in which the initial guess was zero, as well as in which it was set to the value of μ_b used to draw the random biases.

In all estimations, the initial covariance matrix consists of all zeroes, with the exception of some of the diagonal components: the components corresponding to the cartesian state were set to 250000 m^2 and 0.01 m^2/s^2 respectively.

To see the effect on the estimation performance of a single station compared to multiple stations, the estimation has been performed using both the pseudo-observations of only a single station, as well as all three stations.

The resulting orbital state estimation error and time bias estimation error are shown in Section 5.4 for the different configurations discussed in this section.

4.3. Temperature and Stability Performance in Laboratory

As a first test to check the temperature behavior of operating the setup in an air-constricted box, as well as investigating how the observed stability of a signal changes when the electronics experience temperature changes, the Fitlet3, RSPduo and mini-GPS clock were placed inside a plastic junction box. Then, following the method described in Section 4.1.2, three 4000 seconds recordings of a 10 MHz signal were made and analyzed, of which the results are shown in Section 5.3.

The first recording was made using the original cable between the GPS clock and the SDR, while the second and third were made using a new cable. For the first and second recordings, the box had remained open for several hours to start in a stable environment. Then, five minutes before the recording started, the box was closed to reduce the cooling effect of airflow over the devices, and thus enforce rising temperatures inside the box. Between the second and third recordings, a dead-time of 10 minutes with the box closed was kept to allow the devices to settle again before starting a new recording. During the last 5 minutes of the third recording, the box was opened again, such that the influence on a rapid decrease in temperature on the stability could be investigated.

The air temperature in the box was monitored using a BMP180 GY-68 barometric pressure and temperature sensor board, which was read out once a minute using an Arduino Nano Every. A picture of these components is shown in Figure 4.3. This temperature sensor is capable of measuring temperatures from -40°C to $+40^{\circ}$C and a resolution of 0.1° C, with an accuracy of $\pm 1^{\circ}$ C. In addition to the air temperature, temperature measurements from the Fitlet3's internal components were retrieved once a minute as well.

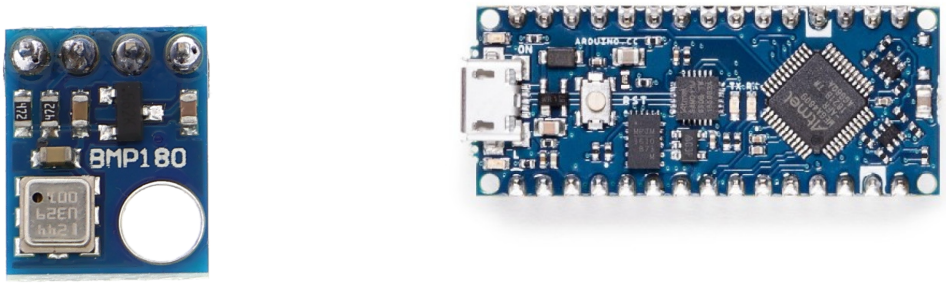

(a) BMP180 GY-68 **(b)** Arduino Nano Every

Figure 4.3: BMP180 GY-68 temperature sensor and Arduino Nano Every board used to monitor the temperature inside the DopTrackBox prototype. Images obtained from (*Luchtdruksensor / temperatuursensor / hoogtesensor BMP180 5V* 2025; *Arduino Nano Every with headers* 2025)

4.4. Real-world Performance

To assess the real-world performance of the prototype, the selected SDR and GPS clock needed to be placed inside a suitable box. Within the resources of this project there were two options: acquiring a COTS box, or designing one to be 3D printed. The default materials that were present to be printed on the available FDM printers were PLA and PET-G. These materials degrade under UV-light exposure and are therefore not recommended for long durations in an outside environment (Amza et al., 2021). In addition, 3D prints are often difficult to waterproof, without treating them with some sealant or coating, (*Running an RPI outside? - Raspberry Pi Forums* 2025; MijnEchteUsername, 2023; *How to Make Waterproof 3D Prints | All3DP* 2025). For these reasons, it was decided to acquire a COTS box instead of designing one and 3D printing it. As it is unclear how the temperature inside the box will behave in a realistic environment, the simplest box from the ”outdoor cabinets without ventilation” category described in 2.3.2 was chosen to use as prototype. It is an IP66 rated steel wall box, with dimensions of 400 by 300 by 150mm.

After building the prototype, it was placed together with a VHF optimized eggbeater antenna on the roof of the Aerospace Engineering faculty of the TU Delft. Figures 4.4 and 4.5 show the internals of the box and the experimental setup on the roof. At first, the system was connected to the TU Delft internet network using WiFi, but it was found that the wireless network was not stable enough to maintain a connection. Although the connection was able to restore itself at first several times after losing connection, at some point the connection was permanently lost, until it was connected to the network again using an Ethernet connection.

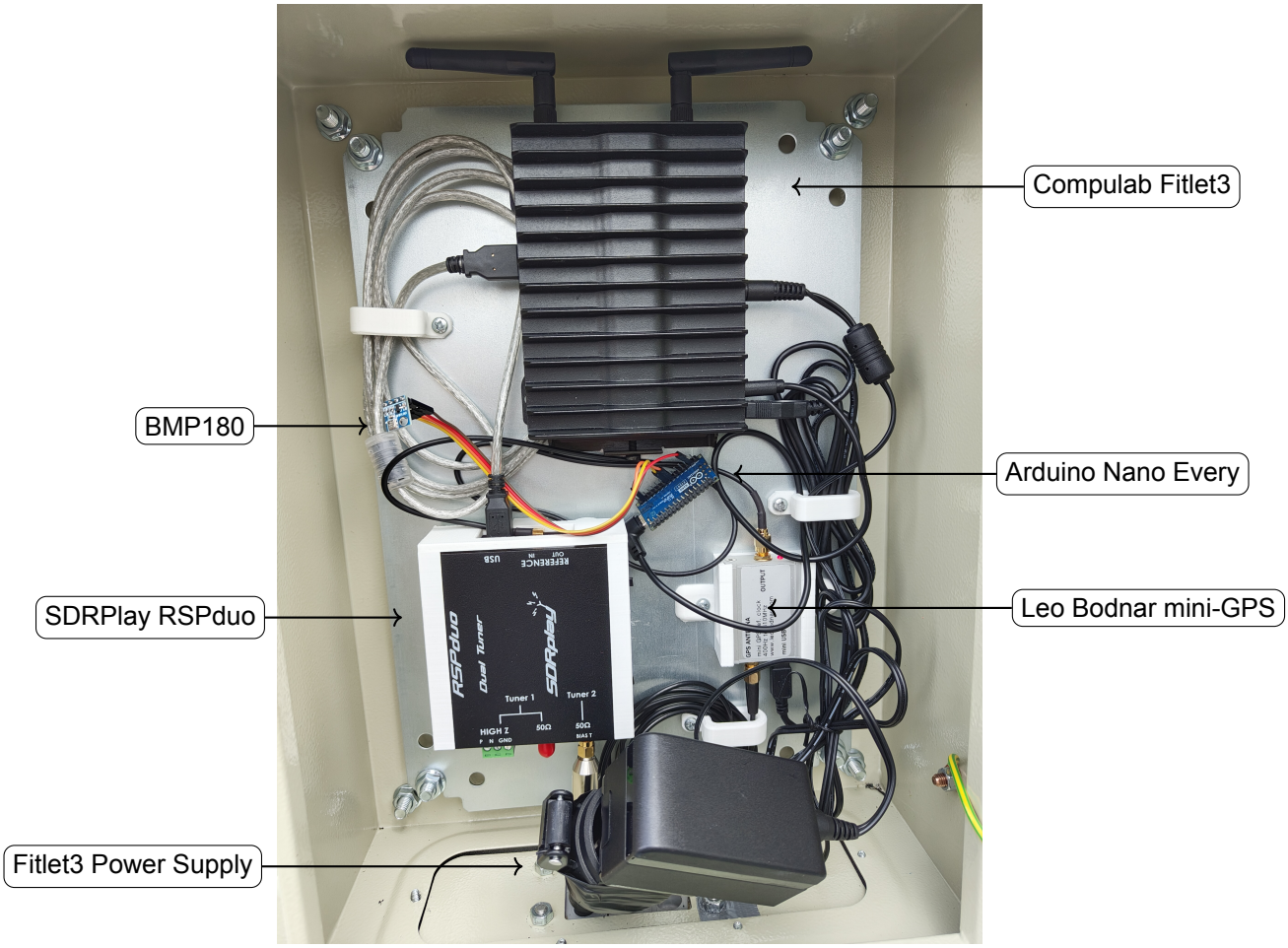

Figure 4.4: The internal components of the DopTrackBox prototype.

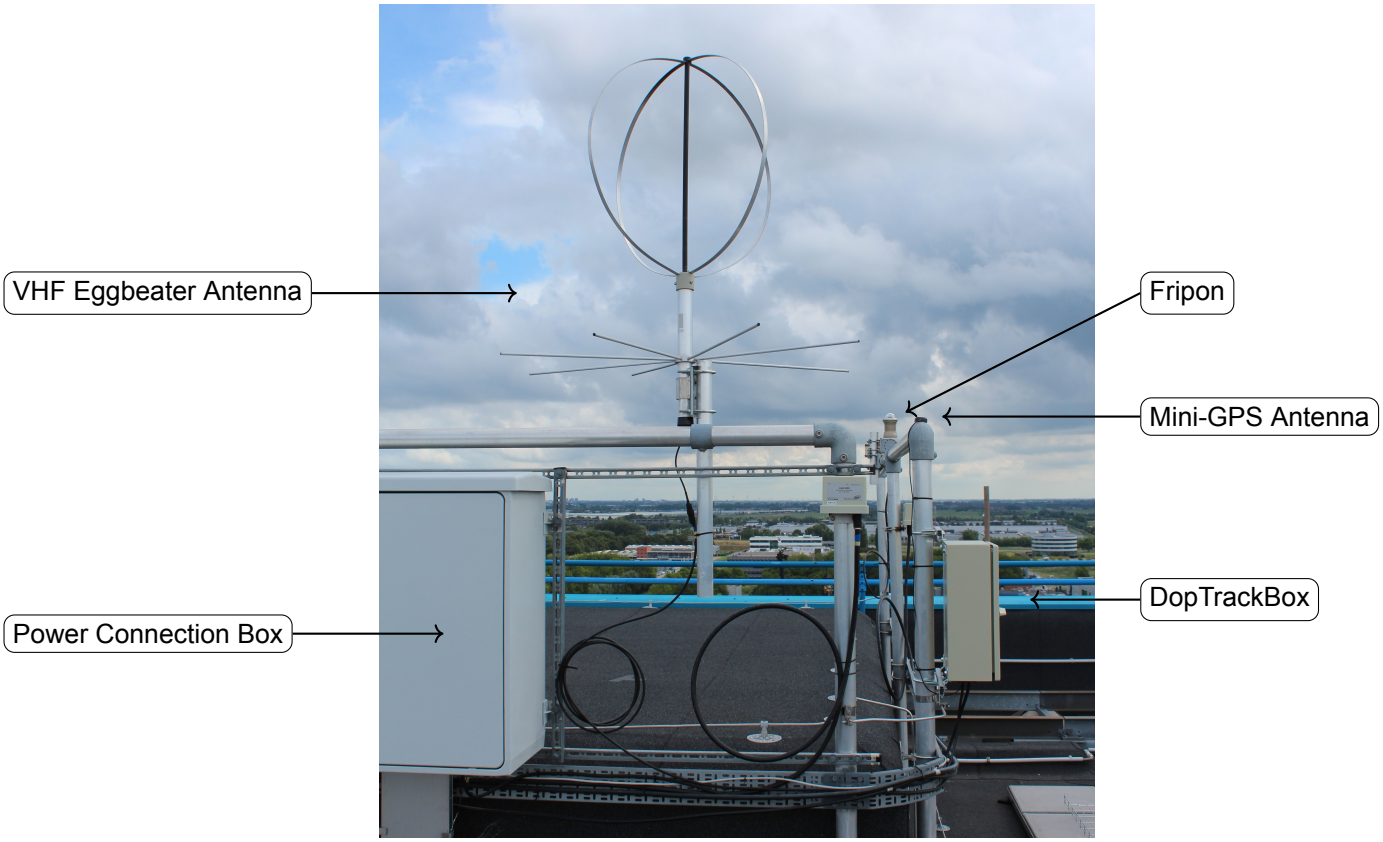

Figure 4.5: The DopTrackBox prototype, connected to a VHF eggbeater antenna at the roof of the TU Delft Aerospace Faculty building. Electrical power for DopTrackBox is supplied through the power connection box. Fripon is a different experiment that will later on in this thesis discussed as a potential noise source.

The setup has been operational from the 24th of July to the 25th of August 2025 in the standard configuration. After this, between the 26th of August and the 7th of October 2025, the system was operated in both the standard configuration as well as various test configurations to perform the system verification tests described in section 4.5.

During the operational period, DopTrackBox has autonomously performed recordings of satellite passes using the protocols described in the work of Sprenkels (2023) with minor modifications, while monitoring the temperature inside the box. The recordings were made using *rx tools* and *SoapySDR*, while the scheduling and initiation of these recordings is performed using scripts developed by the DopTrack project. More information on the installation of the software can be found in Appendix C.2.

In an effort to prevent a failure of the equipment, an automatic failsafe had been implemented that brought the Fitlet3 computer into sleep mode for a preset time of one hour if the mean temperature over five consecutive minutes has been higher than $40°$C, as measured every minute by the BMP180 sensor. This would lead to a significantly reduced power usage and therefore possibly a drop in temperature. The condition was automatically evaluated every 10 minutes. This gives room for four or five new measurements to take place after the machine wakes up, and thus prevents it from repeatedly going to sleep right after waking up even when the temperature has decreased to safe levels.

4.4.1. Temperature Analysis

To analyze the temperature behavior of the prototype, the temperature measured by the BMP180 sensor, as well as the internal temperatures of the Fitlet3 were recorded every minute. Because the BMP180 board is the temperature sensor located the farthest from the Fitlet3, it should be the least susceptible to variations caused by computational load on the Fitlet3, and is therefore assumed to be most representative of the air temperature inside the box. For the full set of temperatures measured by the BMP180 board between the 24th of July 2025 and 21st of September 2025, an hourly mean was then computed to get an indication of the typical temperatures inside the box. As this is the warmest period during the year in The Netherlands, these measurements provide a good baseline to investigate the likelihood of overheating in locations with similar climates.

In order to predict what the temperature inside the box might be in slightly different weather conditions, it must be known how the temperature inside the box correlates to the weather conditions outside. To this end, a dataset containing hourly measurements of temperature, average wind speed, cloud coverage, precipitation, dew point temperature and sunshine duration in Voorschoten (about 14 kilometers from Delft) was retrieved from the Koninklijk Nederlands Meteorologisch Instituut (KNMI) and correlated to the mean temperature inside the box.

In addition to this, histograms have been made of the temperature sensors on the Fitlet3's components. These provide insight into the typical temperatures of the components and whether they are likely to overheat. The results of this analysis are shown in Section 5.5.1.

4.4.2. Satellite Recordings Analysis

To evaluate range-rate accuracy, signal-to-noise ratio, and time bias of the recorded satellite signals, the IQ samples were first loaded in chunks of 0.5 seconds of samples. Then, on each chunk, a Fast Fourier Transform was performed to transform the samples from the time domain to the frequency domain. Within this time bin, the signal strength in each frequency bin was first used to compute the mean and standard deviation of the spectrum. Then, each frequency bin is classified as either signal, noise, or unclear. Following the work by Sprenkels (2023), a bin is considered signal if the strength is more than two standard deviations above the mean of that time bin. Unlike in the work of Sprenkels, instead of defining a frequency bin as noise if the strength is within one standard deviation above or below the mean, in this work the frequency bin is classified as noise when the strength is below one standard deviation above the mean, such that parts of the spectrum with low noise contribute to the computation of the noise floor. A frequency bin is unclear when it satisfies neither the signal nor the noise criterion.

The noise floor strength was determined by computing the median of all frequencies classified as noise for that particular time bin. For each frequency bin, the signal-to-noise ratio was then computed by dividing the signal strength by the computed noise floor.

As the recordings often contain signals from various land transmissions, or even other satellites, in addition to the satellite signal of interest, the frequencies are filtered such that only a window of 20 kHz around the expected signal frequency remains. Even in this window, several signals with a relatively constant frequency often still remain. To filter these out, all remaining frequencies that satisfy the signal criterion were first binned into a histogram. Then, all frequency bins were masked out that have a higher amount of entries in the histogram bin than the median plus one standard deviation of the 20 closest bins around each bin. Then, an initial guess for the signal frequency as function of time is made based

on a hyperbolic tangent function of the shape

$$y = -a \tanh\left(b(x - c)\right) + d, \tag{4.2}$$

where x is the time, f the expected frequency, and a, b, c, and d are the estimated parameters. The c and d parameters describe the time of closest approach (TCA) and frequency at closest approach (FCA) of the signal, while a and b stretch the shape of the curve.

If the same pass had been recorded and processed by the DopTrack setup itself as well, the initial guess for the parameters of the hyperbolic tangent were retrieved from that data. If not, the initial guess was set to [4000, 0.01, $t_{1/2}$, f_0] for a FUNcube-1 pass, and [2500, 0.005, $t_{1/2}$, $f_0 - 1200$] for other satellite passes. Here, $t_{1/2}$ represents the half time point of the recording, and f_0 the expected frequency of the signal which is typically the tuning frequency.

Then, for each time bin, the frequency of the remaining signal points with the highest signal-to-noise ratio in a 2.5 kHz band around the hyperbolic tangent were retrieved when no DopTrack initial guess was available, or 1 kHz when there was a DopTrack initial guess available. These points were then used to perform a least-squares fit on the parameters of the hyperbolic tangent. The parameters of the hyperbolic tangent were updated with the estimated values, which were then used to compute the remaining signal points again, now in a band 0.9 times narrower than the previous band. Then the strongest remaining signals in the band were then used to update the estimation again. This cycle was repeated until the band would become smaller than 500 Hz in the next step. The next step of the process depends on the analysis under consideration.

Signal-to-noise ratio comparison

In order to compare the signal-to-noise ratio of the DopTrackBox system with respect to DopTrack, the signal-to-noise ratio of the extracted signals by both systems needed to be known. However, as the DopTrack data processor does not output the signal-to-noise ratio of the extracted signal points, the passes recorded by DopTrack corresponding to the passes recorded by DopTrackBox have been processed using the same procedure as described in Subsection 4.4.2.

Due to differences in both hardware and recording software, the start time of the recordings are not exactly the same between DopTrack and DopTrackBox. In DopTrackBox, the only known times are the times right before the start and right after the end of the recording. These will be referred to as t_1 and t_2 respectively. In DopTrack, the recording software is also capable of providing an estimate between receiving the command to commence the recording, until the actual first sample is taken. Using this information, and a 1PPS signal used to synchronize the time, a more accurate start time of the recording is determined, called $t_{\text{start, DT}}$. Based on the known duration of the recording, this time is also used to compute the supposed more accurate end time of the recording, $t_{\text{stop,DT}}$.

As a time bias is assumed to be more likely to originate from a delay in the start of the recording, rather than at the end of the recording, an potentially more accurate start time, $t_{\text{start, DTB}}$, of DopTrackBox has been computed based on $t_{2,\text{DTB}}$ and the known duration of the recording, $T_{\text{rec, DTB}}$, as $t_{\text{start, DTB}} = t_{2,\text{DTB}} - T_{\text{rec, DTB}}$. Figure 4.6 shows a schematic illustration of the these start and end times, as well as a hypothetical time bias at the start, Δt_s, and end, Δt_e of the recording. The computed variable $t_{\text{start, DTB}}$ corresponds to the $t_{\text{start, est}}$ point in the upper part of the timeline, as the real start time is not know. For DopTrack, the obtained values for t_{start} and t_{end} are assumed to be close enough to the true value to not make an impact, but a verification of this will be discussed in the next section.

To compare the signal-to-noise ratio of the systems, the signal-to-noise ratio as a function of time is shown in both cases with respect to the $t_{\text{start, DT}}$, in Section 5.5.2. To compute these times for the DopTrackBox recording, the DopTrackBox timestamps with respect to their start time have been corrected by subtracting $t_{\text{start, DT}} - t_{\text{start, DTB}}$.

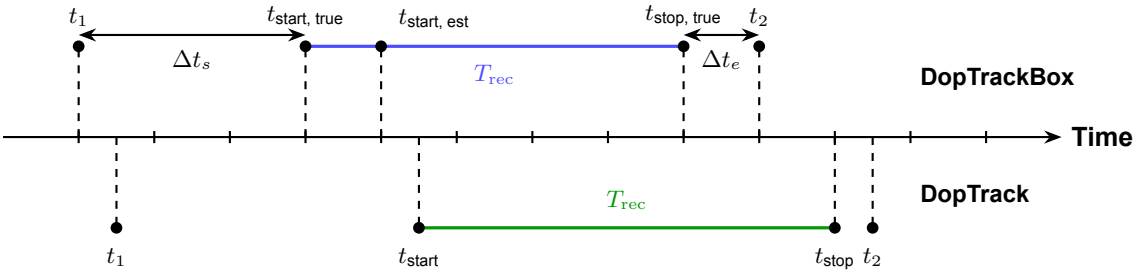

Figure 4.6: Schematic illustration of the recording timeline of DopTrackBox (top) and DopTrack (bottom), with a hypothetical unknown time bias at the start and end of the DopTrackBox recording. The illustration is not to scale.

Time and Frequency Bias Estimation

To estimate the time bias of the observations, the same method as described in the previous subsection was used. However, instead of processing the DopTrack data using the methods described previously, the DopTrack data was processed by DopTrack's own processing.

After applying only the start time correction described in the previous section, the extracted frequencies for both systems were displayed with respect to $t_{\text{start, DT}}$. To also show the frequency difference between the systems, the DopTrack frequencies were first linearly interpolated at the timestamps of the DopTrackBox data.

Then, a least-squares estimation was performed to estimate the time and frequency bias, Δt and Δf, of the DopTrackBox system with respect to DopTrack, such that for all DopTrackBox observations $t_{\text{true}} = t_{\text{obs}} - \Delta t$ and $f_{\text{true}} = f_{\text{obs}} - \Delta f$. In the estimation, only datapoints 180 seconds before and after the DopTrack estimated TCA have been used, to keep the number of noise points used in the estimation limited. Then, the estimated time and frequency bias were used to correct the DopTrackBox datapoints and a new frequency comparison between the DopTrack and DopTrackBox system was made.

As this method yielded unsatisfactory results, the frequency bias was forced to 0. The initial guess of the time bias was also set to zero, with a lower and upper bound of -10 and 10 seconds respectively.

In addition, the Jacobian matrix was retrieved and used together with the residuals to compute an uncertainty on the estimated biases.

As even with a time bias, the frequency difference between the DopTrack and DopTrackBox datapoints was typically below 125 Hz, the least squares estimation was repeated while taking only DopTrackBox datapoints into account that are less 150 Hz from the DopTrack datapoints. A new frequency comparison between DopTrackBox and DopTrack was made after correcting for these bias estimations as well.

To get an indication of whether $t_{1,\text{DTB}}$ or $t_{\text{start, DTB}}$ is a better estimate of the recording start time, this bias and frequency estimation was performed using $t_{1,\text{DTB}}$ as recording start time instead of $t_{\text{start, DTB}}$ as well. The results of the analysis described in this section are shown in Section 5.5.2.

This time and frequency bias estimation procedure relies on the assumption that the DopTrack system has a negligible time and frequency bias itself, such that the time bias with respect to DopTrack represents the time bias with respect to absolute time well enough. To verify the truth of this statement, an upper limit on the DopTrack time bias was also computed using the time difference between $t_2 - T_{\text{rec}}$ and t_{start} for DopTrack. The results of this are also shown in Section 5.5.2.

4.5. System Components Verification

As the DopTrackBox system had a lower than expected signal-to-noise ratio for passes recorded during the operational time on the roof, further investigation was warranted to rule out any defective or disruptive components of the system. Therefore, multiple configurations have been tested in which hardware components have been replaced, moved or deactivated. The system was then used to record either new FUNcube-1 passes, or the Rotterdam Airport Automatic Terminal Information Service (ATIS) signal, broadcasting at 128.565 MHz.

When evaluating the recorded passes, it appeared that the noise values were higher than those reported in the work of Sprenkels (2023). One of the possible sources of noise in recording could be electromagnetic fields of the electronics inside DopTrackBox (in particular the Fitlet3 computer) coupling to the antenna. To exclude this, the first test was to move the DopTrackBox antenna further from the box, while using the same cable between the antenna and the SDR. The default distance from the center of the box to the center of the eggbeater antenna was about 160 ± 10 cm. Additional locations that have been tested are about 220 ± 10 and 280 ± 10 cm. If the noise was caused by the box, a drop in noise, and increase in signal-to-noise ratio would be expected when moving the antenna further from the box.

When making recordings with *rx tools*, automatic gain control (AGC) was turned on by default. Although this was also used in the work of Sprenkels, it is possible that the default setpoint of the AGC has been changed between *rx tools* or *SoapySDR* (used as an interface between *rx tools* and the SDR) software revisions. To test the impact of the AGC setpoint on the noise and the signal-to-noise ratio, recordings of the ATIS signal have been performed using AGC setpoint values of -10, -20, -30, -40 and -60 dBFS.

To exclude certain hardware components from being faulty, a first test was performed by recording the ATIS signal using the DopTrack antenna instead of the DopTrackBox antenna, changing the coax cable between the antenna and DopTrackBox, and using a new RSPduo device connected outside the box to possibly reduce radio frequency interference of the Fitlet3 on the SDR. This test was performed on September 1st, and all subsequent recordings with DopTrackBox on the roof have been performed using this coax cable between the DopTrackBox antenna and SDR.

As the DopTrack system itself had shown an increase in noise since around February or March 2025, it was suspected that a new experiment on the roof (Fripon) installed during this period, might be partly responsible for the high noise. To investigate the influence of this new experiment on the noise, additional FUNcube-1 passes have been recorded while the experiment was turned off between the 12th and 19th of September around 17:00 local time.

Even though the DopTrack and DopTrackBox antennas are both eggbeaters, one is older than the other and could have a different gain as function of frequency. Since the ATIS signal frequency is not at the optimized frequency of the antenna, it might not be a suitable signal to compare measurements made with DopTrack and DopTrackBox to eliminate potential faulty components. Therefore, additional

FUNcube recordings were made in several configurations: the new RSPduo and Fitlet3 were first used without GPS clock in the server rack of the lab that hosts the rest of the DopTrack system. Instead of using the DopTrackBox antenna and cable, the SDR was connected to the DopTrack antenna system using a splitter in the lab using a coax cable previously used for one of the DopTrack SDRs. Then, this cable between the splitter and SDR was exchanged with the DopTrackBox cable that was used before September 1st in the primary operational period. Then, to investigate the influence of the Low Noise Amplifier (LNA) used in the DopTrack system, the LNA was turned off.

After these tests, the original DopTrackBox setup was used again to record FUNcube-1 passes, but without Leo Bodnar GPS clock. Then, the antenna of DopTrack was swapped with the antenna of DopTrackBox to test whether the original DopTrackBox antenna was faulty. After this, the entire DopTrackBox system (without antenna and coax cable) was placed in the lab as a whole, and connected to the DopTrack antenna system using the splitter and the original DopTrackBox cable. Subsequently, the DopTrackBox system was placed back on the roof, and connected to its original antenna with the new cable, at a location about further located from an electronics power box on the roof. Finally, to test if a lack of heat dissipation of the SDR when the box is closed influences the signal-to-noise ratio, the door of the box was opened during recorded FUNcube-1 passes.

An overview of the test configurations to test each of the influences are shown in Table 4.4.

Measurements Group	**Test Aspect**	**Fripon [on/off]**	**DT LNA [on/off]**	**GPS clock [on/off]**	**SDR [old/new]**	**DTB Antenna [DT/DTB]**	**DT Antenna [DT/DTB]**	**Radio Cable [old/new/DT]**	**SDR Location [roof/lab]**	**DTB to Antenna Distance [m]**	**Data [ATIS/ FUNcube-1]**
Default	N/A	on	N/A	on	new	DTB	DT	both	roof	1.6 ± 0.1	Both
Antenna Distance	N/A	on	N/A	on	old	DTB	N/A	old	roof	1.6 ± 0.1 2.2 ± 0.1 2.80 ± 0.1	ATIS
AGC	N/A	on	N/A	on	new	DTB	N/A	old	roof	2.8 ± 0.1	ATIS
Components on roof with ATIS	Default	on	N/A	off	old	DTB	N/A	old	roof	2.8 ± 0.1	ATIS
	Antenna	on	N/A	off	old	DT	N/A	old	roof	3.8 ± 0.1	ATIS
	Coax Cable	on	N/A	off	old	DTB	N/A	new	roof	2.8 ± 0.1	ATIS
	SDR	on	N/A	off	new	DTB	N/A	new	roof	Fitlet3 2.8 ± 0.1 SDR ± 0.2	ATIS
Components with FUNcube-1 on roof	Fripon	off	on	on	old	DTB	N/A	new	roof	2.8 ± 0.1	FUNcube-1
	GPS Clock	on	on	off	old	DTB	DT	new	roof	2.8 ± 0.1	FUNcube-1
	Antenna Swap	on	on	off	old	DT	DTB	new	roof	2.8 ± 0.1	FUNcube-1
	Different Location	on	on	off	old	DTB	DT	new	roof	0.8 ± 0.2	FUNcube-1
	Box Door Open	on	on	off	old	DTB	DT	new	roof	0.8 ± 0.2	FUNcube-1
Components with FUNcube-1 in lab	SDR	on	on	off	new	DT	DT	DT	lab	2.8 ± 0.1	FUNcube-1
	Coax Cable	on	on	off	new	DT	DT	old	lab	2.8 ± 0.1	FUNcube-1
	LNA	on	off	off	new	DT	DT	old	lab	2.8 ± 0.1	FUNcube-1
	Fitlet3 to SDR Noise Coupling	on	on	off	old	DTB	DTB	new	lab	2.8 ± 0.1	FUNcube-1

Table 4.4: An overview of the different test configurations used to tests the influence of components, environment and software settings on the signal-to-noise ratio performance of the DopTrackBox system.

5

Results

This chapter presents the results of the experiments described in Chapter 4. First, Section 5.1 covers the stability of the GPS clocks tested in this project. Then, Section 5.2 shows the stability of the SDRs when using these GPS clocks, and how they differ when not using them. Section 5.3 then shows how this stability is impacted by temperature fluctuations.

The subsequent Section, 5.4, shows the impact of an observation time bias on the estimation performance of a simulated satellite, and if this bias can be estimated to mitigate its effects. This is followed by Section 5.5, in which the bias of the DopTrackBox prototype is extracted, and comparisons with passes recorded by DopTrack are made. This section also demonstrates the observed temperature behavior of the prototype. Finally, Section 5.6 covers the results of the systematic verification of the hardware.

5.1. GPS-clock Stability

Figures 5.1 and 5.2 show the unwrapped phase differences between the EC20S and the Leo Bodnar mini-GPS and LBE-1421 as measured using the TinyPFA, respectively. Each of the measurements contains a linear drift of the phase, which represents the average difference in frequency difference between the EC20S and the device under test (DUT). For the mini-GPS, the linear drift is similar between the different measurement runs, while for the LBE-1421 the drift is less consistent. For two of the measurements with the LBE-1421, the linear drift is larger than for all of the measurements using the mini-GPS, indicating a larger average frequency difference. For all of the measurements, there are phase jumps at seemingly random points in time. In addition, in particular the third run of measurements with the LBE-1421 has smaller periodic jumps in the phase.

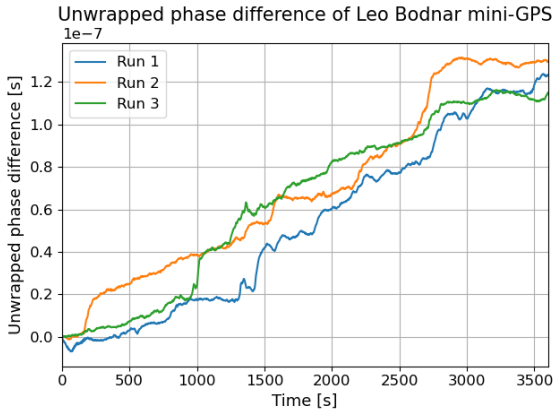

Figure 5.1: Unwrapped phase difference between the output of a 10MHz reference frequency and a Leo Bodnar mini-GPS clock, measured using a TinyPFA.

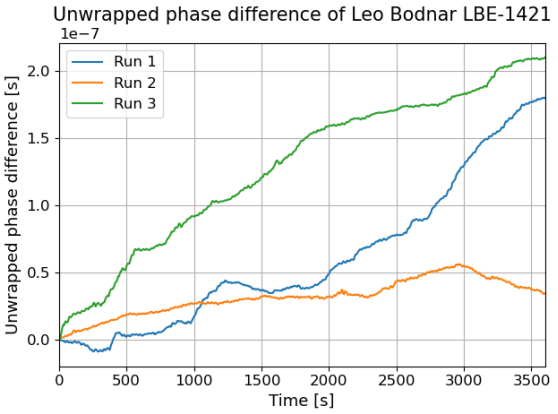

Figure 5.2: Unwrapped phase difference between the output of a 10MHz reference and a Leo Bodnar LBE-1421, measured using a TinyPFA.

The overlapping Allan deviation of the Leo Bodnar mini-GPS and LBE-1421 are shown in Figures 5.3 and 5.4 respectively. Based on these figures, both clocks have a better stability than the requirement of 10^{-8} (identifier DTB-TECH-3.02) over the range of interest between 0.5 and 10^3 seconds. For $\tau \leq 10$s, the newer LBE-1421 model seems to be more stable than the older mini-GPS model. For $\tau \geq 10$s, the clocks seem to have a similar stability, although this cannot be stated with certainty as the consistency in the measured stability is much lower for the LBE-1421 than the mini-GPS. Furthermore, both models show a 'bump' in the stability, with their peaks around 3 and 10 seconds, respectively. There is no discernible difference between the first and second run, and the third run of the mini-GPS in which the experimental 'correct' pulling setting of the TinyPFA was used. In addition, there is no discernible difference between run one, and run two and three of the mini-GPS measurements in which it was placed inside a cardboard box.

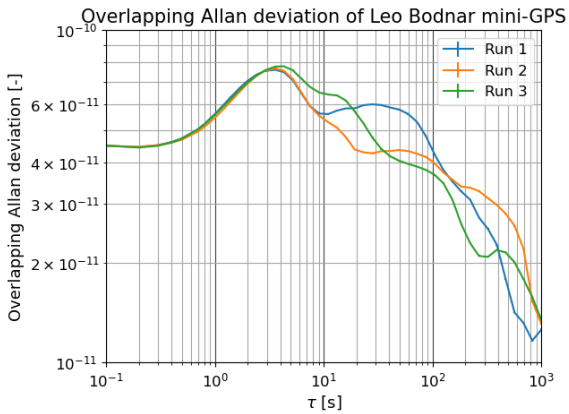

Figure 5.3: Overlapping Allan deviation of the Leo Bodnar mini-GPS clock output. Over the range of interest between $\tau = 0.5$ s and $\tau = 10^3$ s, the stability of the clock output is better than the requirement of 10^{-8}.

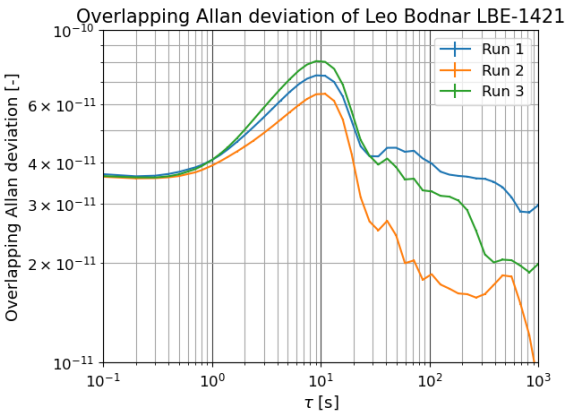

Figure 5.4: Overlapping Allan deviation of the Leo Bodnar LBE-1421 clock output. Over the range of interest between $\tau = 0.5$ s and $\tau = 10^3$ s, the stability of the clock output is better than the requirement of 10^{-8}.

5.2. Software Defined Radio Stability

After establishing that the GPS clocks themselves have a sufficient stability to satisfy the requirements, this section first shows the stability when using the RSPduo with and without GPS clock in Section 5.2.1. This is followed by Section 5.2.2 in which the measured stability of the USRP N210 with both GPS clocks is shown.

5.2.1. SDRPlay RSPduo

Following the procedure discussed in Section 4.1.2, the instantaneous frequency as function of time has been extracted for each of the measurements, and is shown in figures 5.5 and 5.6 for the measurements with the old and new cable between the SDRduo and mini-GPS clock, respectively.

In Figure 5.5 it can be seen that the measurements in which the mini-GPS clock was not connected to the RSPduo (RSPduo, run 1,2 and 3), the frequency of the signal has a drift on the order of 0.2 to 1 Hz over the span between 100 and 400 seconds, while the measurements in which the mini-GPS was connected(RSPduo + mini-GPS (+ Inf. Circuit) run 1,2 and 3) have a no significant drift over that timespan with the exception of the first run with the interface circuit. In addition, the measurements with mini-GPS clock connection are grouped together, while only two of the measurements without a GPS clock are grouped. Furthermore, it can be seen that all measurements contain a downward drift in frequency of approximately 0.5 Hz for the first 100 seconds. In all measurements, the frequency is between 1.4 and 3.0 Hz higher than the theoretical 10 MHz than the EC20S is supposed to output.

Figure 5.6 shows, however, that when using a new cable between the mini-GPS and the RSPduo, this downward drift in frequency in the first 100 seconds is no longer observed, while for the measurements without GPS clock the drift is still present. This led to the belief that the original cable was defective. In addition, the frequency bias of the measurements with GPS clock (RSPduo + mini-GPS (+ Intf. Circuit), run 1,2 and 3) is around 0.485 Hz, compared to approximately 1.9 Hz in Figure 5.5. The fluctuations on this frequency bias are on the order of $\pm 0.025 Hz$ and constant over time.
A difference with Figure 5.5 is that in the measurements without GPS clock, there is only a limited drift of less than 0.2 Hz after the initial 100 seconds, stabilizing to a frequency bias of approximately 2.05 Hz, compared to values of 1.5 to 2.8 Hz in Figure 5.5. Furthermore, the first run without GPS clock (RSPduo, run 1) shows a bigger initial drift in the first 100 seconds of approximately 0.7 Hz, compared to the second and third run with a drift of 0.05 Hz.

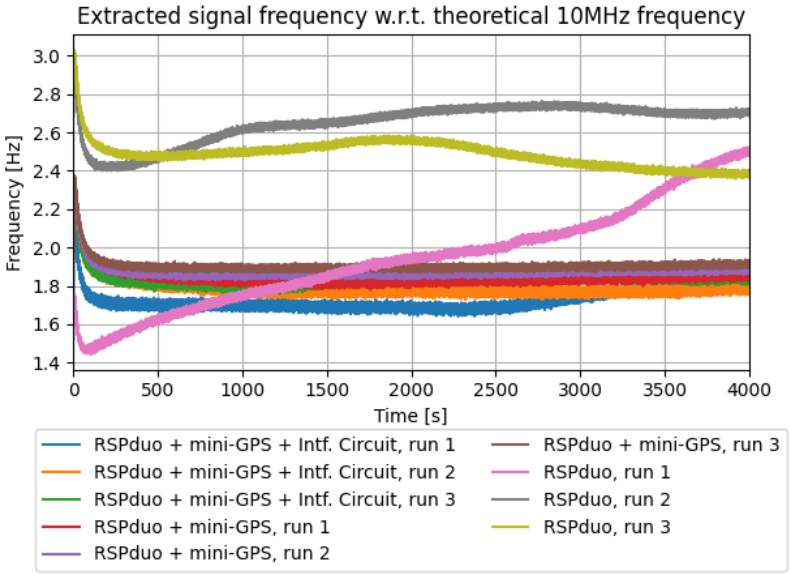

Figure 5.5: Measured signal frequency with respect to the 10 MHz frequency supplied to the RSPduo input, in hardware configurations with and without GPS clock and interface circuit. The measurements with a GPS clock appear more consistent and contain less drift than the measurements without GPS clock.

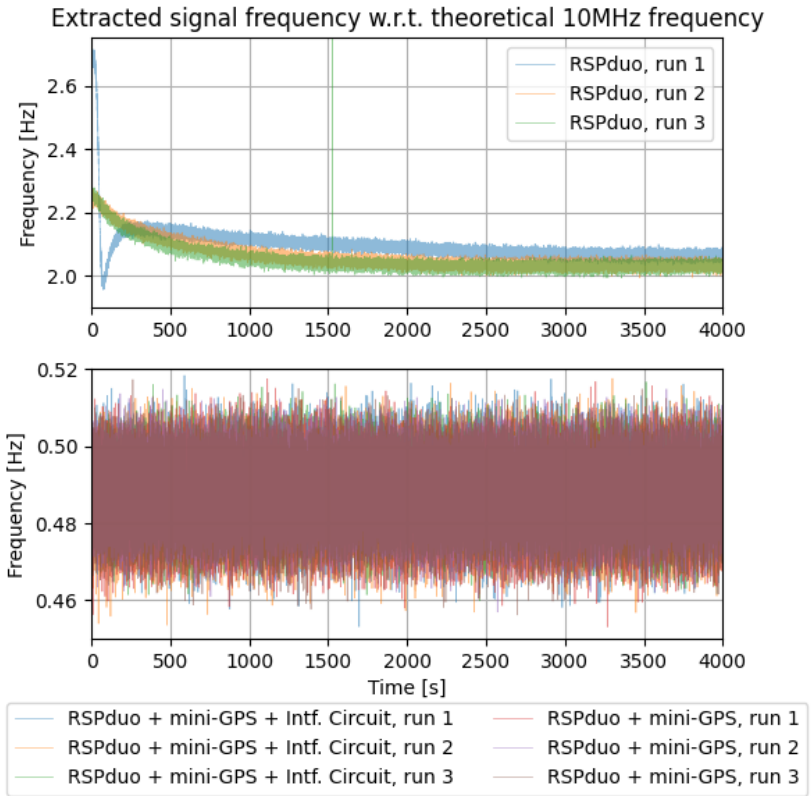

Figure 5.6: Measured signal frequency with respect to the 10 MHz frequency supplied to the RSPduo input, in hardware configurations with and without GPS clock and interface circuit, using a new cable to connect the GPS clock to the SDR. The absolute frequency error is much smaller in the measurements made using a GPS clock than the measurements without GPS clock.

A similar difference between the old and new cable is observed in the overlapping Allan deviations. Figure 5.7 first shows the measurements with the old cable, which all follow a similar pattern: the stability first improves from approximately 10^{-9} to between 2×10^{-10} and 4×10^{-10} with longer averaging periods (τ), but for $3 \times 10^0 \lessapprox \tau \lessapprox 5 \times 10^1$ s, the stability deceases again to approximately 10^{-9}. From this point onward, there seems to be a distinction between each of the three configurations. For the measurements without GPS clock (RSPduo, run 1,2 and 3), the stability continues to decrease to levels upwards of 4×10^{-9} for $\tau = 10^3$ s, with one of the measurements above the requirement of 10^{-8} (identifier DTB-TECH-2.06). The stability in the measurements with a GPS clock, but without interface circuit (RSPduo + mini-GPS, run 1,2 and 3), levels off at 10^{-9} or slightly improves to 4×10^{-8} for $\tau = 10^3$ s. The stability in the measurements with a GPS clock and interface circuit (RSPduo + mini-GPS + Intf. Circuit, run 1,2 and 3) is between these two configurations, with values between 10^{-9} and 4×10^{-9} for $\tau = 10^3$ s.

Also between $3\times10^0 \lessapprox \tau \lessapprox 5\times10^1$ s, there seems to be a difference between the configurations. While the measurements using no GPS clock or only the GPS clock have a similar stability, the measurements using the interface circuit have a stability between 1×10^{-9} and 2×10^{-9} higher than the other two configurations.

Figure 5.8 shows the measurements performed using the new cable. In this case, for $10^{-1} \leq \tau \lessapprox 10^0$ the stability is below 10^{-9} for all measurements, with the exception of run 3 of the measurements without GPS clock (RSPduo, run3). For $\tau \gtrapprox 10^0$, the stability of the measurements using the GPS clock, with out without interface circuit, keep improving with increasing τ to levels between 10^{-11} and 3×10^{10} at $\tau = 10^3$. For the measurements without GPS clock however, the stability starts to decrease again, but at different values of τ. For $\tau = 10^3$, all three of the measurements converge to a similar value of 2×10^{-9}. Compared to Figure 5.7, the most notable difference is that instead of following the same pattern of increasing stability followed by decreasing stability as a function of τ, both configurations with GPS clock now only have an increasing stability as function of τ. The measurements without GPS clock again experience a decrease in stability for values of τ around 10^0 and 10^1, although less consistent then in Figure 5.7. Unlike in that figure, all the measurements have a stability that satisfies the requirement (Identifier DTB-TECH-2.06).

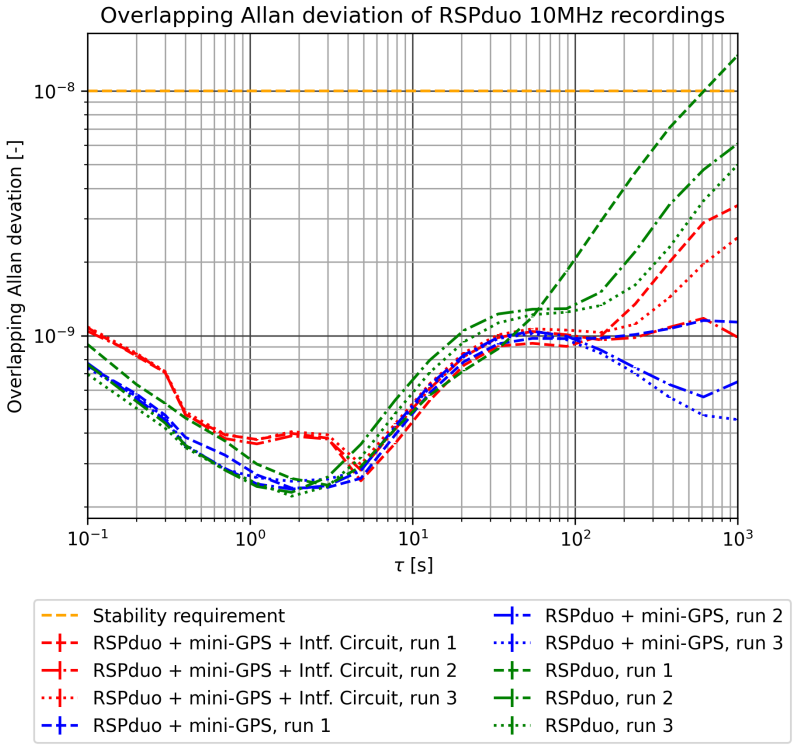

Figure 5.7: Overlapping Allan deviation of the RSPduo in different configurations, using the old cable to connect the GPS clock to the SDR. While the measurements with GPS clock are more stable than the requirement, one measurements without GPS clock has a stability worse than requirement.

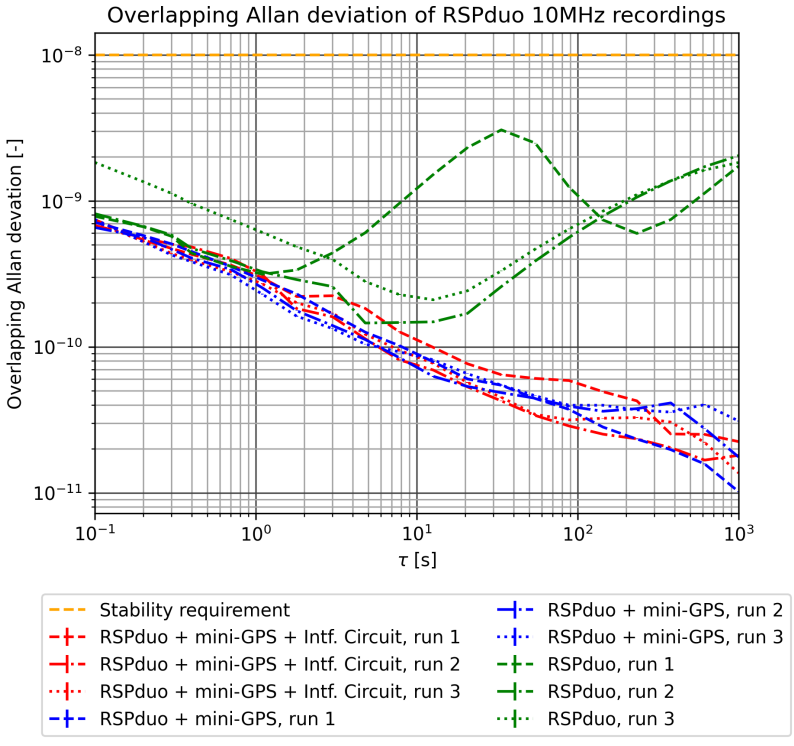

Figure 5.8: Overlapping Allan deviation of the RSPduo in different configurations, using the new cable to connect the GPS clock to the SDR. All measurements have a stability better than requirement.

5.2.2. Ettus Research USRP N210

For the N210, the instantaneous frequency as function of time is shown in Figure 5.9. The first thing to notice is the large spikes in frequency of the measurements taken with the LBE-1421 in FLL mode. The other measurements, with the exception of a single 3Hz spike in the first mini-GPS measurement, do not contain such frequency spikes. Overall, the average frequency biases of the measurements are approximately 0.005 Hz from the theoretical 10 MHz signal supplied by the EC20S. This is significantly smaller than in the approximately 0.485 Hz bias found in the measurements performed with the RSPduo and new cable between the GPS clock and the SDR (Figure 5.6). In addition, the fluctuations on the frequency are only on the order of ± 0.005 Hz as well, compared to ± 0.025 Hz in Figure 5.6.

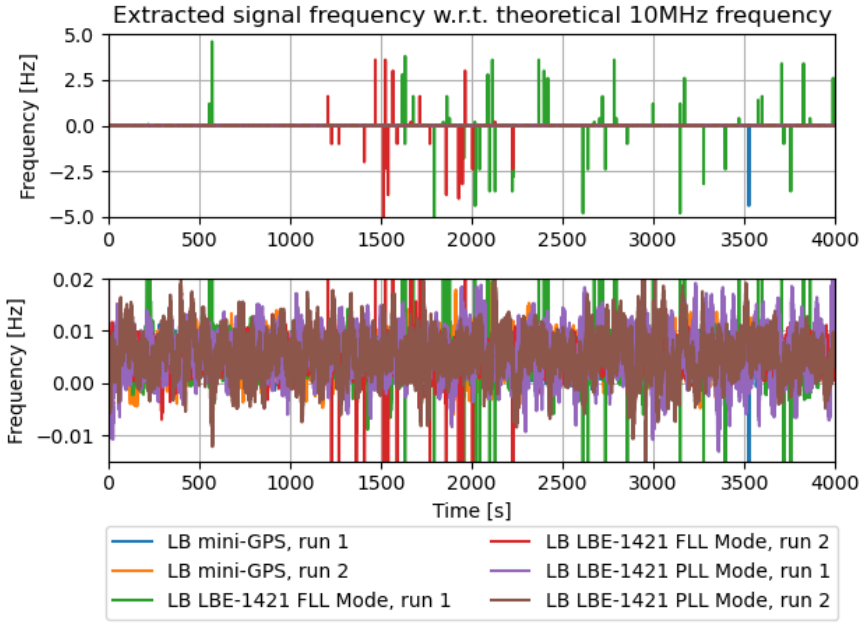

Figure 5.9: The measured frequency of a 10 Mhz reference signal using an Ettus Research USRP N210, using Leo Bodnar mini-GPS and LBE-1421 clocks as external reference. The bottom plot is a zoomed version of the top plot.

Figure 5.10 shows the resulting overlapping Allan deviations. The measurements taken with the LBE-1421 in FLL mode that showed frequency spikes in Figure 5.9 have the highest overlapping Allan deviation, but still below the requirement of 10^{-8} in the range of interest between $\tau = 0.5$ sand $\tau = 10^3$ s.

The measurements with the LBE-1421 in PLL mode have an overlapping Allan deviation that is significantly lower for $\tau \lessapprox 20$ s. After this, it increases to levels similar to the measurements in FLL mode, at which point it goes back down with values slightly lower than those of the measurements in FLL mode.

For low averaging periods, the measurements performed using the mini-GPS have a higher overlapping Allan deviation than was measured with the mini-GPS connected to the RSPduo as was shown in Figure 5.8, but for higher averaging periods it decreases to similar levels.

All measurements have a stability better than the requirement in the averaging period range of interest between 0.5 and 10^3 seconds.

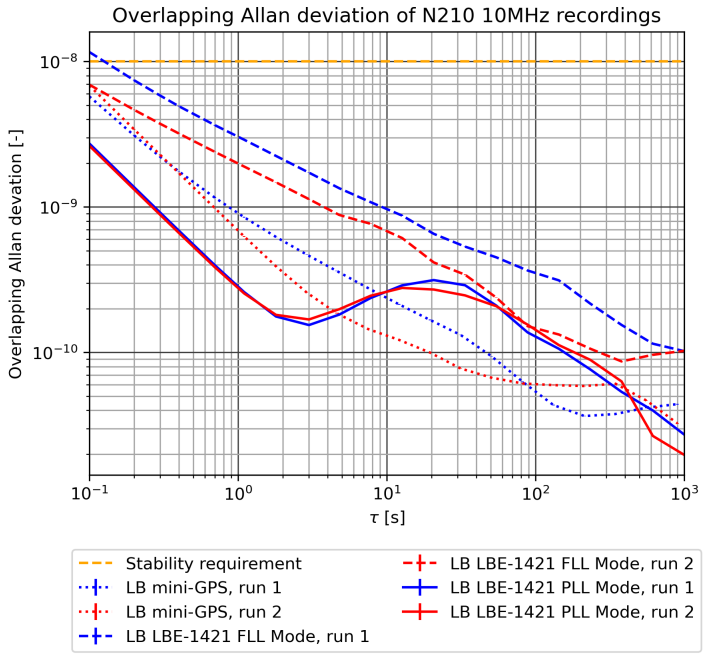

Figure 5.10: Overlapping Allan deviation of the Ettus Research N210 in different configurations. All configurations show a stability better than the requirement.

5.3. Laboratory Setup Temperature Stability

Following the steps described in Section 4.3, Figure 5.11 shows the instantaneous frequency as function of time, together with the measured temperatures, during a recording with the old cable between the SDR and GPS clock, to investigate the influence of temperature fluctuations on the stability. Figures 5.12 and 5.13 show the same, but with the new cable instead.

In Figure 5.11, the frequency as a function of time shows a similar downward trend as observed in other measurements using the RSPduo without GPS clock. However, the magnitude of this drift is now approximately 0.9 Hz, compared to a maximum of approximately 0.6 Hz observed before. In addition, the duration of the drift is about 2000 seconds, compared to the approximately 100 seconds that was observed before. Moreover, the downward trend is less smooth and contains a sudden jump in frequency of about 0.1 Hz. During the measurement, the temperatures inside the box increased from approximately 23.5 to 29°C.

With the new cable between the RSPduo and the mini-GPS clock, there is again no downward drift in the measured frequency anymore as can be seen in Figure 5.12 and 5.13. In Figure 5.12, from around 900 seconds onward, the frequency fluctuations suddenly increase from approximately $\pm 0,0175$ Hz to $\pm 0,0325$ Hz. From the temperatures reported by the BMP180 and internal Fitlet3 components, this point does not seem to coincide with a specific event that would cause a significant increase in temperature. During this measurement, the temperature inside the box increased from around 28 to 32°C.

Figure 5.13 does not show a similar sudden increase in frequency fluctuations, and over the full range the stability seems to be similar to the first 900 seconds of Figure 5.12. Between the first and second run with the new cable, the temperature has dropped from 32 to 31.5°C, and during the second run the temperature slowly increased again to about 32°C, before dropping rapidly to 24° in the last five

minutes of the recording when the box was opened. This decrease in temperature does not show a significant impact on the measured instantaneous frequency.

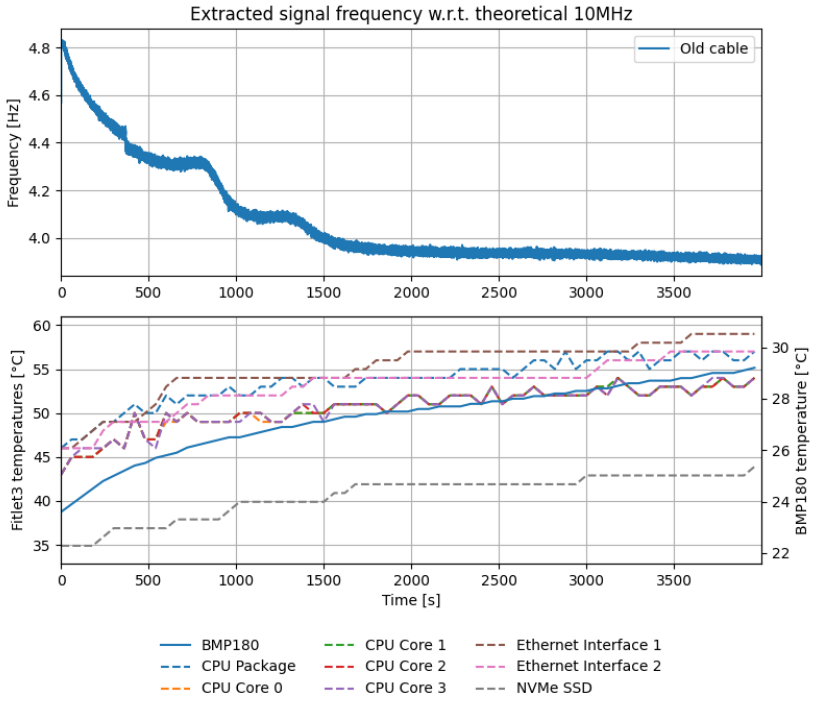

Figure 5.11: Top: Measured signal frequency with respect to the 10 MHz frequency supplied to the RSPduo input, when connecting the mini-GPS using the old cable to the SDR. Bottom: The temperatures measured in the box using the BMP180 and the internal components of the Fitlet3.

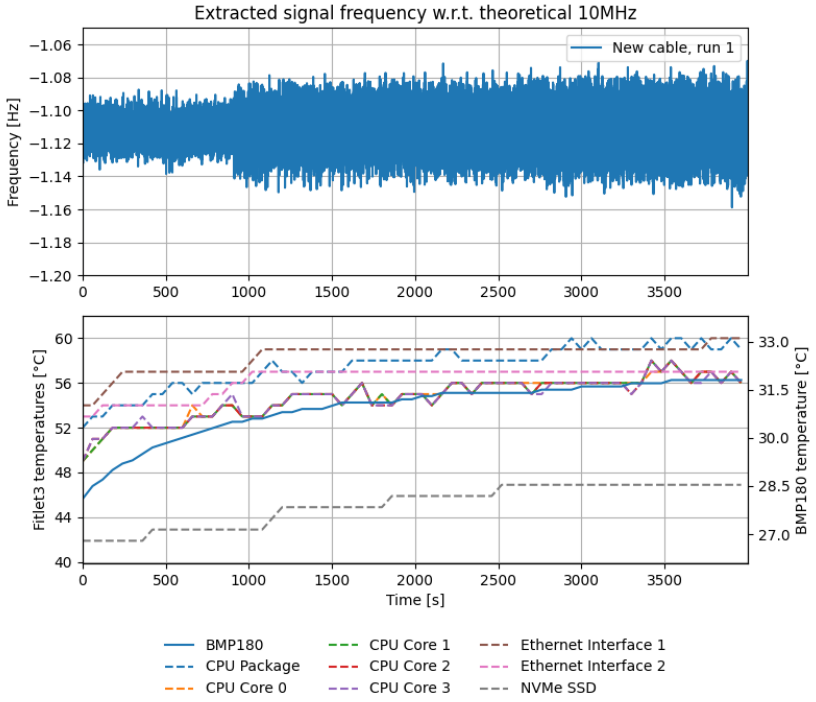

Figure 5.12: Top: Measured signal frequency with respect to the 10 MHz frequency supplied to the RSPduo input, when connecting the mini-GPS using the old cable to the SDR. Bottom: The temperatures measured in the box using the BMP180 and the internal components of the Fitlet3.

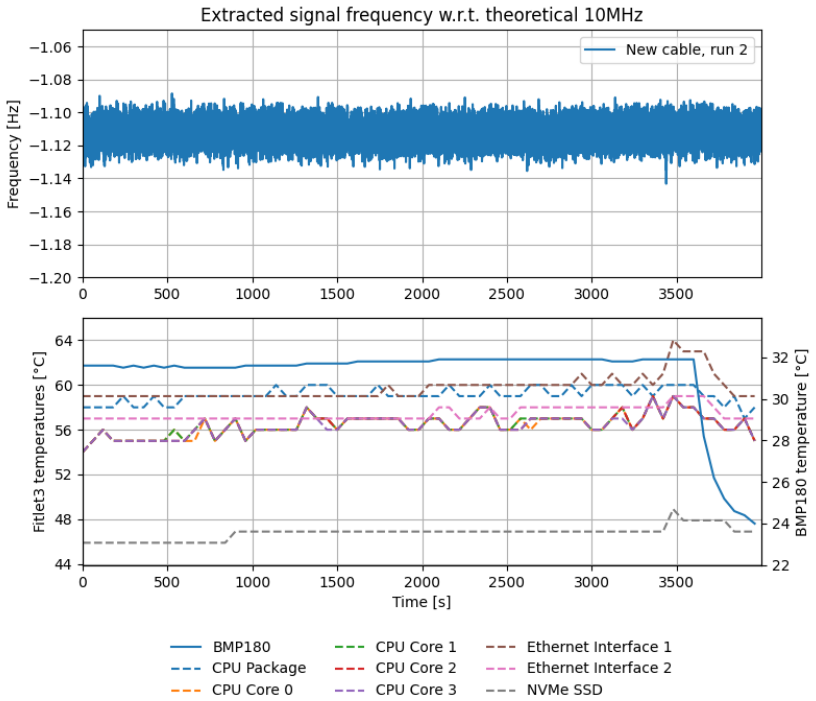

Figure 5.13: Top: Measured signal frequency with respect to the 10 MHz frequency supplied to the RSPduo input, when connecting the mini-GPS using the old cable to the SDR. Bottom: The temperatures measured in the box using the BMP180 and the internal components of the Fitlet3.

Figure 5.14 shows the overlapping Allan deviation of the measurements shown in Figures 5.11, 5.12 and 5.13. In this figure, the measurements show a shape similar to the other measurements taken with the old and new cable, which were shown in Figure 5.7 and 5.8. The the measurements using the new cable show a similar increase in stability from approximately 10^{-9} to 1×10^{-11} between $\tau = 10^{-1}$ and $\tau = 10^{3}$ s, while the measurement taken using the old cable again first has an increase in stability from about 10^{-9} to 2×10^{-10} between $\tau = 10^{-1}$ and $\tau \approx 2 \times 10^{0}$, and then a decrease in stability to about 10^{-8} at $\tau = \times 10^{3}$.

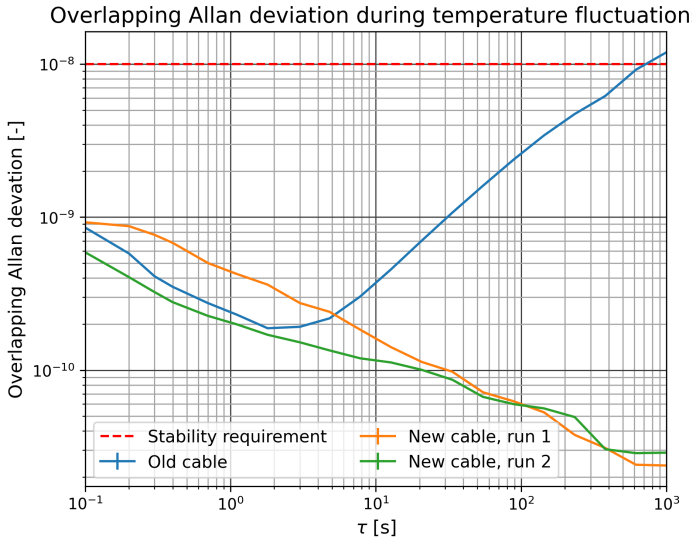

Figure 5.14: Overlapping Allan deviation of the RSPduo when subjected to temperature fluctuations. When using the new cable to connect the mini-GPS to the SDR, the stability is better than the requirement, while this is not the case when the old cable is used.

5.4. Simulated Orbit Estimation

As the RSPduo does not have any means to synchronize the time of a recording to an absolute reference, it is crucial to know how a time bias on the observations impacts the orbit estimation, and if this time bias can be estimated to reduce its impact. This section presents the results of the simulated orbit estimation analysis that addresses this topic. The figures shown in this chapter correspond to the tracking arc of three days. The same figures for the per day and per pass arcs are shown in Appendix B, together with more combinations of parameter estimations. In the following subsections, the simplest and perfect configuration should be assumed, unless otherwise specified. This means that a perfect initial guess for all estimated parameters, and only the parameters that are mentioned are estimated.

5.4.1. Constant Bias

To simplify the problem, first the results are examined when the time bias is constant, such that the bias is the same for each satellite pass in the estimation.

State Only Estimation

Figures 5.15 and 5.16 show the position and velocity error of the estimated arcs as function of the time bias, for the single and multiple stations configurations respectively. Without any bias, in the single station case the state estimation error is already on the order of a hundred meters for the simulations with the lowest noise values, and a few hundred meters for the simulations with the highest noise. For

the lowest tested time bias, the state estimation error is already several hundred meters for all range-rate noise levels. For higher time bias values, the position and velocity estimations keep increasing in the same way for the different noise values. The exception is for a the time bias of 10 seconds, in which the error for the low and medium noise cases are significantly higher between 10^7 and 10^8 meters, instead of between 10^4 and 10^5 for the high noise case. This indicates a divergence of the estimation.

In the case of multiple stations, the position and velocity estimation errors are similar to those in the single station case, with the exception being the case in which the time bias is zero. Instead of several hundreds of meters, the position error is only on the the of one to ten meters for the low noise case, while being on the order of one to several tens of meters for the medium noise case, and (several) hundred meters for the high noise case.

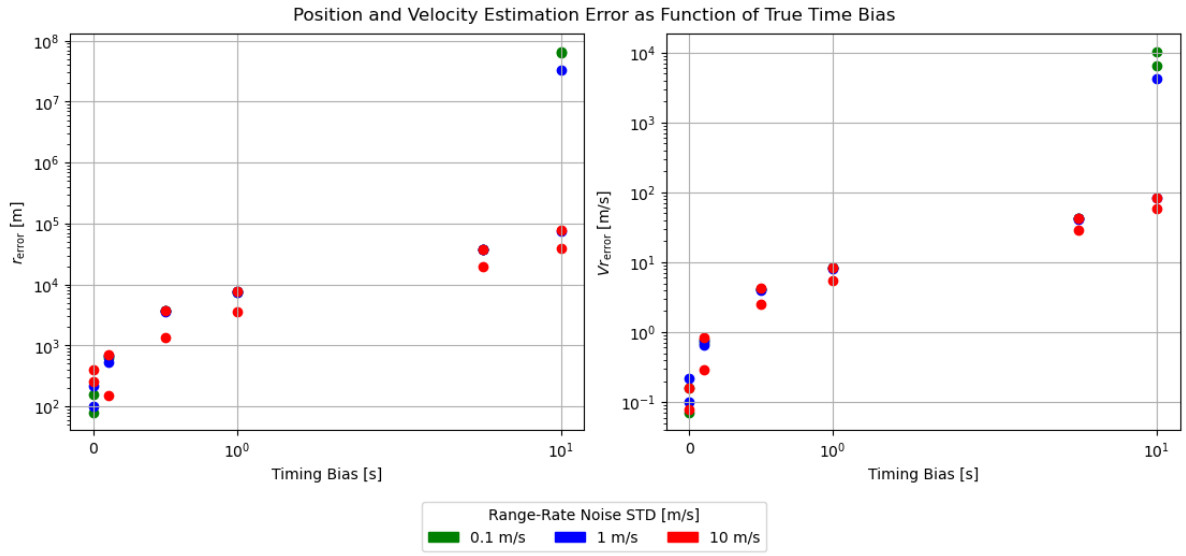

Figure 5.15: Cartesian state estimation error when using a single tracking station, with two tracking arcs of 3 days each. In this estimation, only the cartesian state is estimated.

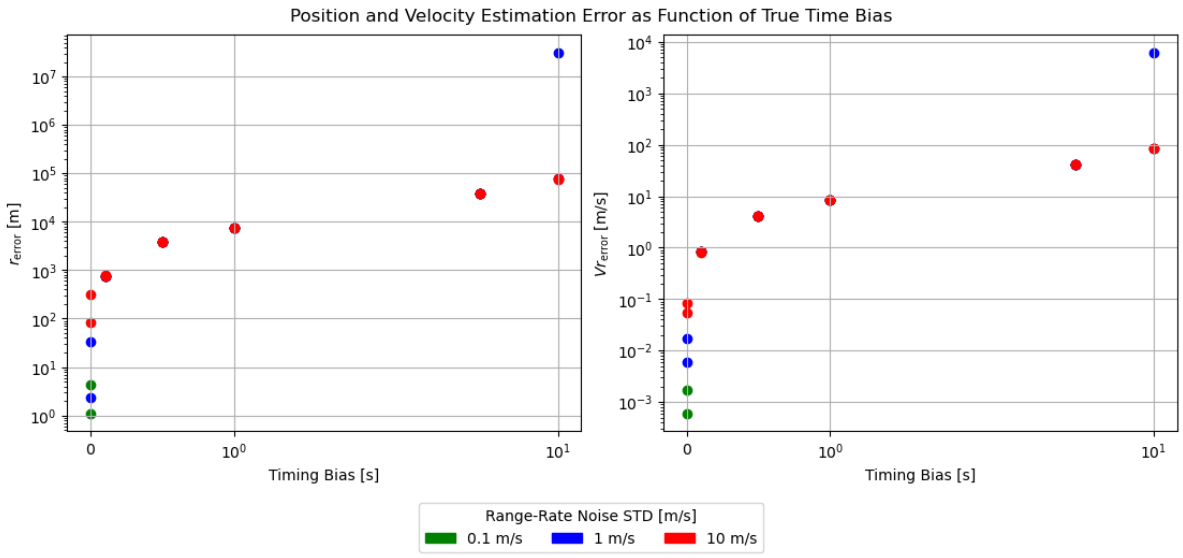

Figure 5.16: Cartesian state estimation error when using three tracking stations, with two tracking arcs of 3 days each. In this estimation, only the cartesian state is estimated.

State & Time Bias Estimation

In Figures 5.17 and 5.18, in addition to the orbital state, the time bias has been estimated as well for the single and multiple stations case, respectively.

In both the single and multiple station cases, the estimation error has become a constant as function of time, with the exception of a slight increase for 5 and 10 seconds of bias in the single station case. For the single station case, the estimation error is on the order of hundred meters in the medium noise scenario, while it is several hundreds of meters for the low and high noise scenarios. For the multiple stations case however, the state estimation error decreases with a decrease in noise, from several hundreds of meters for the high noise scenario, several tens of meters for the medium noise scenario, and about 10 meters or less for the low noise scenario.

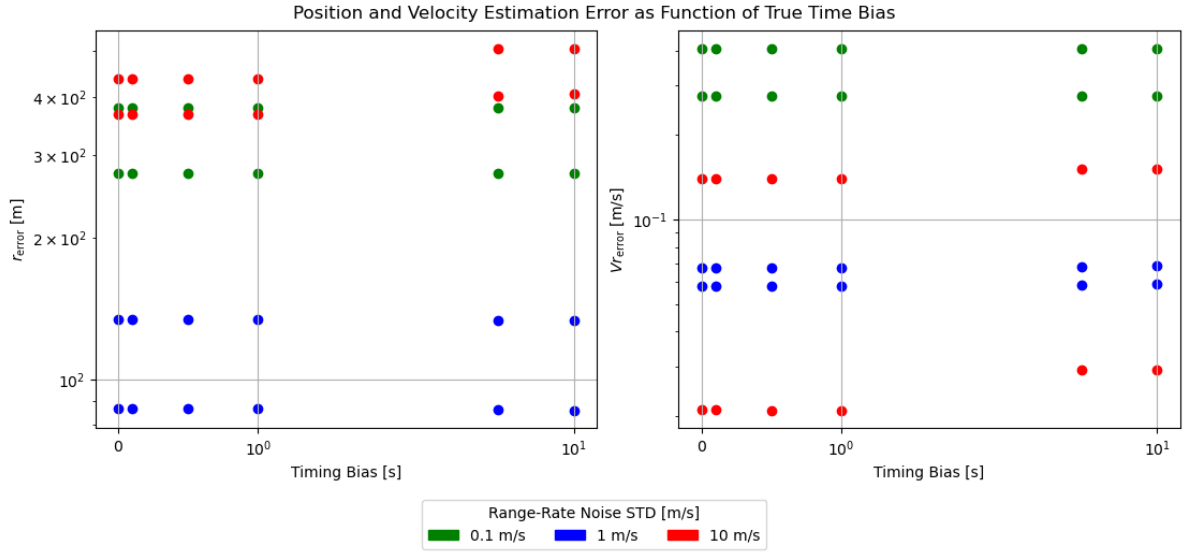

Figure 5.17: Cartesian state estimation error when using a single tracking station, with two tracking arcs of 3 days each. In this estimation, both the cartesian state, and a per pass time observation bias is estimated.

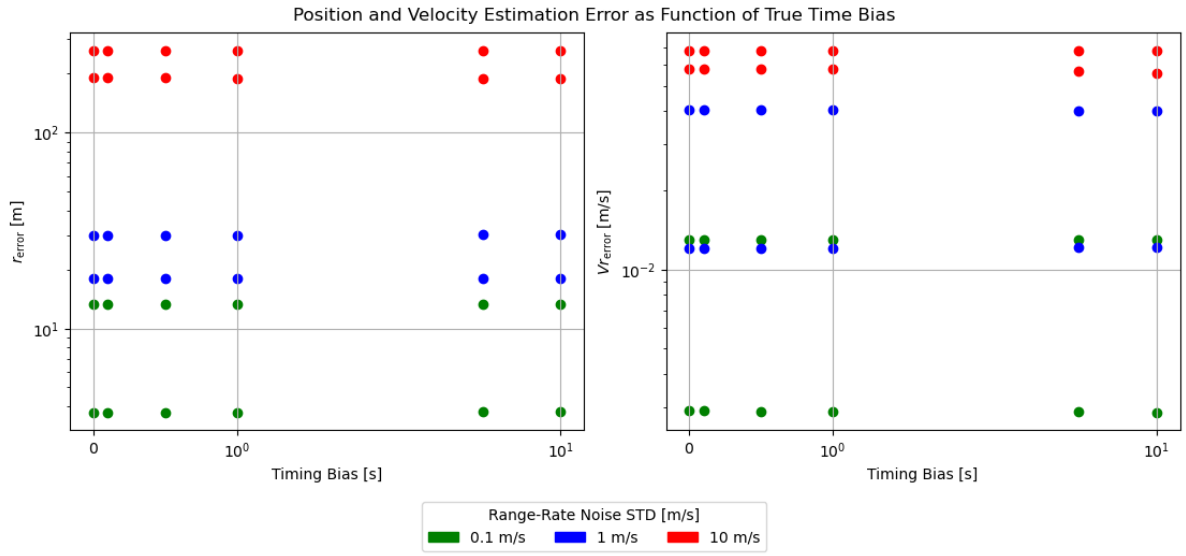

Figure 5.18: Cartesian state estimation error when using three tracking stations, with two tracking arcs of 3 days each. In this estimation, both the cartesian state, and a per pass time observation bias is estimated.

Figures 5.19 and 5.20 show the estimation error of the time bias parameters for the single and multiple case scenarios. Just like the state estimation error, in both cases the bias estimation error is constant as a function of time bias. While in the single station case the bias estimation error decreases only slightly for a decreasing range-rate noise and has significant overlap, in the multiple stations case the decrease in bias estimation error is much more pronounced.

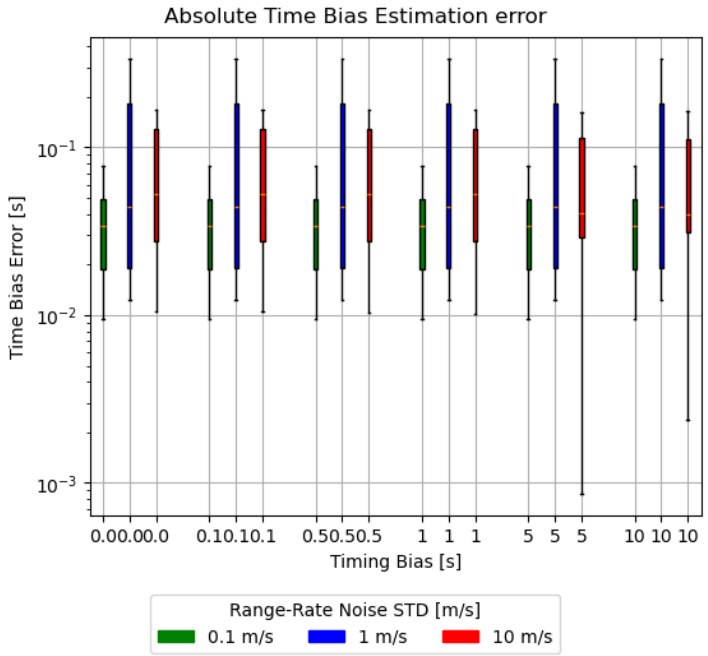

Figure 5.19: Per pass time bias estimation error, using a single tracking station, with two tracking arcs of 3 days each. In this estimation, both the cartesian state, and a per pass time observation bias is estimated.

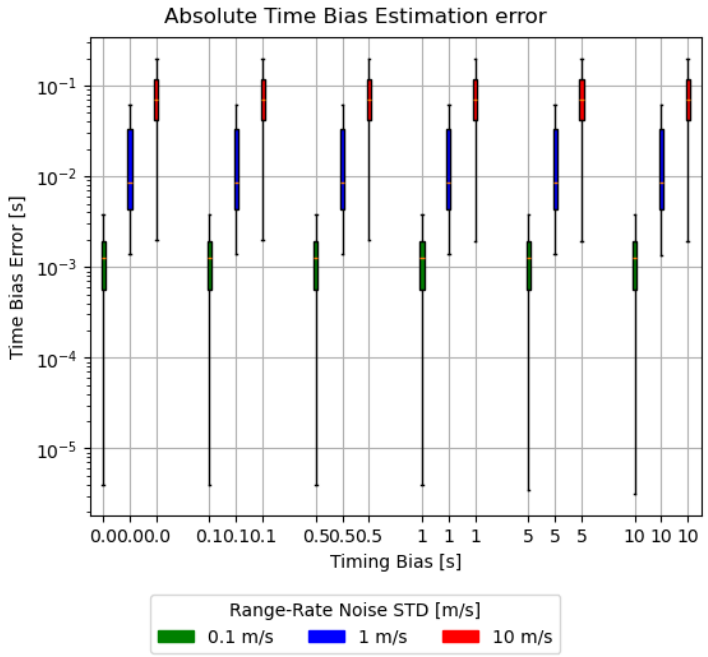

Figure 5.20: Per pass time bias estimation error, using three tracking stations, with two tracking arcs of 3 days each. In this estimation, both the cartesian state, and a per pass time observation bias is estimated.

State, Time Bias, Range-Rate Bias & Drag Estimation

Figure 5.21 shows the state estimation error in the single station case after estimating the range-rate bias and drag coefficient in addition to the time bias. While for the high noise scenario the estimation error is similar to when only the time bias was estimated, for the medium and high noise the estimation

error have decreased to approximately hundred meters and several tens of meters respectively. As the range-rate bias and drag coefficient values were set to the true values in the case they were not estimated, this decrease indicates that these parameters are absorbing some effect not related to the estimated parameter.

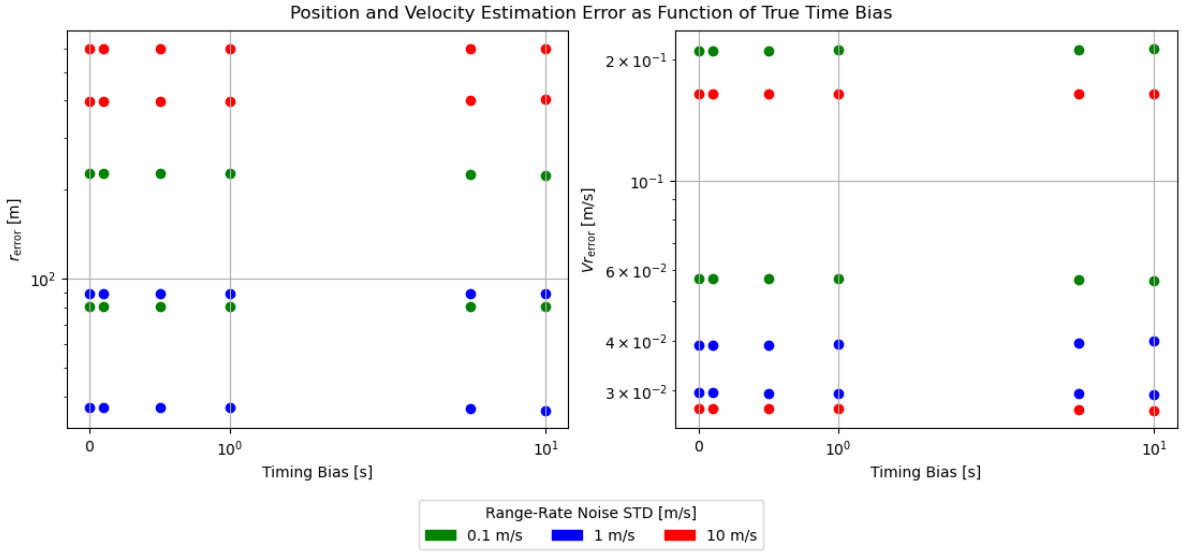

Figure 5.21: Cartesian state estimation error when using a single tracking station, with two tracking arcs of 3 days each. In this estimation, a cartesian state, and a per pass time observation bias is estimated, as well as a per arc drag parameter and per pass range-rate bias.

Figure 5.22 shows the corresponding time bias estimation error. For all three noise scenario's, both the mean and spread of the bias estimation error have increased, indicating that the range-rate bias and drag estimation cannot be independently estimated without affecting the time bias estimation.

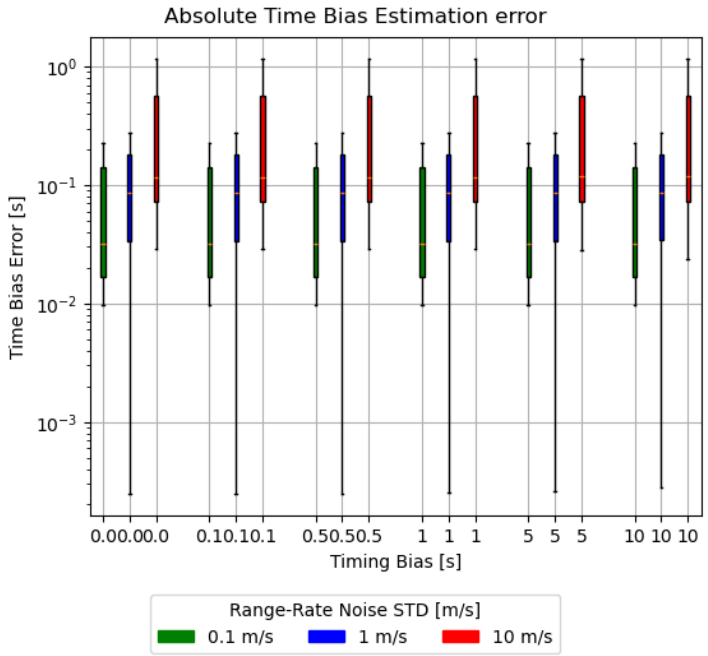

Figure 5.22: Per pass time bias estimation error, using a single tracking station, with two tracking arcs of 3 days each. In this estimation, a cartesian state, and a per pass time observation bias is estimated, as well as a per arc drag parameter and per pass range-rate bias.

Perturbed State & Time Bias Estimation

Figures 5.23 and 5.24 show the state estimation error when the state and time bias are estimated, but instead of a perfect initial guess the initial guess of the arc state was perturbed.

In the single station case of Figure 5.23, the estimation error is still approximately constant as a function of time bias, but has significantly increased compared to when the initial state was not perturbed. In the high noise scenario the state estimation error is now on the order of a kilometer, while in the medium noise scenario the estimation error is only approximately hundred meters for one arc, but several kilometers for the other. In the low noise scenario, the arcs now have an estimation error between one and 10 kilometers.

In the multiple stations case of Figure 5.24, the low noise scenario has failed to converge. While the high noise scenario has an position estimation error of several hundred meters, similar to when the initial guess was not perturbed, the medium noise scenario has a much higher position estimation error, being on the order of one to several kilometers.

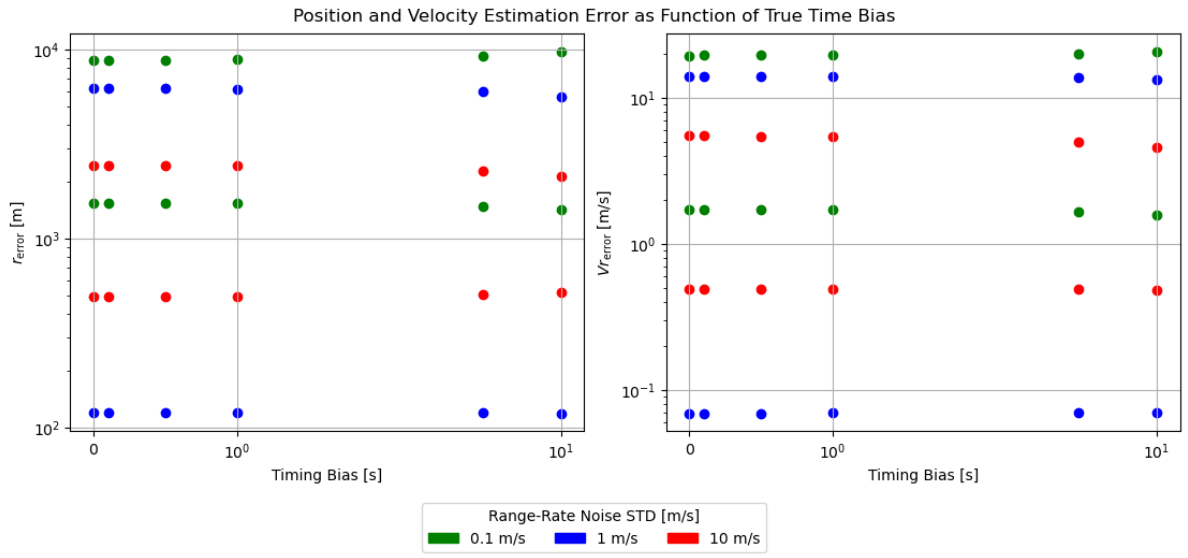

Figure 5.23: Cartesian state estimation error when using a single tracking station, with two tracking arcs of 3 days each. In this estimation, both the cartesian state, and a per pass time observation bias is estimated. For this estimation, the initial guess of the cartesian state was perturbed.

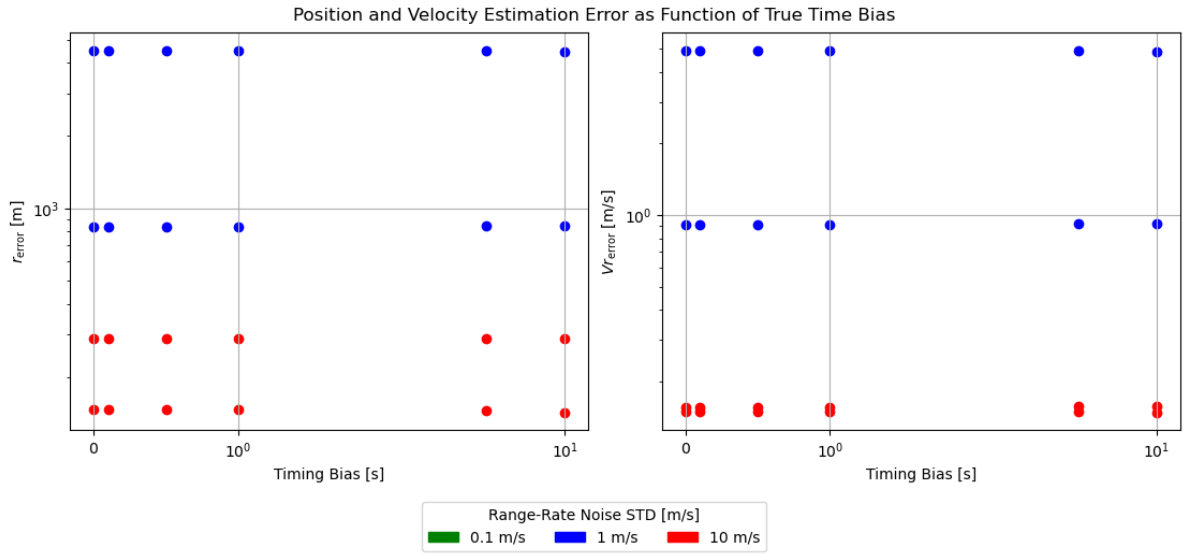

Figure 5.24: Cartesian state estimation error when using three tracking stations, with two tracking arcs of 3 days each. In this estimation, both the cartesian state, and a per pass time observation bias is estimated. For this estimation, the initial guess of the cartesian state was perturbed.

Figures 5.25 and 5.26 show the estimation error of the bias parameters for the single and multiple case scenarios. For the single station case, in all three noise scenarios the median of the time bias estimation is still on the order of a tenth of a second, but there are outliers upwards to (several) tens of seconds. The multiple station case does not have such outliers, but the median of the medium noise scenario has increased to about six tenth of a second. In the high noise scenario however, the median has decreased to below a tenth of a second.

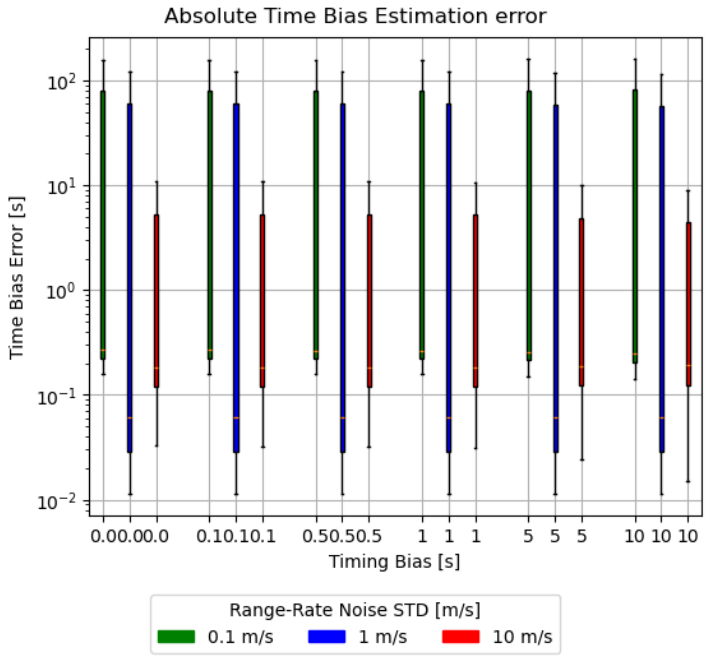

Figure 5.25: Per pass time bias estimation error, using a single tracking station, with two tracking arcs of 3 days each. In this estimation, both the cartesian state, and a per pass time observation bias is estimated. For this estimation, the initial guess of the cartesian state was perturbed.

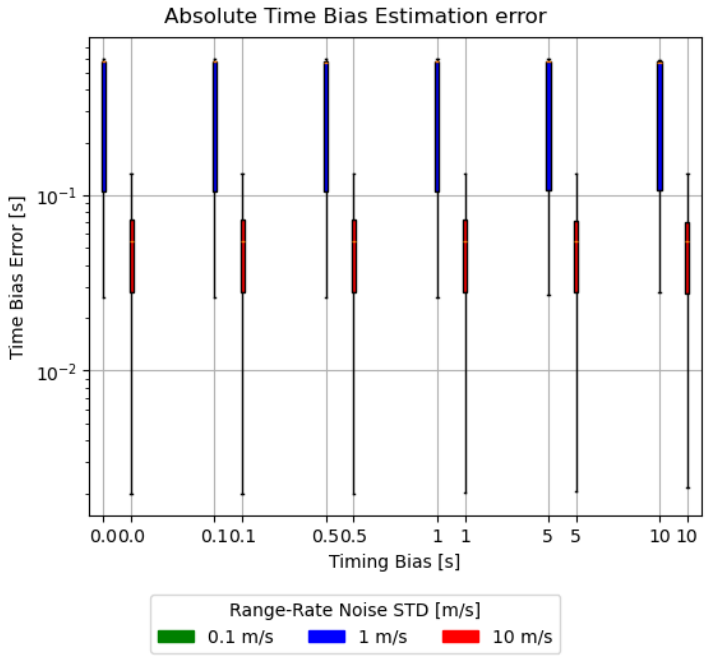

Figure 5.26: Per pass time bias estimation error, using three tracking stations, with two tracking arcs of 3 days each.In this estimation, both the cartesian state, and a per pass time observation bias is estimated. For this estimation, the initial guess of the cartesian state was perturbed.

Perturbed State & Perturbed Time Bias Estimation

Figures 5.27 and 5.28 show the state estimation error when the state and time bias are estimated, but instead of only a perturbed initial guess for the arc states, the initial value of the time bias was now set to zero.

In the single station case of Figure 5.27, the state estimation error is no longer constant over time. In fact, until 1 second of bias, the position estimation error slightly decreases in the high noise scenario. For the medium noise case there is a slight increase in state estimation error, until the estimation did not converge for 10 seconds of bias. For the low noise case, the state estimation error does stay constant as function of time bias, but did not converge for a bias of 5 seconds or higher.

In the multiple stations case of Figure 5.28, none of the low noise scenario's converged, similar to when the initial bias value was perfect. For the medium noise scenario, the estimation failed to converge for bias values of 5 seconds or higher. Below this, the state estimation error has a slight increase as function of the time bias for one of the arcs. In the high noise scenario, the position estimation error is approximately constant as function of the time bias, around several hundred meters.

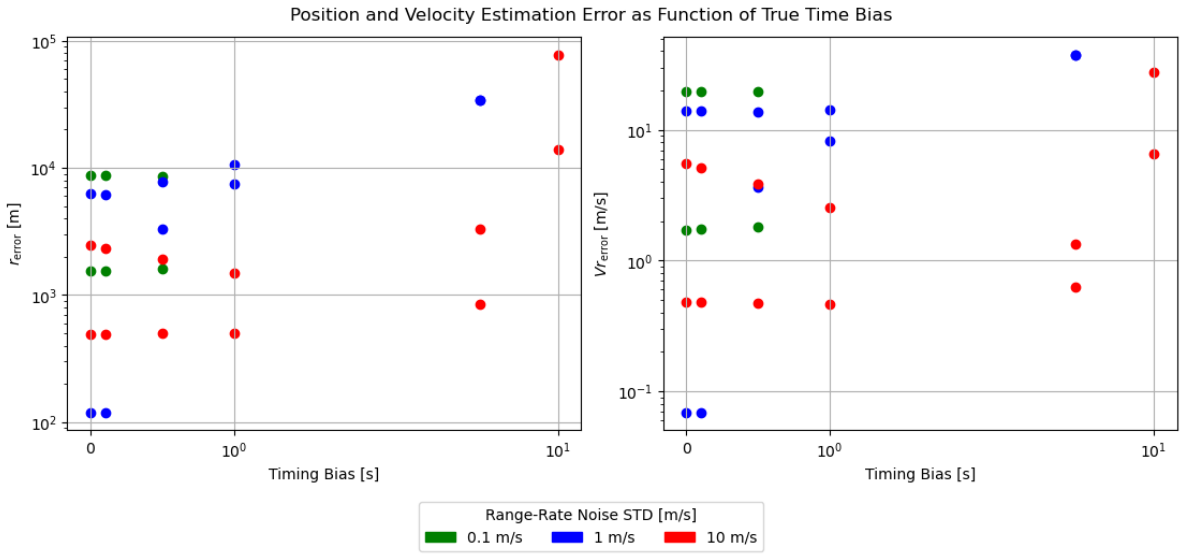

Figure 5.27: Cartesian state estimation error when using a single tracking station, with two tracking arcs of 3 days each. In this estimation, both the cartesian state, and a per pass time observation bias is estimated. For this estimation, both the initial guess of the cartesian state and the time bias were perturbed.

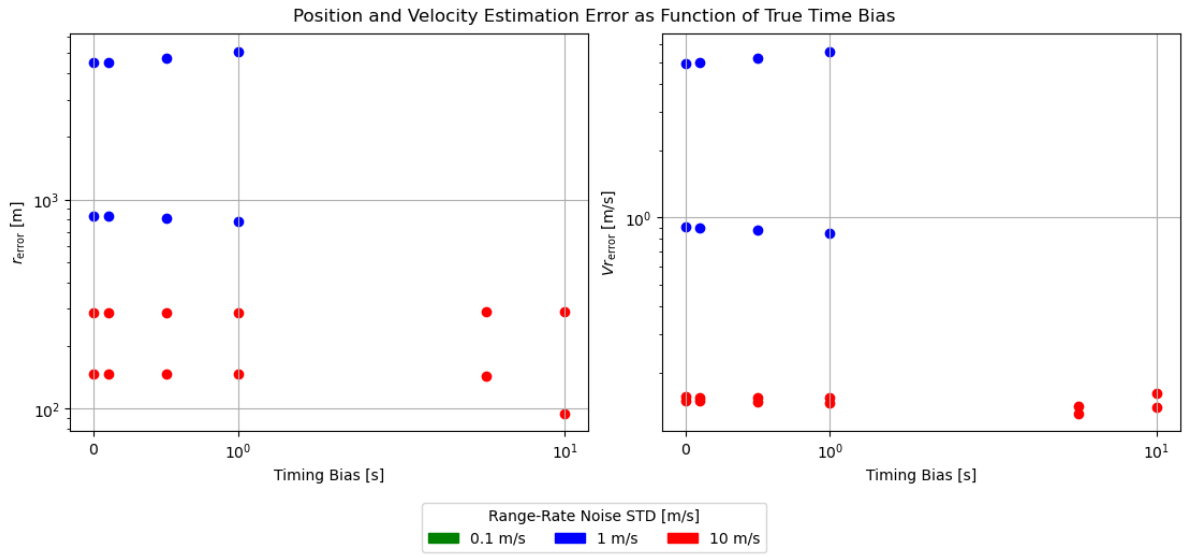

Figure 5.28: Cartesian state estimation error when using three tracking stations, with two tracking arcs of 3 days each. In this estimation, both the cartesian state, and a per pass time observation bias is estimated. For this estimation, both the initial guess of the cartesian state and the time bias were perturbed.

Figures 5.29 and 5.30 show the estimation error of the bias parameters for the single and multiple case scenarios. Similar to the state estimation error, the time bias estimation error is similar to when the initial guess of the bias was perfect, with the difference being that some of the cases have not converged.

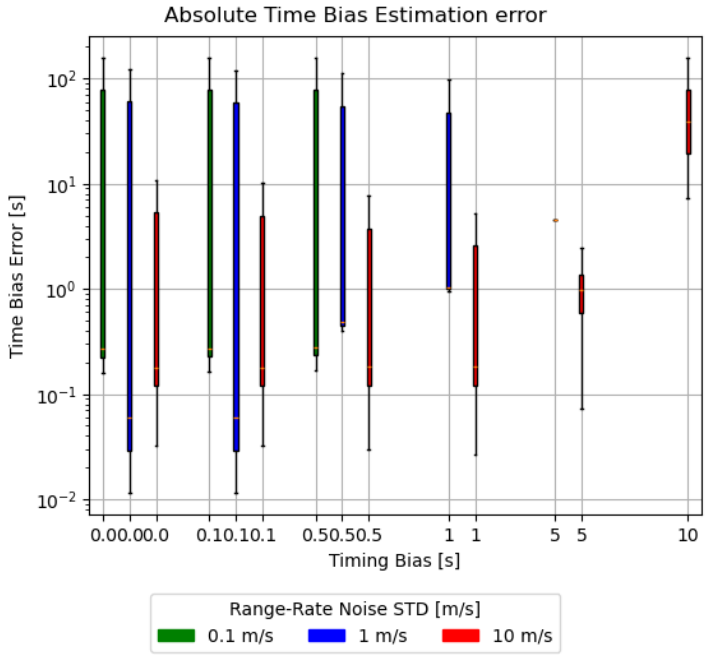

Figure 5.29: Per pass time bias estimation error, using a single tracking station, with two tracking arcs of 3 days each. In this estimation, both the cartesian state, and a per pass time observation bias is estimated. For this estimation, both the initial guess of the cartesian state and the time bias were perturbed.

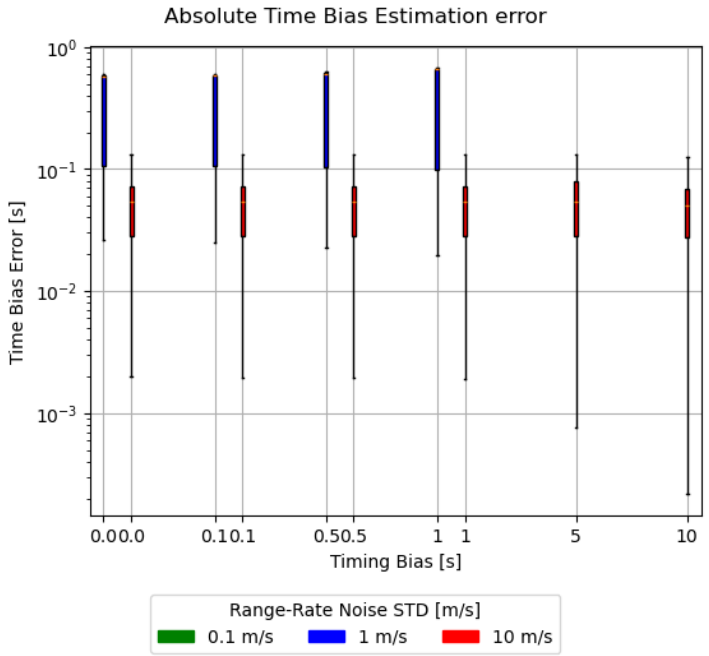

Figure 5.30: Per pass time bias estimation error, using three tracking stations, with two tracking arcs of 3 days each.In this estimation, both the cartesian state, and a per pass time observation bias is estimated. For this estimation, both the initial guess of the cartesian state and the time bias were perturbed.

5.4.2. Fluctuating Bias

As Section 5.5.2 will show that the time bias of the real system is likely on the order of one to a few seconds, with fluctuations of halve a second to a second, this section will show the simulated time bias analysis results under the assumption of a spread on the time bias of 0.5 and 1 seconds.

Perturbed State & Perturbed Time Bias Estimation

Figures 5.31 and 5.32 show the estimated state and time bias for a single tracking station with a bias spread of 1 second, respectively. These are the same as in the case no spread on the bias was applied, suggesting that a spread of 1 second does not make the time bias estimation more difficult to converge when the initial guess is already not perfect. This also holds for the same scenario with multiple tracking stations.

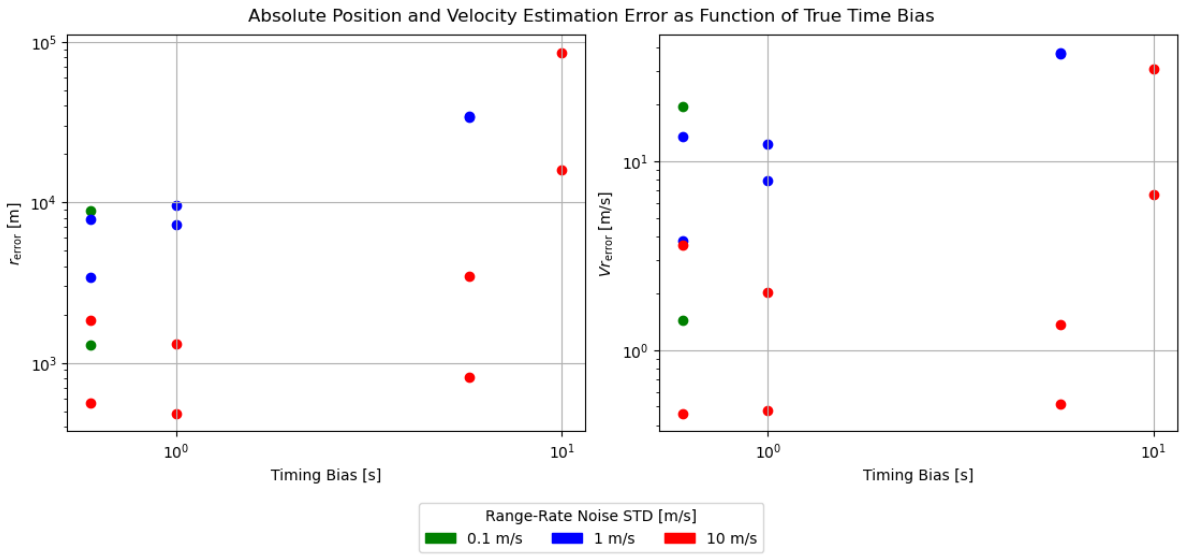

Figure 5.31: Cartesian state estimation error when using a single tracking station, with two tracking arcs of 3 days each. In this estimation, both the cartesian state, and a per pass time observation bias is estimated. For this estimation, both the initial guess of the cartesian state and the time bias were perturbed. Instead of a constant bias per pass, there was a spread on the true bias.

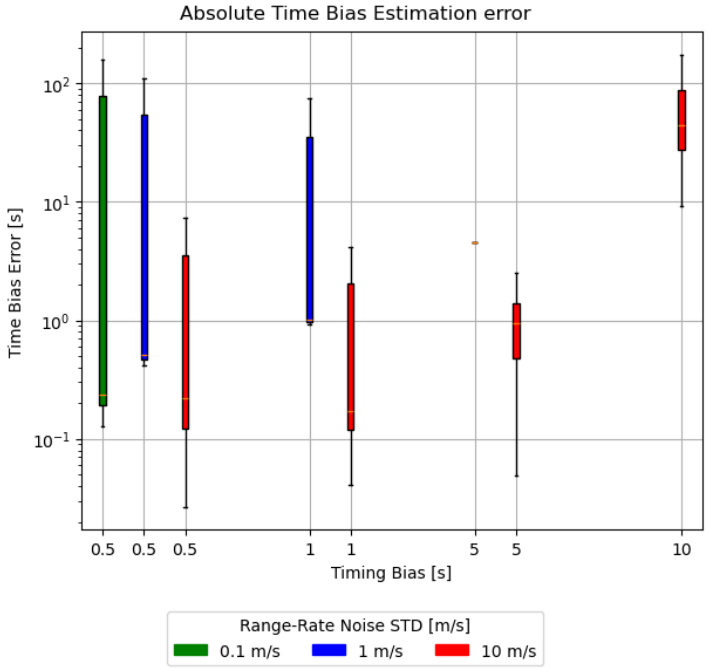

Figure 5.32: Per pass time bias estimation error, using a single tracking station, with two tracking arcs of 3 days each. In this estimation, both the cartesian state, and a per pass time observation bias is estimated. For this estimation, both the initial guess of the cartesian state and the time bias were perturbed. Instead of a constant bias per pass, there was a spread on the true bias.

To get a better overview of the influence of all effects, a summary of all estimation results shown in this section are shown in Table 5.1. The values reported in this table correspond to an assumed time bias of 1 second, and for the case of a fluctuating bias, a spread of 0.5 seconds is assumed.

Stations	Estimation	Noise [m/s]	r_{error} [m]		Vr_{error} [m/s]		Absolute Time bias error [s]				
			Arc 1	Arc 2	Arc 1	Arc 2	Q1-1.5IQR	Q1	Median	Q3	Q3+1.5IQR
Single	State Only	0.1	8×10^{3}	8×10^{3}	8×10^{0}	8×10^{0}	N/A	N/A	N/A	N/A	N/A
		1	8×10^{3}	8×10^{3}	8×10^{0}	8×10^{0}	N/A	N/A	N/A	N/A	N/A
		10	3×10^{3}	8×10^{3}	8×10^{0}	8×10^{0}	N/A	N/A	N/A	N/A	N/A
	State & Time Bias	0.1	3×10^{2}	4×10^{3}	3×10^{-1}	4×10^{-1}	1×10^{-2}	2×10^{-2}	3×10^{-2}	5×10^{-2}	8×10^{-2}
		1	9×10^{1}	1×10^{2}	6×10^{-2}	7×10^{-2}	1×10^{-2}	2×10^{-2}	4×10^{-2}	2×10^{-1}	3×10^{-1}
		10	4×10^{1}	4×10^{1}	2×10^{-2}	1×10^{-1}	1×10^{-2}	3×10^{-2}	5×10^{-2}	1×10^{-1}	2×10^{-1}
	State, Time Bias, Range-Rate Bias & Drag	0.1	8×10^{1}	2×10^{2}	6×10^{-2}	2×10^{-1}	1×10^{-2}	2×10^{-2}	3×10^{-2}	1×10^{-1}	2×10^{-1}
		1	4×10^{1}	9×10^{1}	3×10^{-2}	4×10^{-2}	3×10^{-4}	3×10^{-2}	8×10^{-2}	2×10^{-1}	3×10^{-1}
		10	4×10^{2}	6×10^{2}	3×10^{-2}	2×10^{-1}	3×10^{-2}	7×10^{-2}	1×10^{-1}	6×10^{-1}	1×10^{0}
	Perturbed State & Time Bias	0.1	1×10^{3}	9×10^{3}	2×10^{0}	2×10^{1}	1×10^{-1}	2×10^{-1}	1×10^{-1}	8×10^{1}	2×10^{2}
		1	1×10^{2}	6×10^{3}	7×10^{-2}	1×10^{1}	1×10^{-2}	3×10^{-2}	6×10^{-2}	6×10^{1}	1×10^{2}
		10	5×10^{2}	2×10^{3}	5×10^{-1}	5×10^{0}	3×10^{-2}	1×10^{-1}	2×10^{-1}	5×10^{0}	1×10^{-1}
	Perturbed State & Perturbed Time Bias	0.1	N/A	N/A	N/A	N/A	N/A	N/A	N/A	N/A	N/A
		1	7×10^{3}	1×10^{4}	8×10^{0}	1×10^{1}	1×10^{0}	1×10^{0}	1×10^{0}	5×10^{1}	1×10^{2}
		10	5×10^{2}	1×10^{3}	5×10^{-1}	3×10^{0}	3×10^{-2}	1×10^{-1}	2×10^{-1}	3×10^{0}	6×10^{0}
	Perturbed State & Perturbed Time Bias (fluctuating bias)	0.1	N/A	N/A	N/A	N/A	N/A	N/A	N/A	N/A	N/A
		1	7×10^{3}	1×10^{4}	8×10^{0}	1×10^{1}	2×10^{0}	1×10^{0}	1×10^{0}	4×10^{1}	7×10^{1}
		10	5×10^{2}	1×10^{3}	5×10^{-1}	2×10^{0}	4×10^{-2}	1×10^{-1}	2×10^{-1}	2×10^{0}	4×10^{0}
Multiple	State Only	0.1	8×10^{3}	8×10^{3}	8×10^{0}	8×10^{0}	N/A	N/A	N/A	N/A	N/A
		1	8×10^{3}	8×10^{3}	8×10^{0}	8×10^{0}	N/A	N/A	N/A	N/A	N/A
		10	8×10^{3}	8×10^{3}	8×10^{0}	8×10^{0}	N/A	N/A	N/A	N/A	N/A
	State & Time Bias	0.1	4×10^{0}	1×10^{1}	3×10^{-3}	1×10^{-2}	4×10^{-5}	6×10^{-4}	1×10^{-3}	2×10^{-3}	4×10^{-3}
		1	2×10^{1}	3×10^{1}	1×10^{-2}	4×10^{-2}	1×10^{-3}	4×10^{-3}	8×10^{-2}	3×10^{-2}	6×10^{-2}
		10	2×10^{1}	3×10^{2}	6×10^{-2}	7×10^{-2}	2×10^{-3}	4×10^{-2}	7×10^{-2}	1×10^{-1}	2×10^{-1}
	Perturbed State & Time Bias	0.1	N/A	N/A	N/A	N/A	N/A	N/A	N/A	N/A	N/A
		1	8×10^{2}	4×10^{3}	9×10^{-1}	5×10^{0}	3×10^{-2}	1×10^{-1}	6×10^{-1}	6×10^{-1}	6×10^{-1}
		10	1×10^{2}	3×10^{2}	2×10^{-1}	2×10^{-1}	2×10^{-3}	3×10^{-2}	5×10^{-2}	7×10^{-2}	1×10^{-1}
	Perturbed State & Perturbed Time Bias	0.1	N/A	N/A	N/A	N/A	N/A	N/A	N/A	N/A	N/A
		1	8×10^{2}	5×10^{3}	8×10^{-1}	6×10^{0}	2×10^{-2}	1×10^{-1}	6×10^{-1}	6×10^{-1}	6×10^{-1}
		10	1×10^{2}	3×10^{2}	2×10^{-1}	2×10^{-1}	2×10^{-3}	3×10^{-2}	5×10^{-2}	6×10^{-2}	1×10^{-1}

Table 5.1: A summary overview of the cartesian state and time bias estimation errors using different estimation settings, for a simulated time bias of 1 second. The arcs are sorted from lowest to highest error. A row containing "N/A" for all estimation errors means the estimation did not converge, while a a row of "N/A" in only the time bias estimation means the time bias was not estimated for that estimation configuration. The reported time bias errors are the median error, the first and third quartile, and 1.5 times the interquartile range below the first, and above the third quartile.

5.5. DopTrackBox Prototype Data

This section contains the results gathered during the operational phase of the DopTrackBox prototype. Section 5.5.1 shows the temperature behavior of the prototype, while Section 5.5.2 analyzes the satellite recording data obtained using the prototype.

5.5.1. Temperatures

Figure 5.33 shows the hourly mean temperature measured inside the box against the KNMI measured air temperature in Voorschoten during the period of continuous prototype operations on the roof. A Pearson's correlation of $r = 0.81$ was found between these two variables. In addition, the measured temperatures inside the box are always equal to or higher than the outside temperature, with the exception of the outlier around 18°C. For increasing temperatures, the spread of the box temperatures increases as well. Moreover, on average, the mean temperature difference between the outside air and box temperature seems to increase from about 7 degrees at air temperatures around 10°C to around 10 to 12 degrees for air temperatures around 25°C and beyond. On 10 occasions, spread out over 4 days (August 11, 12, 13 and 19), the temperature threshold of 40°C was surpassed, triggering an automatic sleep mode for an hour. On these occasions, the outside air temperature was between 23 and 30°C.

Figure 5.34 shows the measured internal temperatures against the KNMI dew point temperatures. From this figure it becomes apparent that although the temperature has always been higher than the dewpoint temperature, on some occasions, the internal temperature has been less than two degrees above the dewpoint temperature.

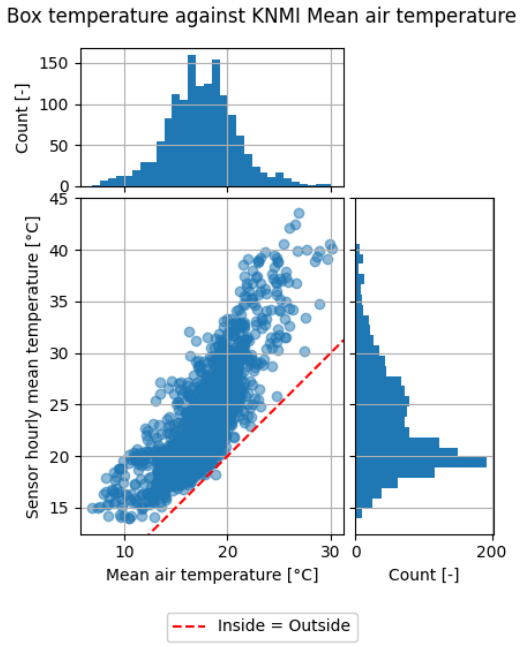

Figure 5.33: Measured internal DopTrackBox temperature using the BMP180 sensor, against the hourly mean temperature in Voorschoten, as measured by the KNMI.

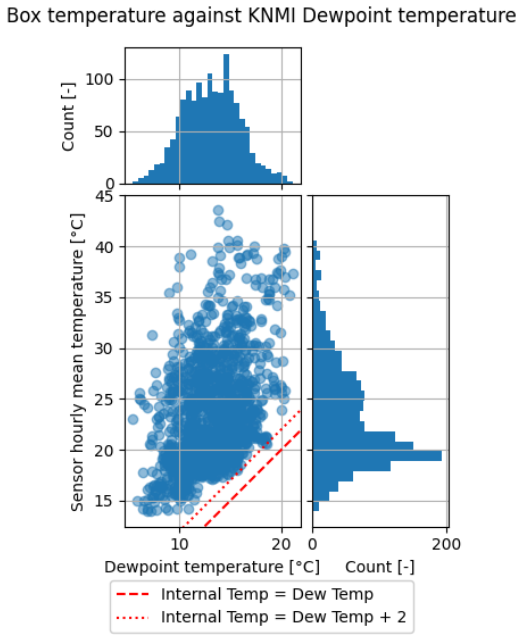

Figure 5.34: Measured internal DopTrackBox temperature using the BMP180 sensor, against the hourly mean dewpoint temperature in Voorschoten, as measured by the KNMI.

Figure 5.35 shows the internal box temperature against the KNMI hourly cloud coverage fraction, measured in eights. A value of 9 indicates an invisible sky. There is an anti-correlation of -0.15 between these variables. Furthermore, it becomes apparent that most of the hours were fully or almost fully clouded, followed by fully clear skies.

Figure 5.36 shows the internal box temperature against the KNMI hourly sunshine duration. These two variables are positively correlated by 0.58. Similar to the cloud coverage, most of the hours had no sunshine, followed by hours with continuous sunshine.

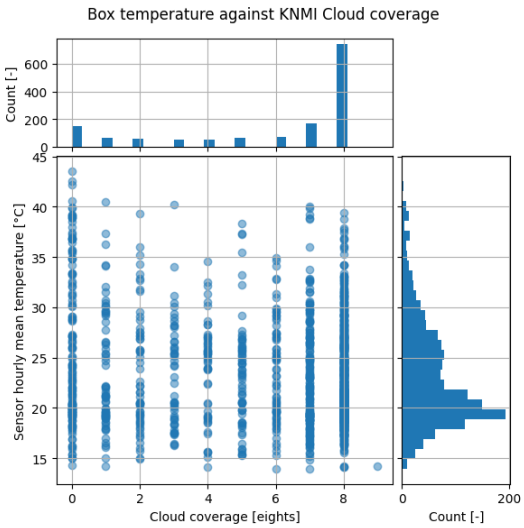

Figure 5.35: Measured internal DopTrackBox temperature using the BMP180 sensor, against the hourly mean cloud coverage in Voorschoten, as measured by the KNMI.

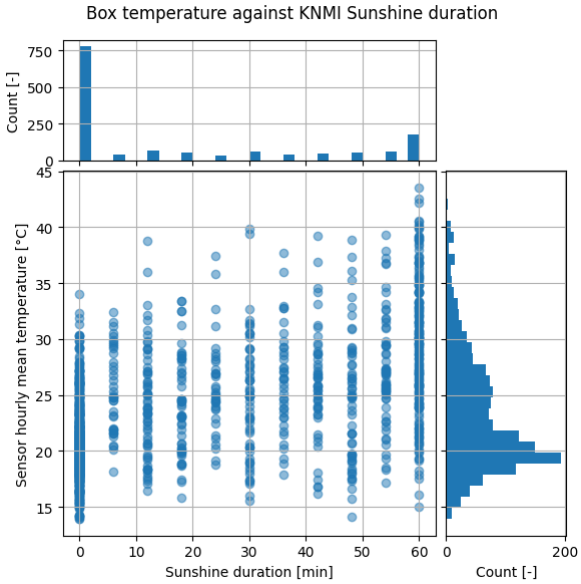

Figure 5.36: Measured internal DopTrackBox temperature using the BMP180 sensor, against the hourly mean dewpoint temperature in Voorschoten, as measured by the KNMI.

Figure 5.37 shows the internal box temperature against the KNMI hourly precipitation duration. From this figure it becomes clear that most hours had no or less than 5 minutes of rain. In addition, none of the hours with any rain had an internal temperature with more than 30 degrees.

Figure 5.38 shows the internal box temperature against the KNMI hourly average windspeed. From this figure it becomes apparent that high internal temperatures typically occurred during hours with a low to moderate average windspeed.

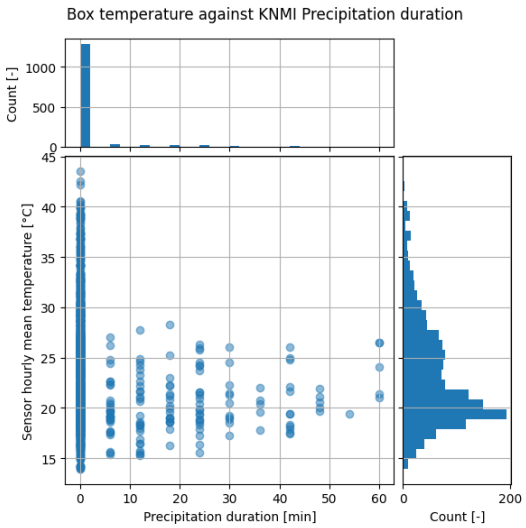

Figure 5.37: Measured internal DopTrackBox temperature using the BMP180 sensor, against the hourly precipitation duration in Voorschoten, as measured by the KNMI.

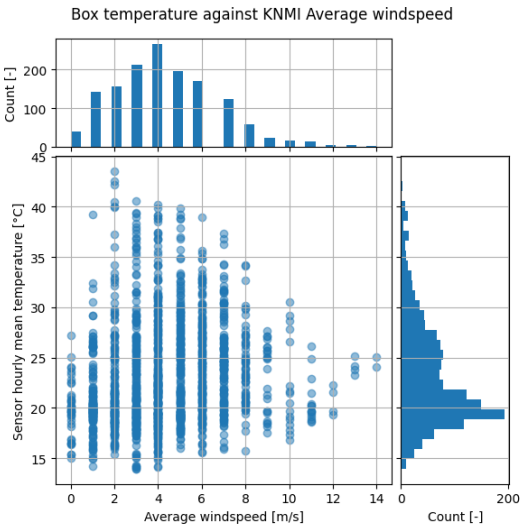

Figure 5.38: Measured internal DopTrackBox temperature using the BMP180 sensor, against the hourly mean windspeed in Voorschoten, as measured by the KNMI.

Figure 5.39a shows a histogram of the CPU package temperature of the Fitlet3 computer. The temperatures typically range between 40 and 80°C, with a minimum of 31°C, and a maximum of 91°C. As such, the critical temperature of 105°C has not been surpassed. Similarly, figure 5.39b shows a histogram of the highest temperature core for each timestamp. The distribution is similar to that of the package, but has a minimum of 27°C, while having the same maximum of 91°C. This also means that none of the cores has surpassed its critical temperature of 105°C.

Figure 5.39c shows the temperature at the interface of the internal data storage device of the Fitlet3. The minimum and maximum are 19°C and 54°C, although the clear peak at 54 indicates that this might be the maximum temperature the sensor is able to output.

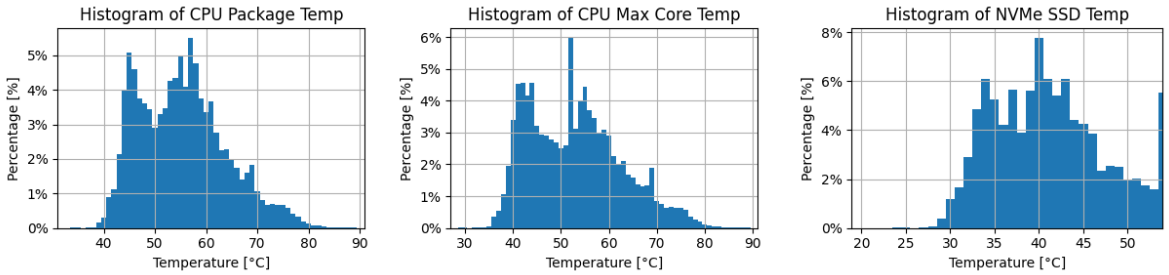

(a) CPU Package **(b)** CPU Core with highest temperature **(c)** NVMe SSD interface

Figure 5.39: Distribution of the temperature of several internal components of the Fitlet3.

Figures 5.40a, 5.40b and 5.40c show the temperatures of the Fitlet3's two Ethernet interfaces and WIFI interface, respectively. All three interfaces show clear peaks in the temperatures, indicating some measured values seem to be "preferred" over others. In addition, there is a bit more spread on the temperatures of interface 1 than interface 2 and the WIFI interface. With maximum temperatures of 87, 80 and 83°C, none of the interfaces have surpassed their critical level of 100°C.

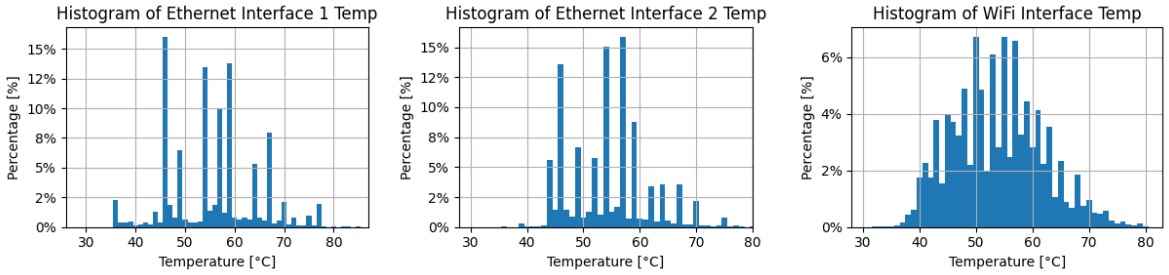

(a) Ethernet interface 1 **(b)** Ethernet interface 2 **(c)** WIFI interface

Figure 5.40: Distribution of the temperature of several internal components of the Fitlet3.

5.5.2. Satellite Recordings

Shortly after the start of the operational phase, it became apparent that the signal of the intended comparison satellite, FUNcube-1, was not as strongly visible in the data as expected. Therefore, 15 different additional satellites have been recorded for various periods in time, summarized in table 5.2. In total, 646 satellite passes have been recorded, 258 of which are from the FUNcube-1 satellite. The only satellites for which passes have been recorded in which an extractable signal was present are

NOAA-15, NOAA-19 and FUNcube-1.

Satellite Name	Recording Start	Recording End	Number of Passes	Extractable Data?
FUNcube-1	25-07	07-10	258	Yes
NOAA-2	30-07	10-08	38	No
NOAA-9	30-07	10-08	25	No
NOAA-15	30-07	19-08	47	yes
NOAA-19	30-07	10-08	40	yes
ESEO	30-07	07-08	22	No
FOX-1B	30-07	09-08	20	No
ISS	01-08	08-08	12	No
RIDU-Sat-1	31-07	08-08	21	No
TRANSIT5B-5	30-07	08-08	14	No
VELOX-PII	01-08	08-08	21	No
SONATE-2	30-07	08-08	14	No
DIWATA-2	08-08	27-08	37	No
JY1Sat	09-08	26-08	31	No
Z-Sat	09-08	27-08	46	No

Table 5.2: An overview of the recorded satellite passes using DopTrackBox.

Spectrograms

Figures 5.41, 5.42 and 5.43 show a spectrogram of a recorded pass for the NOAA-15, NOAA-19 and FUNcube-1 satellites respectively. The NOAA-15 and NOAA-19 passes contain signal of the Automatic Picture Transmission (APT) system of the satellites. The transmitted images are first amplitude modulated on a 2400 Hz subcarrier, which is then frequency modulated on the carrier frequency around 137 MHz, with a 34 kHz bandwidth. As such, the full signal does not fit into the 20 kHz window. The recorded FUNcube-1 signal consists of a Binary Phase Shift Keying telemetry signal modulated on a carrier frequency of about 145.935 MHz.

In all three spectrograms, the signal-to-noise ratio colorbar is clipped between the mean and mean plus three standard deviations to allow for a better visual contrast in the spectrogram. As a consequence, the peak signal-to-noise ratio thus could be higher than what is indicated in the colorbar.

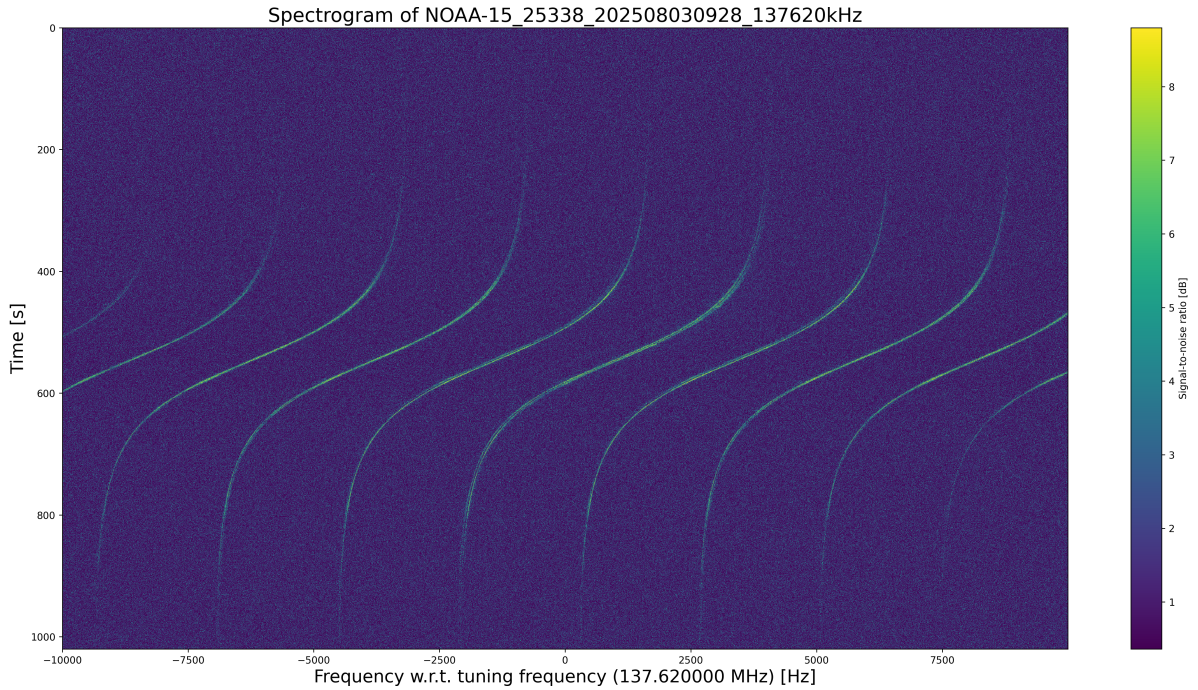

Figure 5.41: Spectrogram of satellite pass NOAA-15_25338_202508030928 as recorded by DopTrackBox. The colorbar is clipped between the mean and the mean plus three standard deviations for better visual contrast.

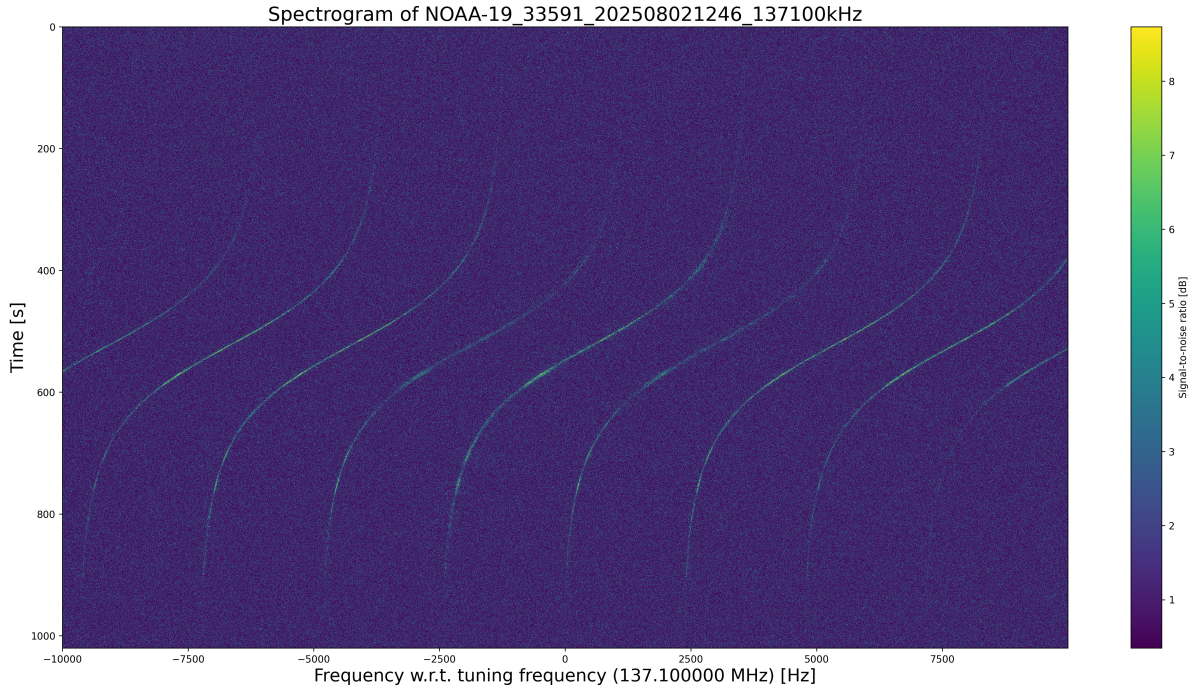

Figure 5.42: Spectrogram of satellite pass NOAA-19_33591_202508021246 as recorded by DopTrackBox. The colorbar is clipped between the mean and the mean plus three standard deviations for better visual contrast.

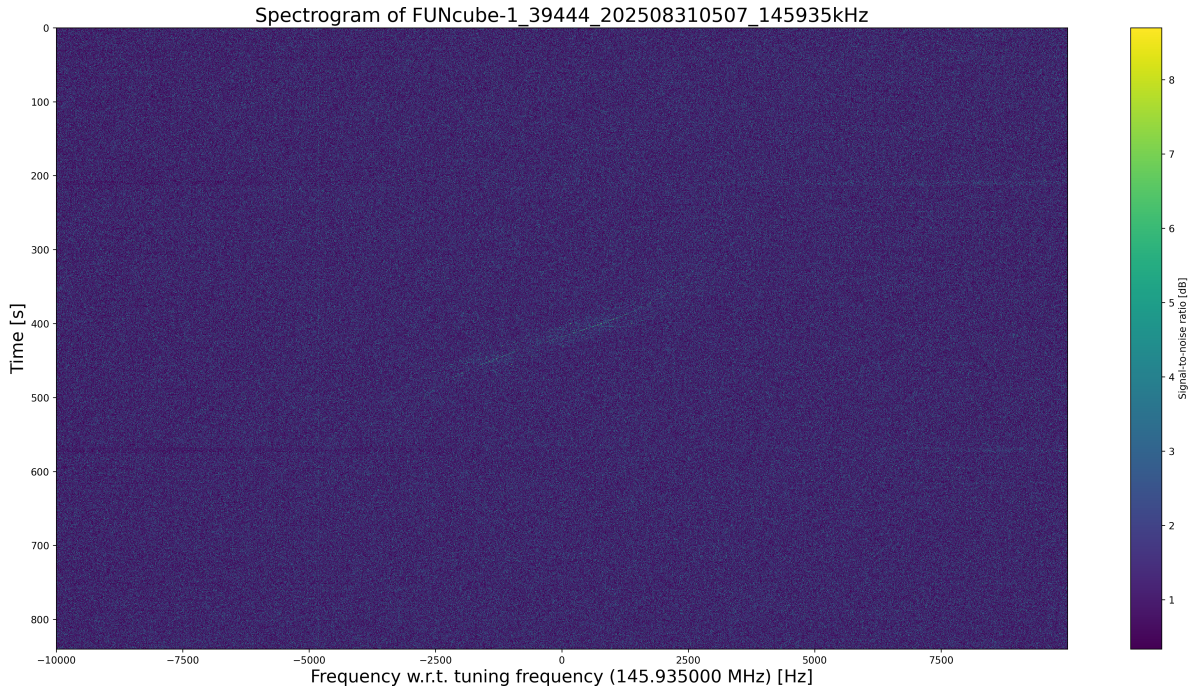

Figure 5.43: Spectrogram of satellite pass FUNcube-1_39444_202508310507 as recorded by DopTrackBox. The colorbar is clipped between the mean and the mean plus three standard deviations for better visual contrast.

Extracted Signal

To demonstrate the result of the signal frequency extraction algorithm, Figures 5.44, 5.45 and 5.46 show the extracted signal frequency as function of time, for the passes shown in Figures 5.41, 5.42 and 5.43. From these figures it can be seen that around the TCA, the signal has the highest signal-to-noise ratio, and the least amount of noise points are extracted instead of real signal, but the further in time from the TCA, the less strong the signal becomes and more noise points have been selected.

In the NOAA satellite passes, the algorithm sometimes tends to converge to a fit in which one part of hyperbolic tangent matches well to one sideband, while in another part of the hyperbolic tangent it matches well to another sideband. An example of this is shown in figure 5.47. As the FUNcube-1 signal does not have such sidebands, this does not pose an issue for the remainder of the analysis in this thesis.

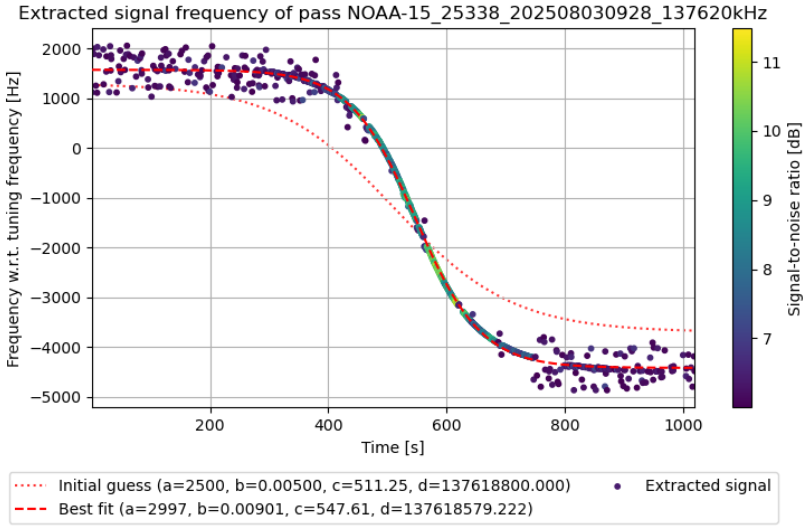

Figure 5.44: Extracted signal frequency of pass NOAA-15_25338_202508030928, recorded by DopTrackBox.

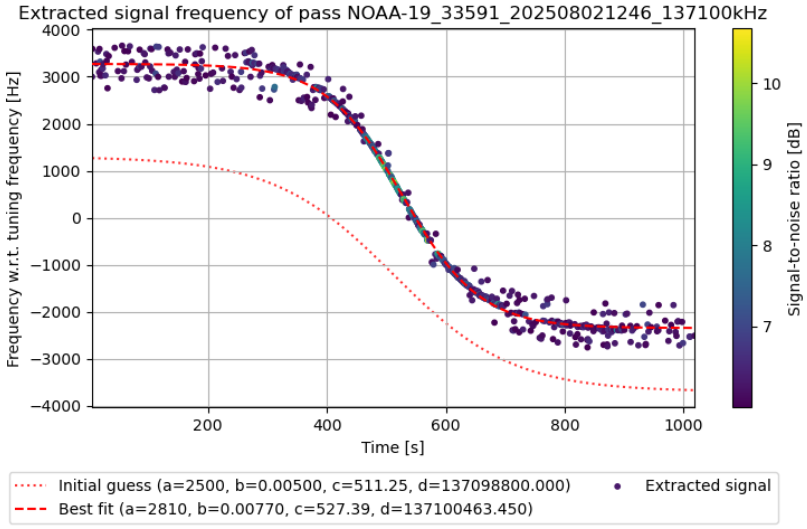

Figure 5.45: Extracted signal frequency of pass NOAA-19_33591_202508021246, recorded by DopTrackBox.

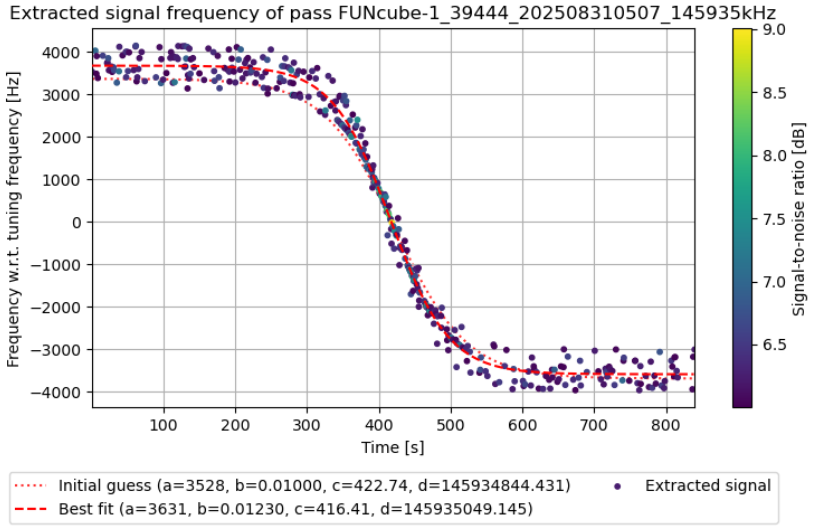

Figure 5.46: Extracted signal frequency of pass FUNcube-1_39444_202508310507, recorded by DopTrackBox.

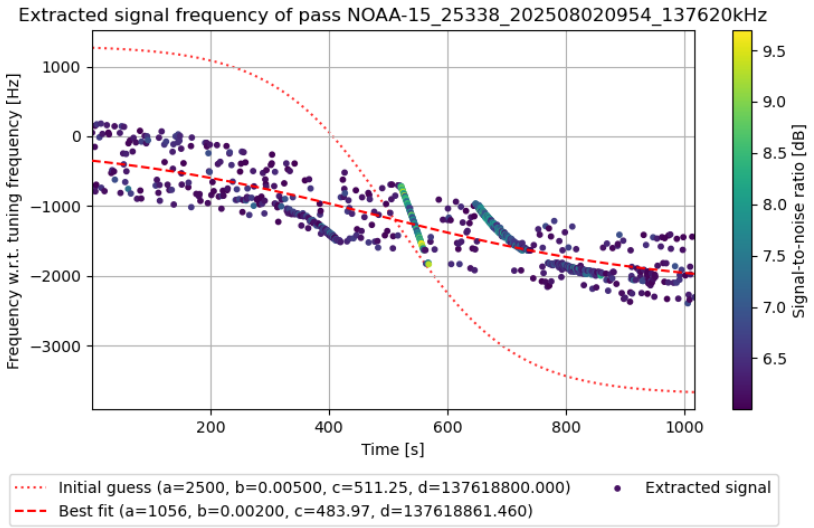

Figure 5.47: A failed signal extraction of pass NOAA-15_25338_202508020954, recorded by DopTrackBox.

As the signal-to-noise ratio of FUNcube-1 passes is lower than expected, most of the extractions do not contain any useful FUNcube-1 signal. For the analyses in the coming sections, the datasets that are used will therefore be listed.

Signal-to-noise ratio comparison with DopTrack

Figure 5.48 and 5.49 show the spectrogram and extracted signal of the same FUNcube-1 pass as in the previous section, but recorded by DopTrack. From these figures it might already seen that the signal is stronger than when recorded by DopTrackBox, and the extracted signal frequency contains FUNcube-1 signal for a longer duration with respect to the TCA. This difference becomes even clearer in Figure 5.50, where the signal-to-noise ratio of the extracted FUNcube-1 signal for DopTrack and DopTrackBox are shown together. While DopTrack achieves a peak SNR of about 19 dB, DopTrackBox achieves

only about 9 dB. This is equivalent to a 10 signal with 10 times more power in DopTrack compared to DopTrackBox. The lower bound of 6 dB on all datapoints is artificial and originates from the 6dB cut on the signal-to-noise that was used to aid in the distinction between selecting signal and noise points.

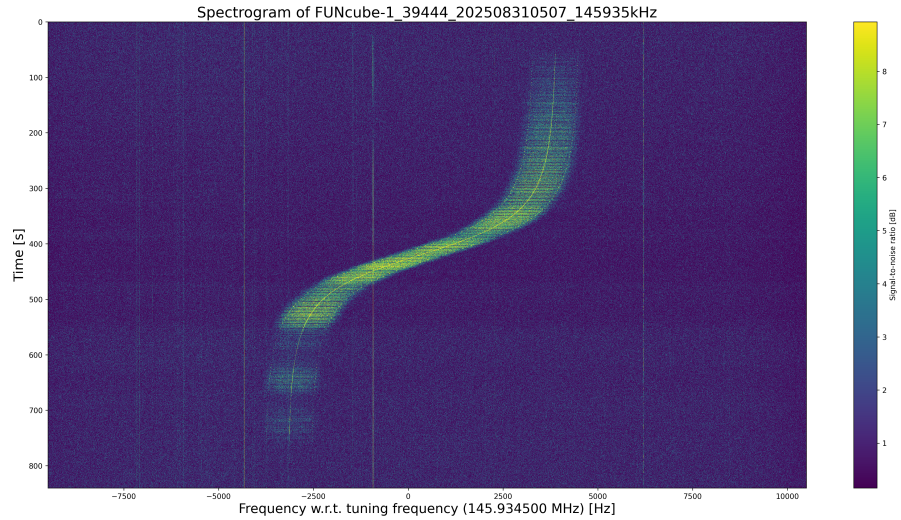

Figure 5.48: Spectrogram of satellite pass FUNcube-1_39444_202508310507 as recorded by DopTrack. The colorbar is clipped between the mean and the mean plus three standard deviations for better visual contrast.

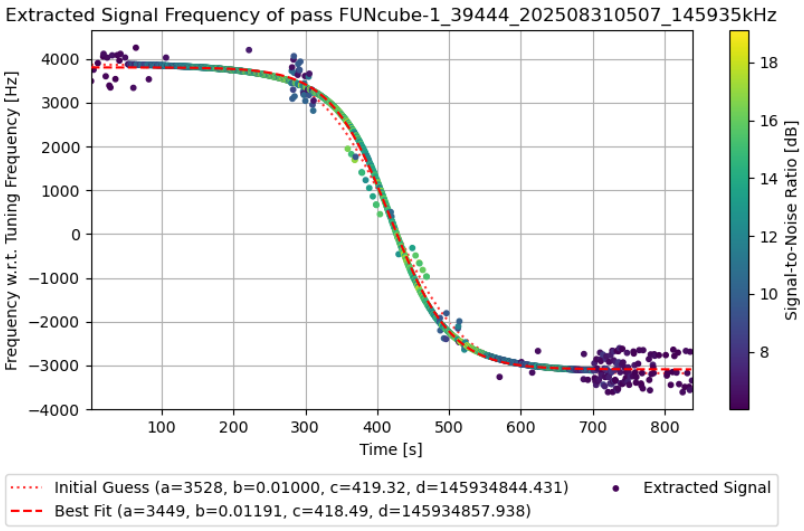

Figure 5.49: Extracted Signal Frequency of pass FUNcube-1_39444_202508310507, recorded by DopTrack.

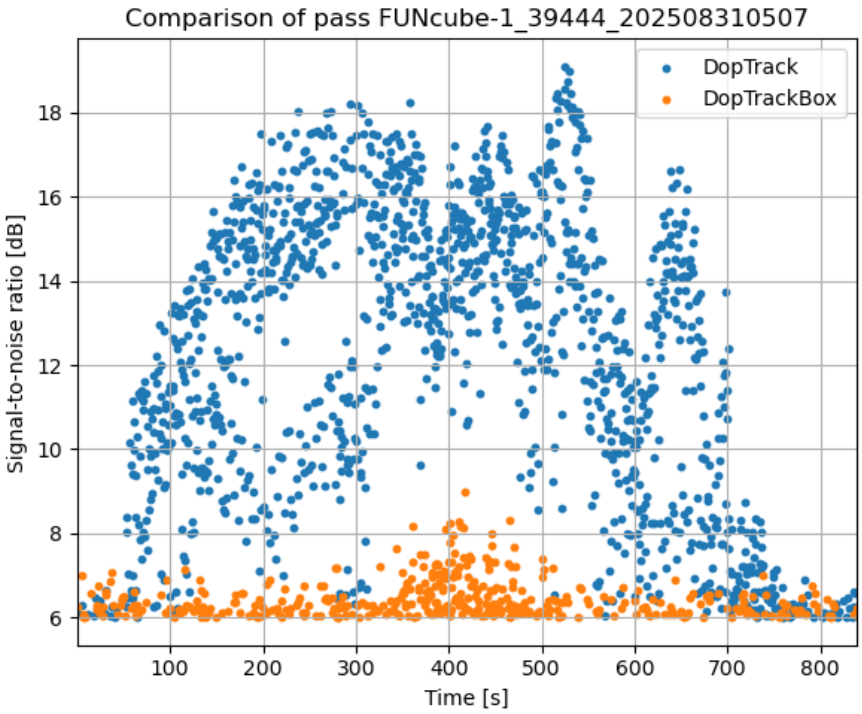

Figure 5.50: Signal-to-noise ratio comparison between DopTrack and DopTrackBox for pass FUNcube-1_39444_202508310507.

This has been repeated for multiple passes in which there is some extracted DopTrackBox signal. The mean and peak signal-to-noise ratios of these passes recorded by the DopTrack and DopTrackBox systems, and the difference between them are shown in Table 5.3. The identifier represents the month, day, hour and minute part the recording label

The mean over all passes of the mean signal-to-noise ratio of the DopTrack recordings is 10.93 dB with a standard deviation of 0.99 dB. For DopTrackBox this is a mean of 6.30 with a standard deviation of 0.05. This indicates that many of the DopTrackBox recordings likely have a very limited amount of actual signal points, making the mean signal-to-noise ratio of 4.63 dB between DopTrack and DopTrackBox not a useful quantity.

The mean of the peak signal-to-noise ratio of the passes recorded by DopTrack is 17.23 dB with a standard deviation of 1.28 dB. For DopTrackBox this mean is 7.80 dB with a standard deviation of 0.52 dB. Te resulting mean difference between the peak signal-to-noise ratio of these systems is 9.44 dB, with a standard deviation of 1.28 dB. Based on this table there seems to only be a weak influence of the pass elevation on the peak signal-to-noise ratio of the recordings, but this was not investigated during this thesis.

		Mean [dB]			Peak [dB]		
Identifier	**Elevation [deg]**	$\mathbf{SNR_{DT}}$	$\mathbf{SNR_{DTB}}$	$\mathbf{\Delta SNR}$	$\mathbf{SNR_{DT}}$	$\mathbf{SNR_{DTB}}$	$\mathbf{\Delta SNR}$
08281604	78	10.50	6.30	4.20	16.08	8.36	7.71
08300509	71	12.31	6.37	5.95	18.97	8.58	10.39
08301600	85	10.10	6.35	3.75	17.21	8.83	8.38
08310507	67	12.33	6.46	5.87	19.10	9.01	10.10
09010505	63	12.30	6.39	5.90	19.67	8.38	11.29
09020502	59	12.12	6.25	5.88	18.64	7.13	11.51
09040458	53	12.12	6.29	5.84	18.71	7.60	11.11
09050455	49	12.01	6.26	5.75	18.03	7.39	10.64
09051546	65	9.36	6.26	3.09	15.11	7.36	7.76
09060453	46	11.89	6.24	5.64	18.43	7.36	11.07
09070450	44	11.67	6.27	5.40	18.11	7.52	10.59
09080448	41	11.49	6.26	5.23	17.54	7.16	10.38
09100443	37	11.24	6.25	4.99	17.22	7.31	9.91
09111532	45	9.71	6.26	3.45	15.06	7.36	7.70
09160428	26	11.06	6.29	4.78	16.64	8.15	8.49
09160603	34	11.06	6.33	4.73	17.90	7.79	10.11
09161519	34	9.26	6.27	2.99	16.05	7.81	8.24
09170425	25	10.60	6.33	4.26	16.59	7.83	8.76
09170600	36	10.71	6.30	4.41	18.02	7.39	10.63
09171517	32	9.88	6.24	3.63	16.49	8.21	8.29
09171652	26	9.72	6.27	3.46	15.60	7.88	7.72
09180423	23	10.88	6.33	4.55	16.47	8.41	8.06
09180558	38	10.84	6.28	4.57	17.77	7.16	10.61
09190420	22	10.86	6.33	4.54	16.30	7.80	8.50
09200418	21	10.13	6.31	3.83	15.74	7.28	8.46
09210550	46	10.91	6.33	4.58	17.72	7.84	9.88
09211641	33	9.03	6.27	2.75	15.17	7.35	7.82
09220547	49	12.01	6.35	5.65	18.13	8.03	10.10
Mean		10.93	6.30	4.63	17.23	7.80	9.44
STD		0.99	0.05	0.97	1.28	0.52	1.28

Table 5.3: The mean and peak signal-to-noise ratio of recorded FUNcube-1 passes by both DopTrack and DopTrackBox, and the difference between them.

Time-bias with respect to DopTrack

The extracted signal of the previously shown FUNcube-1 recording by DopTrackBox is now shown together with the recording made and processed using the DopTrack system in Figure 5.51. The time is with respect to DopTrack's estimate of t_{start}. For this figure, DopTrackBox's start time was assumed to be t_1. Close to the midpoint of the S-curve, it can be seen that the DopTrackBox points do not fully overlap with the DopTrack points, and seem to be shifted with respect to each other by a time bias, frequency bias, or both. The datapoints that are likely to be real signal points, rather than noise points can be recognized from the frequency difference plot. The real signal points are clustered together in a slight V-shape, in this case between approximately 0 and -90 Hz, while the noise plots are more spread

out among the figure. When the DopTrackBox start time is assumed to be $t_{\text{start, DTB}}$ the figure changes to Figure 5.52.

In this case, the lack of overlap is now on the other side of the DopTrackBox signal, and the frequency difference of the signal points has swapped from being negative to being positive, suggesting that recomputing DopTrackBox's start time as as $t_{\text{start, DTB}}$ overshoots the time bias, or there is a frequency bias, or both. In case the time bias is overshot, this would suggest that the assumption that the delay at the end of the recording is negligible with respect to the delay at the start of the recording is incorrect.

Instead of a peak frequency difference of the signal around -90 Hz, the V-shape has inverted, and the peak frequency difference has now changed to approximately +70 Hz. As the frequency difference of the signal points is not a flat line, nor is it centered around a difference of zero, it is likely that there is both time and frequency bias.

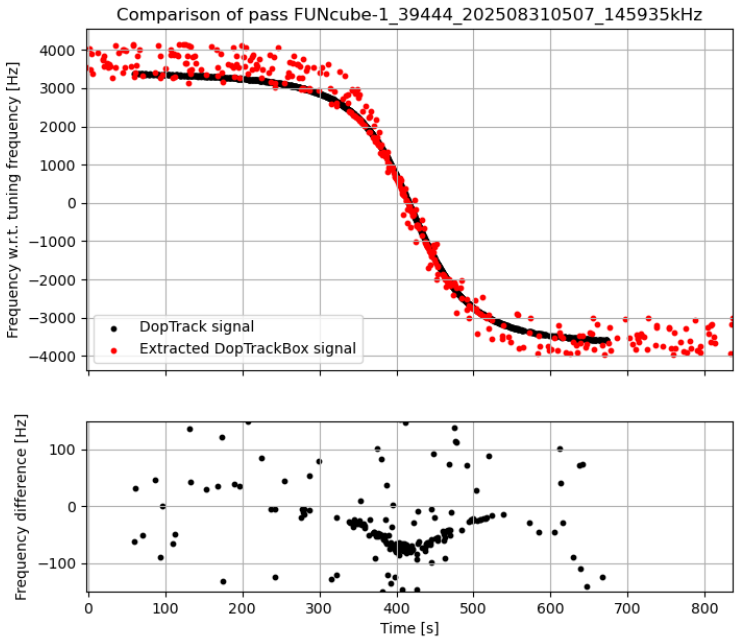

Figure 5.51: Comparison of the extracted signal frequency between DopTrack and DopTrackBox for pass FUNcube-1_39444_202508310507, when using t_1 as DopTrackBox recording start time.

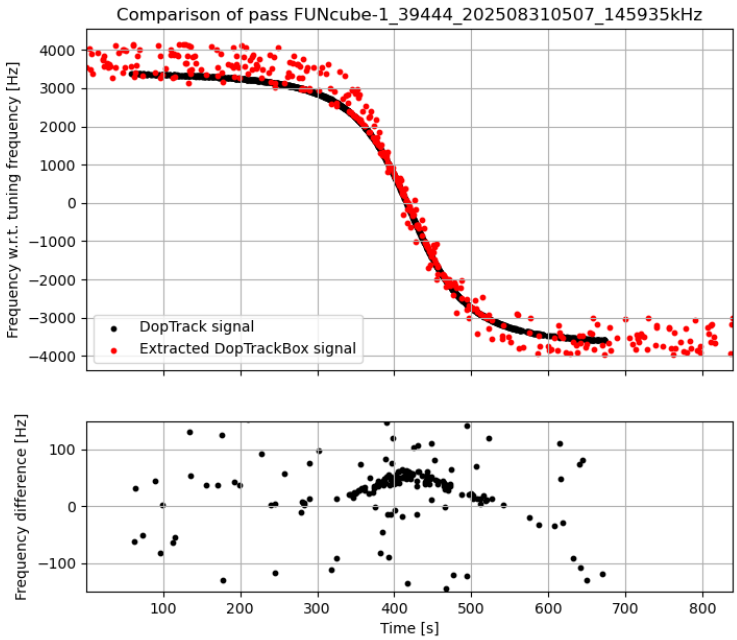

Figure 5.52: Comparison of the extracted signal frequency between DopTrack and DopTrackBox for pass FUNcube-1_39444_202508310507, when using t_{start} as DopTrackBox recording start time.

After estimating a time bias and frequency on the DopTrackBox points 180 seconds before and after the DopTrack TCA estimate, the resulting frequency comparisons when using either $t_{1,\,\text{DTB}}$ or $t_{\text{start},\,\text{DTB}}$ as DopTrackBox start time are in Figures 5.53 and 5.54. When the frequency bias was also estimated using these datasets, the model converged to the scenario in which all the DopTrackBox data is as vertically centered on the DopTrack data as possible. As there is still a significant amount of noise datapoints, the resulting frequency bias estimate does not necessarily correspond to the best overlap between the real signal points. Therefore, the frequency bias estimate was forced at zero.

Compared to when the time bias was not estimated, the peak frequency difference has shrunk from approximately -90 to -70 Hz when using $t_{1,\,\text{DTB}}$ as start time, and kept the same magnitude but swapped sign from approximately $+70$ to -70 Hz when using $t_{\text{start},\,\text{DTB}}$. In both cases the characteristic V-shape has remained similar to what it was before.

The estimated time biases are -0.41 and 2.44 s when using t_1 or t_{start} respectively. These estimated biases will be referred to as Δt_1 and Δt_{start}. The difference in the estimated bias corresponds to the difference between the values of t_1 and t_{start} (2.86 s) to within 0.01 s. This shows that the two estimations converged to essentially the same best estimate in terms of frequency difference between DopTrack and DopTrackBox.

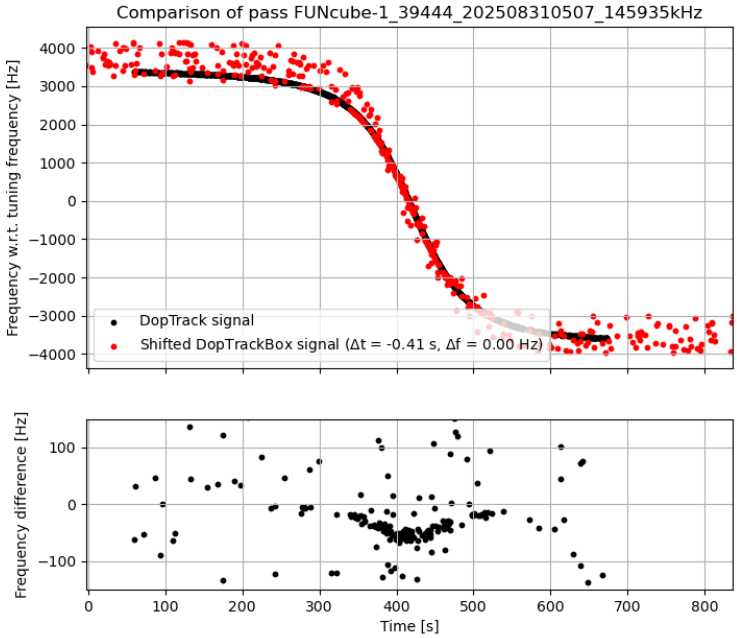

Figure 5.53: Comparison of the shifted DopTrackBox signal with the DopTrack signal for pass FUNcube-1_39444_202508310507, after estimating a time bias, when using t_1 as DopTrackBox recording start time.

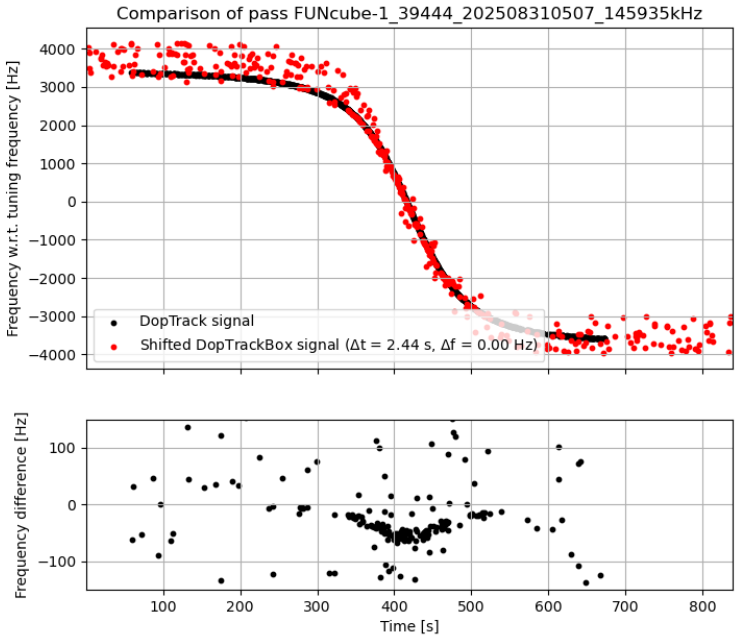

Figure 5.54: Comparison of the shifted DopTrackBox signal with the DopTrack signal for pass FUNcube-1_39444_202508310507, after estimating a time bias, when using t_{start} as DopTrackBox recording start time.

After removing the DopTrackBox datapoints that are more than 150 Hz from the DopTrack points and

repeating the time and frequency bias estimation, the previous two figures become Figures 5.55 and 5.56. Instead of of having a peak frequency difference of approximately -70 Hz, the peak frequency differences are now only about -20 Hz when using $t_{1,\,\text{DTB}}$ as DopTrackBox start time, and approximately $+20$ when using $t_{\text{start,\,DTB}}$. In addition, instead of a clear characteristic V-shape, in both cases the frequency difference is now flatter and the points are more spread out instead of being line-like. This is indicative of a more realistic time bias estimation. Yet, in both cases all signal points seem to have frequency either below, or above 0, respectively. This means that that the time and frequency bias estimations are not as good as they could be.

The estimated time biases are -1.46 and 0.88 s when using t_1 and t_{start} respectively. This means that when t_1 the estimated time bias has now increased by 1.05 s, compared to when more datapoints were used in the estimation, while when using t_{start} the bias has decreased by 1.56 s. In addition, the difference between the bias estimations is 2.34, which is smaller then the difference in time between t_1 and t_{start}, which is to be expected as the frequency difference pattern was not the same, indicating a difference in the best solution found by the estimation. Furthermore, this can also be seen from the frequency bias estimate, as this is 3.16 Hz when using t_1 as start time, but 4.73 Hz when using t_{start}.

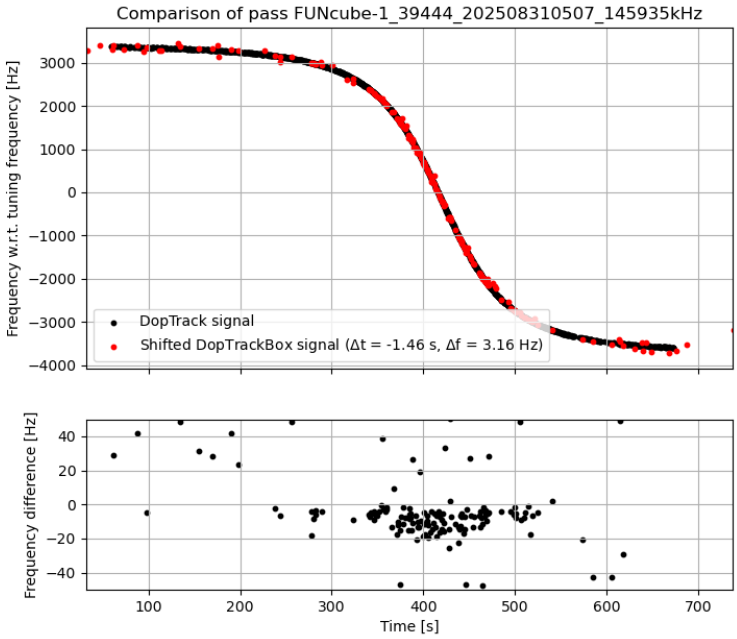

Figure 5.55: Comparison of the shifted DopTrackBox signal with the DopTrack signal for pass FUNcube-1_39444_202508310507, after estimating a time and frequency bias, when using t_1 as DopTrackBox recording start time. Only the DopTrackBox datapoints with less than 150 Hz difference with respect to DopTrack have been used in the estimation to reduce the effect of extracted noise datapoints.

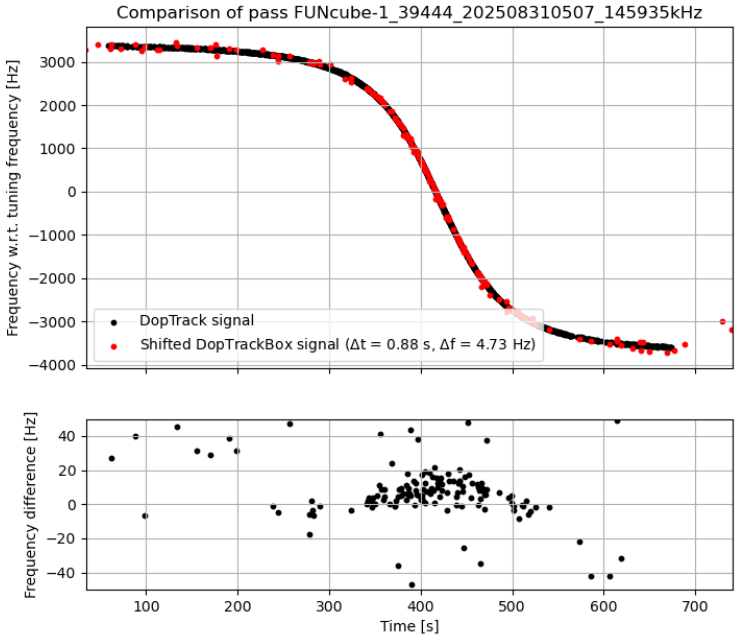

Figure 5.56: Comparison of the shifted DopTrackBox signal with the DopTrack signal for pass FUNcube-1_39444_202508310507, after estimating a time and frequency bias, when using t_{start} as DopTrackBox recording start time. Only the DopTrackBox datapoints with less than 150 Hz difference with respect to DopTrack have been used in the estimation to reduce the effect of extracted noise datapoints.

This process has been performed for all FUNcube-1 passes that contain signal points in the extracted signal, across a few different configurations. For the recordings made in the default operational configuration, the resulting estimates are shown in Table 5.4. The average time difference between $t_{\text{start, DTB}}$ (the recomputed recording start time, based on the Fitlet3 system time after the recording has ended and the known duration of the recording) and $t_{1,\text{ DTB}}$ (the Fitlet3 system time before executing the command to commence recording) is rather constant, with a value of 2.84 ± 0.09 s. Under the assumption that the only time bias in the system comes from a delay in the start the recording, this value is an upper bound on the average time bias. Depending on how this time difference between $t_{\text{start, DTB}}$ and $t_{1,\text{ DTB}}$ is distributed among the start and end of the recording, the mean of the estimated time bias will be closer to zero when using $t_{\text{start, DTB}}$ or $t_{1,\text{ DTB}}$ as recording start time.

For the estimations in which the wide 500 Hz band was used, the mean of the estimated biases is -1.94 and 0.69 s when using $t_{1,\text{ DTB}}$ or $t_{\text{start, DTB}}$ respectively. The uncertainty on the estimated bias values is a significant portion of the actual value itself, and the spread on the estimated biases are several seconds. For the estimations in which only points 150 Hz around the DopTrack data are taken, the mean of the estimated biases is -0.81 and 0.52 s when using $t_{1,\text{ DTB}}$ or $t_{\text{start, DTB}}$ respectively, and both the uncertainty on the estimated time biases, as well as the spread (0.77 and 0.59 s) are much lower, even though an extra parameter is estimated. The uncertainty on the frequency bias itself is however typically on the same order of magnitude as the estimated value itself, both being typically on the order of 10 Hz.

Table 5.6 shows the results of recordings made when DopTrackBox was operated in the lab. As the

signal-to-noise ratio of the DopTrackBox signal was significantly higher in these recordings (see Section 5.6.5), there are more real signal datapoints used in these estimations instead of noise points, leading to a better estimate. This can be seen from the uncertainty on the estimated biases. Yet, as the number of passes is small, this dataset is unsuitable to draw conclusion about the mean estimated time biases of -1.69 and 0.29 s, when using $t_{1,\,\mathrm{DTB}}$ or $t_{\mathrm{start},\,\mathrm{DTB}}$ respectively and only using the narrow 150 Hz band of points. Compared to -1.02 and 3.01 Hz in the previous configuration, the mean frequency bias is here 21.45 and 31.76 Hz, due to the Leo Bodnar GPS clock being disabled for these measurements, leading to a less precise absolute frequency reference.

Table 5.6 shows the results of recordings made using a new RSPduo device separately in the lab. Also in this case no GPS clock was used, leading to mean frequency bias estimates of 21.45 and 31.76 Hz. Even though a different RSPduo device is used, the difference between $t_{\mathrm{start},\,\mathrm{DTB}}$ and $t_{1,\,\mathrm{DTB}}$ is with a mean value of 2.88 ± 0.10 s similar to what was found in the datasets taken with the full DopTrackBox. The spread on the estimated biases when using only the datapoints less than 150 Hz from the DopTrack data are approximately two to three times higher compared to in the dataset of the full DopTrackBox. The estimated time biases itself, when only considering the narrow 150 Hz band of datapoints, are -1.07 and 1.61 s, when using $t_{1,\,\mathrm{DTB}}$ or $t_{\mathrm{start},\,\mathrm{DTB}}$ as start time respectively.

Identifier	$t_{\text{start, DTB}} - t_{1,\text{DTB}}$ [s]	Δt_1 [s]	Δt_{start} [s]	Δt_1 (N) [s]	Δt_{start}(N) [s]	Δf_1(N) [Hz]	Δf_{start}(N) [Hz]
08281604	2.94	-0.90 ± 0.87	2.03 ± 0.87	-0.81 ± 0.25	2.03 ± 0.25	-12.49 ± 9.49	-34.32 ± 9.01
08300509	2.96	-0.81 ± 0.82	1.57 ± 0.81	-1.40 ± 0.25	1.25 ± 0.20	2.21 ± 7.54	-7.21 ± 6.18
08301600	2.95	-2.32 ± 0.71	0.63 ± 0.71	-0.55 ± 0.27	0.85 ± 0.21	-9.59 ± 9.74	-11.88 ± 8.30
08310507	2.86	-0.41 ± 0.59	2.44 ± 0.60	-1.46 ± 0.17	0.88 ± 0.14	3.16 ± 6.09	4.73 ± 5.27
09010505	2.99	-2.33 ± 0.61	0.66 ± 0.61	-2.13 ± 0.22	0.55 ± 0.17	30.01 ± 6.99	9.52 ± 5.88
09200502	2.96	-5.83 ± 1.58	-2.86 ± 1.58	-0.56 ± 0.34	0.42 ± 0.39	-36.27 ± 10.26	-7.00 ± 11.69
09040458	2.98	-0.91 ± 1.20	2.13 ± 1.31	-0.60 ± 0.53	0.38 ± 0.45	-8.15 ± 13.04	1.65 ± 11.40
09050455	2.72	-2.65 ± 1.31	0.80 ± 1.19	0.10 ± 0.49	0.77 ± 0.31	-2.37 ± 11.29	21.08 ± 7.55
09051546	2.83	-0.18 ± 1.14	1.79 ± 1.05	-2.43 ± 0.42	0.15 ± 0.33	64.05 ± 15.16	36.78 ± 12.33
09060453	2.77	-4.87 ± 1.34	-2.09 ± 1.34	0.04 ± 0.50	0.12 ± 0.54	-17.13 ± 13.70	0.39 ± 14.91
09070450	2.80	-9.22 ± 1.80	-7.42 ± 1.88	-0.42 ± 0.42	-0.17 ± 0.60	-19.85 ± 10.62	-2.59 ± 12.38
09080448	2.84	1.41 ± 1.06	5.48 ± 1.18	0.28 ± 0.48	0.10 ± 0.43	-14.67 ± 14.83	8.14 ± 10.79
09100443	2.78	6.21 ± 1.75	8.99 ± 1.73	-0.29 ± 0.50	0.99 ± 0.55	9.94 ± 12.07	3.21 ± 12.70
09111532	2.83	-4.76 ± 1.93	-1.85 ± 1.93	0.08 ± 0.52	-0.18 ± 0.64	-7.70 ± 14.49	12.45 ± 16.28
09160428	2.92	0.79 ± 1.39	2.36 ± 1.22	-0.32 ± 0.41	0.79 ± 0.38	-13.54 ± 8.21	-0.42 ± 8.08
09160603	2.83	2.09 ± 1.15	4.90 ± 1.13	-1.41 ± 0.36	1.52 ± 0.26	-1.97 ± 7.96	-25.43 ± 6.60
09161519	2.90	4.42 ± 1.73	6.82 ± 1.71	-0.70 ± 0.55	-0.18 ± 0.38	-8.98 ± 12.58	11.55 ± 9.33
09170425	2.89	-3.67 ± 1.15	-0.78 ± 1.15	0.26 ± 0.55	0.65 ± 0.61	-23.00 ± 10.01	-8.04 ± 11.27
09170600	2.88	0.19 ± 1.75	2.57 ± 1.67	-2.31 ± 0.44	-0.18 ± 0.60	38.24 ± 11.61	16.44 ± 13.27
09171517	2.73	2.43 ± 1.88	5.17 ± 1.88	-1.82 ± 0.71	0.92 ± 0.59	22.20 ± 14.97	3.72 ± 12.62
09171652	2.77	-6.29 ± 1.92	-3.83 ± 1.80	-1.04 ± 0.77	0.48 ± 0.58	2.80 ± 14.84	6.78 ± 10.37
09180423	2.65	2.35 ± 1.29	5.53 ± 1.12	-0.76 ± 0.47	0.48 ± 0.44	-5.87 ± 8.78	6.83 ± 7.86
09180558	2.84	-2.54 ± 1.56	0.79 ± 1.55	-1.04 ± 0.47	0.04 ± 0.46	16.49 ± 9.55	36.18 ± 10.13
09190420	2.75	-3.43 ± 1.51	-1.43 ± 1.58	-0.14 ± 0.43	-0.36 ± 0.42	-13.63 ± 7.89	11.47 ± 7.38
09200418	2.76	-5.07 ± 1.69	-2.89 ± 1.74	-0.78 ± 0.61	1.22 ± 0.72	-6.73 ± 10.74	-15.37 ± 12.46
09210550	2.80	-5.47 ± 1.27	-2.68 ± 1.24	-1.66 ± 0.38	-0.42 ± 0.41	26.92 ± 8.57	26.70 ± 9.71
09211641	2.76	-10.00 ± 1.17	-9.72 ± 1.00	0.15 ± 0.67	0.66 ± 0.70	-36.15 ± 14.17	-26.64 ± 15.78
09210547	2.89	-2.59 ± 0.99	0.30 ± 0.99	-0.95 ± 0.21	0.81 ± 0.28	-6.49 ± 5.48	5.61 ± 8.28
Mean	2.84	-1.94	0.69	-0.81	0.52	-1.02	3.01
STD	0.09	3.73	4.05	0.77	0.58	21.59	16.55

Table 5.4: Estimated time (Δt) and frequency (Δf) biases when using passes from the prototype when it was on the roof. The subscripts in the bias indicate if DopTrackBox's t_{start} or t_1 time was used as recording start time in the estimation. An (N) indicates that only the datapoints in a narrow band of 150 Hz around the DopTrack points were used in the estimation.

Identifier	$t_{\text{start, DTB}} - t_{1,\text{DTB}}$ [s]	Δt_1 [s]	Δt_{start} [s]	Δt_1(N) [s]	Δt_{start}(N) [s]	Δf_1(N) [Hz]	Δf_{start}(N) [Hz]
10021436	2.85	0.79 ± 0.69	3.54 ± 0.69	-0.21 ± 0.44	1.63 ± 0.30	-5.53 ± 6.47	4.13 ± 4.54
10021746	2.81	-0.19 ± 0.72	2.62 ± 0.73	-3.66 ± 0.30	-0.88 ± 0.31	54.96 ± 3.94	53.66 ± 4.09
10030515	2.84	-0.68 ± 0.15	2.16 ± 0.15	-1.50 ± 0.03	1.15 ± 0.04	20.51 ± 0.85	21.84 ± 0.95
10030651	2.96	0.40 ± 0.30	3.36 ± 0.30	-1.39 ± 0.12	-0.74 ± 0.12	19.88 ± 1.78	47.41 ± 1.72
Mean	2.86	0.08	2.92	-1.69	0.29	21.45	31.76
STD	0.06	0.56	0.56	1.24	1.11	22.45	19.91

Table 5.5: Estimated time (Δt) and frequency (Δf) biases when using passes from the prototype when it was in the lab. The subscripts in the bias indicate if DopTrackBox's t_{start} or t_1 time was used as recording start time in the estimation. An (N) indicates that only the datapoints in a narrow band of 150 Hz around the DopTrack points were used in the estimation.

Identifier	$t_{\text{start, DTB}} - t_{1,\text{DTB}}$ [s]	Δt_1 [s]	Δt_{start} [s]	Δt_1(N) [s]	Δt_{start}(N) [s]	Δf_1(N) [Hz]	Δf_{start}(N) [Hz]
09221504	3.01	1.35 ± 0.35	4.32 ± 0.35	-0.86 ± 0.10	1.72 ± 0.12	40.83 ± 1.90	45.28 ± 2.36
09221638	2.97	1.04 ± 0.37	4.00 ± 0.37	-0.87 ± 0.09	2.03 ± 0.10	40.65 ± 2.20	38.23 ± 2.40
09230410	3.01	2.75 ± 0.36	5.76 ± 0.38	-1.85 ± 0.14	-0.24 ± 0.16	60.06 ± 2.06	74.71 ± 2.48
09230544	2.98	1.11 ± 0.29	4.08 ± 0.31	-1.55 ± 0.07	1.30 ± 0.09	55.65 ± 1.76	52.28 ± 2.21
09230720	2.97	4.55 ± 0.51	7.45 ± 0.50	-0.79 ± 0.34	1.68 ± 0.40	46.72 ± 3.89	49.71 ± 4.55
09231635	2.94	1.66 ± 0.34	4.16 ± 0.33	-1.18 ± 0.07	1.81 ± 0.10	52.41 ± 1.69	46.64 ± 2.30
09240407	2.91	2.94 ± 0.23	5.48 ± 0.23	-0.16 ± 0.09	2.76 ± 0.11	40.64 ± 1.54	39.22 ± 1.73
09240542	2.99	2.17 ± 0.29	5.16 ± 0.29	-1.58 ± 0.05	1.16 ± 0.07	59.22 ± 1.09	59.82 ± 1.62
09240717	2.98	-0.02 ± 0.55	2.95 ± 0.55	0.19 ± 0.27	3.16 ± 0.31	28.61 ± 3.20	27.22 ± 3.68
09241458	2.80	1.53 ± 0.32	4.32 ± 0.32	-1.35 ± 0.13	2.08 ± 0.18	57.32 ± 2.36	41.92 ± 3.19
09241633	2.98	-0.47 ± 0.27	2.37 ± 0.27	-1.46 ± 0.07	1.26 ± 0.09	55.99 ± 1.68	55.93 ± 2.15
09250404	2.79	3.29 ± 0.27	6.08 ± 0.27	-0.67 ± 0.08	2.14 ± 0.09	47.36 ± 1.33	46.33 ± 1.50
09250539	2.82	2.37 ± 0.32	5.19 ± 0.32	-1.48 ± 0.05	1.10 ± 0.07	58.15 ± 1.10	59.14 ± 1.70
09250714	2.70	3.89 ± 0.49	6.85 ± 0.50	-4.89 ± 0.23	-2.31 ± 0.27	90.51 ± 2.79	88.91 ± 3.28
09251456	2.89	2.53 ± 0.28	5.41 ± 0.29	-1.24 ± 0.13	1.15 ± 0.17	56.40 ± 2.13	59.80 ± 2.86
09251630	2.73	1.38 ± 0.29	4.13 ± 0.29	-1.45 ± 0.06	1.32 ± 0.07	56.13 ± 1.56	52.64 ± 1.77
09260402	2.85	2.38 ± 0.17	5.23 ± 0.17	-1.40 ± 0.07	1.56 ± 0.08	56.36 ± 1.06	53.93 ± 1.36
09260536	2.83	0.30 ± 0.27	3.11 ± 0.27	-1.17 ± 0.07	1.32 ± 0.07	47.49 ± 1.65	51.65 ± 1.73
09260712	2.71	3.26 ± 0.31	5.99 ± 0.31	4.30 ± 0.20	7.00 ± 0.21	-17.61 ± 2.67	-17.74 ± 2.73
09261627	2.73	0.24 ± 0.32	2.98 ± 0.32	-1.17 ± 0.07	1.11 ± 0.11	51.42 ± 1.66	53.39 ± 2.70
09270533	2.98	0.18 ± 0.22	3.16 ± 0.22	-1.52 ± 0.08	1.24 ± 0.08	48.69 ± 1.82	51.56 ± 1.91
09271624	2.99	-0.41 ± 0.42	2.60 ± 0.41	-0.17 ± 0.13	2.24 ± 0.17	10.98 ± 3.11	11.84 ± 4.07
09280530	2.75	-0.29 ± 0.21	2.46 ± 0.21	-1.43 ± 0.07	1.27 ± 0.08	49.58 ± 1.75	49.04 ± 1.83
09281621	2.80	0.82 ± 0.37	3.61 ± 0.38	-1.35 ± 0.07	1.06 ± 0.11	58.19 ± 1.91	60.27 ± 2.98
09290527	2.94	-0.69 ± 0.32	2.28 ± 0.32	-1.63 ± 0.05	1.35 ± 0.08	61.08 ± 1.35	57.36 ± 1.91
Mean	2.88	1.51	4.37	-1.07	1.61	48.51	48.36
STD	0.10	1.44	1.42	1.41	1.48	19.09	19.50

Table 5.6: Estimated time (Δt) and frequency (Δf) biases when using passes recorded by a new RSPduo device in the lab. The subscripts in the bias indicate if DopTrackBox's t_{start} or t_1 time was used as recording start time in the estimation. An (N) indicates that only the datapoints in a narrow band of 150 Hz around the DopTrack points were used in the estimation.

For the passes analyzed in this analysis, the maximum DopTrack time bias (computed using the mean time difference between DopTrack's $t_2 - T_{\text{rec}}$ and t_{start} times) was found to be 0.03 ± 0.01 s.

5.6. System Components Verification

In this Section, the noise and/or signal-to-noise ratio performance of DopTrackBox is shown with respect to itself in different configurations, or recordings made by DopTrack. First, Section 5.6.1 shows the impact of moving the DopTrackBox antenna with respect to the DopTrackBox electronics. Then, Section 5.6.2 demonstrates the effect of changing the AGC settings on the noise and signal-to-noise ratio of DopTrackBox. The is followed by the results of shutting down a potential noise source in Section 5.6.3. Section 5.6.4 then shows the results of the hardware tests performed by measuring the ATIS signal. And finally, Section 5.6.5 shows hardware tests performed by measuring FUNcube-1 passes in different hardware configurations.

5.6.1. Antenna Distance

Figure 5.57 shows the extracted noise floor as function of time for three ATIS signal recordings at different antenna distances from the box. Although some of the lowest noise values are in the recordings where the antenna was moved further from the box, these recordings also contain the highest values. Moreover, all three recordings have seemingly discrete jumps in the noise floor, indicative of gain adjustments by the AGC. Therefore, the noise values on their own cannot be interpreted without considering the signal-to-noise ratio of the ATIS signal in the three recordings, shown in Figure 5.58. From this figure, it becomes clear that moving the antenna to 220 cm from the box led to a lower ATIS signal-to-noise ratio by about 1.5 dB on average, while moving it to 280 cm led to a higher signal-to-noise ratio by about 2.5 dB on average.

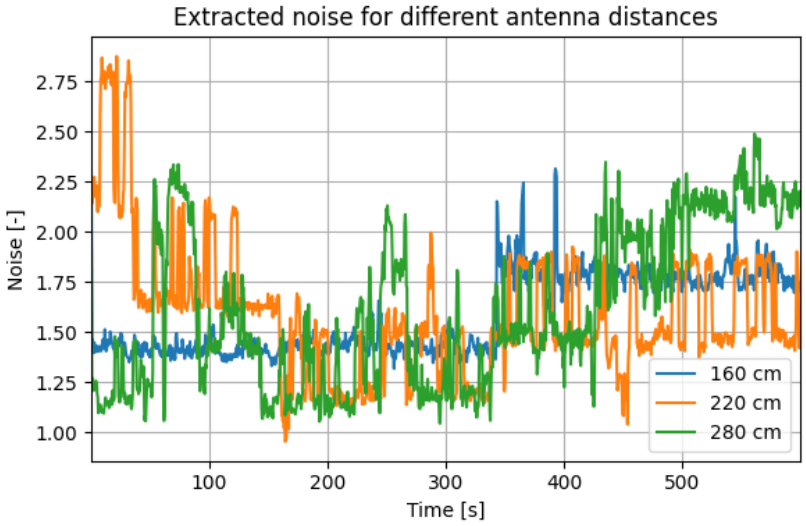

Figure 5.57: Extracted noise values for ATIS recordings made with the VHF antenna at distances of 160, 220 and 280 cm from the DopTrackBox.

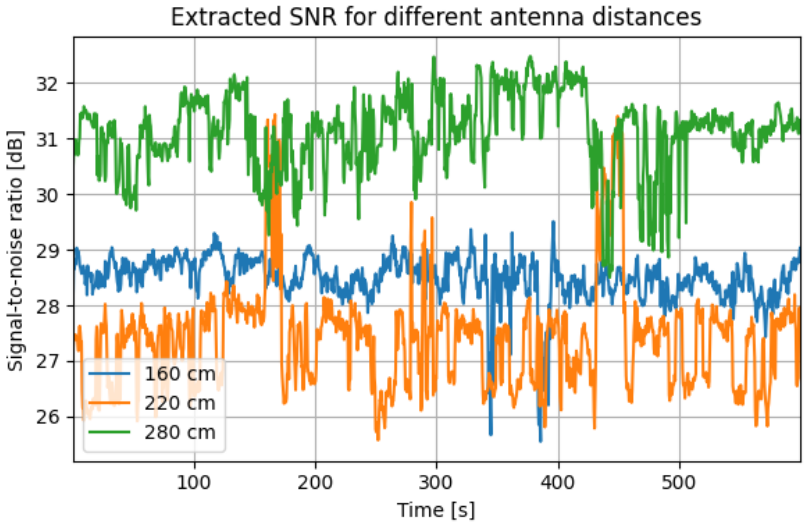

Figure 5.58: Extracted signal-to-noise ratios for ATIS recordings made with the VHF antenna at distances of 160, 220 and 280 cm from the DopTrackBox.

5.6.2. Automatic Gain Control Setpoint

Figure 5.59 shows the computed noise values as function of time for the different AGC setpoint values. For higher values than the default value of -30 dBF, much higher noise is achieved, while for lower values the noise is similar. But again, the noise alone does not describe the quality of the signal well, so it is more useful to look at the signal-to-noise ratio as well, shown in Figure 5.60. From this figure, it can be seen that the default value of the AGC setpoint leads to the best signal-to-noise ratio, with all other cases being approximately 1.5 dB lower.

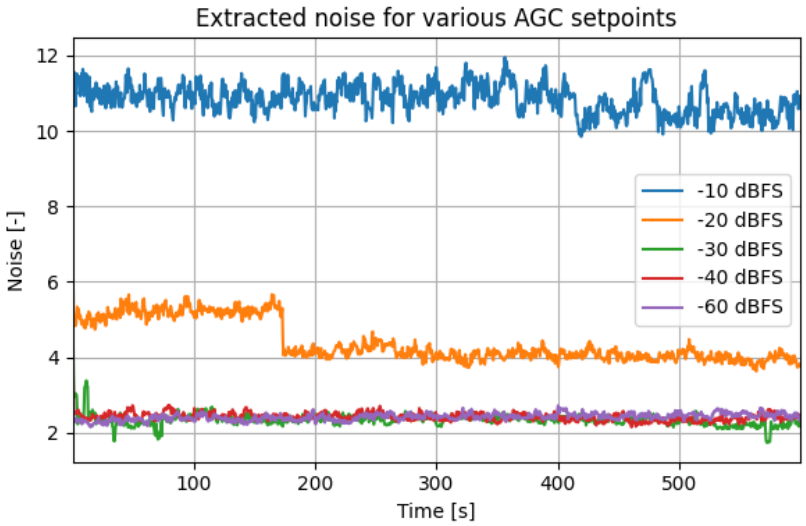

Figure 5.59: Extracted noise values for ATIS recordings made with at different automatic gain control setpoint values.

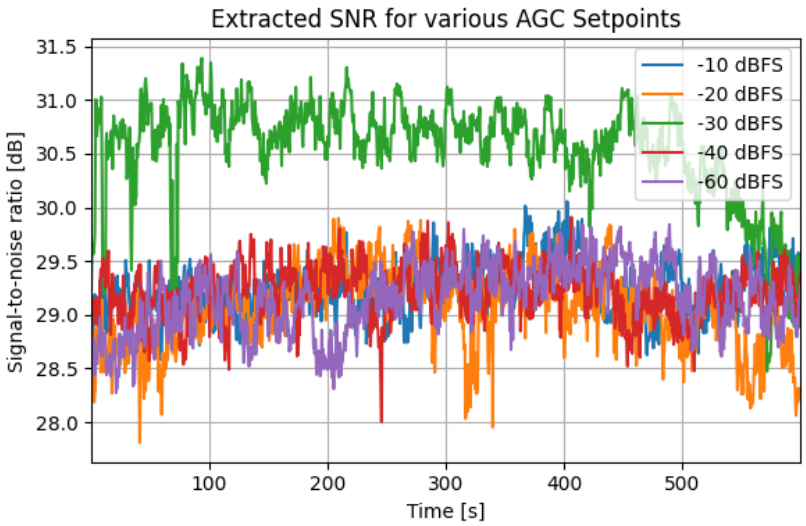

Figure 5.60: Extracted signal-to-noise ratios for ATIS recordings made with at different automatic gain control setpoint values.

5.6.3. Potential Noise Source Shutdown

Figures 5.61 and 5.62 show a typical pass for which there is an extractable signal in the DopTrackBox recording before and during the shutdown of the Fripon experiment on the roof, which could be a potential noise source. From these figures it becomes apparent that there is no significant difference in the computed noise floor. The signal-to-noise ratio of the signal, visible in both passes between approximately 300 and 600 seconds, is about 0.5 dB higher during the pass in the shutdown period compared to before the shutdown period, but this is well within typical pass-to-pass fluctuations of the signal.

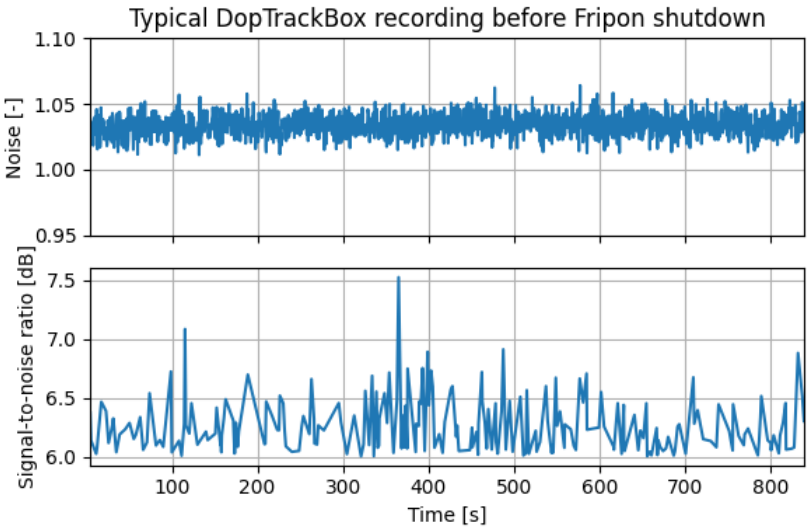

Figure 5.61: Extracted noise and signal-to-noise values of a typical satellite recording made with DopTrackBox, before shutting down a potential noise source.

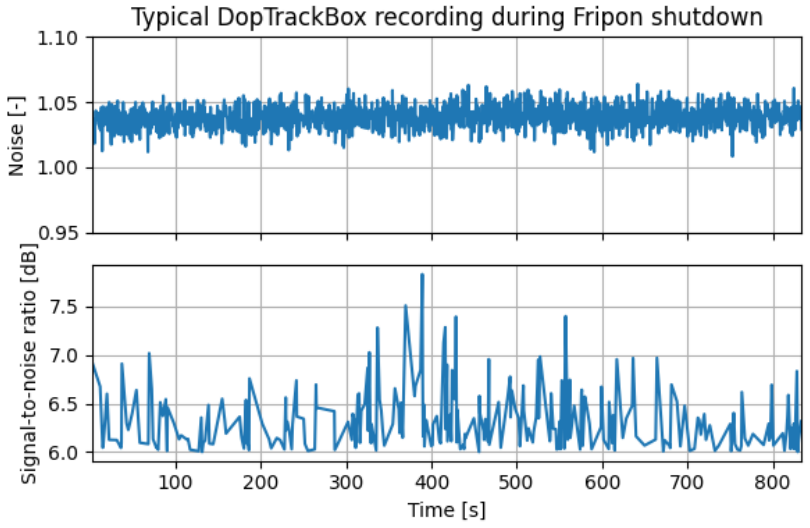

Figure 5.62: Extracted noise and signal-to-noise values of a typical satellite recording made with DopTrackBox, after shutting down a potential noise source.

5.6.4. Hardware Components Test With ATIS

Figure 5.63 shows the extracted noise during ATIS recordings in different hardware configurations. From this figure it seems that using a different coax cable leads to a slightly higher noise, but when using both a different coax cable and different RSPduo device (located about 1.2 meters from the box to limit electronic noise by the Fitlet3), the noise is similar to the default setup. The extracted noise in the recording made using the DopTrack antenna shows a much higher noise than the other cases. However, as stated before, the noise depends on the gain selected by the AGC, and this cannot be guaranteed to be the same across the measurements, the signal-to-noise ratio needs to be evaluated as well. Figure 5.64 shows this signal-to-noise ratio for these measurements. In this figure, it does appear that the DopTrack antenna is worse than the DopTrackBox antenna, as the signal-to-noise ratio is approximately 8 dB lower than the default case using the DopTrackBox antenna. In addition, using a different coax cable seems to lead to a slightly lower and much less stable signal-to-noise ratio compared to the default case. Using the new RSPduo together with the different cable leads to a signal-to-noise ratio between the default case and the case using a different coax cable, but has a similar instability to when using the different coax cable on its own.

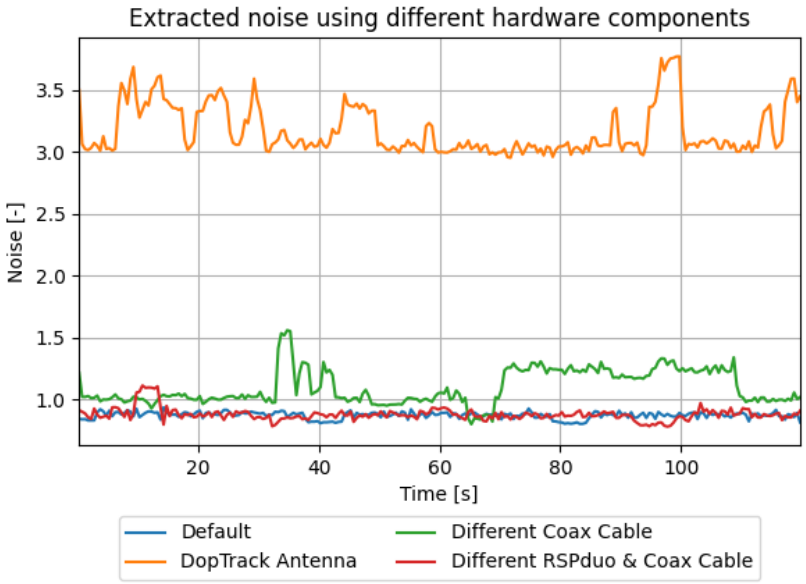

Figure 5.63: Extracted noise values from ATIS recordings made using different hardware configurations.

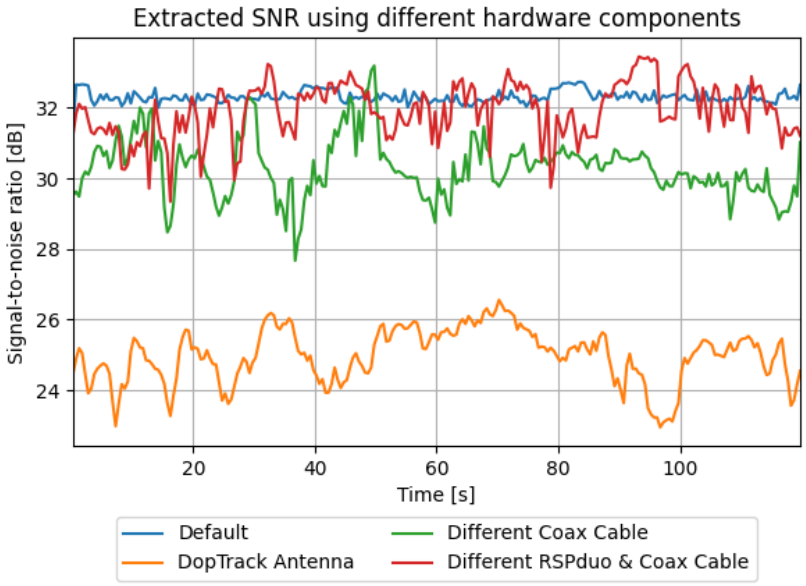

Figure 5.64: Extracted signal-to-noise ratio values from ATIS recordings made using different hardware configurations.

5.6.5. Hardware Components Test with FUNcube-1

Recording Setup on the Roof

Figure 5.65 shows the signal-to-noise ratio of FUNcube-1 passes recorded by DopTrack and DopTrackBox, while for one of the passes recorded by DopTrackBox the Leo Bodnar GPS clock had been disabled. Although the signal-to-noise ratio of the extracted signal has increased slightly for DopTrackBox when disabling the GPS clock, so has the signal-to-noise ratio of the extracted signal from the DopTrack system. In both passes, the peak signal-to-noise ratio of the DopTrackBox system is approximately 8 dB lower than that of DopTrack.

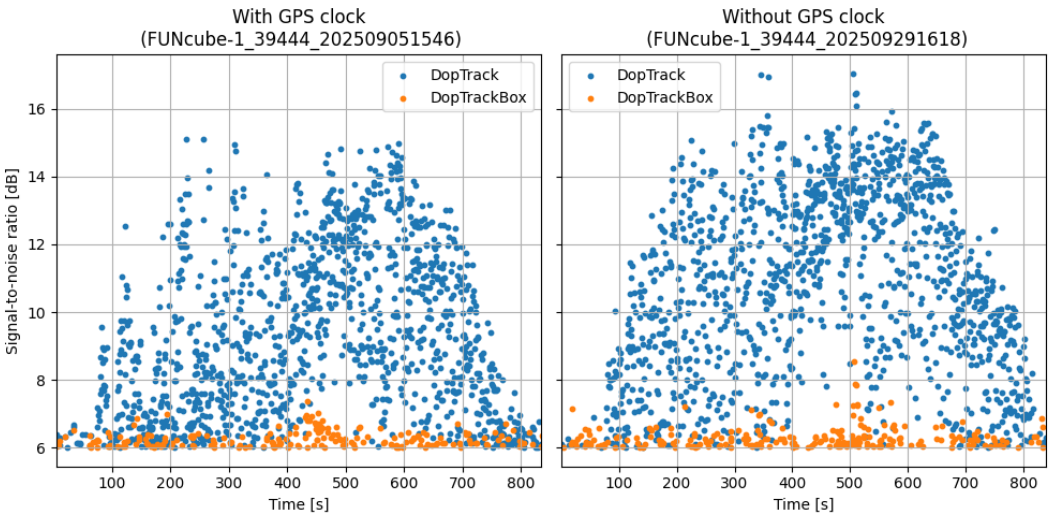

Figure 5.65: Comparisons between the DopTrack and DopTrackBox signal-to-noise ratio for FUNcube-1 passes, before and after disabling the DopTrackBox GPS clock.

Figure 5.66 shows the signal-to-noise ratio of FUNcube-1 recordings by DopTrack and DopTrackBox, during various hardware tests performed while the setup was on the roof. In all cases, the Leo Bodnar GPS clock was disabled. Swapping the antenna's of the DopTrack and DopTrackBox systems reveals that the typical shape of the signal-to-noise ratio as a function of time for a satellite pass recording is different between the antennas. In addition, although for most of the recording the DopTrack signal-to-noise ratio seems to be slightly lower compared to typical passes, the DopTrackBox signal-to-noise ratio is not significantly higher. After moving the DopTrackBox and its antenna to a different location on the roof, the extracted signal-to-noise ratio has not increased with respect to DopTrack. In fact, instead of about 8 dB of peak signal-to-noise ratio difference, the difference is now approximately 10 dB. During the passes in which the door to the DopTrackBox was opened, while being at its relocated spot on the roof, the difference was only approximately 8.5 dB, closer to what was observed in the default case at its original location.

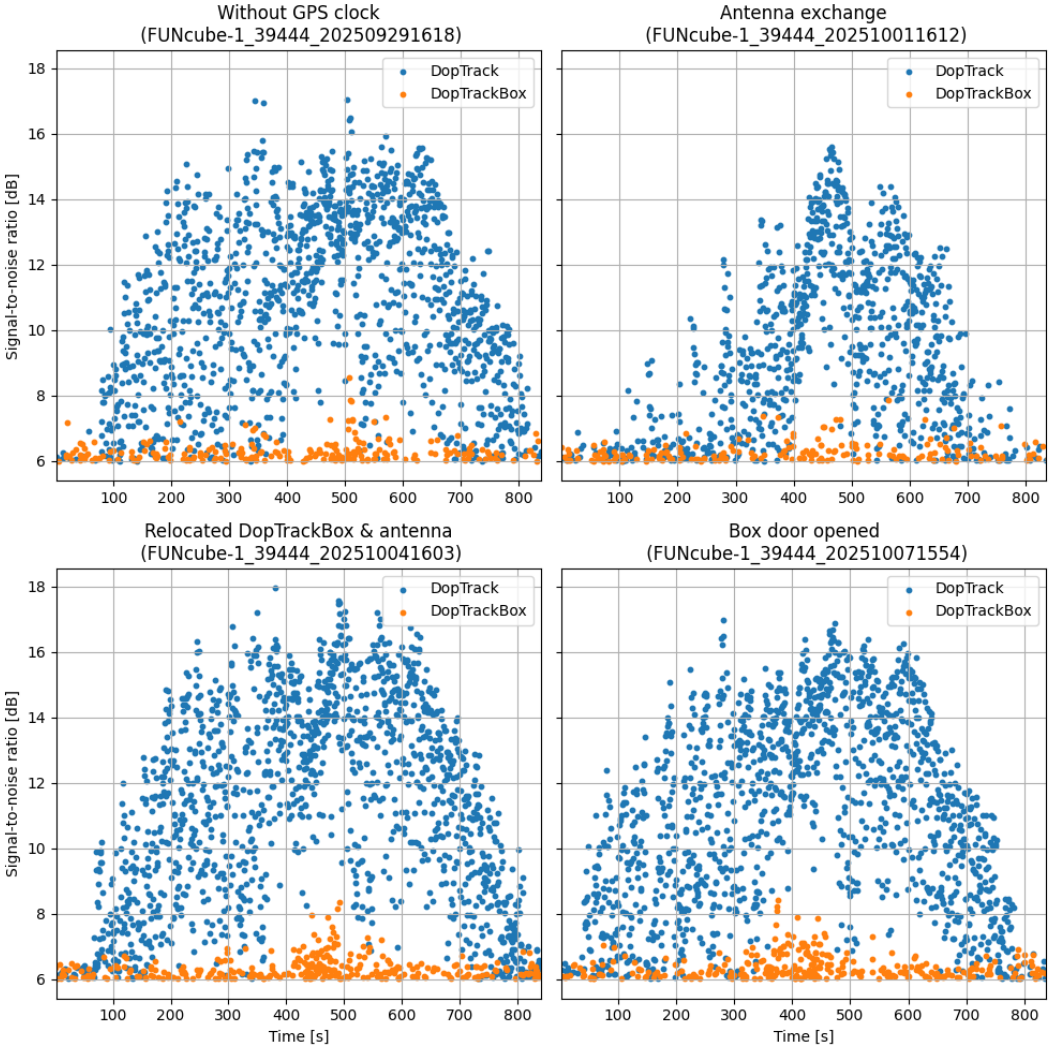

Figure 5.66: Comparisons between the DopTrack and DopTrackBox signal-to-noise ratio for FUNcube-1 passes, in DopTrackBox's normal configuration but without active GPS clock, a configuration in which the antenna of DopTrack and DopTrackBox have been swapped with each other, a configuration in which DopTrackBox and its antenna were placed at a different location on the roof, and a configuration in which the box door of DopTrackBox was opened during the recording.

Recording Setup in the Lab

Figure 5.67 shows the signal-to-noise ratio of FUNcube-1 recordings by DopTrack and DopTrackBox, during various hardware configurations when connected to the DopTrack antenna system using a radio splitter in the lab. When only a separate new RSPduo device was used together with the Fitlet3 to record the pass, the signal-to-noise ratio of the extracted DopTrack and DopTrackBox recordings are similar. Also when the cable between the splitter and RSPduo was exchanged for the original DopTrackBox cable, the signal-to-noise ratio of the two systems was similar. When the low noise amplifier (LNA) was then turned off, the signal-to-noise ratio of both systems dropped by approximately 3 dB over the full recording duration. After turning on the LNA, and connecting the full DopTrackBox system (but without GPS clock) to the splitter using its original coax cable, the signal-to-noise ratio of the DopTrack and DopTrackBox systems were still similar. For this configuration the shape of the signal-to-noise ratio over time is similar to Figure 5.66, as in this configuration the DopTrackBox antenna was replaced by the DopTrack Antenna.

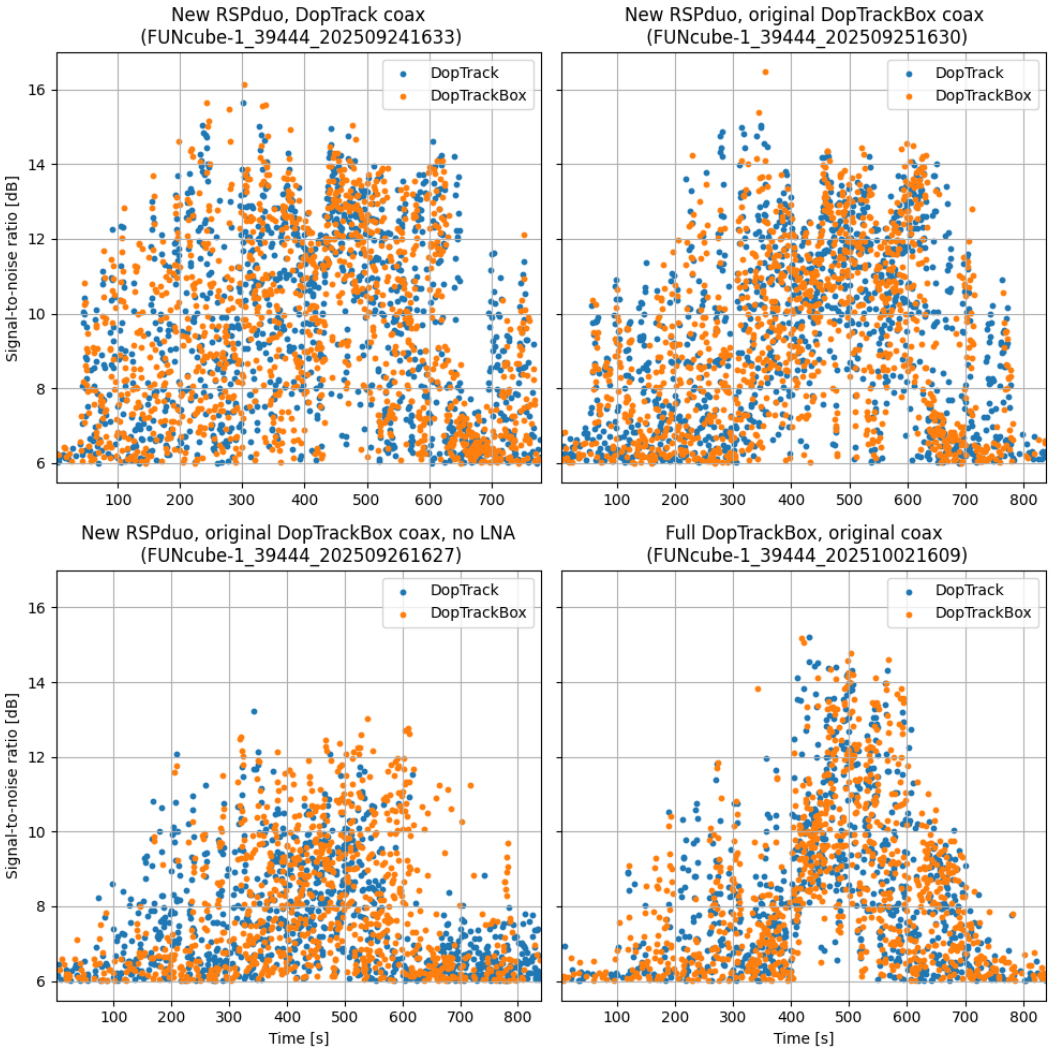

Figure 5.67: Comparisons between the DopTrack and DopTrackBox signal-to-noise ratio for FUNcube-1 passes, in a configuration of using only a new RSPduo in the lab connected to the DopTrack system using a radio cable from DopTrack, the same configuration but using DopTrackBox's original radio cable, the same configuration but without LNA, and the full DopTrackBox system with the old RSPduo.

6

Discussion

The results described in the previous chapter are meaningless without a discussion of the shortcomings of the analysis and interpretation of the findings. First, this chapter presets a discussion relevant for the initial selection of the hardware in Section 6.1. This is followed by a discussion on the findings of the data gathered using the prototype in Section 6.2. Lastly, Section 5.6 discussed the results of the component verification analysis.

6.1. Hardware Selection

To develop a system with the the desired orbit estimation accuracy, two key factors must be considered. The first factor is the frequency stability with which a satellite signal can be measured. A discussion on the findings of this thesis is presented in Section 6.1.1. The second factor is the impact of a time bias on the orbit estimation accuracy, with the relevant discussion on the results presented in Section 6.1.2.

6.1.1. Frequency Stability

GPS Clocks

The unwrapped phase measurements of the mini-GPS and LBE-1421 shown in Figures 5.1 and 5.2 showed jumps in the phase at seemingly random points in time. According to the manufacturer of the TinyPFA, such jumps could originate from touches of the device, cable or changes in temperature (Kaashoek, n.d.). It cannot be ruled out that the device or cable was touched during the measurements, and that this is the cause of the observed phase jumps. In addition, one of the jumps appears to have occurred around the time the lab door was opened, leading to an influx of warm air in the air-conditioned room. As a result, it is possible that the actual stability of the tested devices is higher than reported in this thesis, when not touched and less temperature fluctuations occur.

The stability of the mini-GPS and LBE-1421 clocks found in Section 5.2.1 is for most averaging times similar to the expected values between 5×10^{-11} and 5×10^{-12}. However, between around $\tau = 10^{0}$ and $\tau = 10^{1}$, there was a 'bump' visible where the stability decreases to around 8×10^{-11}. This is supposedly caused by a frequency pulling effect due to a difference in average frequency between the DUT and the EC20S (Kaashoek, 2023). This effect should make the observed stability only worse than

the real stability, and as such the stability of the mini-gps and LBE-1421 should be sufficient to achieve the required stability (requirement identifier DTB-TECH-3.02).

These measurements also show that the stability of the mini-GPS is more consistent than that of the LBE-1421. However, it must be noted that the mini-GPS has had significant runtime before, while LBE-1421 only had a few hours of runtime at most. As a consequence, the internal PID loops were still settling during these measurements, as it can take more than a month to fully settle (*Question about the Bodnar mini GPSDO unit* 2025; *Another question about the Bodnar Mini GPS Unit* 2025). In addition, auto-tuning of short-term PID loops could be the cause of the periodic spikes in the phase, as observed in the measurements performed on the LBE-1421.

Furthermore, it must be noted that the measured stability is that of the least stable input. It is not ruled out that the Leo Bodnar GPS clocks could be more stable for certain averaging times than the EC20S reference clock. In that case, the measured stability is actually that of the EC20S, but because this means that the Leo Bodnar GPS clocks must be at least as stable, this does not influence the conclusion as the observed stability satisfies the requirement.

For the measurements in which the setup was placed inside a box to investigate the influence of temperature fluctuations on the stability, it must be considered that the overlapping Allan deviation is not the perfect tool to express the stability: by definition, the allan deviation assumes that the noise properties of a system remain the same during the period of the measurements. As the goal of these measurements was to investigate how the stability changes due to changing noise caused by temperature fluctuations, this assumption does not hold, possibly leading to an overestimation of the stability. However, considering that the measured stability was lower than the requirement, this effect has no impact on the conclusions.

Software Defined Radio

Although it seems based on Figures 5.7 and 5.8 that the performance of the RSPduo without external GPS clock reference varies between the first and second dataset, it must be noted that the second dataset was produced using a newly acquired RSPduo device, unlike any of the other measurements. As a result, the runtime between the devices are much different and it is not excluded that internal components of the RSPduo have changed. Both could lead to differences in stability when used on their own.

This logic does not apply to the measurements using the mini-GPS as an external reference clock, shown in Figure 5.14, because the measurements using the GPS clock from this figure have been performed using the older RSPduo device.

From comparing the measurements shown in Figures 5.8 and 5.10, it could be that for low averaging periods the RSPduo has a higher stability than the N210. It must however be noted that because attenuators with different attenuation factors have been used, the signal strength provided to the SDR is not equal. As a result, the relative size of the phase noise of the SDR with respect to the signal strength is different, purely by having a different input signal strength. In addition, while the sample rate of the measurements with the RSPduo was 62.5 kHz, the sample rate of the measurements with the N210 was 250 kHz. This increase in sample rate could to lead to more ADC noise which might show up in the analysis as a lower stability for low averaging times.

6.1.2. Time Bias Analysis

In the state and time bias estimation analysis, only the properties of a single satellite in a single orbit have been simulated. As such, any conclusions about the effect of a potential time bias in the DopTrack-Box system on its expected performance rely on the assumption that the estimation behaves similarly for satellites with different properties and in different orbits.

Considering that satellites that use the amateur VHF or UHF bands to communicate are often CubeSats with similar properties and orbits to the satellite simulated in this thesis, it is assumed that this has no significant effect on the conclusions of this analysis.

The radio transmitters of real satellites typically drift over time due to instabilities in the on-board clock. This was not simulated in this analysis, and could lead to more difficulties in estimating the orbital state and time biases, when it is taken into account. The analysis in this thesis therefore represents a best case scenario, in which a particular satellite has no significant frequency drift.

6.2. DopTrackBox Prototype

This Section provides a discussion on the results obtained during the operational phase of the Dop-TrackBox prototype. It starts with the findings related to the temperature behavior of the system in Section 6.2.1, followed by the results of the satellite recording performance in Section 6.2.2.

6.2.1. Temperature

The measured temperatures by the DopTrackBox system were correlated to KNMI data of a weather station located in Voorschoten, approximately 12 kilometers from Delft. As a result, the KNMI data used does not perfectly describe the weather conditions at the DopTrackBox location. Although the temperature can be assumed to be similar within a few degrees, the cloud coverage and sunshine duration and precipitation duration can vary widely over small spatial distances. In addition, the KNMI station is located on ground level, while the DopTrackBox system was located on the roof of the Aerospace Faculty building, approximately 60 meters high. At these heights there is naturally much more wind and a slightly different temperature than at ground level. All of these effects tend to weaken any correlations between the KNMI data variables and the measured temperature.

In addition, the correlations must be interpreted with care. Although there is a correlation between most of the variables, this does not mean they are necessarily causally related. For example, warm days in the Netherlands typically have less clouds, more sunshine and less precipitation than cold days. Since the temperature of the box is strongly correlated to the outside temperature, the box temperature will thus also be correlated to the cloud coverage, sunshine duration and precipitation duration, even if they might not have a causal relationship with the box temperature.

Moreover, it is assumed that the measured temperature inside the box is representative of what it will be when operating in normal circumstances. However, it must be taken into account that the computational load, which is related to the amount of heat generated by the Fitlet3, is different than during normal operations. On one hand, the system should be designed to handle almost continuous recording of passes throughout the day, while during most of the time in this thesis the system had only been tracking one or a few satellites, leading to a reduced the computational load. On the other hand, during some of the time the system was also used to process the recorded data, leading to bursts of high computational load that would not occur if the processing would be handled by a centralized and dedicated sever.

Furthermore, when drawing conclusions based on the measured temperature, one must realize that the data only describes approximately two out of twelve months of the year. As these months contained the hottest days of the year, they provide a good benchmark for the upper limit of what the system will endure when operating in the Netherlands. However, when evaluating whether the system will stay warm enough on cold days to prevent condensation inside the box or even freezing of the components, the data is not sufficient.

In addition, when interpreting the data on warm days, one must realize there there is an artificial bias in some of the the measured temperatures, because of the automatic shutdown that occurred when surpassing the 40°C threshold to prevent overheating of the components. During these shutdown periods the temperature measurements stop, resulting in an incomplete dataset for that specific hour, during which the temperature might or might not have continued to rise.

To solve the issue of overheating, there are two possible routes:

- **Add cooling:** A different box could be chosen that has options for ventilation. However, as some potential DopTrackBox station locations achieve higher air temperatures during the warmest days, then the lowest temperature constraint of 40°C, adding only ventilation would still lead to overheating. To counter this, the cooling options discussed in Section 2.3.2 could be tested by modifying the prototype. Although electro-thermal cooling is less efficient, the lack of any moving parts makes it a more suitable choice for DopTrackBox than electro-mechanical.
- **Change hardware components:** No cooling may be needed if the electronics is capable of enduring higher temperatures. As the constraining component is currently the power supply to the Fitlet3, a new power supply could be acquired that is capable of handling higher temperatures. In that case, the new constraining component is the Fitlet3 itself with a maximum temperature of 45°C. However, as a different variant of the Fitlet3 is available with a maximum temperature of 60°C, changing the Fitlet3 to this variant increases the system temperature limit further to 60°C. Under the assumption that the box temperature is approximately 15°C higher than the outside temperature, the box should then be capable of operating in locations with a maximum outside air temperature of 45°C.

From the list of candidate locations, only Khartoum (Sudan) and Sydney (Australia) have higher maximum temperatures than 45°C. For these locations, combining the upgraded components, together with either fans or electro-thermal cooling might be sufficient to operate in these conditions as well.

6.2.2. Satellite Recordings

Signal-to-noise ratio Analysis

From the FUNcube-1 recordings made during the operational phase of DopTrackBox, it becomes clear that the resulting extracted signal has a peak signal-to-noise ratio that is on average 9.44 dB lower than the same passes recorded by DopTrack. In addition, the signal is visible for a much shorter duration, or not at all, compared to the recordings made with the DopTrack system.

There are several differences in the setups that could be responsible for this observed discrepancy.

- **SDR differences**: As the DopTrack system used an Ettus Research USRP N210, while DopTrackBox used an SDRPlay RSPduo as SDR, even if the signal power would be the same in both systems, the signal-to-noise ratio could be different if the noise generated by the SDR is differ-

ent. However, in the work of Sprenkels (2023), the RSPduo was also as SDR to compare with DopTrack, and no such discrepancy in signal-to-noise ratio was found. In fact, in some of the measurements the signal-to-noise ratio of recordings with the RSPduo were found to be higher than using the DopTrack setup. Although the exact same RSPduo device was used, in the meantime it could have become defective, it the recording software could have changed settings leading to a lower signal-to-noise ratio.

- **Environmental noise**: The operational environment of the DopTrackBox is different than DopTrack. While DopTrack operates in an air-conditioned laboratory, the DopTrackBox SDR is located in a box on the roof near the antenna's, unlike during the measurements made by Sprenkels. As there was no active cooling of the box, the temperatures were often higher than in the air-conditioned laboratory. This could lead to higher thermal noise and thus a lower signal-to-noise ratio. In addition, as DopTrackBox is close to the antenna, radio-frequency interference could be generated by the electronics in the box, and either enter the system by coupling to the antenna, or possibly to the SDR directly.
- **Different antenna**: Although DopTrack and DopTrackBox both use eggbeater antenna's, they are not physically the same antenna. This could lead to a different antenna efficiency, and thus different signal-to-noise ratio. Furthermore, the DopTrackBox antenna was missing one of the spokes of the reflector plane of the antenna. This can impact the antenna efficiency, although it is not clear by how much.
- **Cable length and LNA**: As the DopTrack setup is located in the lab, the cables are much longer than what was used for DopTrackBox, leading to higher cable losses. To compensate for this loss, the DopTrack system has an LNA close to the antenna. If the noise is dominated by electronic noise of the SDR, it is possible that the LNA boosts the signal by more than the cable loss, leading to a higher signal-to-noise ratio in the recording. As DopTrackBox does not use an LNA, it is possible this causes a difference in signal-to-noise ratio between DopTrack and DopTrackBox, considering the work of Sprenkels used the DopTrack antenna system with LNA as well. In addition, the cable used for DopTrackBox could be defective or has too high losses compared to the DopTrack system.
- **Influence of GPS clock**: It is unclear if using the Leo Bodnar GPS clock as external oscillator has any effect on the signal-to-noise ratio of the received signal. Although in the work of Sprenkels this GPS clock was also used, it was found during this work that the cable used to connect the GPS clock to the SDR was defective. It is unclear if this could have been the case during the measurements taken by the work of Sprenkels, considering the same cable was used, and the conclusion was drawn that the range-rate accuracy (which is tied to the frequency stability) did not meet the expectations.

To find the cause(es) of the observed discrepancy in signal-to-noise ratio between DopTrack and DopTrackBox, the analysis presented in Section 4.5 was developed to systematically eliminate as many options as possible. The discussion on the results of this analysis is presented in Section 6.3.

Time Bias Analysis

In this analysis, it was assumed that the only contribution to the time bias in the system is caused by the delay in the recording. This assumption is only true if the internal time of the Fitlet3 computer has negligible drift with respect to true time. To realize this, the Fitlet3 clock is synchronized to an NTP

server, reporting an expected clock error of less than 1 millisecond, making this contribution to the time bias negligible. In addition, it was found that the time bias in DopTrack itself is 0.03 ± 0.01 s, indicating that the DopTrack time bias is also negligible for the purposes of this analysis.

This does however not guarantee that the estimated time biases are accurate, as they depend on several factors in the estimation process. In the dataset containing the recordings made with DopTrackBox in the operational phase, it was observed that when using the wide band of 500 Hz in the estimation, the typical estimated time biases and the spread on these biases were larger than the expected upper limit of the bias, based on the time difference between $t_{\text{start, DTB}}$ and $t_{\text{1,DTB}}$. This indicates that using this method does not provide good estimates of the time bias.

That this does not occur for the method in which only the points 150 Hz around the DopTrack points are used does however not indicate that the fit is much better: by selecting only the points closely around the DopTrack points, the estimation becomes more biased. This is an issue if by selecting points closer around the DopTrack data less real signal and more noise points are selected, but the figures containing the frequency difference between the two systems before and after changing the selection of datapoints show that this is not the case.

When using only the datapoints 150 Hz around the DopTrack data, the resulting estimated time biases and their spread are both lower. In this case, the mean of the estimated biases are on the same order of magnitude as the spread on the estimated biases, both when using $t_{\text{start, DTB}}$ or $t_{\text{1,DTB}}$ as recording start time. Since the mean of the estimated biases swaps sign after switching the recording start time estimate, it appears that the true mean of the bias lies, as expected, between using $t_{\text{start, DTB}}$ and $t_{\text{1,DTB}}$. As the means of the estimated biases are similar in size, a significant fraction of the time difference between $t_{\text{start, DTB}}$ and $t_{\text{1,DTB}}$ could originate from a delay after the end of the recording.

In the results of the stability analysis presented in Section 4.1, a frequency offset of approximately 0.5 Hz was observed when using the GPS clock, and approximately 2 Hz when not using a GPS clock. Under the assumption that the offset scales with the tuning frequency, the expected offsets at the FUNcube-1 frequency are approximately 7.25 and 29 Hz respectively. This slightly lower than what was observed, however, the higher temperatures inside the box could cause a higher frequency error. In addition, as the extracted frequency is discrete, and then interpolated during the estimation, the estimator does not estimate the frequency bias smoothly. There seem to be jumps in the estimated values between iterations, which might lead to a higher than expected frequency bias.

6.3. System Components Verification

Many of the potential causes for the observed discrepancy between the DopTrackBox and DopTrack signal-to-noise ratio when recording FUNcube-1 passes, presented in Section 6.2.2, can be eliminated by the results of the analysis presented in Section 5.6.

Figure 5.67 showed that when the full DopTrackBox system with its original cable but without GPS clock was placed inside the lab and connected to the DopTrackBox antenna system, it achieved a similar signal-to-noise ratio to DopTrack, in agreement with what was found in the work of Sprenkels (2023). Therefore, the possibilities of the SDR being defective or receiving significant amounts of electromagnetic interference from the Fitlet3 could be eliminated. In addition, it rules out that the coax cable is defective or has too much loss. In addition, this figure shows that even without LNA, there is still a much higher signal-to-noise ratio in DopTrackBox when operated in the lab, versus when it was

operated on the roof, indicating that a lack of LNA is not the sole cause either.

It may seem that the lack of GPS clock caused the signal-to-noise ratio to improve, but but Figure 5.66 showed that there was no difference between enabling and disabling the GPS clock when DopTrackBox was operated on the roof. In addition, it showed that opening the door for aided cooling to reduce thermal noise does not improve the signal-to-noise ratio either.

However, it was found that the shape of the signal-to-noise ratio as function of time is different for the DopTrackBox antenna than the DopTrack antenna. There are multiple possible causes for this. The missing antenna spoke of the DopTrackBox antenna could lead to a lower antenna efficiency. In addition, the slightly different locations of the antennas could lead to different obstructions of the antenna, with a reduced signal power as a consequence. However, as the difference in peak-signal-to-noise ratio did not change significantly when swapping the antennas, this is likely not the cause of the observed discrepancy.

Combined, it indicates that the discrepancy is related to DopTrackBox being operated on the roof instead of in the lab. As Figure 5.58 showed, changing the antenna distance to the box did not improve the signal-to-noise ratio of the ATIS signal significantly. In fact, between moving the antenna from its closest position to the box to the position with a distance in the middle, the signal to noise ratio even got slightly worse. But as the ATIS beacon is located at Rotterdam Airport at ground level, this could be explained by blockage of the signal by the building, roof or other elements on the itself, as the tested antenna locations are not directly in line with each other, nor with the ATIS beacon location. Although, noise being generated by the box coupling to the antenna seems not likely to be the cause, it can also not be eliminated. What else remains is that by being operated on the roof, the SDR itself could pick up significant amounts of noise. If this is the cause, it could possibly be mitigated using a better shielding of the SDR, or its second antenna port not used during the recordings.

7

Conclusion & Recommendations

In this thesis, several aspects of the design of DopTrackBox have been investigated that required attention, as defined by the research questions presented in the introduction. The conclusions on these matters are addressed in the following sections. First, Section 7.0.1 addresses the suitability of the RSPduo and N210 as SDR in DopTrackBox in terms of frequency stability. Then, Section 7.0.2 discusses the suitability of the RSPduo as SDR in terms of observation time bias. After this, Section 7.0.3 discusses the environmental protection box aspect of the DopTrackBox design. This is followed by Section 7.0.4, which discusses the signal-to-noise ratio performance of the design prototype. Lastly, Section 7.1 draws conclusions about the prototype design based on the established requirements.

7.0.1. Hardware Tracking Stability

In the requirements analysis presented in Chapter 3, a stability requirement of 10^{-8} was derived based on the desired position estimation accuracy needed to compete with TLE ephemerids provided by NORAD. By measuring and comparing the frequency of a signal of a precisely known frequency source, the stability of the potential SDR and GPS clocks were investigated and compared to the requirement.

First, it was found that the Leo Bodnar mini-GPS has a stability better than 10^{-10} for all averaging periods between $\tau = 0.5$ and $\tau = 10^3$ s. Therefore, the answer to research question 1A:*"Is the Leo Bodnar mini-GPS clock output sufficiently stable for the desired range-range accuracy?"* is that it is plenty sufficient, under the assumption that the relation between the required stability and the expected orbit estimation performance is correct.

Then, it was also found that by combining the SDRPlay RSPduo software defined radio, together with the Leo Bodnar mini-GPS clock, a stability better than 6×10^{-10} is achieved for $\tau > 0.5$ s, improving, to 3×10^{-11} at $\tau = 10^3$ s, even when subjected to temperature fluctuations. Consequently, the answer to research question 1B:*"Is the frequency stability of the SDRplay RSPduo sufficient for the desired range-rate accuracy when using the Leo Bodnar mini-GPS clock as an external reference clock?""* is that this combination of SDR and GPS clock is sufficient, under the assumption that the relation between the required stability and the expected orbit estimation performance is correct. In addition, considering that the stability was measured under forced temperature fluctuations of $\pm 8°$C without

significant degradation of the stability, the answer to research question 2B: *"Is passive temperature control of the box sufficient to satisfy the frequency stability requirements?"* seems to be that passive temperature control should be sufficient.

In addition, it was found that using an interface circuit between the mini-GPS clock and SDR has no benefit or drawback on the stability, but does add an extra point of failure to the design. The answer to research question 1C: *"How does the use of an interface circuit after the output of the Leo Bodnar mini-GPS clock influence its output frequency stability?"* is that there is no impact was found. Therefore, it is recommended to not use the interface circuit in the design.

Furthermore, similar tests were performed with the Ettus Research USRP N210 together with a Leo Bodnar mini-GPS and LBE-1421 GPS clock as external reference frequency sources to answer research question 1E: *"What is the frequency stability of the Ettus Research USRP N210 when using the Leo Bodnar mini-GPS as an external reference clock?"*. It was found that a frequency stability better than 2×10^{-9} for $\tau > 0.5$ s can be achieved, improving to 5×10^{-11} at $\tau = 10^3$ s. As such, this combination also satisfies the stability requirement. When the LBE-1421 was used, an even higher stability of 5×10^{-10} for $\tau > 0.5$s, improving to 3×10^{-11} at $\tau = 10^3$ s was achieved. However, as this research was unable to make the N210 work with the Fitlet3 computer, and since the N210 was found to be not being manufactured anymore, the N210 is not recommended as of software defined radio is for DopTrackBox.

7.0.2. Time Bias

To find the time bias of the DopTrackBox system when the RSPduo is used as SDR, recordings were made of the FUNcube-1 satellite. The extracted frequency of these recordings were then compared against the extracted frequency of the DopTrack system, which was found to have a negligible time bias of $0.030.01$s with respect to the absolute time. An estimation of the time and frequency bias in DopTrackBox was performed by minimizing the frequency difference between the two systems during a satellite pass.

Considering only measurements performed using the DopTrackBox prototype in its full form, the answer to research question 3B:*"What is the time bias of the DopTrackBox system?"* is that the a mean time bias of -0.81 s, with a standard deviation of 0.77 s was found. But, when an attempt was made to correct for this bias by recomputing the start time using the end time of the recording and the known duration of the recording, the mean time bias decreased to $+0.52$ s with a standard deviation of 0.58 s. In addition, it was found that the absolute maximum of the bias should be less than 3 s. As the frequency residuals showed that the bias estimation is suboptimal, there is a significant uncertainty on the estimated bias. To get a better estimate on the distribution of the bias, several steps are recommended.

First, more passes should be analyzed, with preferably a higher signal-to-noise ratio. This allows for more datapoints to be used in the optimization, leading to a better estimate. Then, the datapoint selection can be improved such that less noise points are used in the estimation, which deteriorate the estimation.

Alternatively, instead of estimating the biases based on a drifting satellite signal, the bias can be estimated using a different kind of signal with transient effects, such as the ATIS signal shown in a different analysis of this thesis. As this ATIS signal repeats its broadcast approximately every minute, there is a transient in the modulated part of the signal when the message starts again. By observing the times

of these transients using DopTrack and DopTrackBox simultaneously, the bias of DopTrackBox could potentially be extracted with a much higher accuracy than using the approach used in this thesis.

The time bias is only an issue if it has any impact on the orbit estimation performance of the system. Therefore, research question 1D:*"What sample timing accuracy is required to achieve the desired orbit estimation accuracy?"* was investigated. It was found that this research question does not have a single answer, as it depends on many factors, including the range-rate noise of the system, the number of tracking stations, and which parameters are being estimated in addition to the orbital state.

Simulations showed that when a time bias of a second is introduced on the state estimation error is on the order of ten kilometers, when this bias is not estimated, meaning that the bias needs to be much less to achieve the desired estimation error between 100 meters and a kilometer needed to compete with the accuracy of NORAD's TLEs. However, estimating this bias reduces the state estimation error to hundred to several hundred meters when using a single tracking station, depending on the range-rate noise, and possibly to only ten meters when using three tracking stations. This is similar to what was found when there was no time bias at all. But when the initial guess of the state and the time biases were perturbed, the estimation accuracy decreased to values between hundreds of meters and ten kilometers for a single station, and approximately a kilometer for three tracking stations, depending on the range-rate noise.

Introducing a spread of one second on the bias of one second did not impact the time bias and state estimation accuracy. From these simulations it can be concluded that by estimating the time bias of DopTrackBox during the orbit estimation, a position accuracy that competes with TLEs could be achieved when at least three spread-out DopTrackBox stations are to gather passes in estimation arcs of three days in length.

As it was found that the estimation did not always converge when low range-rate noise values were used, the estimation might be improved when estimating the states in a staggered approach, decreasing the observation noise covariance to the range-rate noise value in a stepwise manner. This is only useful if the range-rate noise performance of DopTrackBox is low enough to experience these convergence issues. It is therefore recommended to investigate the range-rate noise performance of DopTrackBox, such that more representative estimations can be made.

In addition, it is recommended to investigate how the estimation performs when even more tracking stations are added to the network, as they might lead to an quicker convergence of the state estimates, and a higher estimation accuracy. As a result, the concerns about a time bias in the observations might be reduced further.

Together with the previous section, it can be concluded that the answer to research question 1.*"Is the current Leo Bodnar mini-GPS and SDRplay RSPduo combination capable enough to compete with NORAD?"* is that this equipment is sufficient, provided that the time bias in the system is being estimated, and multiple tracking stations are used with tracking arcs more than 3 days.

7.0.3. Box Design

For the prototype box in this thesis, a box was chosen with as little features as possible, while still satisfying the liquid and solid particulate ingression requirement. During the operational prototype phase of this project, it was discovered that even in the Dutch weather the temperature constraint (limited by the power supply of the Fitlet3 computer) was violated multiple times. As such, this box is

not suitable to be used in the current hardware configuration. When upgrading the power supply and changing the Fitlet3 variant to an ”extended temperature” variant, the system should not overheat in Dutch climate.

To answer research question 2A: *“What are the environmental constraints the DopTrackBox must be capable of enduring for continuous operations?”* the weather, in particular the minimum and maximum temperatures, at potential DopTrackBox locations was investigated. It was found that using the upgrade proposed above, the system should also be capable of enduring the weather at most other investigated potential DopTrackBox locations, with the exception of Khartoum (Sudan) and Sydney (Australia). However, more research is needed to find the effectiveness of other cooling options discussed in this thesis for the remainder of potential locations for which a box without any additional cooling is not sufficient.

In addition, as the prototype was only used during the warmest months of the year, it remains unclear what the temperature behavior of the box is with colder outside temperatures. It is therefore recommended to keep the prototype operational for the remainder of the year, such that its temperature behavior could be fully characterized. Then, conclusions could be drawn on the potential necessity of additional heating during cold days, to prevent freezing of the components.

Therefore, a full conclusion on research question 2C: *“What box design makes DopTrackBox compliant with weather requirements?”* and 2: *“What is the best physical design for DopTrackBox that satisfies the environmental and performance constraints?”* cannot be given using the data gathered during this thesis project.

As practical considerations for the box design, it is recommended to make a new design for the SDR bracket. The one used in this prototype only supports the SDR in the direction of gravity using two tie-wraps latching behind the legs of the SDR. If the bracket were to be inverted, there would be plastic supporting the weight of the SDR itself as well, but the limited size plastic opening would block the radio cable connector when mounted in this direction. By making a new design with supporting plastic on the other end of the bracket, with openings designed for the connector to fit through, the SDR would be supported in a safer way.

In addition, the cable gland should ideally be placed closer in the direction of the SDR radio cable connectors: the coax cables are relatively rigid, making them difficult to connect to the SDR without tension when the gland is not directly below the SDR. Although this was kept in mind when placing the gland in the prototype, it was found that ideally it should be moved even more direct below the SDR.

7.0.4. Signal-to-noise ratio

When operating the DopTrackBox prototype, a mean peak signal-to-noise ratio of 7.80 dB was found, which is significantly less than expected based on the results of earlier work. Moreover, compared to the same passes recoded by the DopTrack system, a mean difference of 9.44 dB was found. Many of the possible causes of this discrepancy have been investigated and ruled out in this thesis, yet the exact reason for the discrepancy still remains. The primary candidate cause is that purely by being on the roof, the noise of the SDR is significantly higher, compared to when it is placed in the lab. Alternatively, as measurements performed using the ATIS signal seemed less consistent, it could still be possible that the electronic noise caused by the electronics in DopTrackBox couple to its antenna, resulting in high noise.

To investigate this further, it is first recommended attempt to shield the SDR from electromagnetic

interference. In particular, it could be investigated if there is leakage from the second antenna port that is not used during the recordings. In addition, RF cavity filters could be studied as a remedy against electromagnetic interference noise. Furthermore, it could be useful to move the DopTrackBox setup to a different location, to study if this has any impact on the measured noise as well.

As many of the recorded FUNcube-1 passes (with an maximum elevation above 20 degrees) by DopTrackBox did not even have an observable signal in the data, the answer to research question 3A: *"What is the minimum signal-to-noise ratio measured by the refined DopTrackBox setup for elevations above 20 degrees during a satellite pass?"* is that with the data in this thesis a minimum cannot be established. As during the extraction process of the signal a cut of 6 dB was used, it can only be concluded that the minium signal-to-noise ratio for elevations above 20 degrees is less than 6 dB.

7.1. Design Requirements

Based on the prototype design presented in this thesis and the conclusions drawn from it in the previous sections, Tables 7.1 and 7.2 show the compliance of the design with the requirements established in Chapter 3. A checkmark indicates compliance with the requirement, a cross indicates no compliance, and a dash indicates that the status has not been investigated or is not known.

The first requirement that is not met is requirement DTB-OPS-2.06.1, but it was already established before that this is beyond the scope of this thesis. The next requirement that is not satisfied is DTB-OPS-2.08.1, but in the previous section some suggestions were given to investigate why this is not the case. The same is true for requirement DTB-OPS-2.10.

Although requirement DTB-OPS-2.09.1 should be satisfied with the prototype used in this thesis, it has not been explicitly investigated in this thesis if the actual range-rate error is smaller than this requirement, but it is recommended to confirm this in future work. The same holds for requirement DTB-OPS-2.11.

Similarly, the internal data stream of the Fitlet3 is not known, so a checkmark for requirement DTB-TECH-1.07 can not be given, but considering that this requirement was proposed as a solution to crashing recordings and no crashes have taken place during the operational phase of the DopTrackBox prototype, it can be assumed that this requirement is satisfied.

The prototype design from this thesis did not use a surge protector and was thus not protected against lightning surges. Therefore the design does not yet comply with requirement DTB-TECH-7.02. Compliance can be partly achieved using a surge protector, but full protection against direct strikes can not be guaranteed even in that case.

The last requirement, DTB-TECH-7.03, can not be as the threshold limits for the requirement had not been defined yet. Based on the temperatures at potential locations and the temperature limits of the hardware components, it is proposed to set the lower and upper temperature limit to 0 and 45°C outside temperatures. With the proposed upgrades in the previous section the design might comply with this requirement, but more research on this is needed.

Identifier	Requirement	Status
DTB-OPS-1.02	DTB shall include a computer	✓
DTB-OPS-1.03	DTB shall include an SDR	✓
DTB-OPS-1.04	DTB shall include a GPS clock	✓
DTB-OPS-1.05	DTB shall include an antenna	✓
DTB-OPS-1.07.1	DTB shall include a system to receive electrical power	✓
DTB-OPS-2.01	DTB shall be able to record automatically scheduled satellite passes	✓
DTB-OPS-2.03	DTB shall be able to operate without active internet connection during satellite passes	✓
DTB-OPS-2.04	DTB shall be able to record satellite passes without crashing	✓
DTB-OPS-2.06.1	DTB shall be able to operate on battery power for at least 60 minutes	x
DTB-OPS-2.07	DTB shall be able to store satellite data of at least 150 passes	✓
DTB-OPS-2.08.1	DTB shall be able to record FUNcube-1 passes with a mean SNR of 3.0 dB or higher when its elevation is above 20°	x
DTB-OPS-2.09.1	DTB shall be able to record satellite range-rates with a RMS error less than 5 m/s	-
DTB-OPS-2.10	The SNR difference between DTB and DT shall be no smaller than -3 dB	x
DTB-OPS-2.11	The RMS of the range-rate difference over a single pass between DTB and the predicted orbit shall be no larger than 50 m/s	-
DTB-OPS-2.12	DTB shall be able to be operated fully remotely after initial setup	✓
DTB-OPS-2.13	DTB shall be operable in an outside environment	✓

Table 7.1: Compliance of the prototype design with the proposed operational requirements. A checkmark indicates compliance, a cross indicates no compliance, a dash indicates that the status is not known/was not investigated.

Identifier	Requirement	Status
DTB-TECH-1.01.2	The computer shall have at least 2 USB type A ports	✓
DTB-TECH-1.02	The computer shall have the capability of connecting to the internet	✓
DTB-TECH-1.04	The computer shall have the means to connect to a Human Interface Device for interaction with the system	✓
DTB-TECH-1.05	The computer shall have a minimum internal storage capacity of 32 GB	✓
DTB-TECH-1.06	The computer shall be able to run Python 3.9 or newer	✓
DTB-TECH-1.07	The computer shall be able to process a data stream of 2 MB/s	-
DTB-TECH-1.08	The computer shall be capable of access via SSH	✓
DTB-TECH-2.01	The SDR shall have a connection for the antenna	✓
DTB-TECH-2.02	The SDR shall be connected to the computer via a USB type A connection	✓
DTB-TECH-2.03	The SDR shall be capable of receiving VHF signals from 30 to 300 MHz	✓
DTB-TECH-2.05	The SDR shall be capable of sampling at a sample rate of 250 kHz	✓
DTB-TECH-2.06	The SDR shall be capable of recording with a fractional frequency stability better than 10^{-8}	✓
DTB-TECH-3.02	The GPS clock shall provide an output with a fractional frequency stability better than 10^{-8}	✓
DTB-TECH-3.03	The GPS clock shall be capable of producing the reference frequency required by the SDR	✓
DTB-TECH-3.04	The GPS clock shall be capable of producing the reference signal at the shape, voltage and current required by the SDR	✓
DTB-TECH-3.05	The GPS clock output shall be capable of being connected physically to the SDR	✓
DTB-TECH-4.01	The antenna shall be capable of receiving VHF signals from 30 to 300 MHz	✓
DTB-TECH-4.03	The antenna shall be physically compatible with the SDR	✓
DTB-TECH-5.01.1	Any data storage medium shall not have any moving parts	✓
DTB-TECH-5.03.1	The data storage medium shall have a minimum capacity of 512 GB	✓
DTB-TECH-6.01	The Operating System shall be based on Linux	✓
DTB-TECH-6.02	The recorder software shall be compatible with the SDR	✓
DTB-TECH-7.01	DTB shall be dust and waterproof up to at least IP65	✓
DTB-TECH-7.02	DTB shall be protected against lightning surges	x
DTB-TECH-7.03	DTB shall be operational in temperatures between TBD and TBD degrees Celcius	-

Table 7.2: Compliance of the prototype design with the proposed technical requirements. A checkmark indicates compliance, a cross indicates no compliance and a dash indicates that the status is not known/was not investigated.

References

Akeela, Rami and Behnam Dezfouli (Apr. 18, 2018). *Software-defined Radios: Architecture, State-of-the-art, and Challenges*. DOI: 10.48550/arXiv.1804.06564. arXiv: 1804.06564[cs]. URL: http://arxiv.org/abs/1804.06564 (visited on 08/05/2025).

Allan, D.W. (1966). "Statistics of atomic frequency standards". In: *Proceedings of the IEEE* 54.2. Publisher: Institute of Electrical and Electronics Engineers (IEEE), pp. 221–230. ISSN: 0018-9219. DOI: 10.1109/proc.1966.4634. URL: http://ieeexplore.ieee.org/document/1446564/ (visited on 07/08/2025).

Ames, Sam (2025). *What is the minimum IP Rating for outdoor use?* Authority: LoopsDirect. URL: https://loopsdirect.com/blogs/help-guides/what-is-the-minimum-ip-rating-for-outdoor-use (visited on 08/28/2025).

Amza, Catalin Gheorghe et al. (Nov. 26, 2021). "Accelerated Aging Effect on Mechanical Properties of Common 3D-Printing Polymers". In: *Polymers* 13.23, p. 4132. ISSN: 2073-4360. DOI: 10.3390/polym13234132.

Another question about the Bodnar Mini GPS Unit (2025). URL: https://groups.io/g/fmt-nuts/topic/another_question_about_the/87385272 (visited on 08/30/2025).

Arduino Nano Every with headers (2025). URL: https://www.kiwi-electronics.com/nl/arduino-nano-every-with-headers-4331 (visited on 10/28/2025).

Cao, Paul (June 17, 2025). *What is the IP Rating for a weatherproof enclosure? - E-Abel*. Section: Blog. URL: https://www.eabel.com/what-is-the-ip-rating-for-a-weatherproof-enclosure/ (visited on 08/28/2025).

Chadwick, Peter E. (n.d.). "Possibilities and Limitations in Software Defined Radio Design."

Climates to Travel - world climate guide (2025). URL: https://www.climatestotravel.com/ (visited on 10/05/2025).

Csete, Alexandru and Sheila Christiansen (Mar. 20, 2020). *Evaluation of SDR Boards and Toolchains*. 1.0. URL: https://www.klofas.com/blog/2020/satnogs-station-and-minicircuits-lna-modifications/Evaluation_of_SDR_Boards-1.0.pdf (visited on 11/02/2025).

Erik Kaashoek (Jan. 9, 2023). *Using the tinyPFA to measure ADEV*. tex.entrysubtype: video. URL: https://www.youtube.com/watch?v=sBjDdNFdC9w (visited on 08/08/2025).

External Reference Clocks (June 2020).

Flohrer, Tim, Holger Krag, and Heiner Klinkrad (Jan. 1, 2008). "Assessment and Categorization of TLE Orbit Errors for the US SSN Catalogue". In.

Galile0 (Apr. 8, 2025). *G4lile0/tinyGS*. original-date: 2019-11-28T21:02:21Z. URL: https://github.com/G4lile0/tinyGS (visited on 04/11/2025).

Garg, Rakesh Kumar, Ashish Dixit, and Pavan Yadav (2008). *Basic electronics*. OCLC: 227149035. New Delhi: Laxmi Publications. ISBN: 978-81-318-0302-8.

González Martínez, Óscar (July 28, 2017). *Orbit determination of Delfi-C3 using Doppler tracking data from DopTrack ground station*. Master Thesis. Delft University of Technology.

Harding, David (July 16, 2019). *Bad Science: Converting TLEs to Keplerian Elements*. URL: https://blog.hardinglabs.com/tle-to-kep.html (visited on 01/25/2025).

How to Make Waterproof 3D Prints | All3DP (2025). URL: https://all3dp.com/2/waterproof-3d-print-pla/ (visited on 08/28/2025).

IEC (2013). *Degrees of protection provided by enclosures (IP Code)*. Edition 2.2. OCLC: 864643678. Geneva: International Electrotechnical Commission. ISBN: 978-2-8322-1086-4.

Introduction to the RSPduo (n.d.).

ITU (2024). *Radio Regulations*. 1. Geneva, Switzerland. 453 pp. URL: https://www.itu.int:443/en/publications/ITU-R/Pages/publications.aspx?parent=R-REG-RR-2024&media=electronic (visited on 07/28/2025).

ITU-R (Sept. 2016). *Attenuation by atmospheric gases*. URL: https://www.itu.int/dms_pubrec/itu-r/rec/p/R-REC-P.676-11-201609-I!!PDF-E.pdf.

Janes, Noel (Oct. 14, 2019). "ORBIT DETERMINATION USING SATNOGS AND OREKIT". Open Source CubeSat Workshop 2019. Athens. URL: https://events.libre.space/event/3/contributions/69/attachments/35/50/OD-using-Satnogs-orekit.pdf.

Kaashoek, Erik (Jan. 9, 2023). *Using the tinyPFA to measure ADEV*. URL: https://www.youtube.com/watch?v=sBjDdNFdC9w (visited on 08/08/2025).

— (n.d.). "tinyPFA, Measuring phase and frequency". RF Seminar. URL: https://www.50mhzandup.org/show/ukv0.

Luchtdruksensor / temperatuursensor / hoogtesensor BMP180 5V (2025). Funduinoshop. URL: https://funduinoshop.com/nl/elektronische-modules/sensoren/druk-en-gewicht/luchtdruksensor/temperatuursensor/hoogtesensor-bmp180-5v (visited on 10/28/2025).

MijnEchteUsername (Dec. 4, 2023). *How water tight is PLA?* r/3Dprinting. URL: https://www.reddit.com/r/3Dprinting/comments/18ap3jm/how_water_tight_is_pla/ (visited on 08/28/2025).

Mini Precision GPS Reference Clock : Leo Bodnar Electronics (2025). URL: https://www.leobodnar.com/shop/index.php?main_page=product_info&cPath=107&products_id=301 (visited on 08/07/2025).

Orbit Determination from SatNOGS data - SatNOGS (Apr. 18, 2024). Libre Space Community. Section: SatNOGS. URL: https://community.libre.space/t/orbit-determination-from-satnogs-data/11643 (visited on 04/11/2025).

Orbital elements (July 14, 2025). In: *Wikipedia*. Page Version ID: 1300409584. URL: https://en.wikipedia.org/w/index.php?title=Orbital_elements&oldid=1300409584 (visited on 08/06/2025).

pericynthion (Dec. 3, 2014). *Answer to "What is the accuracy / uncertainty of Two Line Elements (TLEs)?"*. Space Exploration Stack Exchange. URL: https://space.stackexchange.com/a/6168 (visited on 03/15/2025).

Question about the Bodnar mini GPSDO unit (2025). URL: https://groups.io/g/fmt-nuts/topic/question_about_the_bodnar/87523478 (visited on 08/30/2025).

Reeve, Whitham D (Nov. 25, 2020). *Using the SDRPlay SDR Receivers with an External Frequency Reference*.

Riley, W J and W J Riley (2008). *Handbook of frequency stability analysis*. Gaithersburg, MD: National Institute of Standards and Technology. DOI: 10.6028/nist.sp.1065. URL: https://nvlpubs.nist.gov/nistpubs/Legacy/SP/nistspecialpublication1065.pdf (visited on 07/10/2025).

Root, Bart et al. (n.d.). *The DopTrack Experiment Operational Manual*.

Running an RPI outside? - Raspberry Pi Forums (2025). URL: https://forums.raspberrypi.com/viewtopic.php?t=242551 (visited on 08/28/2025).

SatNOGS (2025). Open Source global network of satellite ground-stations. URL: https://satnogs.org/ (visited on 04/11/2025).

Semi-major and semi-minor axes (Mar. 13, 2025). In: *Wikipedia*. URL: https://en.wikipedia.org/w/index.php?title=Semi-major_and_semi-minor_axes&oldid=1280281991 (visited on 08/06/2025).

SOCIS 2019 (July 10, 2019). *SOCIS 2019: Orbit Determination with SatNOGS - Orekit usage*. Orekit. Section: Orekit usage. URL: https://forum.orekit.org/t/socis-2019-orbit-determination-with-satnogs/534 (visited on 04/11/2025).

Søndergaard, Martin H.A. (Apr. 16, 2018). *Accuracy of the DopTrack satellite tracking system compared to two-line elements*. Bachelor Thesis. Inholland University of Applied Sciences & Delft University of Technology.

Spectracom (Feb. 26, 2018). *EPSILON CLOCK MODEL EC20S User's Manual*.

Sprenkels, Amber (Oct. 26, 2023). *Portable Doppler Tracking Groundstation*. Master Thesis. Delft: Delft University of Technology.

tinydevices.org | TinyPFA / First Use (2025). URL: https://www.tinydevices.org/wiki/pmwiki.php?n=TinyPFA.FirstUse (visited on 08/07/2025).

tinydevices.org | TinyPFA / Menu Tree (2025). URL: https://www.tinydevices.org/wiki/pmwiki.php?n=TinyPFA.MenuTree (visited on 08/08/2025).

TinyGS (2025). Unleash Your Inner Explorer: Build a Tiny Ground Station and Help Secure Our Space Future. URL: https://tinygs.com/ (visited on 04/11/2025).

USRP Hardware Driver and USRP Manual: Device Synchronization (2025). URL: https://files.ettus.com/manual/page_sync.html (visited on 03/15/2025).

Vig, John R (June 1997). *Introduction to Quartz Frequency Standards*. Research and Development Technical Report CECOM-TR-97-3. U.S. Army Communications-Electronics Command.

Wertz, James R. and Wiley J. Larson, eds. (2008). *Space mission analysis and design: SMAD III*. 3. ed., 10. print. Space technology library 8. Hawthorne, Calif: Microcosm Press [u.a.] 976 pp. ISBN: 978-1-881883-10-4 978-0-7923-5901-2.

A

Model & Simulations Validation

A.1. Numerical Integrator

As the goal is to have an estimation error on the order of 100 meters, the integration error during the propagation should be significantly less than this. It is assumed that one order of magnitude is a sufficient accuracy. Figure A.1 shows the difference in position as function of time when using an RK4 fixed step integrator with timestep Δt versus $\Delta t/2$. To generate the truth orbit, the computational efficiency is less relevant, as it only has to be performed once. The chosen stepsize of 4 seconds leads to an integration error of 0.1 meters, significantly better than the requirement, as can be seen in figure A.2. For the integrator of the estimation, the chosen stepsize of 8 seconds corresponds to an integration error between 1 and 10 meters over the full 6 days propagation span. However, as the estimation arc is at most 3 days, the expected integration error is only on the order of 1 meter.

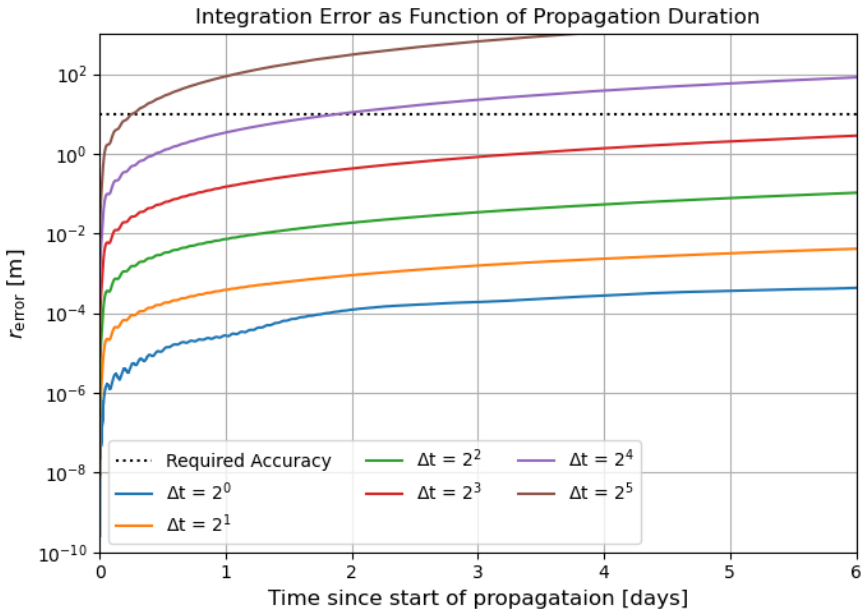

Figure A.1: Integration error as function of propagation duration for a simulated satellite orbit with similar parameters to Delfi-C3, for different fixed time step values of an RK4 integrator.

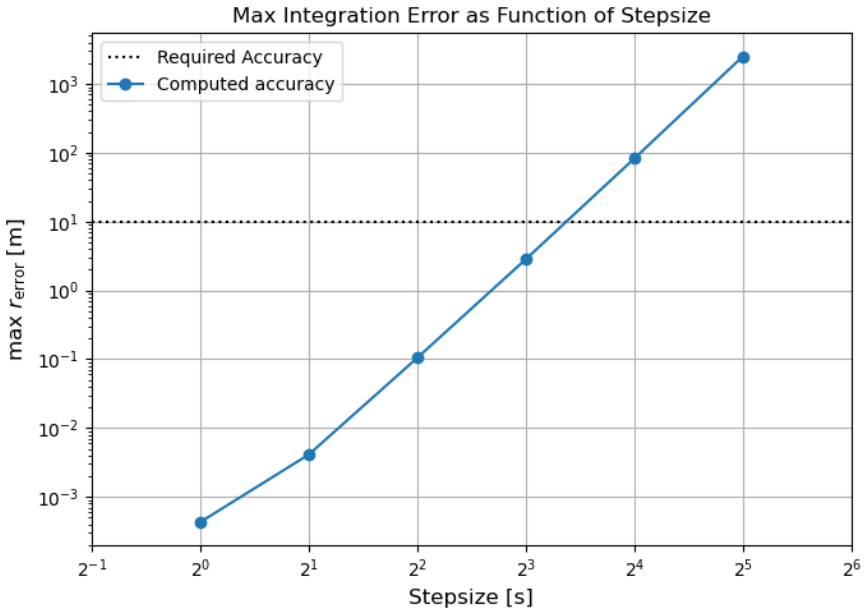

Figure A.2: Maximum integration error of a 6-day propagation for a simulated satellite orbit with similar parameters to Delfi-C3, as function of different fixed time step values of an RK4 integrator.

B

Additional Figures

B.1. Simulated Orbit Estimation

The orbit estimation results as shown in the thesis are shown here again, but for a per pass and per day orbital state arc. An empty image indicates non of the estimations converged.

B.1.1. Per Day Estimation

State Only Estimation

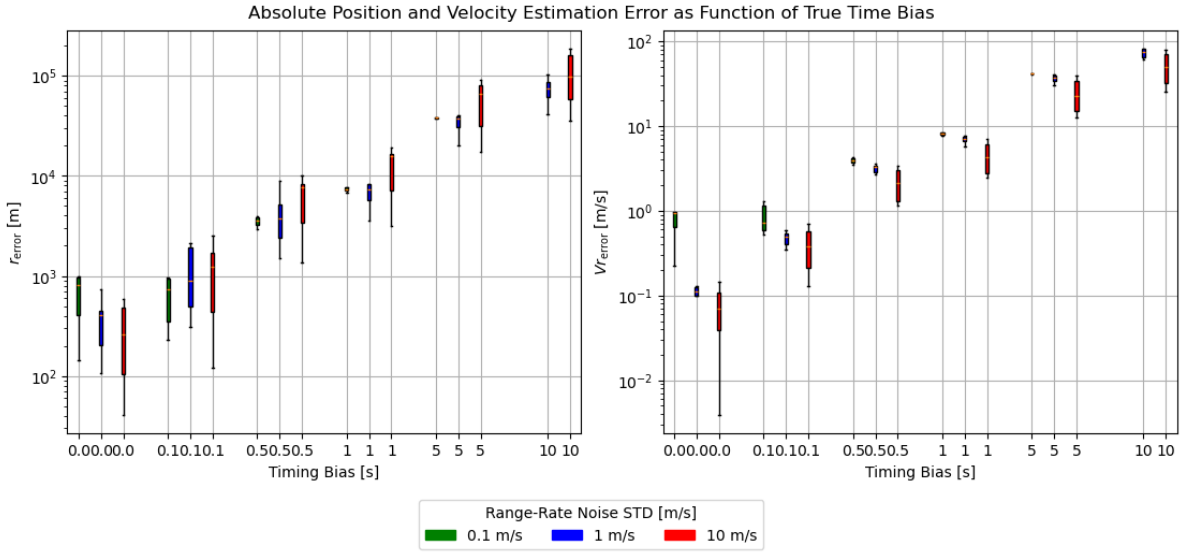

Figure B.1: Cartesian state estimation error when using a single tracking station, with six tracking arcs of 1 day each. In this estimation, only the cartesian state is estimated.

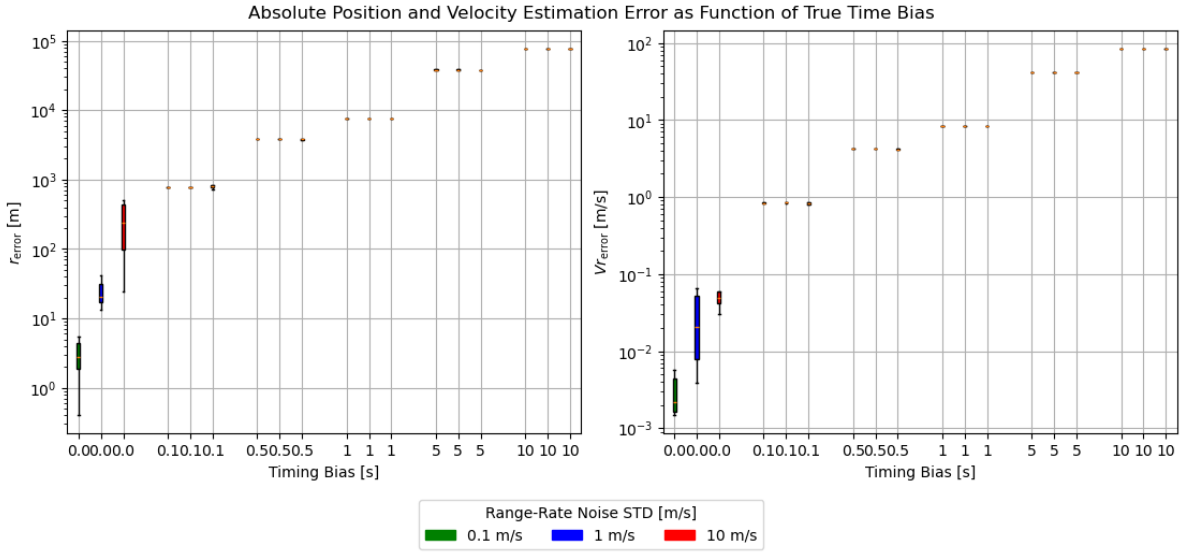

Figure B.2: Cartesian state estimation error when using three tracking stations, with six tracking arcs of 1 day each. In this estimation, only the cartesian state is estimated.

State & Time Bias Estimation

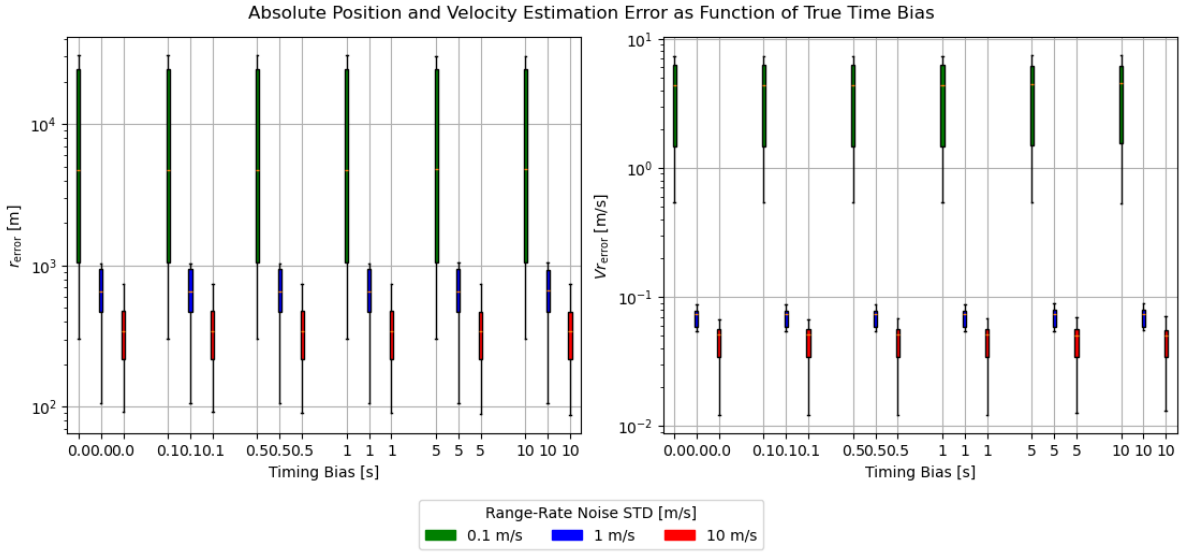

Figure B.3: Cartesian state estimation error when using a single tracking station,with six tracking arcs of 1 day each. In this estimation, both the cartesian state, and a per pass time observation bias is estimated.

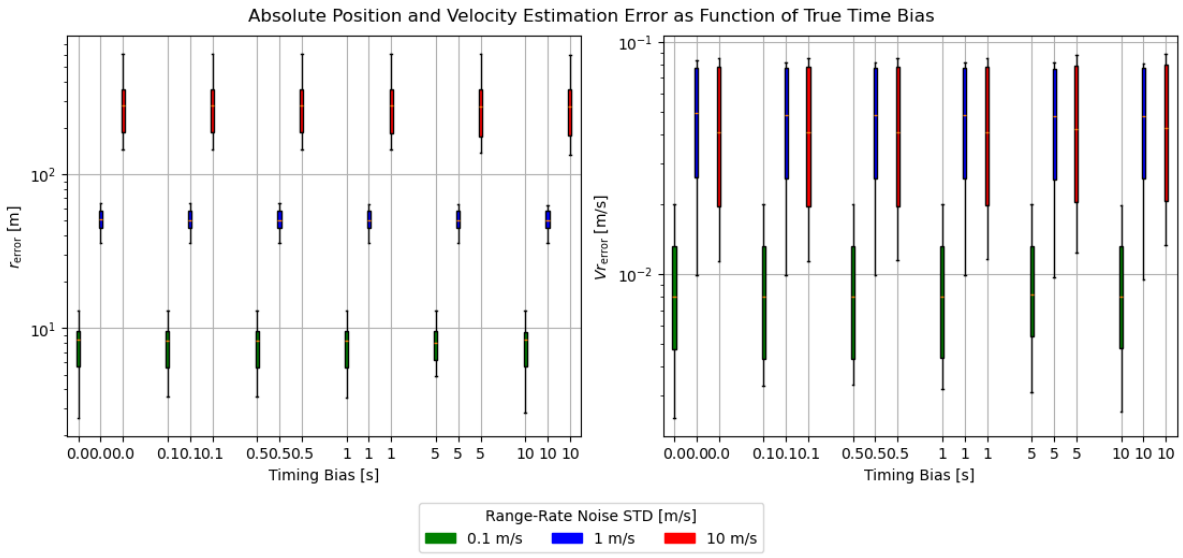

Figure B.4: Cartesian state estimation error when using three tracking stations, with six tracking arcs of 1 day each. In this estimation, both the cartesian state, and a per pass time observation bias is estimated.

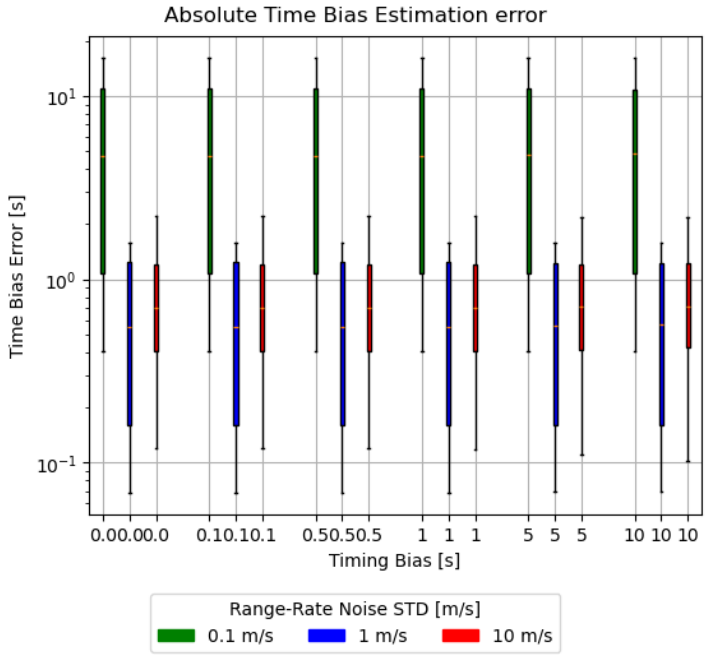

Figure B.5: Per pass time bias estimation error, using a single tracking station, with six tracking arcs of 1 day each. In this estimation, both the cartesian state, and a per pass time observation bias is estimated.

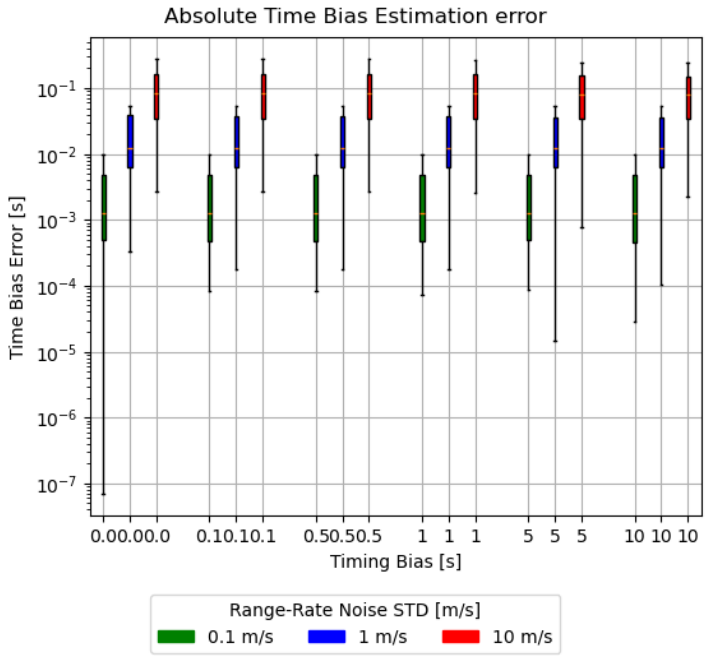

Figure B.6: Per pass time bias estimation error, using three tracking stations, with six tracking arcs of 1 day each. In this estimation, both the cartesian state, and a per pass time observation bias is estimated.

State, Time Bias, Range-Rate & Drag Estimation

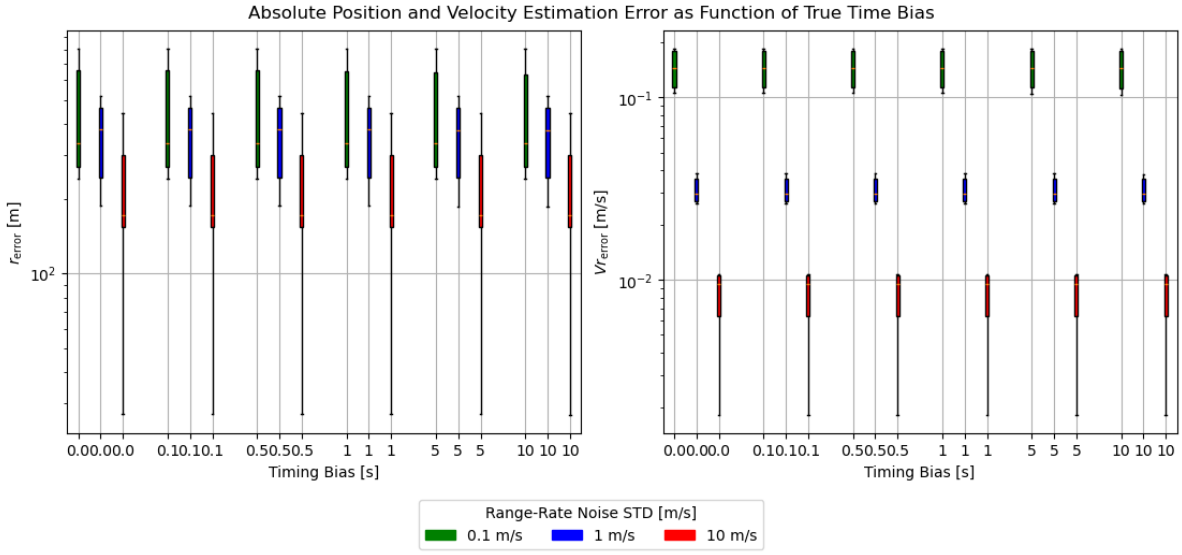

Figure B.7: Cartesian state estimation error when using a single tracking station, with six tracking arcs of 1 day each. In this estimation, a cartesian state, and a per pass time observation bias is estimated, as well as a per arc drag parameter and per pass range-rate bias.

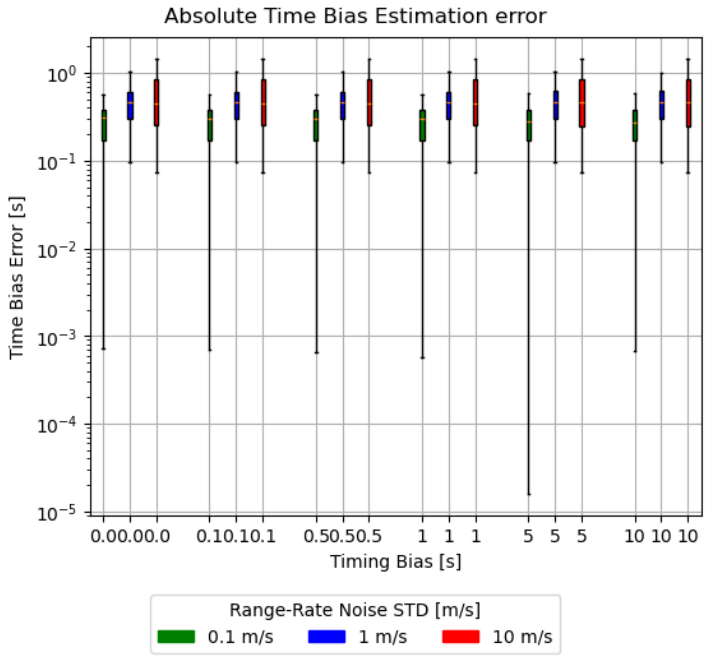

Figure B.8: Per pass time bias estimation error, using a single tracking station, with six tracking arcs of 1 day each. In this estimation, a cartesian state, and a per pass time observation bias is estimated, as well as a per arc drag parameter and per pass range-rate bias.

Perturbed State & Time Bias Estimation

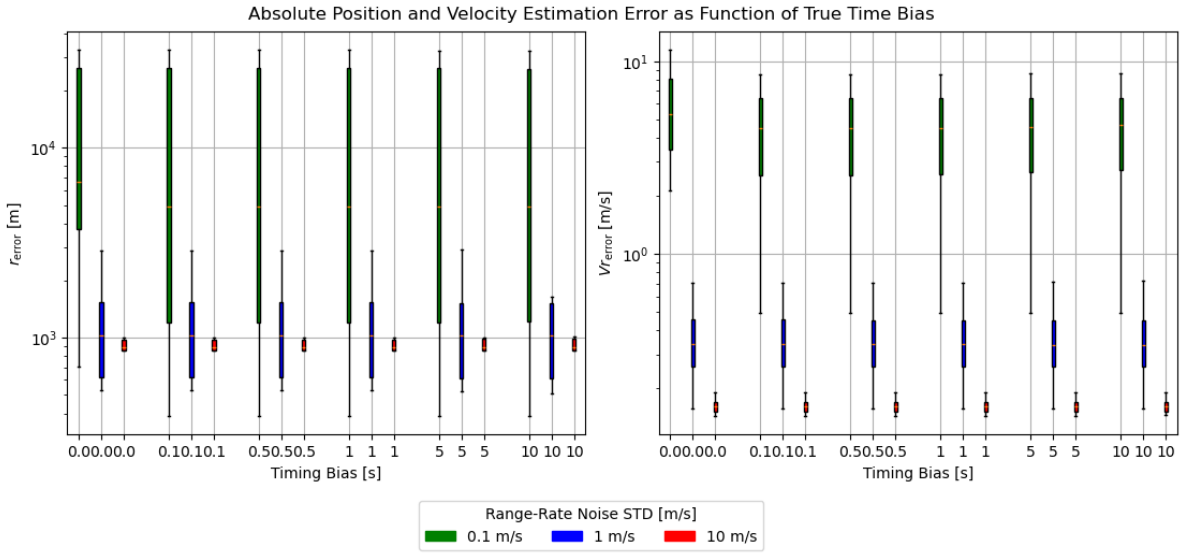

Figure B.9: Cartesian state estimation error when using a single tracking station, with six tracking arcs of 1 day each. In this estimation, both the cartesian state, and a per pass time observation bias is estimated. For this estimation, the initial guess of the cartesian state was perturbed.

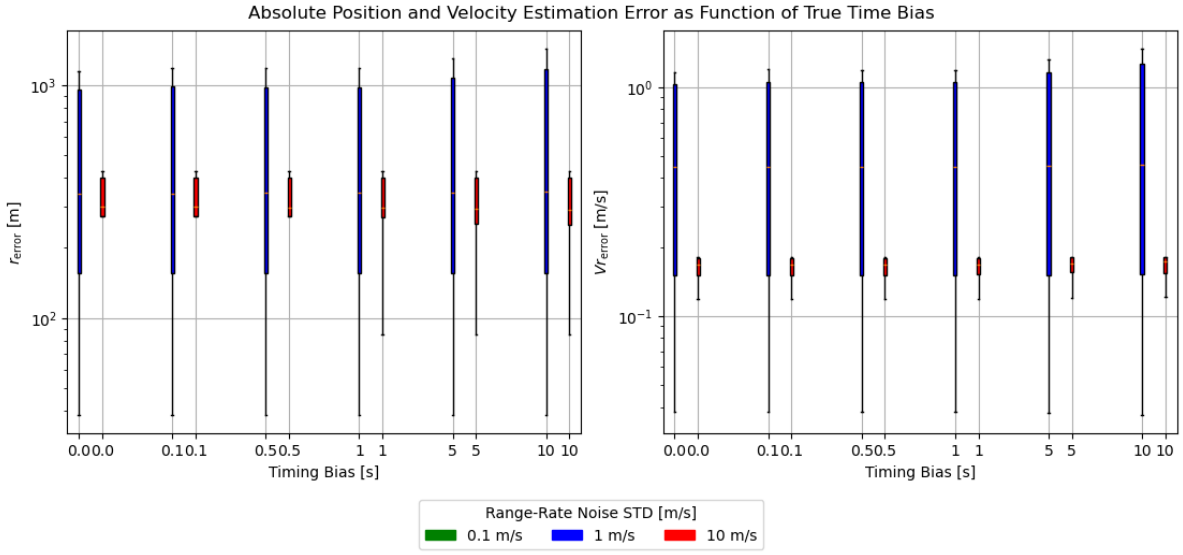

Figure B.10: Cartesian state estimation error when using three tracking stations, with six tracking arcs of 1 day each. In this estimation, both the cartesian state, and a per pass time observation bias is estimated. For this estimation, the initial guess of the cartesian state was perturbed.

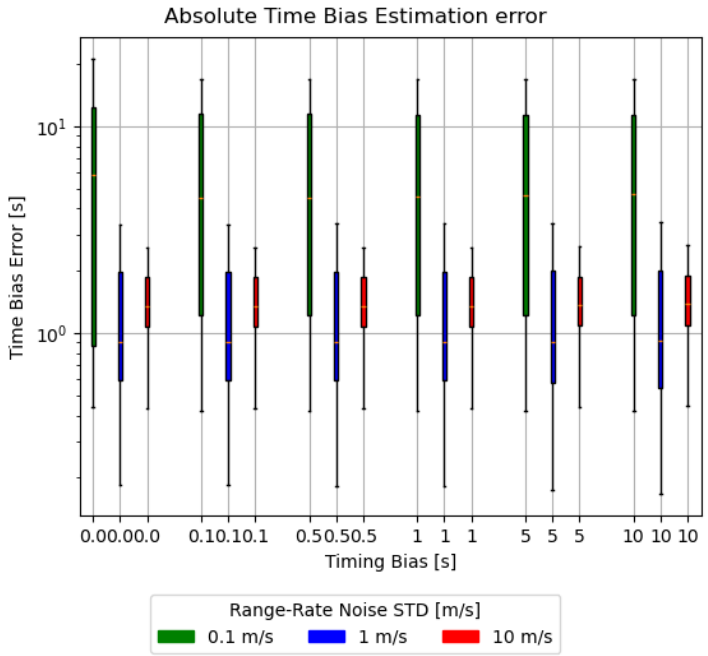

Figure B.11: Per pass time bias estimation error, using a single tracking station, with six tracking arcs of 1 day each. In this estimation, both the cartesian state, and a per pass time observation bias is estimated. For this estimation, the initial guess of the cartesian state was perturbed.

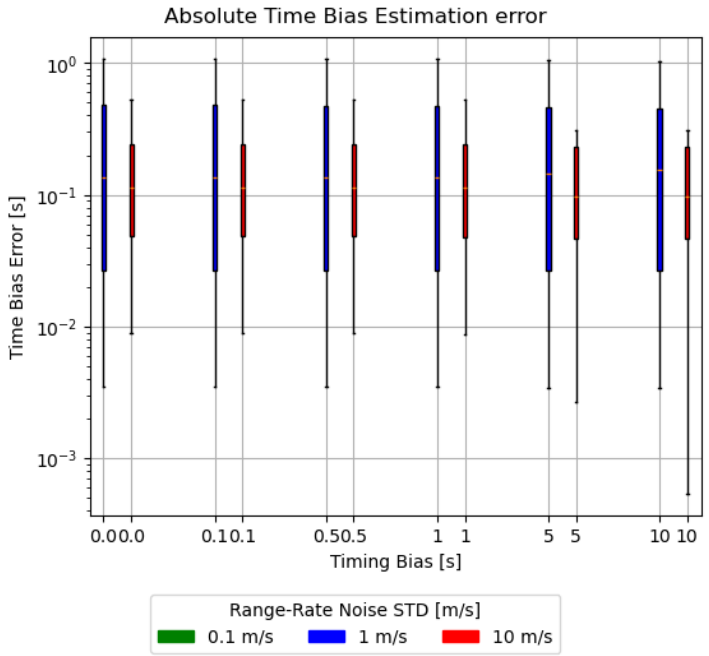

Figure B.12: Per pass time bias estimation error, using three tracking stations, with six tracking arcs of 1 day each. In this estimation, both the cartesian state, and a per pass time observation bias is estimated. For this estimation, the initial guess of the cartesian state was perturbed.

Perturbed State & Perturbed Time Bias Estimation

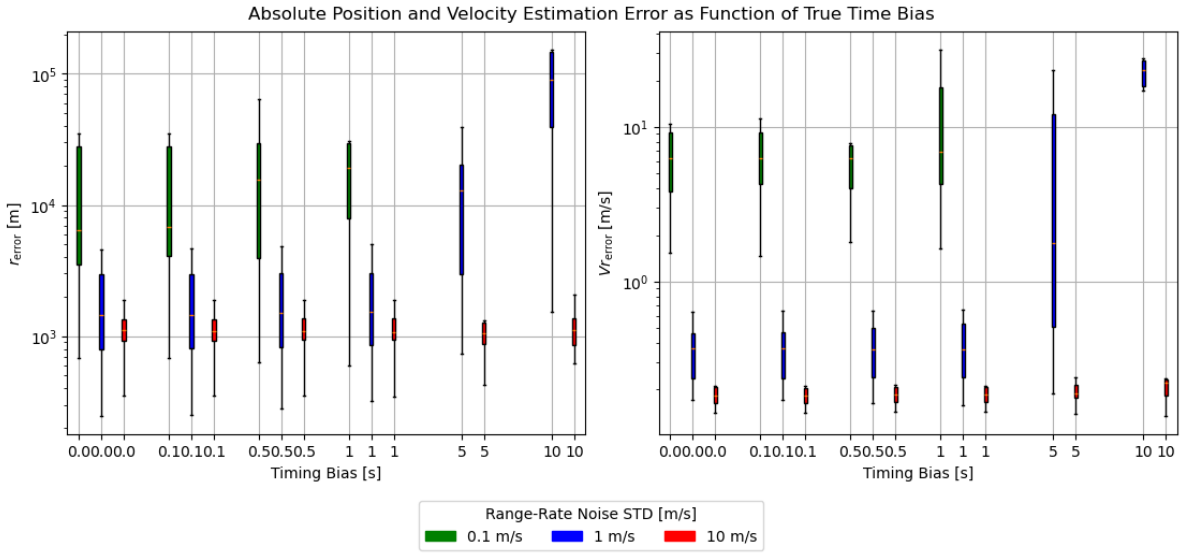

Figure B.13: Cartesian state estimation error when using a single tracking station, with six tracking arcs of 1 day each. In this estimation, both the cartesian state, and a per pass time observation bias is estimated. For this estimation, both the initial guess of the cartesian state and the time bias were perturbed.

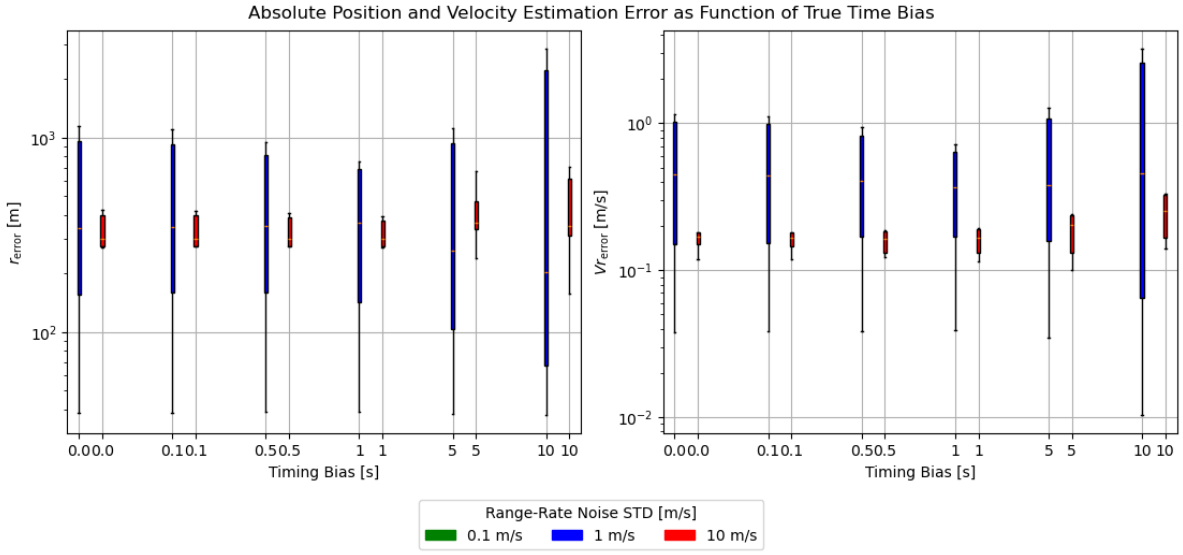

Figure B.14: Cartesian state estimation error when using three tracking stations, with six tracking arcs of 1 day each. In this estimation, both the cartesian state, and a per pass time observation bias is estimated. For this estimation, both the initial guess of the cartesian state and the time bias were perturbed.

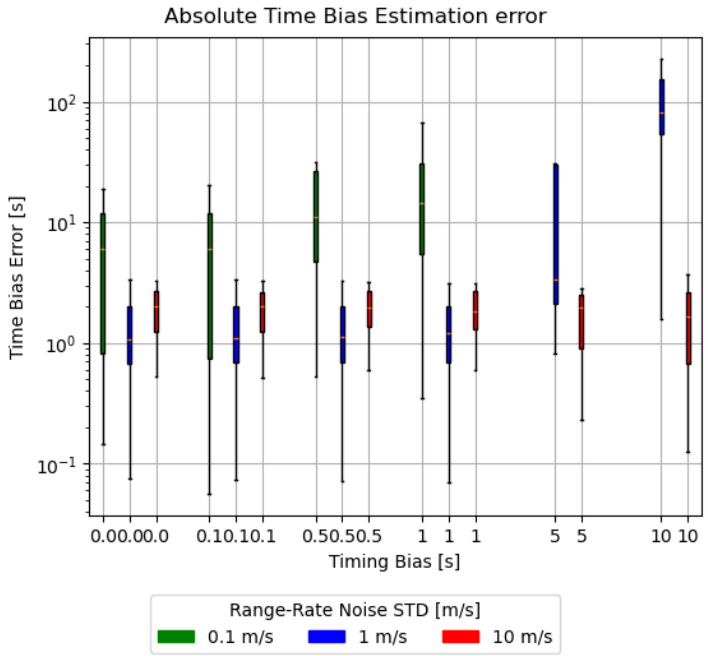

Figure B.15: Per pass time bias estimation error, using a single tracking station, with six tracking arcs of 1 day each. In this estimation, both the cartesian state, and a per pass time observation bias is estimated. For this estimation, both the initial guess of the cartesian state and the time bias were perturbed.

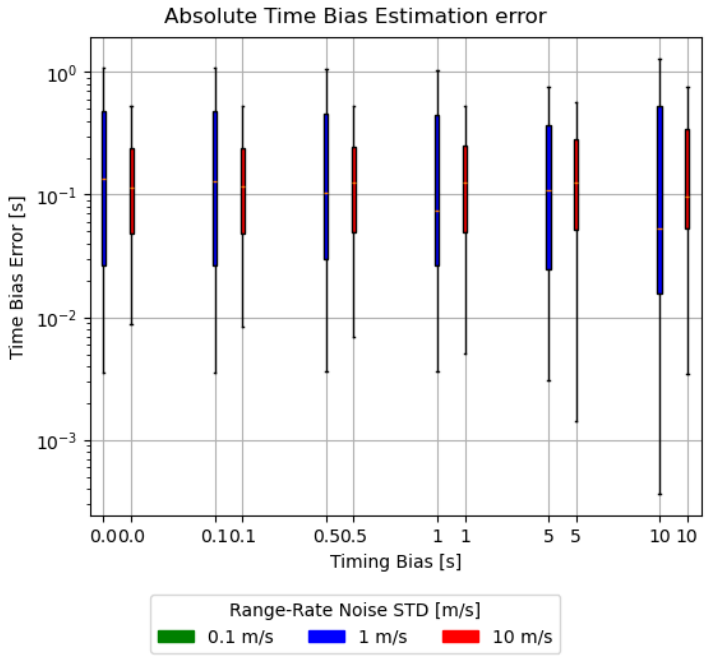

Figure B.16: Per pass time bias estimation error, using three tracking stations, with six tracking arcs of 1 day each. In this estimation, both the cartesian state, and a per pass time observation bias is estimated. For this estimation, both the initial guess of the cartesian state and the time bias were perturbed.

Perturbed State & Perturbed Fluctuating Time Bias Estimation

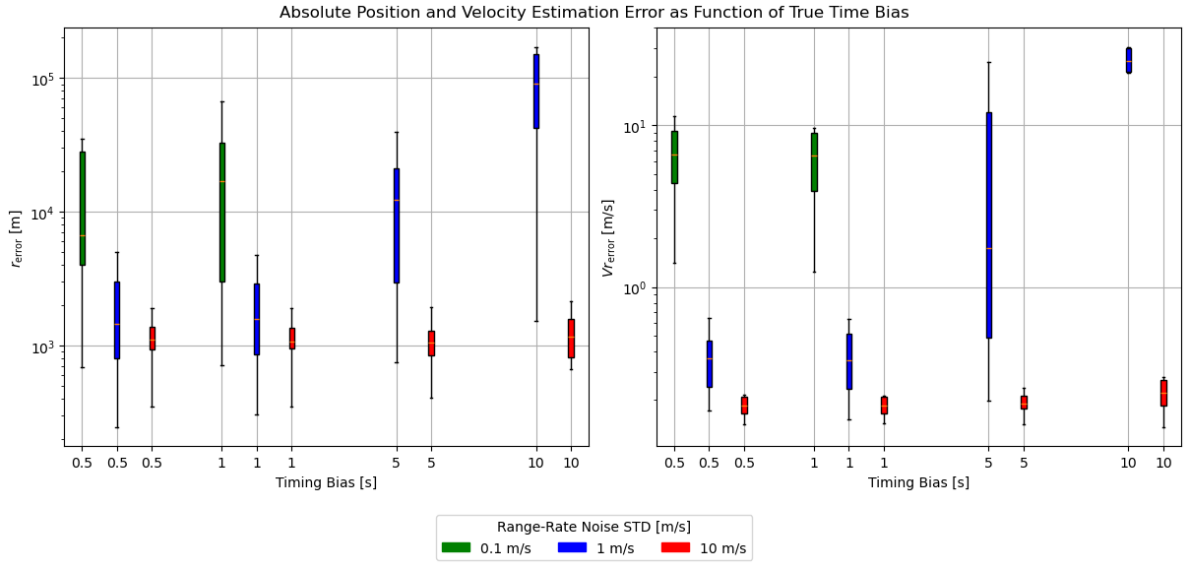

Figure B.17: Cartesian state estimation error when using a single tracking station, with six tracking arcs of 1 day each. In this estimation, both the cartesian state, and a per pass time observation bias is estimated. For this estimation, both the initial guess of the cartesian state and the time bias were perturbed. Instead of a constant bias per pass, there was a spread on the true bias.

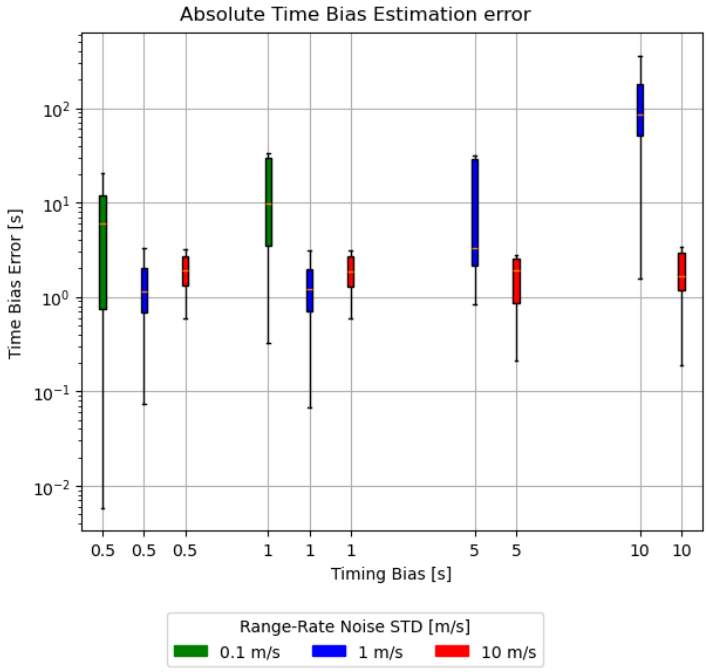

Figure B.18: Per pass time bias estimation error, using a single tracking station, with six tracking arcs of 1 day each. In this estimation, both the cartesian state, and a per pass time observation bias is estimated. For this estimation, both the initial guess of the cartesian state and the time bias were perturbed. Instead of a constant bias per pass, there was a spread on the true bias.

B.1.2. Per Pass Estimation

State Only Estimation

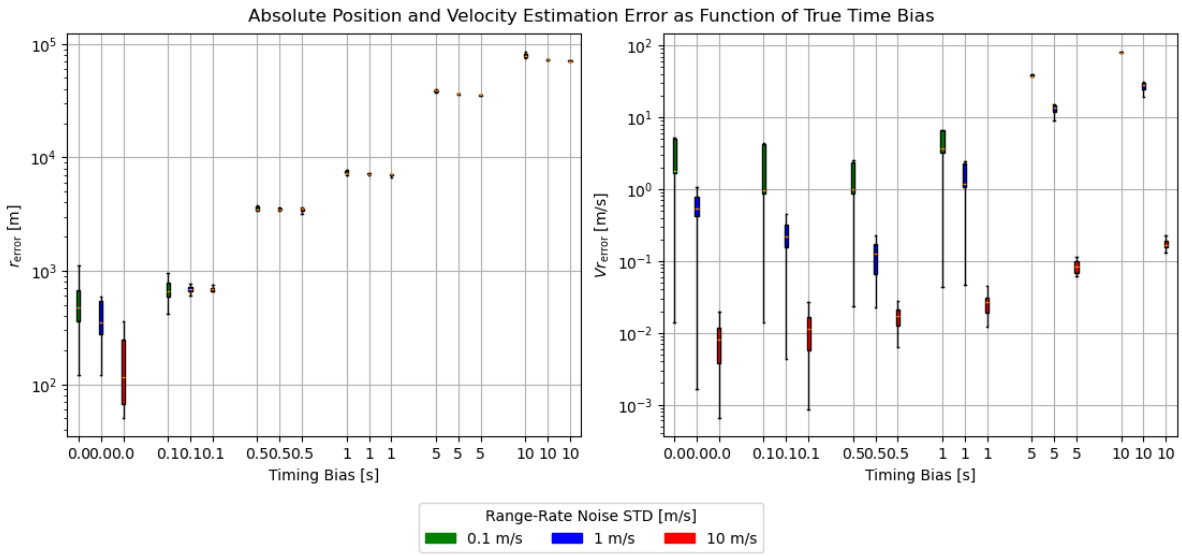

Figure B.19: Cartesian state estimation error when using a single tracking station, with one tracking arc per pass. In this estimation, only the cartesian state is estimated.

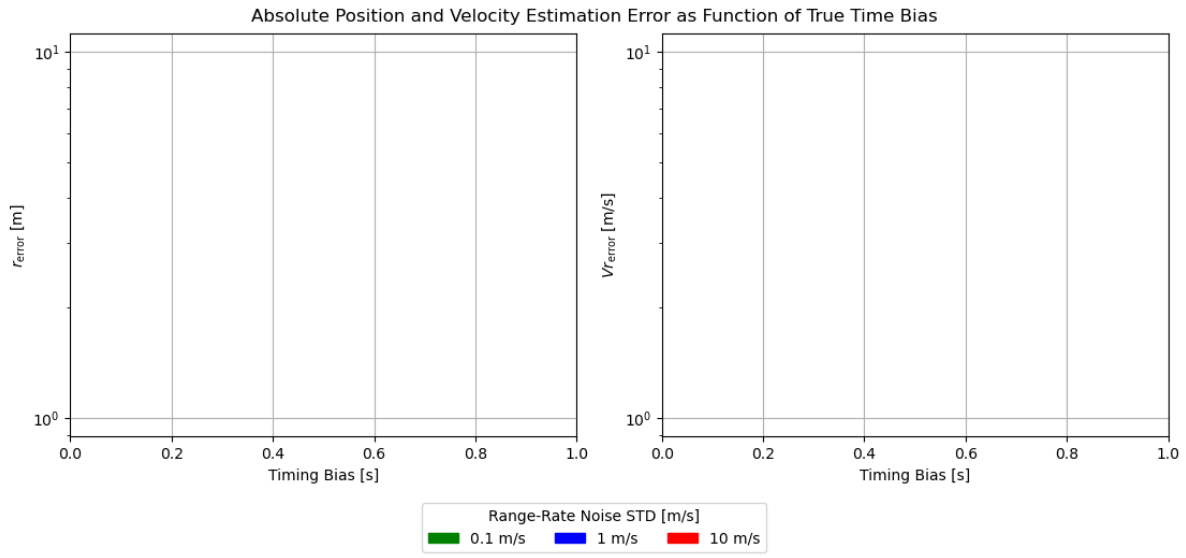

Figure B.20: Cartesian state estimation error when using three tracking stations, with one tracking arc per pass. In this estimation, only the cartesian state is estimated.

State & Time Bias Estimation

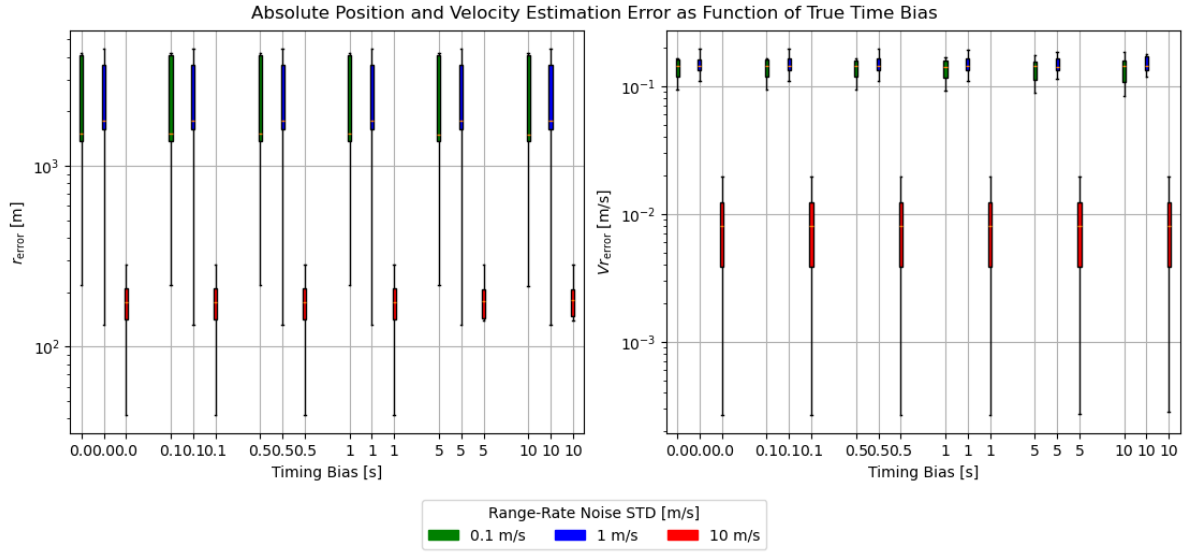

Figure B.21: Cartesian state estimation error when using a single tracking station, with one tracking arc per pass. In this estimation, both the cartesian state, and a per pass time observation bias is estimated.

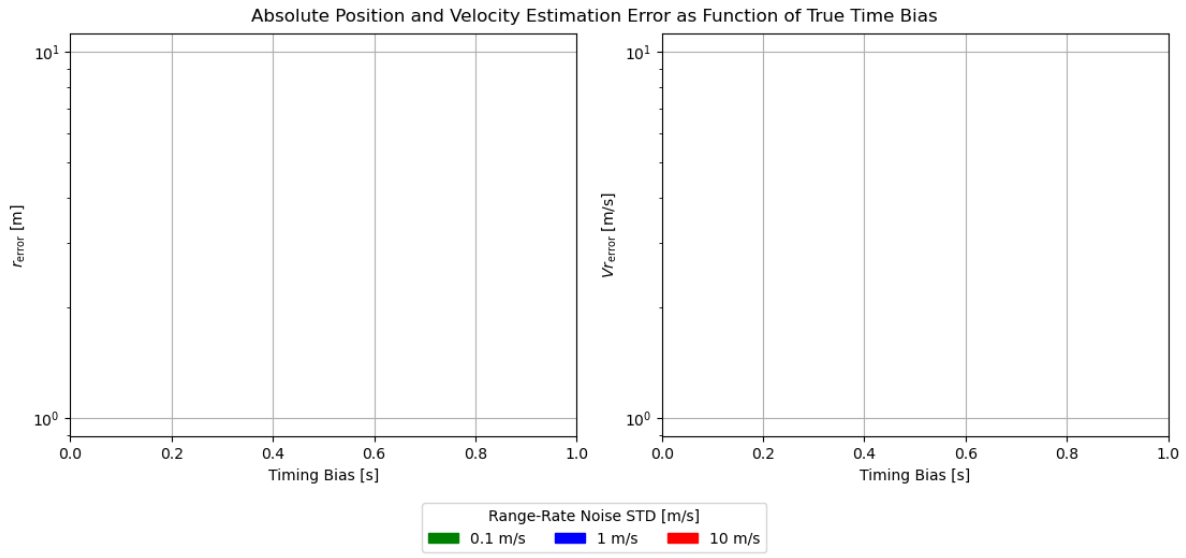

Figure B.22: Cartesian state estimation error when using three tracking stations, with one tracking arc per pass. In this estimation, both the cartesian state, and a per pass time observation bias is estimated.

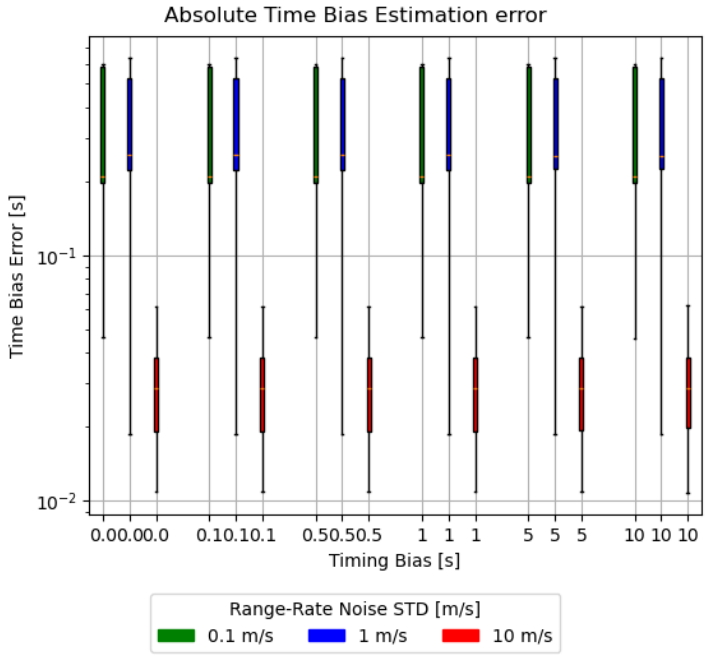

Figure B.23: Per pass time bias estimation error, using a single tracking station, with one tracking arc per pass. In this estimation, both the cartesian state, and a per pass time observation bias is estimated.

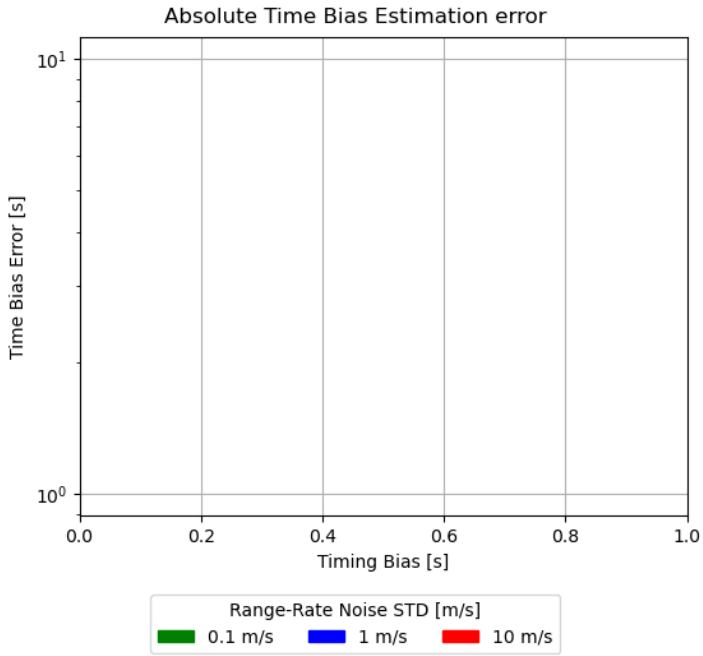

Figure B.24: Per pass time bias estimation error, using three tracking stations, with one tracking arc per pass. In this estimation, both the cartesian state, and a per pass time observation bias is estimated.

State, Time Bias, Range-Rate & Drag Estimation

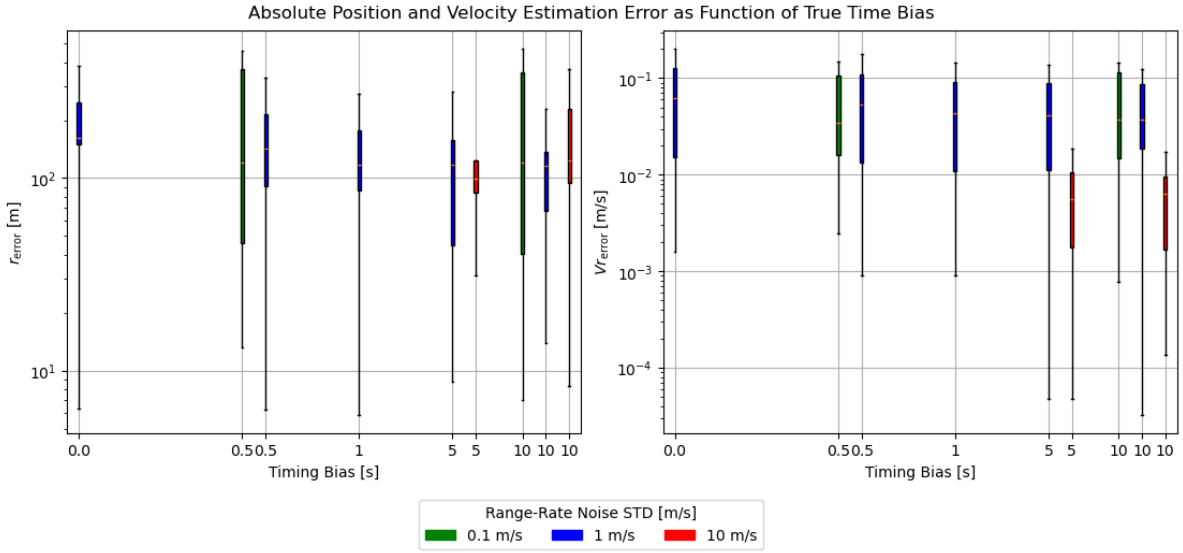

Figure B.25: Cartesian state estimation error when using a single tracking station, with one tracking arc per pass. In this estimation, a cartesian state, and a per pass time observation bias is estimated, as well as a per arc drag parameter and per pass range-rate bias.

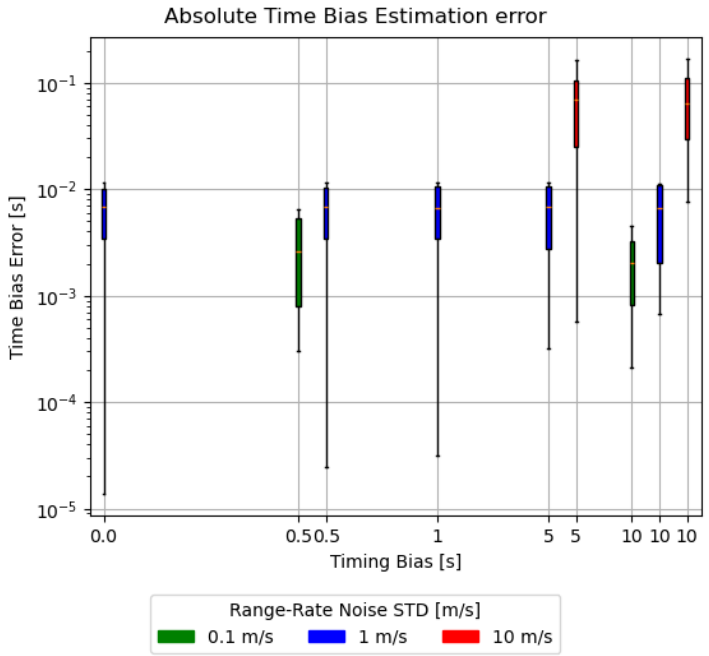

Figure B.26: Per pass time bias estimation error, using a single tracking station, with one tracking arc per pass. In this estimation, a cartesian state, and a per pass time observation bias is estimated, as well as a per arc drag parameter and per pass range-rate bias.

Perturbed State & Time Bias Estimation

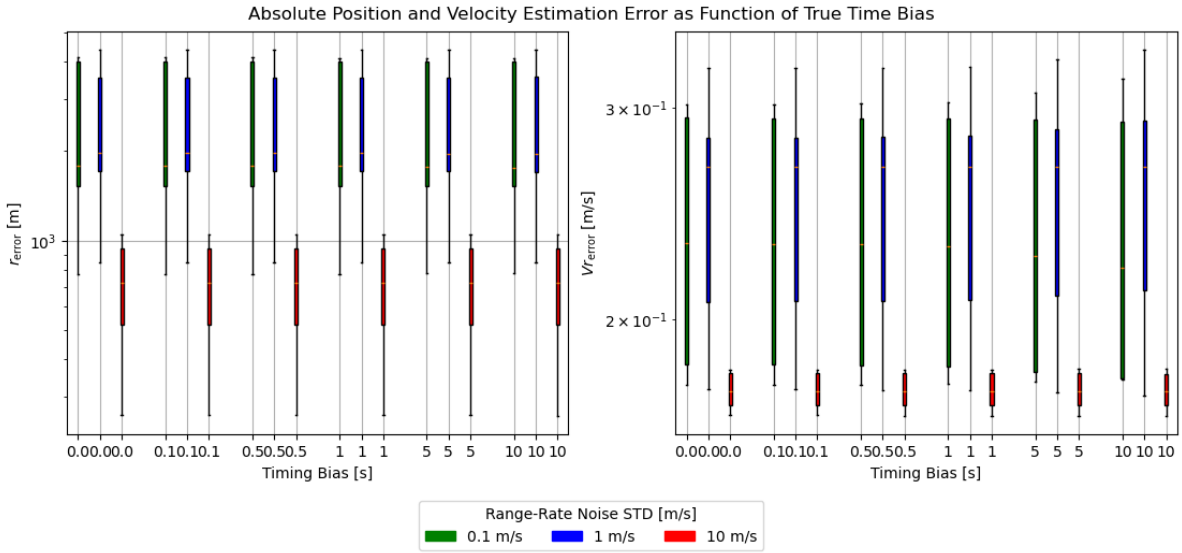

Figure B.27: Cartesian state estimation error when using a single tracking station, with one tracking arc per pass. In this estimation, both the cartesian state, and a per pass time observation bias is estimated. For this estimation, the initial guess of the cartesian state was perturbed.

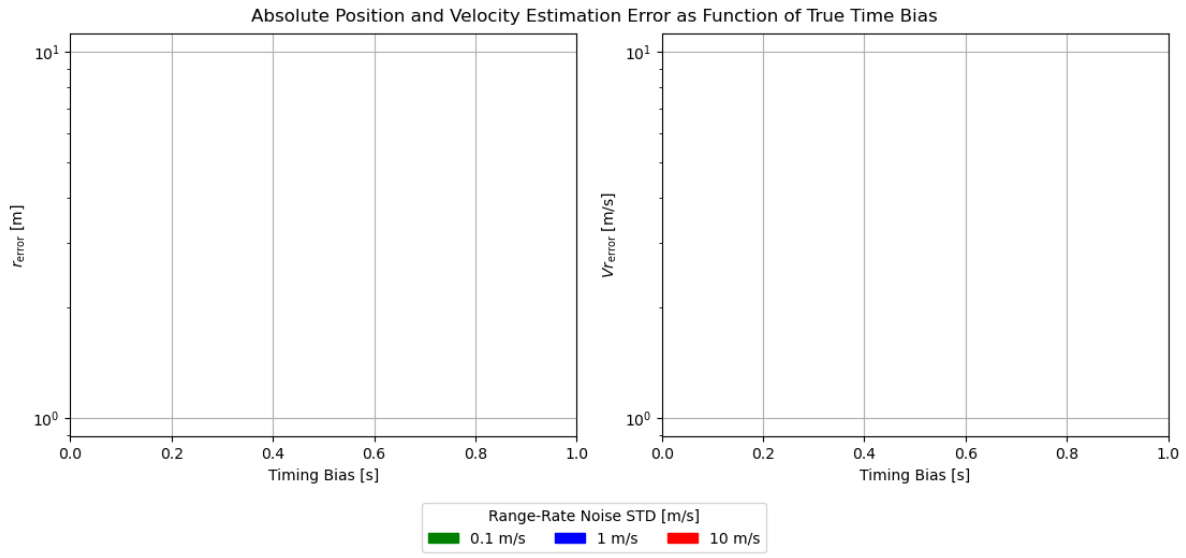

Figure B.28: Cartesian state estimation error when using three tracking stations, with one tracking arc per pass. In this estimation, both the cartesian state, and a per pass time observation bias is estimated. For this estimation, the initial guess of the cartesian state was perturbed.

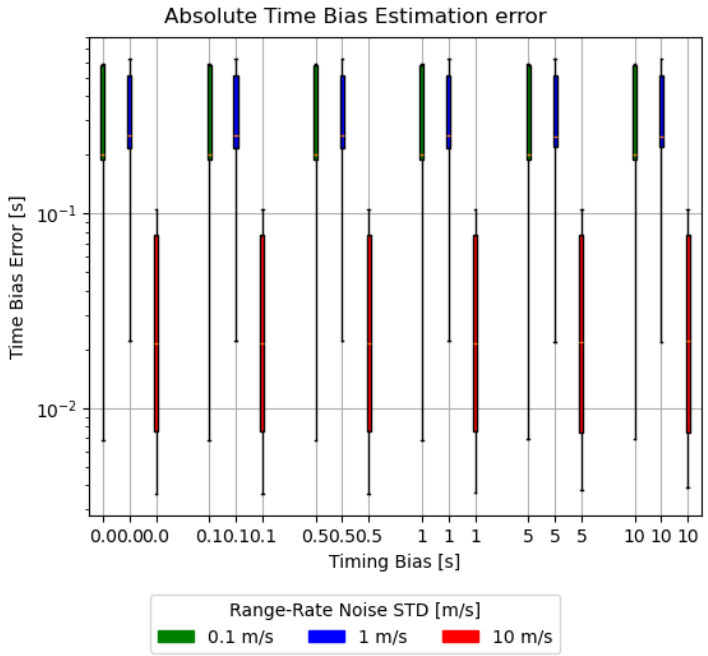

Figure B.29: Per pass time bias estimation error, using a single tracking station, with one tracking arc per pass. In this estimation, both the cartesian state, and a per pass time observation bias is estimated. For this estimation, the initial guess of the cartesian state was perturbed.

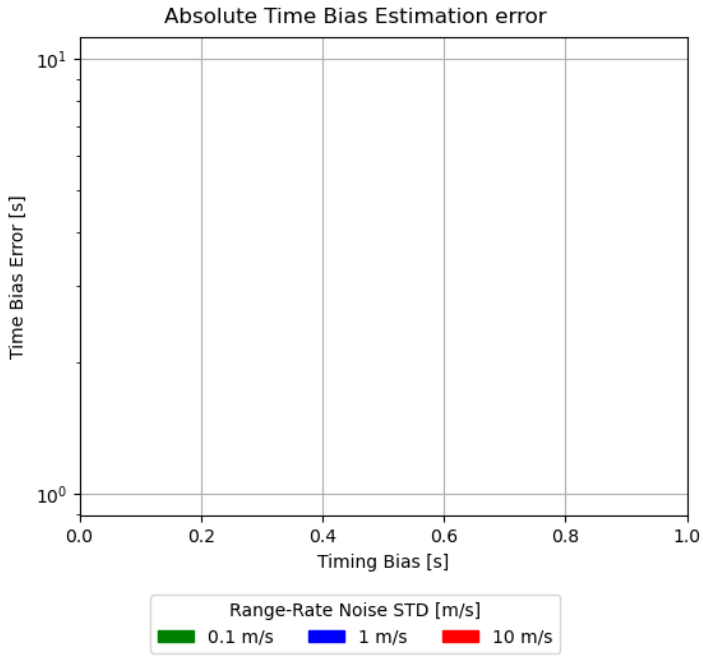

Figure B.30: Per pass time bias estimation error, using three tracking stations, with one tracking arc per pass. In this estimation, both the cartesian state, and a per pass time observation bias is estimated. For this estimation, the initial guess of the cartesian state was perturbed.

Perturbed State & Perturbed Time Bias Estimation

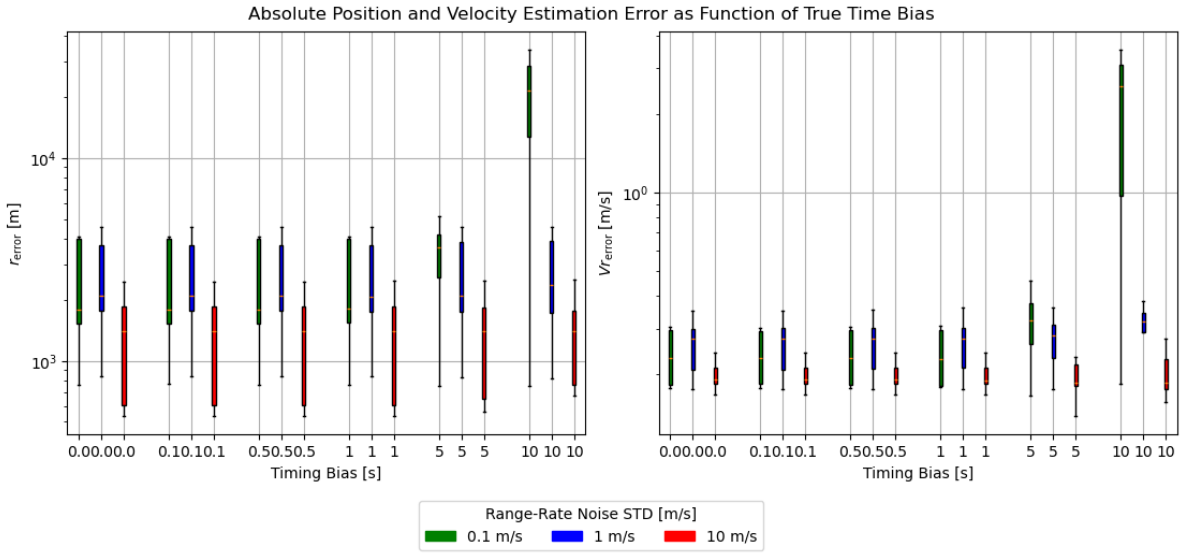

Figure B.31: Cartesian state estimation error when using a single tracking station, with one tracking arc per pass. In this estimation, both the cartesian state, and a per pass time observation bias is estimated. For this estimation, both the initial guess of the cartesian state and the time bias were perturbed.

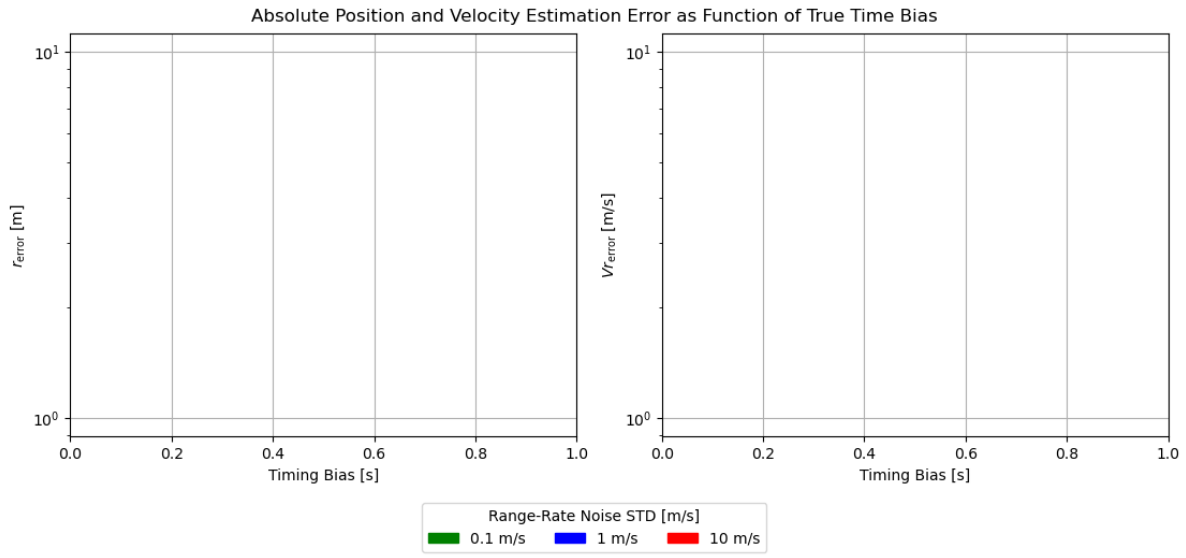

Figure B.32: Cartesian state estimation error when using three tracking stations, with one tracking arc per pass. In this estimation, both the cartesian state, and a per pass time observation bias is estimated. For this estimation, both the initial guess of the cartesian state and the time bias were perturbed.

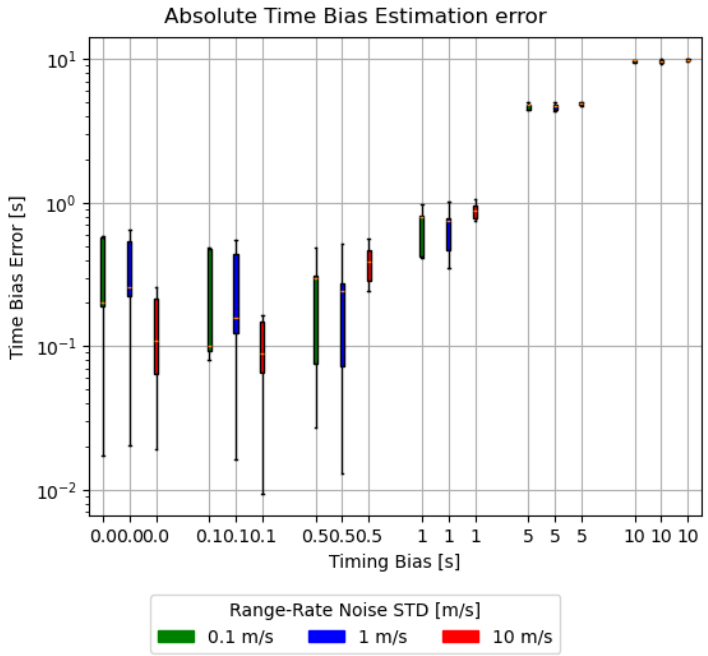

Figure B.33: Per pass time bias estimation error, using a single tracking station, with one tracking arc per pass. In this estimation, both the cartesian state, and a per pass time observation bias is estimated. For this estimation, both the initial guess of the cartesian state and the time bias were perturbed.

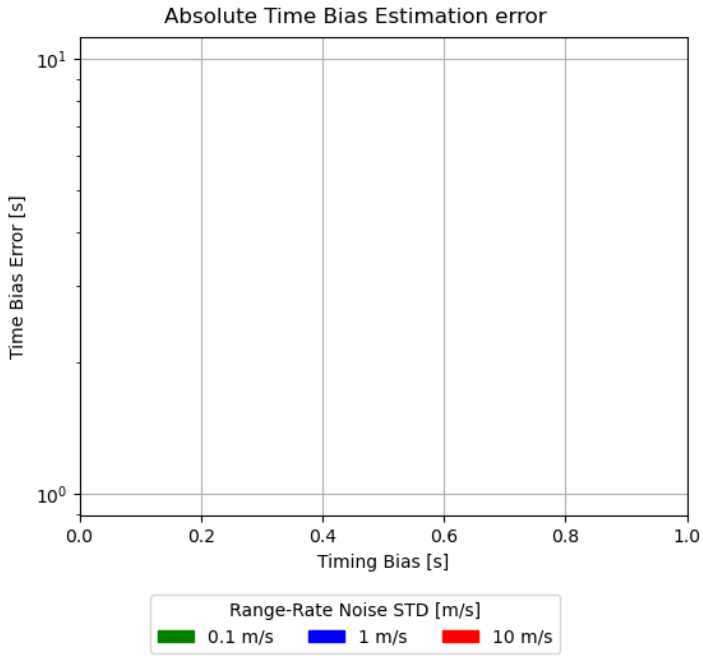

Figure B.34: Per pass time bias estimation error, using three tracking stations, with one tracking arc per pass. In this estimation, both the cartesian state, and a per pass time observation bias is estimated. For this estimation, both the initial guess of the cartesian state and the time bias were perturbed.

Perturbed State & Perturbed Fluctuating Time Bias Estimation

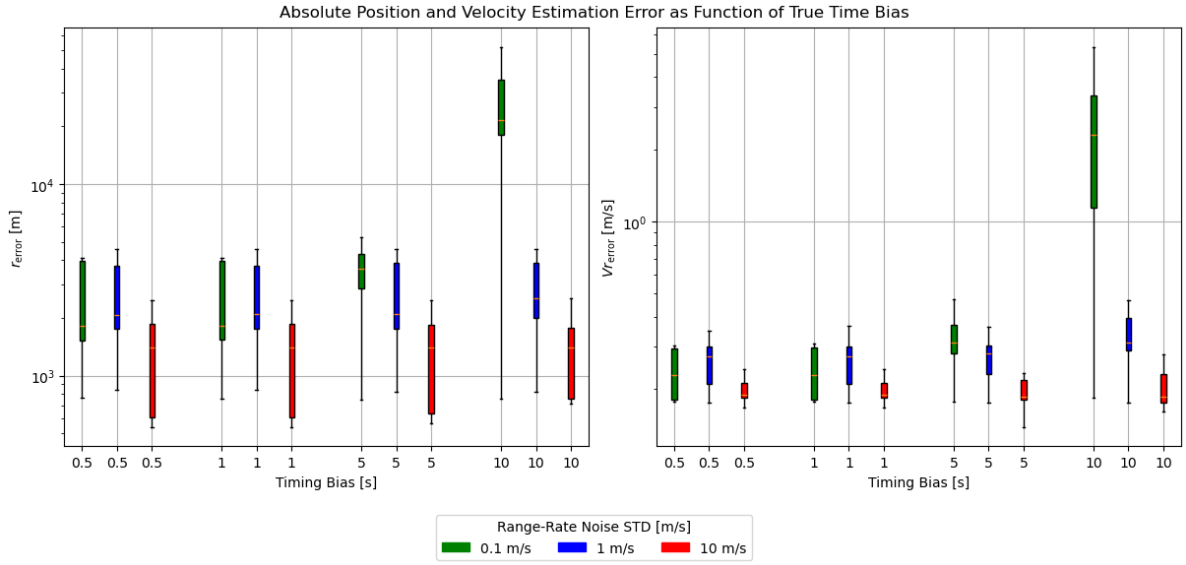

Figure B.35: Cartesian state estimation error when using a single tracking station, with one tracking arc per pass. In this estimation, both the cartesian state, and a per pass time observation bias is estimated. For this estimation, both the initial guess of the cartesian state and the time bias were perturbed. Instead of a constant bias per pass, there was a spread on the true bias.

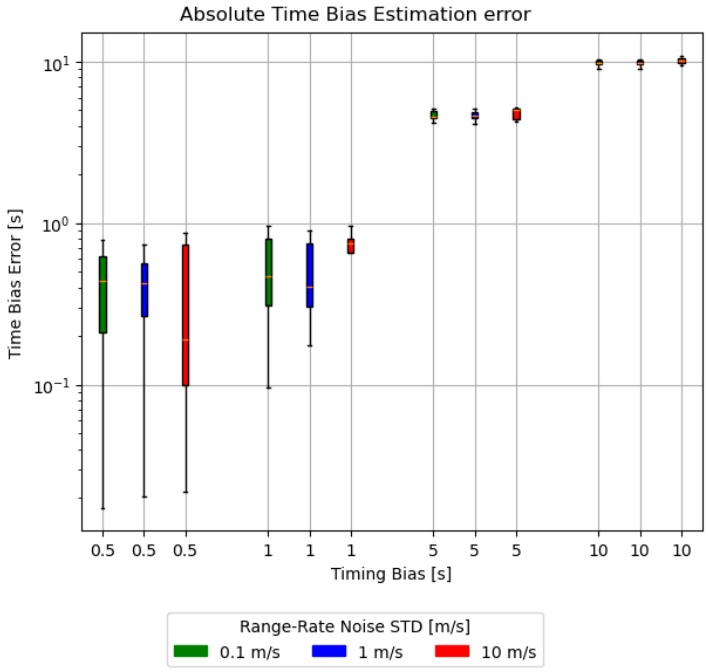

Figure B.36: Per pass time bias estimation error, using a single tracking station, with one tracking arc per pass. In this estimation, both the cartesian state, and a per pass time observation bias is estimated. For this estimation, both the initial guess of the cartesian state and the time bias were perturbed. Instead of a constant bias per pass, there was a spread on the true bias.

C

Manuals

C.1. Hardware Assembly

This section covers the hardware assembly of the box. The subsections are written to be completed consecutively, although some steps could be started simultaneously to speed up the process. When a reference is made to something online, a link to the website should pop up when hovering the mouse over the text in the manual!

C.1.1. Mounting brackets

Before the box itself has arrived, one can start by creating the mounting brackets for the electronics itself.

GPS Clock bracket

For the Leo Bodnar mini-GPS, a 3D printable design from the internet is used:

During this project, it was 3D printed from 2.85mm PLA using an Ultimaker2 with a layer size of 0.2mm at 20% infill. The bracket was printed on its side (with automatic supports under the screw plates) as this is advised by the designer of the bracket, to prevent overhang issues with the small ledge on the upper side of the bracket.

After printing and removing the supports, with a bit of force the GPS clock should be able to fit snugly in the bracket.

SDR bracket

For the RSPduo, a 3D printable design from the internet is used as well. Also this design was printed on its side from 2.85mm PLA using an Ultimaker2 with a layer size of 0.2mm at 20% infill.

The RSPduo should be able to slide freely into the bracket. The SDR can be locked into place by inserting two tie-wraps into the open cavities perpendicular to the sliding direction. These ledge behind the rubber legs of the SDR preventing it from sliding out of the bracket.

As the design has one ”open” (where you slide in the SDR) and one ”closed” side (with a cutout for the

cable connections), there is only one way in which the SDR is properly supported by the bracket itself instead of only the ledge behind the legs. Unfortunately, this is not the side to which the radio cables attach, and as the radio cable enter the box from below, the SDR will be mounted upside-down. It is recommended to redesign the bracket such that is vice versa.

Cable brackets

To secure cables inside the box, 3D printable cable brackets were also made. In the prototype, 3 have been used, but depending on the length of the cables used in the final version, less may be used.

C.1.2. Mounting plate

The box used as prototype is a *RS PRO Steel Wall Box*. The box is 400x300x150 mm, IP66 rated and comes with a metal mounting plate and gland plate.

The next step of the assembly is to mount the brackets on the mounting plate. The screw holes were pre-drilled with a 3.5 mm drill bit.

To mount the Fitlet3 mount, the middle was screwed using two M3 screws that came with the Fitlet3. To fasten it on the backside, two M3 nuts were used. For the corners, four self-tapping M4 screws were used, secured by four M4 nuts on the backside To attach the GPS clock mount, two self-tapping M4 screws were used. As the legs of the mounts are thick, the screws were not long enough to fasten it on the backside using nuts. As the screws grip in the plate quite strong and the GPS clock is light, it doesn't seem to be likely falling off.

The attachment of the SDR mount is a bit more complicated. Instead of screwing the screws from the top, the nuts go into the top of the mount (see Figure C.1). But as the spacing of the holes is not known, the pre-drill holes need to be added from the topside of the SDR mount. Then, to make the holes big enough, an M4 self-tapping screw was used on the backside of the plate in each of the pre-drilled holes. Afterwards, the SDR mount was attached using an M4x12 mm bolt and nut for each of the holes. The result is shown in Figure C.1.

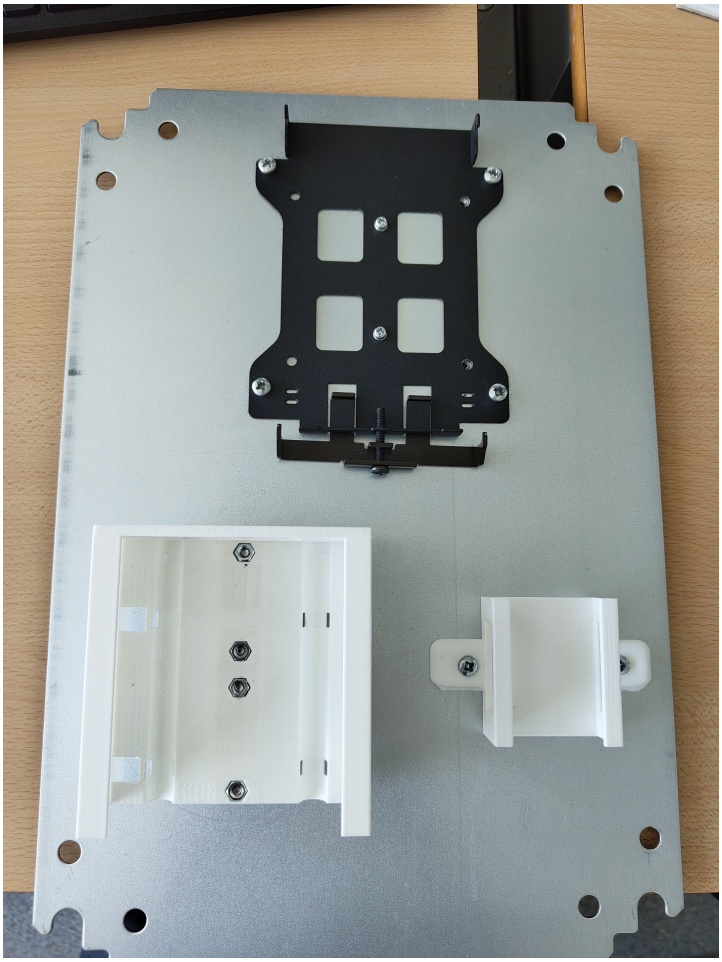

Figure C.1: Mounting plate with assembled mounting brackets

Then, the electronic components were placed inside their brackets. The result is Figure C.2.

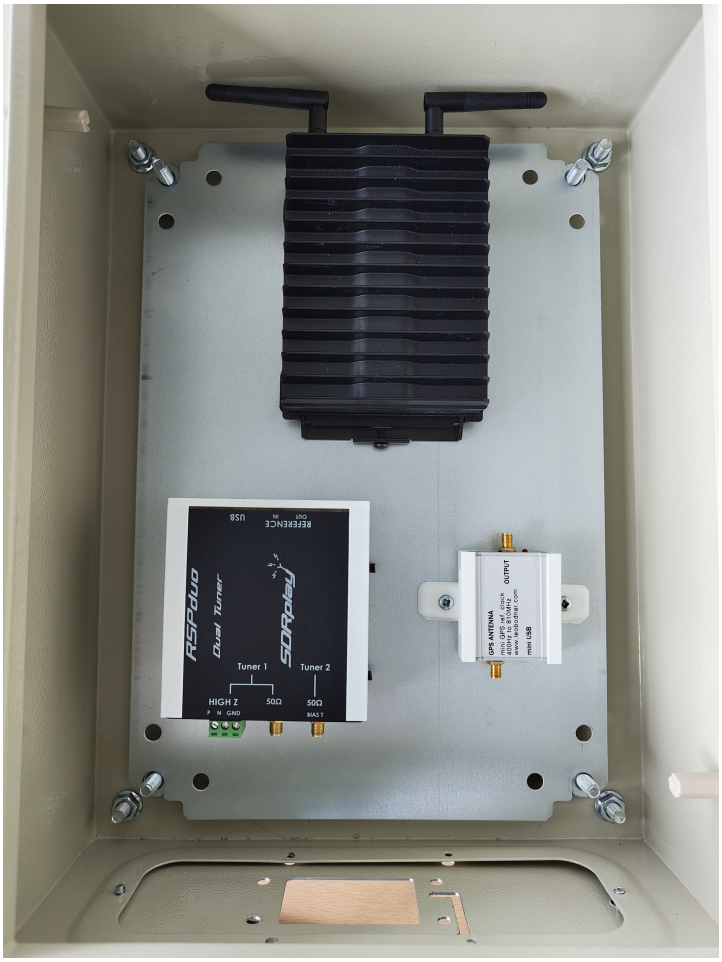

Figure C.2: Components attached to the mounting plate

C.1.3. Cables and connectors

After mounting the components to the mounting plate, the cables were attached. The power and control connection from the GPS clock to the Fitlet3 is done using a USB-A to micro-usb cable, supplied with the GPS clock. The output of the GPS clock is connected to the RSPduo using a male MCX to male SMA cable. The RSPduo was connected to the Fitlet3 using a high-quality USB A to USB B cable with a Ferrite filter. The Arduino Nano Every board is connected to the Fitlet3 using a standard USB-A to micro-USB cable.

After connecting these components, the mounting plate looks like Figure C.3.

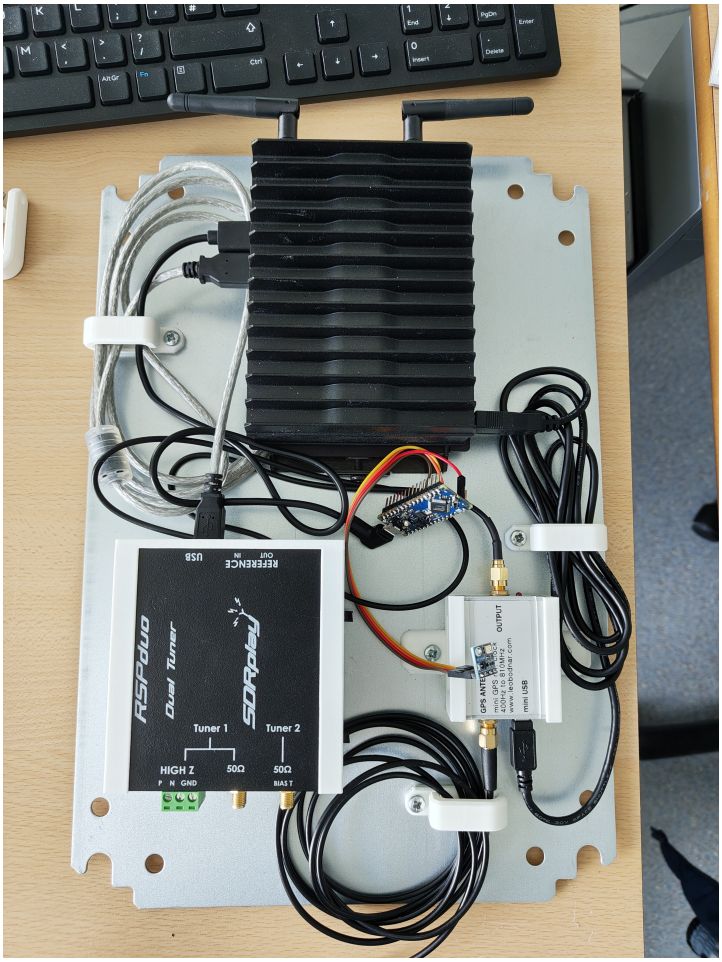

Figure C.3: Mounting plate with electronics after connecting the cables

C.1.4. Cable gland

To make a water and dust-tight seal for the cables going in and out of the box, the gland plate is used. In this particular case, a modular gland from Icotek is used. It has two compartments, sized 1x2 and 2x2 units, but only four units have been used. When a UHF antenna is added to the system this could be 5, if the cabled need to be separated, but units with dual cable pass-through per unit are available. When selecting a gland, two factors need to be kept in mind: the size of the gland plate entry is only 6 cm, so any connectors need to fit through this 6 cm, including the head connector of the power cable into the box.

To attach the gland to the gland plate, a hole was cut based on the inner dimensions of the gland. Then, a rubber seal with self-adhesive glue that was included with the gland was stuck on the outside of the gland plate, after which the necessary cables (GPS antenna cable, VHF coax cable, power supply cable, Ethernet cable) were fed through and the gland was screwed onto the gland plate. Keep in mind that when swapping the position of the units requires the gland to be screwed off the plate.

For future iterations, it might be possible to place the gland on the inside of the box instead of the outside, if the rest of the components are placed differently, and there is still enough room for the Allan key.

C.1.5. Box Pole mounting

To mount the box to a pole, first, the wall mount brackets that came with the box were attached vertically to the box. Then, two pieces of 30cm unistrut profile were cut from a 2m bar using a handsaw. This unistruts were horizontally attached to the wall mount brackets using an M8x25mm bolts and nuts. Then, the box was fastened to a pole using two U-bolt exhaust clamps, one on each unistrut. These are tightened using nuts on the other side of the struts. As the unistrut is open on the side of the nut, washers are used to make it possible to tighten the nut on the strut. It is crucial to use a exhaust clamp that has a diameter with minimum the size of the pole it is going to be mounted on. Figure C.4 shows the unistrut and exhaust clamp assembly on the box. Figure C.5 shows the box attachment to the pole from the other side.

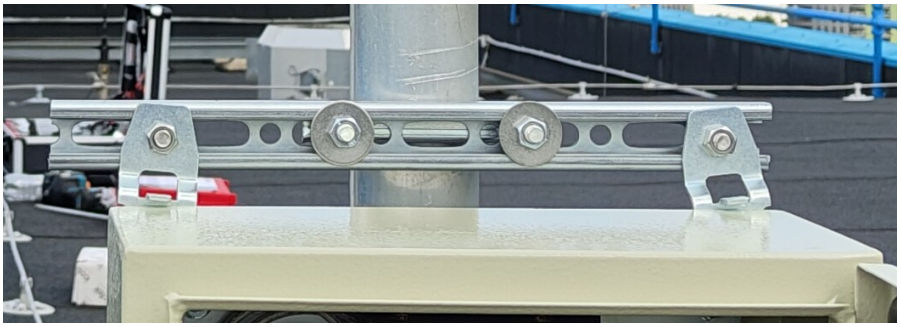

Figure C.4: Components attached to the mounting plate

Figure C.5: Components attached to the mounting plate

C.1.6. Antenna Pole Mounting

Figure C.6 shows the assembly used to mount the antenna to its pole. The antenna is connected to a metal plate using a u-shaped bracket. The metal plate and antenna were then connected to the pole using two v-bolts. Although the V-bolts need to be secured tightly to the pole to prevent it from becoming loose, the nuts should not be tightened to tightly, as it leads to bending of the metal plate, loosening the connection.

(a) Front view **(b)** Side view

Figure C.6: A front and side view of the antenna pole mounting mechanism.

C.1.7. Arduino Temperature Sensor

The DopTrackBox temperature sensor is build using a Arduino Nano Every and a GY-68 BMP180 temperature sensor board. After aquiring these components, the first step is to solder the header pins to the Arduino board and the BMP180 board.

The sensors are read through an I2C protocol, so to use this protocol the correct pins on the Arduino need to be connected to the BMP180 board. There are four connections to be made: VCC, GND, SCL and SDA. Although the BMP180 board *should* be capable of handling both 3.3V and 5V VCC, some boards (depending on the manufacturer) **ONLY** support 3.3V, so it is recommended to use the 3.3V output of the Arduino. The GND pin should be connected to one of the GND pins of the arduino. The SCL and SDA pins should be connected to the A5 and A4 pins of the Arduino respectively, which should be the SCL and SDA I2C pins. For the location of these pins, see the pinout diagram in Figure C.7.

The BMP180 is connected to the arduino using a set of jumper wires/dupont cables.

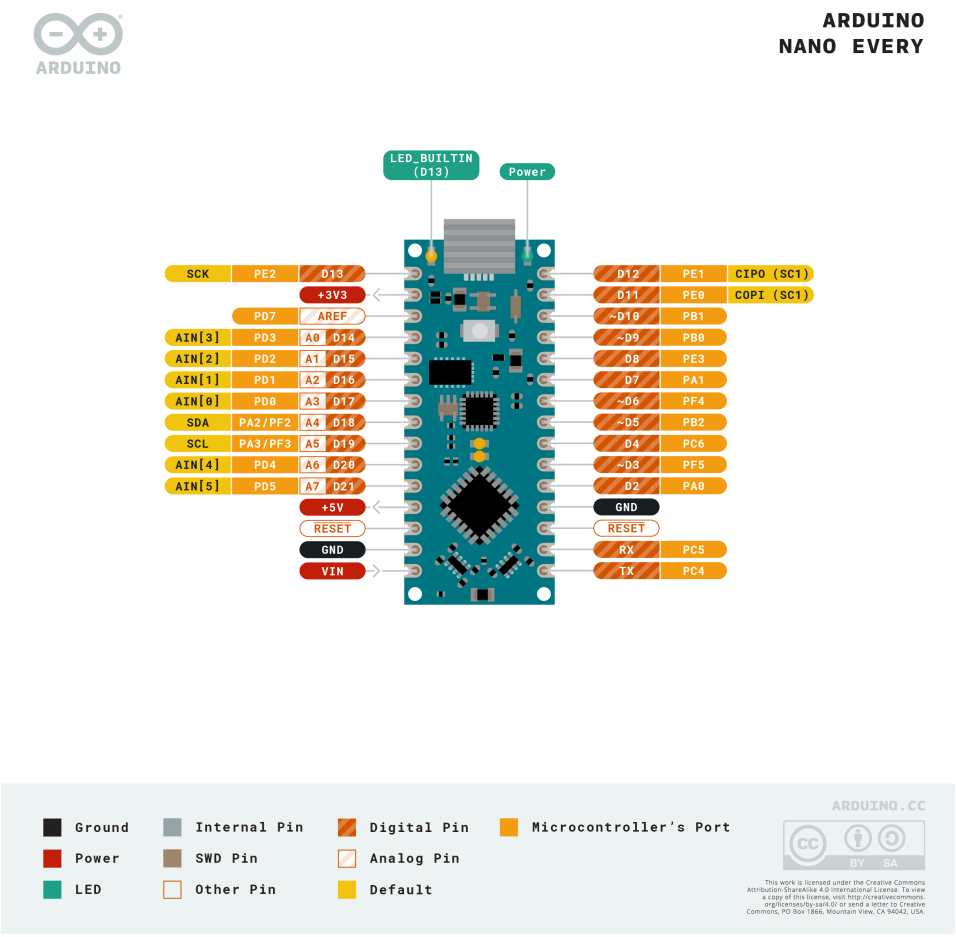

Figure C.7: Pinout diagram of the Arduino Nano Every. Figure taken from here.

C.2. Software Installation

This section covers the software installation needed to operate the DopTrackBox prototype.

C.2.1. Fitlet3 setup

At the time of writing, the officially supported operating system for the Fitlet3 machine is Linux Mint 21. Therefore, Linux Mint 21 Cinnamon was installed using a bootable USB stick. During this process, the Fitlet3 should be connected to a monitor, mouse and keyboard to get through all installation steps.

One of the first steps will be to setup a Linux mint account. This consists of a name, PC name, username and password. The name is not so relevant, but the PC name sets the identification name of the Fitlet3 on a network. The username and password will be the username and password of the administrator account on the machine.

To make sure the device can be turned on remotely, a procedure called Wake-On-Lan is used. Due to a bug in the BIOS of the Fitlet3, it does not only allow the machine to turn on from remotely, it also prevents it from shutting down at all. To enable Wake-On-Lan, follow this tutorial online. For more information, also consult this page.

To make sure that stuck SSH connections prevent you from accessing the machine again remotely, two

lines have been added to `"/etc/ssh/sshd_config"`. These are ”ClientAliveInterval 300”and ”ClientAliveCountMax 5”. The first checks every 300 seconds if an SSH connection still alive. If not, it disconnects the connection. The second sets the maximum number of allowed missed handshakes before a connection is closed.

For proper operation of the machine several packages need to be installed and setup.

SSH

The first package to install is *openssh-server*. This package sets up the machine as an SSH server, allowing remote control of the system using an SSH connection. The steps to install it were as follows:

1. In a terminal, run ”sudo apt install openssh-server” to install the package. When asked for a sudo password, use the sudo password used to setup the machine.
2. To double check that SSH is automatically enabled, use ”sudo systemctl is-enabled ssh”, which should return ”enabled”. If it is disabled, use the following step to enable it: ”sudo systemctl enable ssh”
3. Now start the SSH service using ”sudo systemctl start ssh”
4. Check if the status is ”active” by running ”sudo systemctl status ssh”. If so, the SSH server should be setup to be used

To now connect to the Fitlet3 remotely, one first needs to find the IP-adress of the machine on the network. This can be found under the ”inet” entry when running the ”ifconfig” command in the terminal. To connect to the machine, one can use the command ”ssh username@ip-adress”, where username is replaced by the username of the administrator as setup at the installation of linux mint, and ip-adress is replaced by the ip-adress of the device. A password prompt will come up, to which the correct password is the administrator password connected to the username.

Depending on the network the machine is connected to, additional steps might need to be taken before a connection like this can be established. When the device is connected to the TU Delft SCOM-lab network, one must first be either physically connected to the TU Delft intenet network, or connected to the network using eduVPN. For more information, consult the VPN documentation on the website of the TU Delft. Then, a connection to the SCOM-lab needs to be made using ”ssh netID@scomlab-bastion.lr.tudelft.nl”, where netID is your TU Delft netID. As password promt will come up, for which the password is the password that corresponds to your TU Delft netID. Then, from this terminal one can follow the SSH connection steps described above to communicate with the Fitlet3.

MailUtils

To allow for the setup of an alerting system using emails, the *mailutils* package needs to be installed. It can be installed using the ”sudo apt install mailutils” command. When asked for a selection of postfix configuration, choose the option ”Internet site”.

SSHPass

In order to allow for the automatic backup of satellite pass recordings, *SSHPass* is needed. This package allows for the circumvention of a SSH password prompt (as you would get when mounting the TU Delft webdrive) using a preset SSH passphrase stored on a local file. It can be installed using the command: ”apt-get install sshpass”.

C.2.2. GPS Clock interface

For the first-time setup of the GPS clock, it needs to load the newest firmware. The software to update the firmware is only available on Windows and macOS. After installing the latest firmware, the device can be either configured using officially supported configuration software available on Windows, or third party software for command line control on Linux.

As the Fitlet3 is running Linux, in an operational setting the configuration can only be controlled using a command line package called *lbgpsdo*. Following the instructions on this *GitHub page* of the package, the package can be installed.

C.2.3. SDR Drivers

To control the RSPduo SDR, four software packages are needed. These are *rx_tools*, *SoapySDRPlay3*, *SoapySDR* and *SDRplayAPI* As many updates to these packages have taken place, this procedure is slightly different than what was described in the work of Sprenkels (2023).

As top-level control program, *rx_tools* is used. This is a command line application to record IQ samples using SDRs. It can be downloaded from its GitHub page here. To install this software, following the install guide on in the README file did not work. Instead of using SoapySDR, using SoapySDRPlay3 did make it work. The SoapySDRPlay3 package can be retrieved form it GitHub page here. To install the package, following the steps on the wiki page of the project should work. Before doing so, the third and fourth packages need to be installed first.

The third package is *SDRPlayAPI*. The only version that seems to lead to a recording chain capable of recording without errors is SDRPlayAPI 3.15, obtained from this SDRPlay webpage, and can be installed using this manual provided by SDRPlay.

The fourth package is SoapySDR, and can be installed by following the instructions on its wiki page.

C.2.4. DopTrack(Box) Code Setup

The code that handles the automatic prediction, scheduling and recording of satellite passes is developed by the DopTrack project on the project's GitHub page. At the moment of writing, the specific DopTrackBox code is in a sub-folder of the main folder. This also includes the code to backup files to the project's webdrive, monitor the temperature and automatically checks for disk space management.

The code used to perform automatic processing of the satellite recordings using the methods described in this thesis can be found in a different repository of the project's GitHub. The installation of this software is described in the README of the repository.

The code used perform the conceptual analysis of the design presented in this thesis is found in this GitHub repository. More information on the installation is found in the README of the repository.

C.3. Operations

C.3.1. Data Recording

The code to predict, schedule and record satellite passes follows the same structure as was described by Sprenkels (2023): a shell script called *run_schedule.sh* first obtains the latest TLE for all satellites defined in the *rec.list* file found in the main directory. Using the retrieved TLEs, it makes a prediction for when the satellites will pass over the groundstation. Based on this information, and the priority between

the satellites, a schedule will be made on when to start recording each satellite. To automatically start recording at the correct time, atq jobs are created that call the recording script when a satellite will be flying over.

To automate this process for the DopTrackBox prototype used in this thesis, a cron job is used. To view and edit all running cron jobs, the command ”crontab -e” can be used in the terminal. The cron job runs the *run_schedule.sh* script every day at 07:49 and 19:49. These seemingly random times are because space-track.org (which is used to automatically retrieve the TLEs) requests to avoid using rounded times, as with many people doing that could cause an overload on the system. The *Ground-Control* repository containing these scripts can be found in the DopTrackBox prototype in the path: `/home/doptrackbox/DTB_Software/GroundControl_DTB_Revamp/`.

To also process the recordings automatically, an additional cron job exists that runs the *run_spectrograms.sh* script. This script checks a log for which recordings have been processed before, then looks for new recordings and then processes these new recordings to produce a spectrogram of the recording, as well as an extraction of all points that satisfy the signal and noise requirements, a plot of the signal-noise-ratio as function of time by assuming the signal has the maximum power, and a plot of the computed noise as function of time.

C.3.2. Disk Space Management

The output of the recordings is saved in the `/home/doptrackbox/DTB_Recordings/data` folder on the prototype. To prevent data loss in case of a crash or different failure, a cron job was made that runs each day at 01:00 a script (*backup_recordings.sh*) to backup all recordings of which no backup exists yet to the project’s webdrive.

As the disk space is not unlimited, a script was developed (*check_disk_usage.py*) that checks every 6 hours the disk space of the device, and if it is less than 50 GB, it takes two actions. First, it sends an e-mail to an address that was setup for this project. Then it deletes the 20% oldest recordings in the recordings data folder specified below, as long as it can be confirmed that a backup of the recording exists on the webdrive.

C.3.3. Monitoring

For the monitoring of the temperature two dedicated cron jobs exist. The first one is executes a script (*monitoring_logger.py*) every minute, and has two purposes: it first retrieves a temperature and air pressure measurement from the arduino using the BMP180 sensor. Then, it reads and processes the internal temperatures measured by the Fitlet3. The new data is appended to the sensor log file, located at `/home/doptrackbox/DTB_Recordings/monitoring/sensor_data.csv`.

The second script (*check_temp_shutdown.py*) is executed every 10 minutes, and computes the mean temperature of the last 5 BMP180 temperature measurements. If this is higher than a set threshold of 40°C, three actions are taken: first, a warning email is send to the same e-mail address as the disk space mails go to. Then, if a recording is busy, it kills the recording. Lastly, it suspends itself, meaning it goes to sleep and wakes itself 1 hour later. The n-sample mean should always contain a few more samples than the number of samples taken during the interval between executing this script, to prevent the machine from staying in an endless state of waking up and suspending again because there is no time to take a new measurement. A configurable option exists in the script to shut the machine down instead of suspending it. However, without any electronic power switch or human being close to the

physical device, this is not recommended as there will be no way to turn the machine on again.

C.3.4. Interacting With Components

C.4. Troubleshooting

C.4.1. Fitlet3

SSH Firewall

After installing the SSH server, it is possible that connection to the machine is not possible. If so, it is good to check if the firewall is not the issue: If the firewall is setup using ”ufw”, first use ”sudo ufw allow ssh” in a terminal to add a rule on the firewall to allow SSH connections. To activate the new firewall settings, use ”sudo ufw enable”. Then the settings need to be refreshed using ”sudo ufw reload”. This should solve the issue, if the firewall is managed by ”ufw” and this would be the cause.

C.4.2. RSPduo

It is possible that the RSPduo does not want to start to record for whatever reason. In this case it is recommended to reconfigure the RSPduo using the corresponding *”reconfigure_sdr_hw.sh”* script found in the RSPduo subfolder of the profiles directory.

C.4.3. mini-GPS Clock

When setting up the LB over USB, sometimes it can see that the device cant be opened, or it gives an error when loading a default configuration. In that case, one must reset it. This can be done using the *”configure_clock.sh”* script found in the subfolder of the profiles directory.

C.4.4. Fitlet3 - USRP N210

When trying to use the N210 with the Fitlet3, the same error message keeps appearing. There have been a few random moments in which the error did not show up, but consistently recording for durations longer than a minute was impossible. The error message is shown in Figure C.8. It is supposedly related to a connection issue between the Fitlet3 and the N210, related to the Ethernet protocol used to transfer information.

```
[WARNING] [UHD] Exception caught in safe-call.
  in ~usrp2_clock_ctrl_impl
  at /home/conda/feedstock_root/build_artifacts/uhd_1738255797667/work/host/
lib/usrp/usrp2/clock_ctrl.cpp:81
this->enable_external_ref(false); this->enable_rx_dboard_clock(false); this-
>enable_tx_dboard_clock(false); this->enable_dac_clock(false); this->enable_
adc_clock(false); this->enable_mimo_clock_out(false); this->enable_test_cloc
k(false); -> RuntimeError: fifo ctrl timed out looking for acks
[WARNING] [UHD] Exception caught in safe-call.
  in ~usrp2_codec_ctrl_impl
  at /home/conda/feedstock_root/build_artifacts/uhd_1738255797667/work/host/
lib/usrp/usrp2/codec_ctrl.cpp:101
_ad9777_regs.power_down_mode = 1; this->send_ad9777_reg(0); switch (_iface->
get_rev()) { case usrp2_iface::USRP2_REV3: case usrp2_iface::USRP2_REV4: _if
ace->poke32((0x7000 + (4 * (2))), 0x00); break; case usrp2_iface::USRP_N200:
 case usrp2_iface::USRP_N210: case usrp2_iface::USRP_N200_R4: case usrp2_ifa
ce::USRP_N210_R4: _ads62p44_regs.power_down = ads62p44_regs_t::POWER_DOWN_GL
OBAL_PD; this->send_ads62p44_reg(0x14); break; case usrp2_iface::USRP_NXXX:
break; } -> RuntimeError: fifo ctrl timed out looking for acks
[WARNING] [UHD] Exception caught in safe-call.
  in ~usrp2_fifo_ctrl_impl
  at /home/conda/feedstock_root/build_artifacts/uhd_1738255797667/work/host/
lib/usrp/usrp2/usrp2_fifo_ctrl.cpp:49
this->peek32(0); -> RuntimeError: fifo ctrl timed out looking for acks
Traceback (most recent call last):
  File "/home/doptrackbox/DTB_Software/N210_rec/rec_EC20S.py", line 11, in <
module>
    usrp = uhd.usrp.MultiUSRP(args="addr=192.168.10.6")
  File "/home/doptrackbox/miniconda3/lib/python3.13/site-packages/uhd/usrp/m
ulti_usrp.py", line 36, in __init__
    super(MultiUSRP, self).__init__(args)
    ~~~~~~~~~~~~~~~~~~~~~~~~~~~~~~~~~~^^^^^^
RuntimeError: RuntimeError: fifo ctrl timed out looking for acks
(base) doptrackbox@DTB-fitlet3:~/DTB_Software/N210_rec$
```

Figure C.8: N210 Error message on Fitlet3

To issue was not able to be solved, but multiple attempts have been taken.

- To exclude the UHD / Python version from being the cause, multiple python versions and UHD versions have been attempted, including the one used by the DopTrack station PC to communicate with its USRP. In addition, the exact same version as on the Fitlet3 has also been used on the station computer to test the connection with its USRP, without any issues.
- Different IP addresses and subnet addresses have been tried, including the recommended addresses by the USRP user manual.
- Per suggestion on the internet in similar cases, custom *firewalld* and *iptables* rules have been set to allow packages from the USRP, but this also did not have any effect.
- Lastly, an attempt had been made to install new Ethernet card drivers. Although it is unclear if the installation was successful, the error remained the same.

Based on suggestions on the internet, it appears that the USRP N210 does not communicate well with certain Ethernet cards, causing these kind of errors. Although the Ethernet card of the Fitlet3 was not explicitly mentioned, the Fitlet3 having a relatively obscure industrial Ethernet interface does not aid in finding if this is the cause. It could be attempted to connect the N210 not directly to an Ethernet port, but using an USB adapter instead, but as the N210 was discontinued anyways, this has not been attempted in order to save time.

D

Research Plan

See next page

Refinement and Evaluation of the DopTrackBox Concept

1 Introduction and Relevance of the Project

Over the years, more and more time and resources in the field of space engineering have been dedicated to making satellites more capable, but also smaller and cheaper. This has led to a space industry that is more accessible than ever, with small businesses, universities and small nations being able to build and operate their own satellites. To support the operations of such satellites, it is often required to communicate with the satellites and track their orbital state. The TU Delft is involved in the research and development of a Doppler tracking groundstation, called DopTrack. The operation principle of DopTrack is to extract the satellites range-rate from the observed Doppler shift in VHF or UHF radio beacon of the satellite.

The goal of the DopTrack project is to provide students with hands-on experience with orbit determination, as well as providing an alternative orbital state estimate to NORAD's TLEs [1], [2]**.** To this end, DopTrack should be a cheap and simple setup from using commercial of the shelf (COTS) components, such that other universities and interested parties can participate and form a network, which should increase the performance significantly. One concept that in that direction is DopTrackBox: a simpler version of DopTrack using smaller and cheaper COTS components. A preliminary study has investigated the feasibility of potential DopTrackBox hardware and software configurations, but several aspects of the design require further investigation [3]. Therefore, the goal of this project is to refine the design of DopTrackBox and assess its performance, such that the concept is ready to be cloned and used in a network capable of competing with NORAD.

2 Project Background

2.1 Doppler Tracking Background

In modern times, a wide range of solutions exists for the orbit determination of satellites, but all of them have in common that the orbit is estimated based on a set of position and/or velocity measurements of the spacecraft with respect to some reference frame. Performing these measurements can be done from the ground, on-board, or a combination of both, depending on the chosen navigation solution. Common methods are using on-board GNSS receivers to measure the spacecraft's position and velocity, and performing ground-based range and/or range-rate measurements by either bouncing signals of the satellite from the ground or observing the satellite's telemetry signals [4]. As a consequence, some of these ground-based methods can be used for the orbit determination of satellites even when they do not have any dedicated navigation equipment on-board.

The DopTrack(Box) groundstation relies on the principle of one-way Doppler tracking: as satellites pass over the groundstation, the frequency of their emitted radio telemetry signals undergo a Doppler shift, according to the equation:

$$f_{obs} = (1 + \frac{\Delta v}{c}) f_0$$

In this equation, f_{obs} is the observed frequency as a consequence of a relative line-of-sight velocity $\Delta v = v_s - v_r$ between a receiver r and source s, with respect to the speed of light c, for an frequency f_0 emitted by the source. By measuring the observed frequency as a function of time during the satellite pass, the emitted frequency can be deduced, after which the range-rate as function of time can be calculated by solving the equation above for the line-of-sight velocity for each of the observed frequencies during the pass. At the time of writing, the station is only configured to measure satellites that transmit in the VHF and UHF amateur bands at 2 meters and 70 centimeters respectively due to the size of the antenna's used.

2.2 The DopTrackBox Concept

In the DopTrackBox concept proposed by earlier work, these antenna inputs are collected by an SDRPlay RSPduo Software Defined Radio (SDR). A crucial factor in the noise on the range-rate measurements is the frequency stability of the recorded signal by the SDR. To enhance the stability, SDRs sometimes -among which the RSPduo- have the ability to connect an external reference clock with a higher stability than the internal local oscillator of the SDR. In the DopTrackBox concept, this external reference is a Leo Bodnar mini-GPS clock. In theory, this combination is capable enough to satisfy the attached requirements (Appendix A), but earlier work did not manage to see an improvement in accuracy when using the external reference clock [3]. The SDR is controlled by a compact computer. The preliminary study found that the originally proposed Raspberry Pi3B computer did not have sufficient data processing capacity to successfully record satellite passes consistently. Therefore, the Raspberry Pi3B has been replaced by a Compulab fitlet3 Atom x6425E computer as default measurement computer for the remainder of this research plan.

2.3 Other Tracking Networks

Currently, the North American Aerospace Defense Command (NORAD) is the only provider of publicly available orbital state elements for a wide range of satellites. Supposedly, their orbit determination is performed using a combination of range and range-rate measurements, provided by radar and optical groundstations from the US Space Surveillance Network (SSN) [4], [5]. A common rule of thumb about NORAD's TLEs is that their position error at epoch is on the order of 1 kilometer for LEO satellites [18], but the real error depends on multiple factors, including the shape and orientation of the orbit [19].

Two open-source satellite tracking networks are TinyGS [6], [7], and SatNOGS [8], which both operate in same VHF and UHF bands as the DopTrack project. However, these networks seem to be focused on the decoding of telemetry signals instead of orbit determination. Based on publicly available SatNOGS blog posts, members have made multiple attempts at extracting Doppler curves from the data of the SatNOGS network in order to perform orbit determination, but the exact status of these attempts is not publicly known [9], [10], [11]. For one of these attempts, the TU Berlin offered to share their position and velocity measurements, obtained using on-

board GPS or laser ranging, as they were interested in collaborating on experiments related to amateur radio.

3 Research Question(s)

To achieve the objective, the main question that needs to be researched is:

> *"What cost effective COTS DopTrackBox concept has the potential to compete with the orbital state accuracy of NORAD's TLEs? "*

This question can be split into several researchable questions that cover a separate topic from hardware selection to real-world per multi-station performance.

Hardware Selection

To answer the main question, several research questions that need to be addressed. In order to obtain accurate orbit estimates, the Doppler range-rate measurements need to be as low noise as possible. Therefore, the first question is:

1. *"Is the current Leo Bodnar mini-GPS and SDRplay RSPduo combination capable enough to compete with NORAD?"*

Because earlier work did not find that the Leo Bodnar mini-GPS clock led to less noisy range-rate measurements, even though theoretically it should have, more investigation is needed to address if these sufficient to reach the desired performance requirements. Therefore, the two subquestions to be answered are:

1A. "Is the Leo Bodnar mini-GPS clock output sufficiently stable for the desired range-range accuracy?"

1B. "Is the frequency stability of the SDRplay RSPduo sufficient for the desired range-rate accuracy when using the Leo Bodnar mini-GPS clock as an external reference clock?"

The earlier work used an interface circuit between this clock and the SDR to remove the DC offset of the Leo Bodnar mini-GPS clock and make the signal more stable. According to the SDR manufacturer this is not strictly needed for this model [12],thus the next subquestion is:

1C. "How does the use of an interface circuit after the output of the Leo Bodnar mini-GPS clock influence its output frequency stability?"

To achieve an orbit solution that is as accurate as possible, not only low-noise range-rate measurements are needed, but also the time of recording of these measurements needs to be known with as high precision as possible. Expensive SDRs such as the Ettus Research USRP products used in DopTrack have software support to time synchronization of samples using GNSS time and an accompanying 1 Pulse Per Second (1PPS) signal [13], but cheaper SDRs such as the SDRplay

RSPduo do not have these capabilities. Preliminary tests (see Appendix B) showed that there can be more than a second between a commanded start of recording and the samples being taken with the RSPduo, with an uncertainty on the time of start up of about hundred milliseconds. To find out if the RSPduo is capable of achieving the desired orbit estimation accuracy, the following research question will be investigated:

1D. "What sample timing accuracy is required to achieve the desired orbit estimation accuracy?"

Although the RSPduo is currently the prime option to use as SDR, the results from question 1B and 1D could show that it is not capable enough to satisfy the requirements. Other research showed that the RSPduo should be the best low-price SDR usage as a satellite ground station [14], so in that case the second option is to use a much more expensive Ettus Research USRP N210, which is currently in use in the DopTrack station. To characterize the performance of that potential alternative design, the following research question will be investigated:

1E. "What is the frequency stability of the Ettus Research USRP N210 when using the Leo Bodnar mini-gps as an external reference clock?"

Physical Design

The current design specifies potential components of the setup, but does not provide a design for the physical layout and form factor of the setup. Therefore, a design should be made that ideally provides the station with a compact placement of components, while also being compliant with requirements regarding factors such as temperature stability, weatherproofing, and electromagnetic couplings between the components. This question is encompassed by the second research question:

2. *"What is the best physical design for DopTrackBox that satisfies the environmental and performance constraints?"*

To answer this question, it must first be investigated what environments DopTrackBox will encounter and what the resulting constraints are. Therefore, the first subquestion is:

2A. "What are the environmental constraints on the DopTrackBox must be capable of enduring for continuous operations?"

Various people have reported that fluctuating temperatures influence the stability of the Leo Bodnar GPS clock oscillator significantly [15], [16]. As the Fitlet3 computer can generate significant heat, it is important to investigate how much the temperature fluctuates and how that influences the stability of the GPS clock. Therefore the following subquestion will be investigated:

2B. "Is passive temperature control of the box sufficient to satisfy the frequency stability requirements?"

As DopTrackBox should be capable of operating in the outside environment for extended periods of time, measures should be taken to make the setup resilient

against different weather conditions. Therefore, the following research question will be investigated:

2C. "What measures should be taken to make the DopTrackBox compliant with weather requirements?"

In addition, people have reported coupling of electromagnetic fields (EMF) between their Laptops/PCs/Screens and their antenna when operating an RSPduo SDR [7], [8], [9].This can increase the noise floor and thus decrease the signal-to-noise ratio (SNR). Ways to counteract this are to move the antenna further from the EMF source, or to apply shielding around the EMF source. To investigate the necessity for DopTrackBox to use such methods, the following questions will be researched:

2D. "What combination of antenna distance and EMF shielding leads to satisfaction of the signal-to-noise ratio requirement?

2D1. "What is the relationship between measured noise floor in the SDR and the distance between the antenna and the DopTrackBox electronics?"

If the conclusion from this question is that the antenna cannot be placed within TDB meters from the computer and satisfy the SNR requirements, then the following question will also be investigated:

2D2. "What kind of EMF shielding is suitable to suppress the antenna noise generated by DopTrackBox's electronics?"

2E. "What is the best box for DopTrackBox?"

Refined Design Performance Analysis

After answering the research questions discussed before, a new refined DopTrackBox design should emerge that satisfies the requirements and is ready to copied. To verify the compliance with requirements and find the performance limits of the setup, the refined DopTrackBox setup will be put under test to evaluate the research question:

3. *"What performance of the refined DopTrackBox setup?"*

To concretize this research question, it is split into two subquestions related to the two performance requirements that have a direct impact on the signal extraction and orbit determination capabilities of the network: the signal-to-noise ratio and the range-rate error. The subquestions that characterize the DopTrackBox performance are therefore:

3A. "What is the minimum signal-to-noise ratio measured by the refined DopTrackBox setup for elevations above 20 degrees during a satellite pass?"

3A. "What is the range-rate error performance of the refined DopTrackBox setup?"

DopTrack Network Analysis

Although a single DopTrackBox station could already be used to perform rudimentary orbit determination, the constraining power of the estimation is expected to improve significantly when multiple stations are used that are placed at different physical locations. Therefore, if the first thee research questions have provided satisfactory results and in a timely manner, there is the option to move the DopTrackBox setup to a remote location, and investigate the research question:

4. *"How does the orbit estimation performance change when a remotely located DopTrackBox is operated in coordination with the current DopTrack station?"*

Methods, tools, and expected results

Research Question 1.

Usually, the frequency stability of an oscillator cannot be expressed as a single number, because it depends on the measuring time under consideration as different noise types are dominant at different averaging durations [17]. To characterize this behavior, Allan deviations are typically used, which describe the expected RMS frequency error as a function of averaging time. To answer questions 1A, B, C, and E, these Allan deviations will be measured. For questions A and C, the Leo Bodnar mini GPS clock will be connected to a TinyPFA. This is a modified Vector Network Analyzer (VNA) that can operate as phase/frequency analyzer (PFA), in order to measure the frequency stability with respect to a more stable external reference frequency source. As external reference a EC20S high stability rubidium reference clock will be used. The output of the TinyPFA can be analyzed using software such as Timelab, which can generate Allan deviation plots. The full measurement setup can be seen in Figure 1.

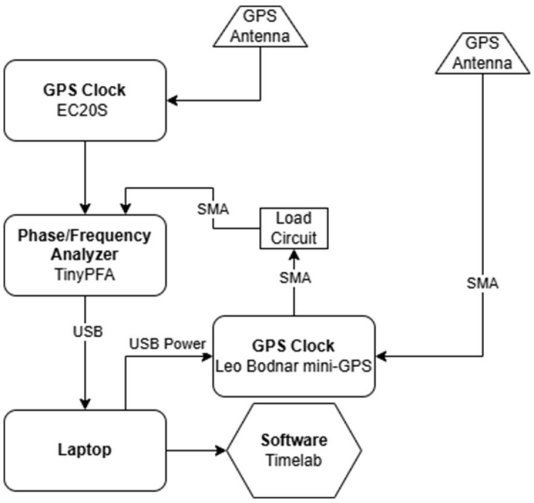

Figure 1 Experiment setup for the Allan Deviation measurement of the Leo Bodnar mini-gps clock.

For question B and E, respectively the RSPduo and USRP N210 will be connected to the Fitlet3 computer. Then, the in-phase and quadrature (I/Q) components of the

signal of a stable VHF or UHF radio beacon will be read out using rx_tools. In this case, a Fast Fourier Transform will be made on 1 second subsets of data. The beacon frequency can then be extracted for each of the subsets, and from this the Allan deviation can be computed. If no sufficiently stable beacon source can be found, the 10 MHz output of the EC20S reference clock will be used as an input to the antenna port of the SDR to act as a reference beacon, at the expense of needing a higher minimum averaging time to reach the same frequency resolution due the frequency being lower than typical VHF and UHF beacon frequencies. The full experiment setup in the latter case is shown in Figure 2. When using a beacon, the EC20S GPS clock and GPS antenna are replaced with a VHF or UHF antenna. To test the different configurations for the different subquestions the load circuit is removed from between the GPS clock and SDR, or removed together with the GPS clock as a whole.

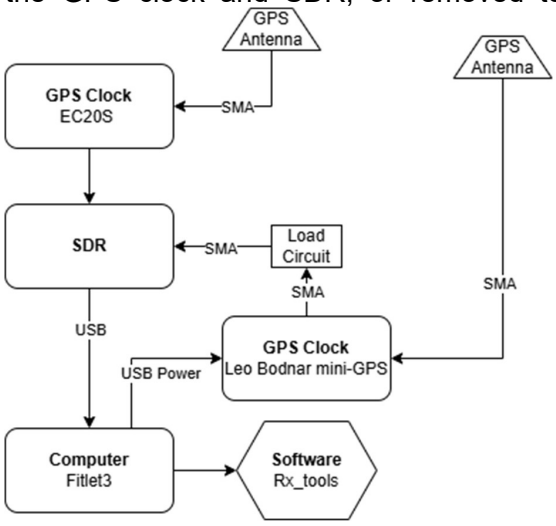

Figure 2 Experiment setup for the Allan Deviation measurements of the Software Defined Radios

To answer question 1D, two strategies will be employed. First, using the TUDAT package, simulated range-rate measurements will be made. These will then be duplicated and shifted in time, to simulate the uncertainty in the absolute timestamp of the samples. Using these simulated measurements, the simulated orbit will be estimated, and the resulting position error with respect to the true simulated orbit. Doing this for multiple timestamp uncertainty values will give insight into the allowable timestamp uncertainty to stay within the orbit estimation accuracy requirements.
The second strategy is to perform orbit determination with datasets gathered using the DopTrack setup, from before and after June/July 2019. Around this time, the DopTrack recording software has been changed from relying on computer system time to using a 1PPS trigger to assign timestamps to samples. The covariances and position residuals of this analysis can be compared with the prediction from the first strategy to verify the analysis approach. In both cases the analysis can be repeated for different arc lengths and estimation settings to get more insight in the effects of the time uncertainty on the orbit estimation process.

Research Question 2

To answer question 2A, literature will be consulted to investigate the environmental factors such as temperatures, humidity and rainfall at a variety of potential future DopTrackBox locations Then, for question 2B, literature will first be consulted to find the temperature sensitivity of the components, and their operation limits. Then, the Fitlet3 computer will be placed in a constricted space together with the GPS clock after which the Allan deviation will be measured again . For question 2C, literature will be consulted to find guidelines for placing electronic equipment in an outside environment. To answer question 2D, question 2D1 will be answered by first by placing the electronic equipment at various distances from the antenna and measuring the noise floor at the frequency of interest. This establishes the relationship between the distance and the noise floor. Then, a link budget analysis can be performed to find the minimum antenna distance needed to satisfy the SNR requirement. If the distance is greater than TBD meters, question 2D2 will be investigated by applying various EMF shielding materials around the electronics and measuring how the noise floor decreases. Then finally, question 2E can be performed by selecting several feasible options and performing a multi-criteria analysis on the different options to select the best one.

Research Question 3

For question 3A, the IQ samples of multiple satellite passes will be recorded, and a fast Fourier transform will be performed on sequentially cut-out timeseries of the data. For each of these subsets, an estimation will be made of the signal and noise levels, after which the signal-to-noise level can be computed. It will be assumed that the stored time of the recordings and the predicted elevation as function of time based on the TLE are accurate enough to compute the time for which the satellite has reached 20 degrees of elevation. The subsets of time for which this is the case will be used to compute the minimum signal-to-noise ratio and evaluate if the setup conforms to the requirement.

To answer question 3B, there are two possible strategies. As the TU Berlin has offered other tracking networks to share their laser-ranging data or on-board GNSS measurements of their satellites, a request can be made to share their data with the DopTrack project as well. If they are willing to share this data, the expected range-rate as function of time can be computed by computing the projection of the satellite's velocity in the line of sight direction of the DopTrackBox station. By recording the passes with DopTrackBox setup, the measured range-rate can be compared with the expected to assess its performance. If this external reference data will not become available for this experiment, the range-rate performance can only be assessed by either computing the range-rate residuals with respect to either the fitted Doppler curve, or the predicted range-rate based on a TLE prediction using SGP4 and python. In the latter case it is crucial to use a pass for which a TLE is created as close as possible to the time of pass to reduce the effects of integrating the orbit error.

Research Question 4

To answer question 4, simulations will first be ran based on the known performance of DopTrack and DopTrackBox to predict the increase in orbit estimation accuracy when using both setups simultaneously. Then, DopTrackBox will be moved to a

physical different location in Renesse (The Netherlands) or Zambujeira do Mar (Portugal), and range-rate measurements will be performed. After collecting measurements of multiple passes, the orbit estimation can be carried out for the setups individually, as well as when combining their data. If the measurements are performed on TU Berlin satellites and their orbit data will be shared with this experiment, the orbit estimation error can be computed. Otherwise, the orbit estimation error needs to be estimated based on uncertainty analysis and cross-checked with the expectation based on simulations.

Expected Data

During these experiments, several types of data are being generated and stored. Table 1 shows the expected data together with why and how it is stored and who will have access.

Table 1: Expected collected data during experiments

Type of data	File format(s)	How will data be collected (for re-used data: source and terms of use)?	Purpose of processing	Storage location	Who will have access to the data
I/Q Timeseries	.32fc files	Measuring using the DopTrackBox hardware and software	To analyze frequency stability of the RSPduo, measure noise floor and asses the range-rate performance of the setup	Doptrack webdata	Anyone with doptrack webdata access directly. Public access via http://doptrack-data.tudelft.nl/ indirectly
Simulated range-rate measurements	.csv files	Using the TUDAT package in python scripts	Assess the expected DopTrackBox performance	Gitlab	Me, supervisor
VNA measurements	.txt files	Measuring frequency differences with VNA device	To measure the Allan deviation of the GPS clock	Gitlab	Me, supervisor

Needed Materials

The full list of materials is attached in Appendix C.

4 Planning

The work can be divided into work packages consisting of subquestions with similar measurements. This gives the following work packages:

1. **GPS clock Allan deviation measurements (1 week):**
   This work package encompasses everything that needs to be done to analyze the Allan deviation of the Leo Bodnar mini-GPS reference clock. The tasks are:
   - Get familiar with Rubidium reference source (0.5 days)
   - Get familiar with VNA device and readout software (1 day)
   - Build setup and perform measurements (1 day)
   - Analyze results (1 day)

2. **SDR Allan Deviation measurements (1 week)**
   This work package contains the work necessary to perform the Allan deviation measurements for the RSPduo and USRP N210. The tasks are:
   - Build setup (0.5 days)
   - Find and test stable beacon (0.5 days)
   - Perform measurements (1 day)
   - Write analysis scripts (1 day)
   - Analyze results (1 day)

3. **Timestamp uncertainty analysis (2 weeks)**
   This work package contains the analysis on the timestamp uncertainty analysis. The tasks are:
   - Make simulations for different scenarios (2 days)
   - Write analysis scripts for simulated data (1 day)
   - Analyze simulated results (1 day)
   - Find appropriate range-rate data to analyze (1 day)
   - Write analysis scripts for real data (1 day)
   - Analyze real data results (1 day)
   - Compare simulated results with real results (1 day)

4. **EMF coupling analysis (1 or 2 weeks)**
This work package involves the analysis of the EMF coupling and consists of the tasks:
   - Build measurement setup (0.5 days)
   - Prepare noise floor vs distance analysis scripts (1 day)
   - Perform noise floor measurements (1 day)
   - Perform link budget analysis (1 day)
   - Analyze noise floor results (0.5 days)
     Potentially:
   - Investigate shielding options (2 days)
   - Perform shielding option measurements (1 day)
   - Analyze shielding options results (1 day)

5. **Finalize DopTrackBox design (1 or 2 weeks)**
This work package encompasses all remaining subquestions regarding the physical design of the setup. In addition, if the decision is make a case ourselves, this work package contains the time allocation to do this.
   - Research weather proofing of electronics (e.g. can we do it ourselves, or need standard weatherproof solution) (2 days)
   - Measure temperature fluctuating Allan deviation (1 day)
   - Either select case (1 day) or: design case (1 week)
   - Build and test full DopTrackBox assembly (1 day)

6. **Construct new DopTrackBox and analyze performance (3 weeks)**
This analysis package involves the testing and analysis of the final (individual) DopTrackBox concept. One must keep in mind that the setup needs to be running for approximately one week to acquire a sufficient amount of passes before being able to start the analysis part of this work package. The tasks of the work package are:
   - Setup hardware for testing (1 day)

- Find satellite with highest pass data quality (1 day)
- Write setup assembly and operations manual (2 days)
- Prepare data acquisition and analysis scripts (2 days)
- Inspect, select and process raw data (1 day)
- Either learn to use TU Berlin data (1 day) or obtain predicted observations from TLE data (1 day)
- Analyze range-rate performance (1 day)
- Analyze SNR performance (1 day)
- Analyze TCA error (1 day)

7. Combined DopTrack and DopTrackBox Analysis (3 weeks)

This work package contains the work to prepare the DopTrackBox setup for operations at a remote location and analyzing its orbit estimation performance when combining its data with the DopTrack station data. In order to carry out the analysis part of this work package, the setup needs to operate at least 1 week simultaneously to gather enough usable passes for the analysis.

- Prepare setup and for fully remote operations over port forwarded SSH (1 day)
- Disassemble DopTrackBox and prepare for moving (1 day)
- Move and set up DopTrackBox (1 day)
- Inspect, select and process raw rata (1 day)
- Create simulations of expected performance increase (1 day)
- Analyze simulated expected performance increase (1 day)
- Prepare analysis scripts (2 days)
- Analyze orbit estimation performance and compare with expectations from simulations (2 days)

8. Thesis Writing (5 weeks)

This work package covers the writing of the thesis from start till “holy draft” completion. This work package can also be worked on when one work package is finished ahead of schedule, and it is more convenient to start a new one a few days later.

With this distribution of work packages, there is room for 0 to 2 weeks of delays, depending on the findings of the EMF analysis and the choice to buy or develop our own hardware case. In case more delays occur, it can be decided to remove research question 4 which corresponds to work package 7. This would yield about 3 extra weeks. Some of the work packages can be worked on in parallel, with a few exceptions: work package 2 should only be carried out after work package 1, because it would be a waste of time to test the RSPduo and USRP with the Leo Bodnar GPS clock if work package 1 shows that the Leo Bodnar GPS clock is not stable enough. In addition, work package 4 can only start after work packages 1, 2 and 3 are finished, as the link budget analysis depends on the choice of the SDR. Similarly, work package 5 can only be carried out after work package 4 has finished, because the will depend on necessity of EMF shielding. In the same way, work package 6 and 7 need to be carried out consecutively, because the design needs to be finished before the performance of the full individual DopTrackBox can be evaluated. Only after having evaluated the performance of the individual setup can it be moved to a remote location to test it in parallel with the DopTrack station. Work package 8 can be started at any point, but only finished after all other work packages have been finished as the results

of all work packages will be present in the thesis. The full planning that incorporates holidays is given in the Gantt chart in Appendix D. If no further delays occur, the estimated date of completion of the research phase is 26-08-2025, with the final dissemination of the project around 6-10-2025 in the form of the thesis defence.

5 Conclusions

To provide students with hands-on experience on orbit determination and provide small businesses, universities and small nations with an alternative orbit estimate than NORAD's TLEs, the TU Delft is involved in the research and development of Doppler tracking ground stations using COTS components, called DopTrack. In an effort to decrease the price and availability further, the DopTrackBox concept has emerged which should utilize even cheaper components without significantly degrading the orbit estimation capabilities. Before the DopTrackBox is ready to be used in a network, several questions regarding the design and its performance need to be answered. In particular, there are concerns that the current hardware might not be capable of achieving the desired orbit estimation accuracy. In addition, there is currently no design for the layout and formfactor of the hardware that allows for continuous operations in an outside environment. Therefore, the proposed research will aim to answer these questions such that a mature and ready-to-use DopTrackBox design will be available for operation in a network.

References

[1] M. H. A. Søndergaard, “Accuracy of the DopTrack satellite tracking system compared to two-line elements,” Inholland University of Applied Sciences & Delft University of Technology, 2018.

[2] Ó. González Martínez, “Orbit determination of Delfi-C3 using Doppler tracking data from DopTrack ground station,” Delft University of Technology, 2017.

[3] A. Sprenkels, “Portable Doppler Tracking Groundstation,” Master Thesis, Delft University of Technology, Delft, 2023.

[4] J. R. Wertz and W. J. Larson, Eds., *Space mission analysis and design: SMAD III*, 3. ed., 10. print. in Space technology library, no. 8. Hawthorne, Calif: Microcosm Press [u.a.], 2008.

[5] D. A. Vallado, *Fundamentals of astrodynamics and applications*, Fifth edition, First printing. in Space technology library, no. 21. Torrance, CA: Microcosm Press, 2022.

[6] “TinyGS,” Unleash Your Inner Explorer: Build a Tiny Ground Station and Help Secure Our Space Future. Accessed: Apr. 11, 2025. [Online]. Available: https://tinygs.com/

[7] Galile0, *G4lile0/tinyGS*. (Apr. 08, 2025). C++. Accessed: Apr. 11, 2025. [Online]. Available: https://github.com/G4lile0/tinyGS

[8] “SatNOGS,” Open Source global network of satellite ground-stations. Accessed: Apr. 11, 2025. [Online]. Available: https://satnogs.org/

[9] “Orbit Determination from SatNOGS data - SatNOGS,” Libre Space Community. Accessed: Apr. 11, 2025. [Online]. Available: https://community.libre.space/t/orbit-determination-from-satnogs-data/11643

[10] N. Janes, “ORBIT DETERMINATION USING SATNOGS AND OREKIT,” presented at the Open Source CubeSat Workshop 2019, Athens, Oct. 14, 2019. [Online]. Available: https://events.libre.space/event/3/contributions/69/attachments/35/50/OD-using-Satnogs-orekit.pdf

[11] “SOCIS 2019: Orbit Determination with SatNOGS - Orekit usage,” Orekit. Accessed: Apr. 11, 2025. [Online]. Available: https://forum.orekit.org/t/socis-2019-orbit-determination-with-satnogs/534

[12] W. D. Reeve, “Using the SDRPlay SDR Receivers with an External Frequency Reference.” Nov. 25, 2020.

[13] “USRP Hardware Driver and USRP Manual: Device Synchronization.” Accessed: Mar. 15, 2025. [Online]. Available: https://files.ettus.com/manual/page_sync.html

[14] A. Csete and S. Christiansen, “Evaluation of SDR Boards and Toolchains,” 1.0, Mar. 2020.

[15] “Question about the Bodnar mini GPSDO unit.” Accessed: Mar. 15, 2025. [Online]. Available: https://groups.io/g/fmt-nuts/topic/question_about_the_bodnar/87523478

[16] “Another question about the Bodnar Mini GPS Unit.” Accessed: Mar. 15, 2025. [Online]. Available: https://groups.io/g/fmt-nuts/topic/another_question_about_the/87385272

[17] W. Riley and D. Howe, “Handbook of Frequency Stability Analysis.” Special Publication (NIST SP), National Institute of Standards and Technology, Gaithersburg, MD, Jul. 01, 2008. [Online]. Available: https://tsapps.nist.gov/publication/get_pdf.cfm?pub_id=50505

[18] pericynthion, “Answer to ‘What is the accuracy / uncertainty of Two Line Elements (TLEs)?,’” Space Exploration Stack Exchange. Accessed: Mar. 15, 2025. [Online]. Available: https://space.stackexchange.com/a/6168

[19] T. Flohrer, H. Krag, and H. Klinkrad, “Assessment and Categorization of TLE Orbit Errors for the US SSN Catalogue”.

Appendix A: DopTrackBox Requirements

In the work of Sprenkels (2023), the following requirements were established for DopTrackBox [3]:

Operational:

Identifier	Requirement
DTB-OPS-1.01	DTB shall be no larger than 0.45 × 0.30 × 0.10 m.
DTB-OPS-1.02	DTB shall include a computer.
DTB-OPS-1.03	DTB shall include an SDR.
DTB-OPS-1.04	DTB shall include a GPS clock
DTB-OPS-1.05	DTB shall include an antenna.
DTB-OPS-1.06	DTB shall include an external data storage medium.
DTB-OPS-1.07.1	DTB shall include a system to receive electrical power.
DTB-OPS-2.01	DTB shall be able to record automatically scheduled satellite passes.
DTB-OPS-2.03	DTB shall be able to operate without active internet connection during satellite passes.
DTB-OPS-2.04	DTB shall be able to record satellite passes without crashing.
DTB-OPS-2.06.1	DTB shall be able to operate on battery power for at least 60 minutes
DTB-OPS-2.07	DTB shall be able to store satellite data of at least 150 passes
DTB-OPS-2.08	DTB shall be able to record satellite data with a mean SNR of 3.0 dB or higher
DTB-OPS-2.09	DTB shall be able to record satellite data with a RMS range-rate difference of 100 m/s or lower
DTB-OPS-2.10	The SNR difference between DTB and DT shall be no smaller than -3 dB
DTB-OPS-2.11	The RMS range-rate difference between DTB and DT shall be no larger than 50 m/s.

Technical:

Identifier	Requirement
DTB-TECH-1.01.1	The computer shall have at least 1 USB type A port
DTB-TECH-1.02	The computer shall have the capability of connecting to the internet.

DTB-TECH-1.04	The computer shall have the means to connect to a Human Interface Device for interaction with the system.
DTB-TECH-1.05	The computer shall have a minimum internal storage capacity of 32 GB
DTB-TECH-1.06	The computer shall be able to run Python 3.9 or newer
DTB-TECH-1.07	The computer shall be able to process a data stream of 2 MB/s.
DTB-TECH-2.01	The SDR shall have a connection for the antenna.
DTB-TECH-2.02	The SDR shall be connected to the computer via a USB type A connection.
DTB-TECH-2.03	The SDR shall be capable of receiving VHF signals from 30 to 300 MHz.
DTB-TECH-2.05	The SDR shall be capable of sampling at a sample rate of 250 kHz.
DTB-TECH-3.01	The GPS clock shall be physically compatible with the rest of the DTB system.
DTB-TECH-4.01	The antenna shall be capable of receiving VHF signals from 30 to 300 MHz.
DTB-TECH-4.03	The antenna shall be physically compatible with the SDR.
DTB-TECH-5.01	The external storage shall not have any moving parts.
DTB-TECH-5.02	The external storage shall be connected to the computer via a USB type A connection.
DTB-TECH-5.03	The external storage shall have a minimum capacity of 256 GB.
DTB-TECH-6.01	The Operating System shall be based on Linux.
DTB-TECH-6.02	The recorder software shall be compatible with the SDR.
DTB-TECH-7.01	The VM shall be capable of USB passthrough.
DTB-TECH-7.02	The VM shall be capable of running a Linux based Operating System.
DTB-TECH-7.03	The VM shall have a minimum allocated storage capacity of 32 GB.
DTB-TECH-7.04	The VM shall have a minimum allocated RAM capacity of 3 GB.

Over time, the scope of the project has been slightly altered, removing the portability aspect as a hard requirement, and it will be assumed that power and ethernet are available. To reflect these changes, several changes to the requirements are proposed. First, as portability is not a concern anymore, the dimensions of DopTrackBox are not as relevant anymore. Therefore, requirement DTB-OPS-1.01: *”DTB shall be no larger than 0.45 × 0.30 × 0.10 m”* should be abolished. A compact as possible form factor could however still be considered as a criteria for the box design. Even though electrical power and ethernet are assumed, the requirements

DTB-OPS-2.06.1: *"DTB shall be able to operate on battery power for at least 60 minutes"* and DTB-OPS-2.03: *"DTB shall be able to operate without active internet connection during satellite passes"* will be kept, but no particular efforts will be made to comply with these requirements during this project.

In addition, since requirement DTB-OPS-1.02: *"DTB shall include a computer"* exist, there should be no need to run a Virtual Machine, which means the requirements on the Virtual Machine, DTB-TECH-7.01 till DTB-TECH-7.04 can be removed.

As the exact computer model to use is not specified in the requirements, the usage of an external storage device is not strictly necessary, depending on the size of the internal storage. Therefore, it is proposed to remove requirements DTB-OPS-1.06*: "DTB shall include an external data storage medium"* and DTB-TECH-5.02: *"The external storage shall be connected to the computer via a USB type A connection"*. In addition, it is proposed to change requirement DTB-TECH-5.01: *"The external storage shall not have any moving parts"* to *"Any storage medium shall not have any moving parts"*.

The size of the needed storage is established in requirement DTB-TECH-5.03: *"The external storage shall have a minimum capacity of 256 GB"*. This number is based on the assumption of 1.44GB per average pass of 12 minutes, and the requirement DTB-OPS-2.07: *"DTB shall be able to store satellite data of at least 150 passes".* It is not clear what the rationale for 150 passes is, but it is suspected to be based on the ability to record three satellites with five passes per day each, for ten consecutive days in case no internet is available. After ten days, the accuracy of TLEs is too low to make accurate predictions of the passing times, and when no internet is available to retrieve new TLE's that would be a suitable point in time to stop recording passes until internet connection has been restored. To future-proof the concept, in this project it will be assumed that many more satellites will be tracked, with the consequence that the station could be recording almost continuously. In that case, if the data rate will be 172 GB per day. One of the variables that dictate this data rate is the sampling rate of the recording. To fully capture the signals, a sample rate of about 30kHz should be sufficient. Yet, DopTrack records at 250 kHz, because the hardware does not support recording at a much lower sampling rate. The RSPduo, intended to be used in DopTrackBox, does support lower sampling rates, with a minimum of 62.5 kHz. Changing the sampling rate to 62.5 kHz would reduce the data rate with a factor of 4 to only 43 GB per day. Maintaining the same 10 days limit, this translates to 432 GB per 10 days. The nearest common storage size that satisfies this minimum is 512 GB, so it is proposed to change requirement DTB-TECH-5.03 to *"Any data storage medium shall have a minimum capacity of 512 GB".*

Currently there are two requirements related to DopTrackBox's performance with respect to DopTrack. These are requirements DTB-OPS-2.10: *"The SNR difference between DTB and DT shall be no smaller than -3 dB"* and DTB-OPS-2.11: *"The RMS range-rate difference between DTB and DT shall be no larger than 50 m/s"*. The requirements should not be interpreted as a design requirement, but as a guideline to monitor if the stations perform as expected when operated under the same circumstances. However, as the hardware is not identical, the in particular the noise level could significantly different between DopTrack and DopTrack box, leading to a

different signal-to-noise ratio. Therefore it is proposed to remove requirement DTB-OPS-2.10.
As the range-rate difference can only be computed when operating the DopTrack and DopTrackBox stations side-by-side, it can only be used to monitor the station in the limited case that the DopTrackBox station is next to DopTrack for testing. To make the requirement more suitable to monitor stations over a longer period (even when placed remotely), it is proposed to change requirement DTB-OPS-2.11 to *"The RMS over a single pass of the range-rate difference between DTB and the estimated orbit shall be no larger than 50 m/s."*

In addition to these requirements, there are requirements based on the desired orbit estimation performance of DopTrackBox. One of these is requirement DTB-OPS-2.08: *"DTB shall be able to record satellite data with a mean SNR of 3.0 dB or higher".* This requirement is a design requirement as it is supposedly the current approximate limit for which the processing script can extract the signal from the background. Similarly, requirement DTB-OPS-2.09: *"DTB shall be able to record satellite data with a RMS range-rate difference of 100 m/s or lower"* exists, but this plan proposes a change for this requirement from 100 m/s RMS error to 2 m/s RMS error in the range-rate based on the following grounds: a rule of thumb about NORAD's TLEs is that their position error at epoch is on the order of 1 kilometer for LEO satellites [18], but the real error depends on multiple factors, including the shape and orientation of the orbit [19]. To compete with this, DopTrackBox should be aiming for about an order of magnitude lower, so about 100 meters. As a rule of thumb, the Doppler range-rate error in meters per second should be a factor 20 lower than the position error in meters, which converts to about 2 m/s. Therefore, it is proposed to change DTB-OPS-2.09 to *"DTB shall be able to record satellite range-rates with a RMS error less than 2 m/s"*. From this requirement, a technical requirement on the performance of the SDR and possible GPS reference clock can be derived: as the range-rate is computed from the change in frequency using the Doppler equation, the required frequency stability can be computed using the same equation when the required range-rate RMS error is known. Specifically, the RMS range-rate error δ_v as a consequence of a change in frequency $\delta_{f,}$ is given by the equation:

$$\delta v = \frac{c\,\delta f}{f0}$$

where c is the speed of light and f0 the carrier frequency of the signal [12]. The frequency stability of the SDR is directly related to the frequency of the local oscillator, so using this equation a requirement on the stability of the local oscillator as fraction of the carrier frequency can be found. Using a 2 m/s RMS range-rate requirement, a fractional stability requirement of 6.67×10^{-9} can be found. Therefore, the following technical requirement is proposed: "*The SDR shall have a frequency stability better than* 6.67×10^{-9}". Typically, SDRs have a relatively low stability oscillator, with the option to connect an external reference clock to increase the stability, which is for the proposed DopTrackBox setup the GPS clock. Therefore, an additional requirement could be added that "*The external reference clock shall have a frequency stability better than* 6.67×10^{-9}". Although requirement DTB-OPS-1.04*: "DTB shall include a GPS clock"* seems to be not strictly necessary, as it seems reasonable that an alternative SDR exists of which the oscillator is stable enough to not need an external clock to meet the requirement, but in practice this does not

occur as GPS disciplining is needed to maintain long-term stability. For sakes of clarity proposed to change requirement DTB-TECH-3.01: "*The GPS clock shall be physically compatible with the rest of the DTB system*" to several requirements that describe the physical compatibility. These will be: "*The external reference clock shall be capable of producing the reference frequency required by the SDR*", "*The external reference clock shall be capable of producing the reference signal at the voltage and current required by the SDR*" and "*The external reference clock shall be capable of being connected to the SDR, albeit using adapters* ".

There are currently a few requirements on the DopTrackBox computer. On of these is DTB-TECH-1.01.1: "*The computer shall have at least 1 USB type A port*". As the current proposed GPS clock needs a USB connection to the computer in order to be configured, as well as the SDR for transfer of data, it is proposed to change this requirement to *The computer shall have at least 2 USB type A ports*". In addition, to allow for fully remote operations, the following technical requirement is proposed: "*The computer shall be capable of access via SSH*". Linked to this, the following operational requirement is proposed: "*DTB shall be able to be operated fully remotely after initial setup*".

Currently, there are no requirements regarding the Box part of DopTrackBox, apart from the requirement on the dimensions that was proposed to be removed. However, although the portability aspect of DopTrackBox is removed, it is still in scope to place the setup in an outside environment. Therefore, the following operational requirements are proposed: "*DTB shall be operable in an outside environment"* and "*The antenna shall be placed less than TBD meters from the electronics box"*.
To facilitate this, two technical requirements are proposed: "*DTB shall be dust and waterproof (what IPS rating?)",* "*DTB shall be protected against lightning surges*" and "DTB shall be operational in temperatures between TBD and TBD degrees Celcius"

Appendix B: Preliminary Absolute Time Uncertainty

To get a first insight into the uncertainty on the timestamps of the recordings made with rx_tools, 100 test recordings of 1 second each were made using a python script, which would store the PC time before executing the rx_tools shell command and after the recording has been finished. The overhead time of the recording was then computed by subtracting the time at the end and start of the recording, and subtracting the recording time. The resulting distribution of overhead times can be seen in Figure 3. There are two clear distinct peaks, separated by about 0.1 seconds, with 24 of the entries in the left peak and 76 in the right one.
This was repeated for recording durations of 5 and 10 seconds as well, and the resulting distributions can be seen in Figure 4 and Figure 5. Interestingly, in these cases the peak around 1.55 seconds got smaller, while the peak around 1.65 seconds got bigger. In addition, in both cases there is an extra case around 2.65 and 1.75 seconds respectively. The lack of such cases for the 1 second recording duration tests could be due to a lack of statistics, but repeating the test but for 1000 recordings gives a similar distribution without cases beyond the 1.65 seconds peak so this seems unlikely.

To get more insight into how this overhead time is distributed before and after the recording, the terminal output has been recorded on video, after which the frames of the different printouts of rx_tools have been keyed. From this it could be deduced that time between rx_tools indicating the start and end of the recording is about 1.3 to 1.4 seconds, so the true start of the recording happens somewhere between 0 and 0.4 seconds after the indicated start of the recording. The time between storing the current time and actually starting the rx_tools script seems to be only around 0.015 seconds. Then, after the recording there is typically also about 1.15 seconds before the script finishes running.

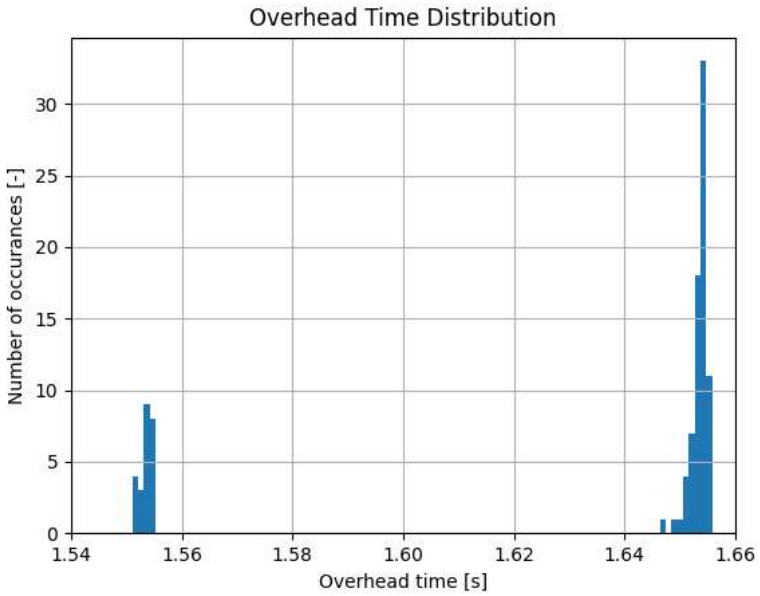

Figure 3:Histogram distribution of the time overhead of 100 recordings of 1 second, performed with rx_tools.

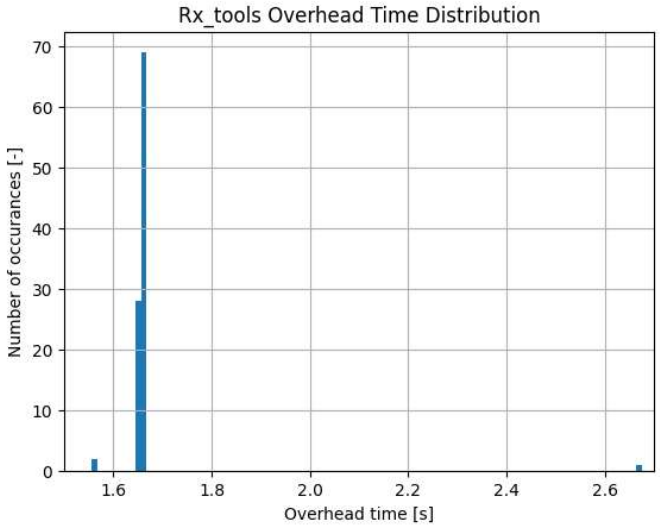

Figure 4: Histogram distribution of the time overhead of 100 recordings of 5 seconds, performed with rx_tools.

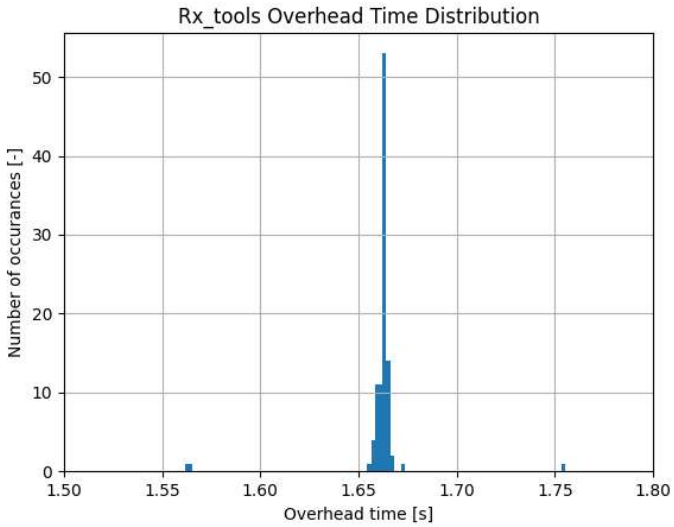

Figure 5: Histogram distribution of the time overhead of 100 recordings of 10 seconds, performed with rx_tools.

Appendix C: List of Materials

Below is a list of needed materials per work package.

GPS clock Allan deviation measurements
LB mini GPSDO + SMA cables to connect to tinyPFA device + ~15 to 20 dB attenuator
TinyPFA device + EC20S reference frequency source + cables to connect them
Load circuit
Personal laptop with TimeLab

SDR Allan Deviation measurements
LB mini GPSDO + cables to connect to SDRs
RSPduo
USRP N210

Antenna capable of receiving beacon signal + cables to connect to SDR, or EC20S reference clock + cables to connect to SDR + ~15 to 20 dB attenuator
Personal laptop with python

Timestamp uncertainty analysis
Personal laptop with python & tudat
Access to DopTrack measurements

EMF coupling analysis
Reference clock + SDR + quality USB cable
Fitlet3
Full omnidirectional VHF antenna + cables to connect to SDR
Datasheets of SDR, cables and antenna
Measuring tape

Optional:
EMF shielding materials

Finalize DopTrackBox design
Fitlet3 + SDR + quality USB cable
Reference clock + cables to connect to VNA device
VNA device (tinyPFA / NanoVNA?) + rubidium reference frequency source OR frequency counter
(Possibly: load circuit)
Personal laptop with TimeLab
Some enclosure (cardboard?)

Construct new DopTrackBox and analyze performance
Selected or made DopTrackBox box.
Fitlet 3
SDR + quality USB cable
GPS clock + cable to connect to SDR
(Possibly: load circuit)
Full VHF antenna + cable to connect to SDR
Personal laptop with tudat

Combined DopTrack and DopTrackBox Analysis
Selected or made DopTrackBox box.
Fitlet 3
SDR + quality USB cable
GPS clock + cable to connect to SDR
(Possibly: load circuit)
Full VHF antenna + cable to connect to SDR
Personal laptop with tudat

Thesis Writing
Personal laptop

Appendix D: Gantt Chart